MAR 31 1950

THE PHYSICAL REVIEW

VOLUME 77 Second Series NUMBER 6

MARCH 15, 1950

Published for the

AMERICAN PHYSICAL SOCIETY

by the

AMERICAN INSTITUTE OF PHYSICS

Lancaster, Pa., and New York, N. Y.

THE PHYSICAL REVIEW

A journal of experimental and theoretical physics established by E. L. Nichols in 1893

Published by the American Institute of Physics
for the
AMERICAN PHYSICAL SOCIETY

Officers

President

I. I. RABI
Columbia University
New York, New York

Vice-President

C. C. LAURITSEN
California Institute of Technology
Pasadena, California

Secretary

K. K. DARROW
Bell Telephone Laboratories
Office:
Columbia University
New York 27, New York

Treasurer

G. B. PEGRAM
Columbia University
New York 27, New York

Local Secretary
for the Pacific Coast

J. KAPLAN
University of California at Los Angeles
Los Angeles, California

Managing Editor

JOHN T. TATE
University of Minnesota
Minneapolis, Minnesota

BOARD OF EDITORS

Editor

JOHN T. TATE

Assistant Editor

J. W. BUCHTA

Associate Editors

S. A. GOUDSMIT — W. E. LAMB, JR. — HARVEY BRINKMAN
R. [illegible] PEIERLS — R. G. HERB — R. F. CHRISTY
W. [illegible] SHOCKLEY — J. BARDEEN — ERNEST KANE

Manuscripts for publication should be submitted to John T. Tate, School of Physics, University of Minnesota, Minneapolis, Minnesota. The authors' institutions are requested to pay a publication charge of $8 per page which, if honored, entitles the author to 100 free reprints. Instructions will be sent with galley proofs.

Please send all correspondence concerning papers in the process of publication and all editorial matters to be addressed to the Publication Manager, American Institute of Physics, 57 East 55 Street, New York 22, New York.

Subscription Price

United States and Canada $25.00
Foreign $27.00

Back Numbers[1]

Single number rate when complete year is available:
Prior to 1949: $20.00
Thereafter: $27.00
Single copies: $2.00 each, prior to July, 1929;
$1.00 each, July, 1929–December, 1941;
$2.00 each, January, 1942–December, 1946;
$1.00 each, January, 1947–December, 1948;
$1.25 each, thereafter.
Volumes, 1893–1920: $4.00.

Subscriptions, renewals, and orders for back numbers should be addressed to the American Institute of Physics, 57 East 55 Street, New York 22, New York.

Changes of address in the case of members of the American Physical Society should be addressed to the Treasurer; in the case of other subscribers to the Publication Manager, American Institute of Physics.

[1] Supplies limited. Inquire of Physics Department, Cornell University, Ithaca, New York.

The Physical Review is published [illegible] at Prince and Lemon Streets, Lancaster, Pennsylvania.

Entered as second-class matter March 6, 1917, at the Post Office at Lancaster, Pennsylvania, under the Act of March 3, 1879.

Acceptance for mailing at special rate of postage provided for in paragraph (d-2), section 34.40, P. L. & R. of 1948, authorized January [illegible]

THE
PHYSICAL REVIEW

A journal of experimental and theoretical physics established by E. L. Nichols in 1893

SECOND SERIES, VOL. 77, NO. 6 MARCH 15, 1950

Low Mass Francium and Emanation Isotopes of High Alpha-Stability*

E. K. HYDE,** A. GHIORSO, AND G. T. SEABORG
Department of Chemistry and Radiation Laboratory, University of California, Berkeley, California
(Received November 30, 1949)

Isotopes of francium with 126 or fewer neutrons have been looked for in bombardments of Th^{232} with 350-Mev protons from the 184-inch cyclotron. Fr^{212}, with an apparent half-life of 19.3 minutes for branching decay by alpha-emission (44 percent) to At^{208} and by orbital electron-capture (56 percent) to Em^{212}, has been found. Em^{212} is shown to be a 23-minute alpha-emitter. At^{208} decays primarily (99.5 percent) by orbital electron-capture to Po^{208}, but shows 0.5 percent alpha-branching. The francium and emanation isotopes have alpha-half-lives completely out of line with the simple predictions based on the previously known isotopes of these elements. Their high alpha-stability is believed to be due to a closed shell of 126 neutrons in analogy to the behavior of elements 83–85. The non-existence of long-lived francium in nature is discussed in the terms of this and other recent work on francium isotopes.

RECENT work with the 184-inch cyclotron has increased greatly the number of alpha-particle emitting isotopes and stimulated the reexamination of alpha-decay systematics in the heavy region.[1–3] The present paper describes experimental work carried out to get more information concerning the abnormalities in alpha-stability for nuclei in the region of 126 neutrons.

A plot of alpha-particle energy *versus* mass number for nuclei of elements above atomic number 85 produces a series of nearly parallel curves (see Fig. 1 which is redrawn from the data of Fig. 1, reference 3, using alpha-particle energies instead of alpha-decay energies). The curves for bismuth, polonium, and astatine (elements 83, 84, and 85) differ markedly in showing sharp maxima and minima. It was of interest to know whether those for emanation (element 86) and francium (element 87) show the same behavior. If the emanation and francium curves of Fig. 1 are simply extrapolated back to lower mass numbers, the alpha-particle energies predicted for all low mass isotopes correspond to half-lives of fractions of microseconds. But if the behavior of the astatine, polonium, and bismuth curves is imitated, one might expect that Fr^{213}, Em^{212}, and isotopes of lower mass number would exhibit alpha-half-lives long enough to permit their chemical isolation from targets bombarded in the 184-inch cyclotron. Should it be possible to do this, it would constitute further evidence for a region of stability at 126 neutrons.[4]

In addition to these considerations, it is of interest to learn more about element 87. No isotopes of this element were known until Perey's work on the 21-minute β-emitting AcK.[5,6] Since then the five shorter-lived isotopes listed in Table I have been discovered. Any new information concerning the isotopes or the chemical properties of this little known element should be welcome.

Therefore we undertook to prepare new francium isotopes by cyclotron bombardment. Without the aid of the high energy beam of the 184-inch cyclotron it would have been impossible as the closest suitable target material is Th^{232}. However, the use of a high energy proton beam (maximum 350 Mev) on thorium easily effected the preparation of isotopes in the region of interest by spallation reactions. We were able to isolate francium and establish the new family of isotopes shown in Fig. 2. The experimental evidence for this scheme is given now.

In addition evidence was found for Fr^{211} decaying principally by successive orbital electron-captures to At^{211} with a half-life of about 8 minutes. This particular work is not complete.

* This research was performed under the auspices of the U. S. AEC.
** On leave of absence from Argonne National Laboratory, Chicago, Illinois.
[1] Perlman, Ghiorso, and Seaborg, Phys. Rev. **74**, 1730 (1948).
[2] Perlman, Ghiorso, and Seaborg, Phys. Rev. **75**, 1096 (1949).
[3] Perlman, Ghiorso, and Seaborg, Phys. Rev. **77**, 26 (1950).
[4] Maria G. Mayer, Phys. Rev. **74**, 235 (1949).
[5] M. Perey, Comptes Rendus **208**, 97 (1939).
[6] M. Perey, J. de phys. et rad. **10**, 435 (1939).

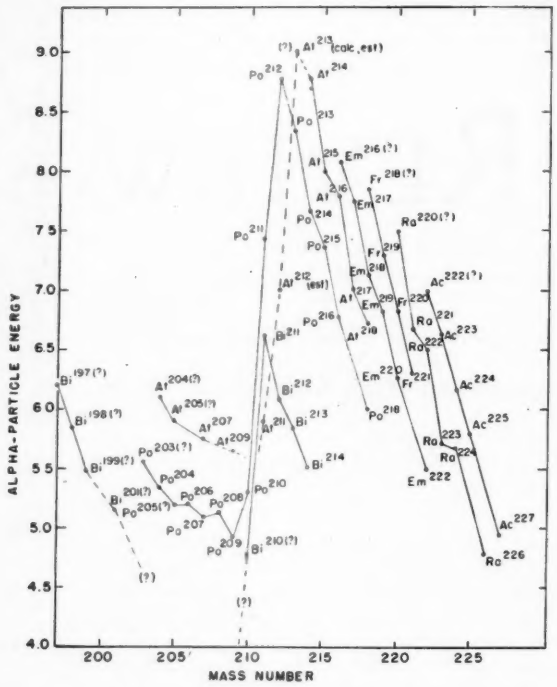

FIG. 1. Plot of alpha-particle energy *versus* mass number for isotopes of elements 83–89. Lines join all isotopes of a single element. Redrawn from paper of Perlman, Ghiorso, and Seaborg, reference 3.

It is quite evident then that the emanation and francium curves in Fig. 1 show the same sharp break in the neighborhood of 126 neutrons as do the curves for elements 83–85. One may safely predict that higher elements will show to some degree the same effect, but the possibility of observing it by the method used here for francium and emanation grows slim, because the half-lives for alpha-decay become very short and the region of greater beta-instability is being penetrated. These matters are discussed in much more detail by Perlman, Ghiorso, and Seaborg.[3]

Many writers of the past decade have pointed out the improbability of the natural occurrence of any long-lived isotopes of element 87. It may be well to reiterate this view in the light of the recent increase of the number of known francium isotopes from one to seven. Known isotopes of mass less than 222 are quite short-lived with respect to alpha-emission. Even the stabilization which occurs around 126 neutrons, although it enormously lengthens the expected half-life, is not enough to raise it to as much as an hour. On the other hand, isotopes 222 and 223 are short-lived with respect to beta-emission and those of higher mass are expected to be even more unstable. At this time we can be virtually certain that no very long-lived francium will ever be found. One cannot completely eliminate the possibility of the existence of a long-lived isomer corresponding to a highly forbidden transition.

EXPERIMENTAL SECTION

(1) Bombardment

Thorium foils 0.005 inch in thickness and 0.5 inch wide were bombarded on edge in the 184-inch cyclotron by full energy protons (max. 350 Mev) for periods ranging from 15 to 50 minutes. Numerous bombardments were made to obtain all the data because of the short half-lives involved.

(2) Chemical Isolation of Francium and Proof of Element Assignment

It was necessary to separate francium out of an exceedingly complex mixture of activities produced by (*p,xn*), (*p,pxn*), and other spallation and fission reactions.

This was done with cesium carrier, using a procedure based on the fission product assay method for cesium reported by Nelson and Glendenin.[7]

The thorium foil was dissolved in hot 6*N* HCl containing 0.1*N* $(NH_4)_2SiF_6$. After dissolution, 2 mg of cesium carrier was precipitated as cesium silicotungstate from 6*N* HCl, washed in HCl, dissolved in NaOH, scavenged of co-precipitated impurities by means of by-product ferric hydroxide precipitation and finally precipitated as cesium perchlorate from anhydrous alcoholic perchloric acid solution.

The activity listed in Fig. 2 as Fr^{212} was identified as the alkali element, francium, by the facts of its co-precipitation on cesium silicotungstate and cesium perchlorate, and its failure to co-precipitate on ferric hydroxide, thorium fluoride, or barium carbonate. It was possible to partially separate it from cesium by passing a 1*N* HNO_3 solution through a short resin column containing colloidal Dowex 50, the francium coming off last as the results of Cohn and Kohn[8] for the other alkali metals would indicate.

TABLE I. Previously known isotopes of francium.

Isotope	Half-life	Mode of decay	Energy of particle (Mev)	Ref.
Fr^{218}	very short	α	7.85	a
Fr^{219}	0.02 sec.	α	7.30	b
Fr^{220}	27.5 sec.	α	6.69	b
Fr^{221}	4.8 min.	α	6.30	c, d
Fr^{222}	14 min.	β^-		e
Fr^{223} (AcK)	21 min.	β^-, γ	1.20	f

[a] Ghiorso, Meinke, and Seaborg, Phys. Rev. **74**, 695 (1948).
[b] Meinke, Ghiorso, and Seaborg, Phys. Rev. **75**, 314 (1949).
[c] Hagemann, Katzin, Studier, Ghiorso, and Seaborg, Phys. Rev. **72**, 252 (1947); more completely given in U. S. AEC declassified document MDDC 1186 (December 10, 1947).
[d] English, Cranshaw, Demers, Harvey, Hincks, Jelley, and May, Phys. Rev. **72**, 253 (1947).
[e] E. K. Hyde and A. Ghiorso, unpublished work (June, 1949).
[f] See references 5 and 6.

[7] C. M. Nelson and L. E. Glendenin, U. S. AEC declassified document AECD 2556C (March 24, 1949).
[8] W. E. Cohn and H. W. Kohn, J. Am. Chem. Soc. **70**, 1986 (1948).

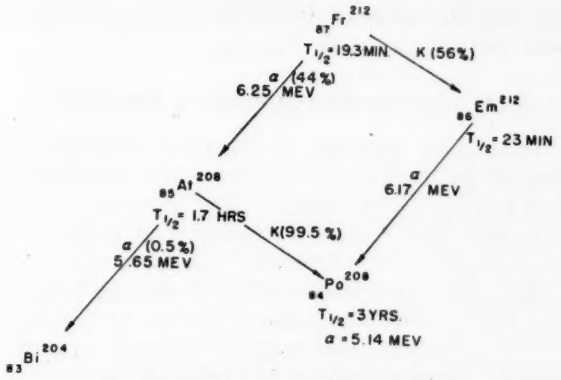

FIG. 2. Disintegration scheme of Fr^{212}.

In addition, it showed the volatility behavior reported for Fr^{221} [9] and the daughters showed the specific behavior of astatine and emanation. It might also be mentioned that the Fr^{223} (AcK) produced in the bombardment followed the behavior of the 19.3-minute alpha-emitter identically.

(3) Determination of Half-Life of Fr^{212}

The gross alpha-activity of francium samples did not show a straight line decay (see Fig. 8). This curve is a composite of the growth and decay of the alpha-activity of Em^{212} superimposed on the direct alpha-decay of Fr^{212} with small contributions from At^{208} and from the alpha-emitting daughters (AcX chain) of Fr^{223}. Ordinarily such a situation can easily be resolved by frequent differential pulse analyses of the alpha-spectrum by which method the peak due to any isotope can be followed independently of the rest. In our alpha-differential pulse analyzer[9] alpha-pulses from an ionization chamber are passed through a series of 48 electronic channels. Each channel records only the pulses falling within a narrow energy band. By plotting alpha-counts per channel *versus* the channel number, a curve is obtained with peaks which indicate the energy and abundance of each alpha-group.

This powerful method failed in this case because the near identity of the Fr^{212} and Em^{212} alpha-particle energies made it impossible to resolve them accurately.

In the method used, aliquots of a francium solution were taken at intervals of 15–30 minutes and volatilized from one platinum plate heated briefly to red heat to a second cooled plate 2 mm above. This volatilization is believed to be due to the disproportionation of the

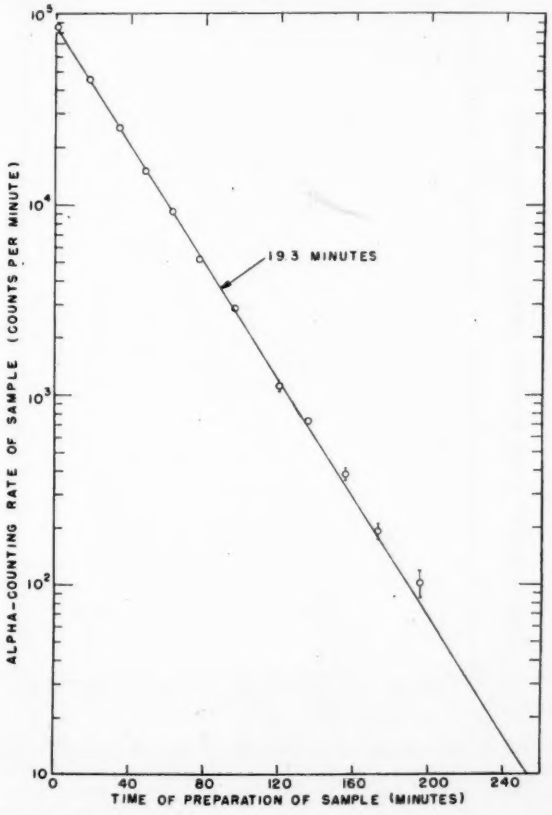

FIG. 3. Determination of half-life of Fr^{212}. Points represent counting rates of equal sized aliquots of a francium solution counted immediately after purification by volatilization.

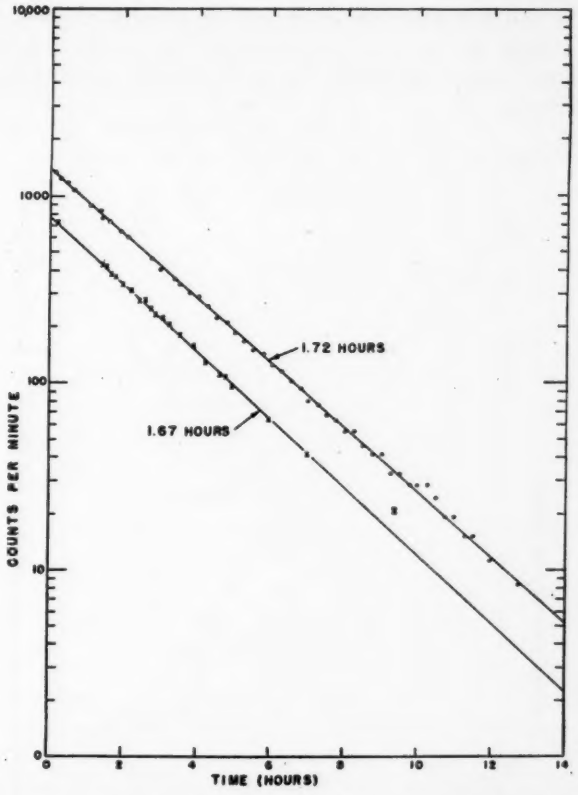

FIG. 4. Determination of half-life of At^{208} by measurement of decay. Upper curve shows decay of x-ray and γ-activity through 1.87 g/cm² beryllium absorber. Lower curve shows alpha-decay.

[9] Ghiorso, Jaffey, Robinson, and Weissbourd, National Nuclear Energy Series, Plutonium Project Record, Vol. 14B, "The transuranium elements: research papers," paper no. 16.8 (1949) (McGraw-Hill Book Company, Inc., New York, 1949); shorter description given in U. S. AEC declassified document MDDC-23 (June 14, 1946).

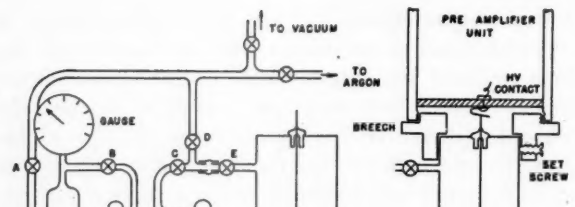

FIG. 5. Apparatus used in the isolation (a) and alpha-counting (b) of Em^{212}.

francium oxide to volatile metal and peroxide coupled with the thermal decomposition of the peroxide in analogy to the behavior of cesium oxide. Thin francium plates could be 99 percent volatilized.

The francium aliquots thus freed of Em^{212} and the Ra^{223} daughter of Fr^{223}, which was also present, were immediately counted before any appreciable re-growth of these had occurred. Corrections were made for an appreciable contribution by At^{208} activity in the later aliquots.

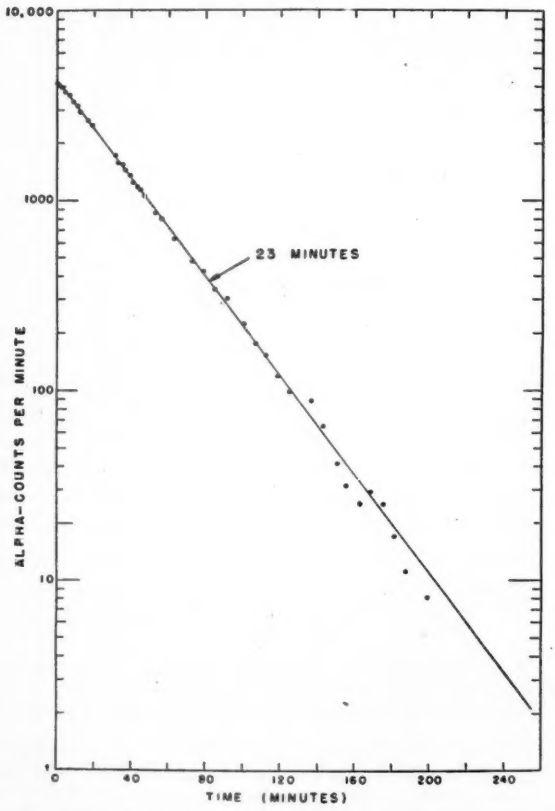

FIG. 6. Determination of half-life of Em^{212} by measurement of decay.

A half-life value of 19.3±0.5 minutes is obtained from the data plotted in Fig. 3.

(4) Identification of Astatine Daughter

Alpha-pulse analyses of francium samples after three hours decay clearly showed a new alpha-activity of 5.65±0.02 Mev energy. This activity could be volatilized from one plate to another at temperatures much lower than the francium could be moved.

High volatility is characteristic of astatine,[10] and this 5.65 Mev activity was judged to be the At^{208} daughter of Fr^{212}. Chemical proof involved carrying the activity on tellurium metal precipitated from $2M$ HCl with SO_2 and extraction into benzene from a $2N$ H_2SO_4 solution saturated with SO_2.

Benzene-extracted astatine samples were observed to have a straight line alpha-decay with a half-life of 1.7 hours. These samples emitted x-rays which also decayed with a 1.7-hour half-life. Representative curves are shown in Fig. 4.

By following decay through 2 grams of beryllium absorber with the sample at 10 percent geometry beneath a xenon-alcohol (10-cm pressure) filled end-

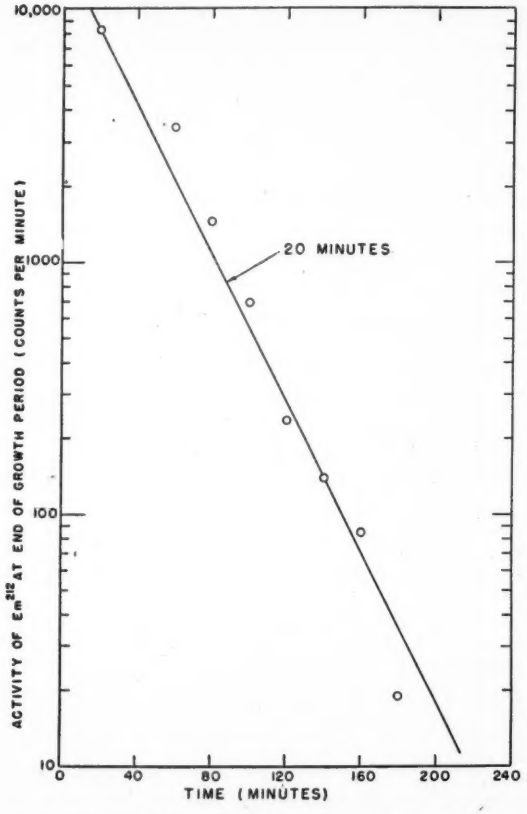

FIG. 7. Determination of half-life of parent of Em^{212}. Points represent counting rate of Em^{212} grown into a sample of Fr^{212} during 20-minute period immediately preceding count.

[10] Johnson, Leininger, and Segrè, J. Chem. Phys. **17**, 1 (1949); also published as U. S. AEC declassified document AECD-1952 (May 10, 1948).

window Geiger tube, we observed one Geiger count per two alpha-disintegrations. This Geiger activity is principally K and L x-rays, but includes some γ-rays. A value of 1.1 Mev was determined by lead absorption for the most energetic γ-ray.

A value of the At^{208} K/α-branching ratio was obtained by comparing the initial alpha-particle counting rate of a pure sample of At^{208} to the alpha-counting rate of the Po^{208} daughter formed from electron-capture observed on complete decay of the At^{208}. From 7830 alpha-counts per minute At^{208} we obtained 88 counts per minute of 3-year Po^{208} alpha-activity.

From this we obtain 178/1 as the K/α-branching ratio for At^{208}. Duplicate samples gave scattered results, the average value being 180 ± 20. This would make the partial alpha-half-life of At^{208} about 13 days.

It should be pointed out that Barton has found evidence for an isomer of At^{208} in astatine fractions of bismuth targets bombarded with high energy helium ions.[11] This isomer decays by orbital electron-capture to Po^{208} with a half-life of 7 hours.

(5) Identification of Polonium Daughter

The alpha-activity found after complete decay of the 1.7-hour astatine activity in the samples mentioned in Section (4) was shown by pulse analysis to be of 5.15 ± 0.05 Mev energy. Templeton *et al.*[12] report a 3-year Po^{208} activity emitting alpha-particles of 5.14 Mev energy. Within statistical error our samples have been decaying with a 3-year half-life for a period of more than 6 months. Large samples of initially pure Fr^{212} (10^5–10^6 alpha-counts per minute) were found weeks later to have the amounts of 5.14-Mev alpha-activity consistent with the production of 3-year Po^{208} by the branching scheme of Fig. 2. This evidence plus the isolation of the same polonium activity from an initially pure sample of the 23-minute emanation is the evidence on which the mass assignments of Fig. 2 rest.

(6) The Emanation Isotope

The apparatus shown in Fig. 5 was used in the isolation and identification of Em^{212}.

A platinum plate with a sample of francium on it was placed in the apparatus. After evacuating the entire system, the part between valves A and B was filled with an atmosphere of pure argon. The platinum plate was brought to red heat with the induction heater to volatilize the francium and deposit it as a readily emanating film on the walls of the vessel. By opening valves B, C, and E with D closed and letting argon flow in from A until the pressure reached atmospheric, the greater part of the emanation could be passed through the dry ice-cooled trap into the counting chamber. The trap removed astatine, water vapor, and

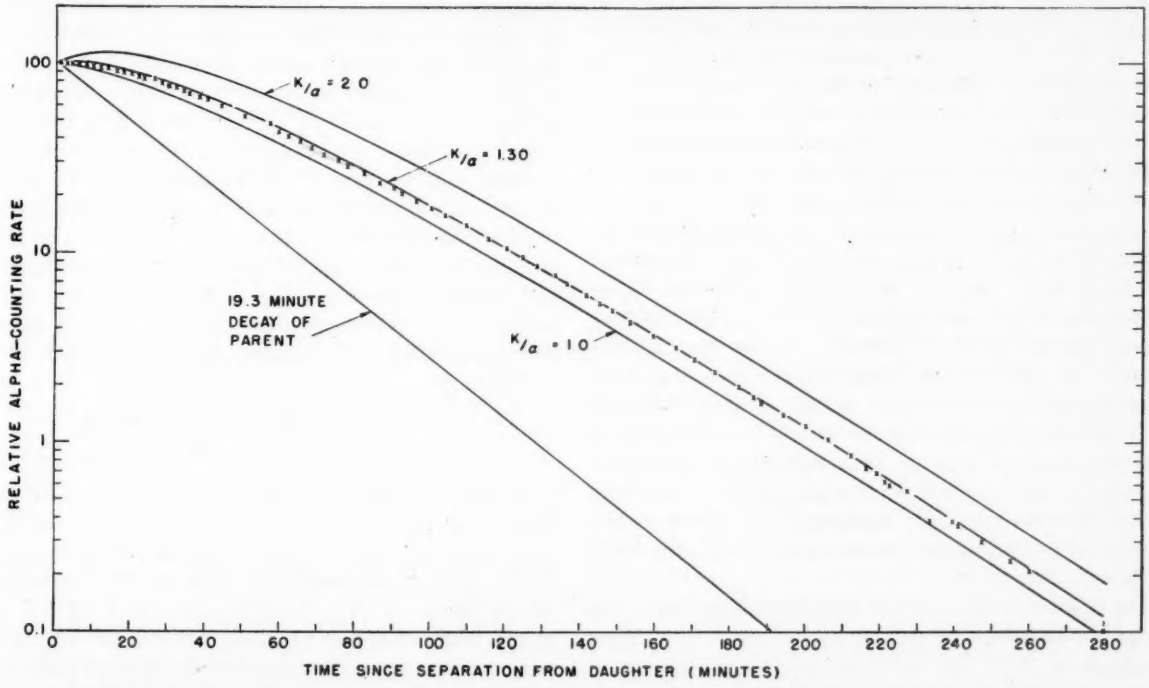

FIG. 8. Determination of the K/α-branching ratio of Fr^{212}. X points are experimental values corrected for small contributions from At^{208} and Ra^{223} and normalized to an initial count of 100. Lines are theoretical curves for the total alpha-counting rate of a 19.3-minute alpha-emitting parent producing a 23-minute alpha-emitting daughter by K-capture with the branching ratio indicated.

[11] Barton, Ghiorso, and Perlman, unpublished work (1949).
[12] Templeton, Howland, and Perlman, Phys. Rev. **72**, 758 (1947).

any low volatility impurities. By inserting this chamber into a special breech and setting the pre-amplifier unit of an alpha-counter into the top of the breech, the central wire of the special chamber made contact with the high voltage lead to the counter (Fig. 5 (b)). The unit then functioned as an argon-filled ionization chamber for the collection of alpha-particle pulses. This comparatively crude arrangement was quite adequate for relative measurements and for half-life determinations.

Using this method, an alpha-emitting emanation activity of 23 minutes half-life was discovered (see Fig. 6). This activity, as well as a second alpha-emitting low mass emanation of 2.3 hours half-life, had been previously found in this laboratory.[13] The present work determined its mass assignment and alpha-energy.

To establish that the 23-minute emanation was the daughter of the 19.3-minute francium, the following "milking" experiment was carried out. After flashing an active francium sample into an atmosphere of argon as above, the system was evacuated. Fresh argon was let in to the section of the apparatus between valves A and B and the emanation permitted to grow for exactly 20 minutes. At the end of this time the gas was transferred to the counting chamber and immediately counted. Then the chamber was again placed in the apparatus and pumped out. The emanation which had grown in during a second 20-minute period was transferred to the counting chamber and counted. This procedure was repeated eight times. Results are shown in Fig. 7. The decay line represents the decay of the francium parent. Considering the experimental error, the half-life value is consistent with the assignment of the 19.3-minute francium as the parent of the emanation.

The alpha-particle energy of Em^{212} is established as nearly identical to that of Fr^{212} from the fact that one peak in pulse analysis curves of the francium fraction accounts for the major part of the activity even though the gross alpha-decay is definitely non-linear. More careful work with the energy scale of the pulse analyzer spread out revealed a difference in the two alpha-energies. A difference of about 80 kev was found by pulse analyzing a francium sample freshly freed of Em^{212} by volatilization and continuing to pulse analyze it as the daughter re-grew. Our best energy values are 6.25 ± 0.03 Mev for the Fr^{212} alpha-particle and 6.17 ± 0.03 Mev for the Em^{212} alpha-particle. These values depend on calibration of the instrument with the Ra^{226} series.

The polonium daughter of alpha-emitting Em^{212} was shown to be identical to the orbital electron-capture daughter of At^{208} by pumping an active sample of emanation through two dry ice traps and letting it decay in an isolated glass tube. When the acid used to wash out this glass tube several hours later was evaporated on a platinum plate and pulse analyzed, alpha-activity of 5.15 ± 0.05 Mev energy was found. This activity, apparently due to Po^{208}, did not decay appreciably in a period of 60 days.

[13] Ghiorso, Meinke, and Seaborg, Phys. Rev. **76**, 1414 (1949).

(7) Determination of Fr^{212} K/α-Branching Ratio

In principle, several methods might be used for making this important measurement, but all involve experimental difficulties.

Counting the francium x-rays directly is rendered impossible by the presence of a high background of cesium fission product activity.

Quantitatively isolating and counting the Em^{212} from a measured sample of Fr^{212} would require developing better counting equipment for the gaseous activity.

One could quantitatively determine the amount of Po^{208} produced in an initially pure alpha-counted Fr^{212} sample. The excess of Po^{208} activity over the amount that would be produced if Fr^{212} decayed only by alpha-particle emission would determine the amount of K-branching. This is insensitive because of the long half-life of Po^{208} and the low K/α-branching of Fr^{212}.

The method selected was to determine carefully the shape of the alpha-growth and decay curve for an initially pure francium sample and compare this curve with theoretical curves drawn for various values of the K/α-branching. A sample of francium containing 10^5 alpha-counts per minute was freed of emanation by volatilizing it from one platinum plate to another, quickly sprayed with a zapon solution to insure the complete retention of Em^{212}, and immediately placed in an alpha-counter. This sample was counted continuously for several hours. The experimentally observed decay points were corrected for a background of Ra^{223} (from the decay of AcK present in the initial sample) amounting to 0.2 percent of the initial count. A small contribution to the counting rate due to the growth and decay of the At^{208} daughter was also subtracted. The resulting points were normalized to make the counting rate equal 100 at the time of volatilization and plotted as shown in Fig. 8. The curves shown were derived from the theoretical equation below, using a Fr^{212} half-life of 19.3 minutes and an Em^{212} half-life of 23.0 minutes.

$$\text{TOTAL ALPHA-COUNTING RATE} = -\lambda_1 N_0 e^{-\lambda_1 t} - [\gamma\lambda_2\lambda_1 N_0(e^{-\lambda_1 t} - e^{-\lambda_2 t})/(\lambda_2 - \lambda_1)]$$

λ_1 and λ_2 are the disintegration constants of Fr^{212} and Em^{212}, t is the time for Em^{212} growth, γ is the K/α-branching ratio of Fr^{212}, and N_0 is the initial amount of Fr^{212}. $-\lambda_1 N_0$ is arbitrarily set equal to 100. From Fig. 8 we estimate the K/α branching to be 1.3 ± 0.1. This would place the partial alpha-half-life of Fr^{212} at 43 minutes, the partial orbital electron-capture half-life at 34 minutes.

ACKNOWLEDGMENTS

The authors are indebted to Mr. James Vale and the operating crew of the 184-inch cyclotron for their assistance in the numerous bombardments required for this work.

Nuclear Shell Models*,†

EUGENE FEENBERG
Washington University, St. Louis, Missouri
(Received December 5, 1949)

The principal features of the several shell models now under discussions are described briefly.

The magnetic moments of odd nuclei have been interpreted as (a) supporting an extreme single particle model (Schmidt limits) and (b) as generally consistent with a uniform model (Margenau-Wigner limits). The evidence is consistent with a composite interpretation based on (a) the approximate validity of the extreme single particle model for nuclei lacking one particle to make a closed shell or possessing one particle in excess of the number making up a closed shell, and (b) the approximate validity of the uniform model for all other odd nuclei.

Remarks on quadrupole moments, isomerism and beta-decay supplement an earlier discussion.

CONTEMPORARY nuclear theory bears some resemblance to the periodic system of the elements and theories of chemical valence and structure. The sources of the parallelism are known: the exclusion principle and the isotropy of space, the latter in the form of the quantum theory of the parity and angular momentum operators.

The number of neutrons N and of protons Z are the basic parameters for the characterization and interpretation of nuclear structure. An imposing body of evidence supports the conclusion that $N=50$, 82, and 126 and $Z=50$ and 82 are associated with particularly stable and abundant nuclear species.[1,2] Other numbers may be added to this list, among them N or $Z=2$, 8, 10, and 20.[3–5]

The interpretation of the "magic" numbers as occupation numbers of single-particle levels in a suitably proportioned potential well was discussed by Elsasser in the same paper in which the special properties of the numbers 50, 82, and 126 were first recognized. Other closely related schemes have been proposed recently. Figure 1 summarizes the various schemes at present under discussion. Column 1 shows the levels and occupation numbers of an isotropic harmonic oscillator. The modifications introduced by distorting the potential into the shape of a rectangular well appear in column 2. These potentials have in common the occupation numbers 2, 8, and 20.[6]

Column 3 exhibits the level order and occupation numbers in the scheme devised by Nordheim.[7] The guiding principle here is the production of the magic numbers with a minimal departure from the level order in the rectangular potential well.

The j–j coupling scheme[8,9] appears in column 4. All levels with orbital angular momentum $l>0$ are split into two, a lower level with total angular momentum $i=l+1/2$ and an upper with $i=l-1/2$. This is essentially the Breit-Inglis[10–12] rule for the effect of spin-orbit coupling. What is new is the assumption that the spin-orbit coupling is large and particularly so for levels with $l\geqq 4$.

The remaining columns 5–9 show the Feenberg-Hammack[13] scheme based on Elsasser's suggestion of a central elevation in the potential well.[1] A physical basis for the central elevation is now provided by the effect of the Coulomb repulsion between protons on the variation of particle density within the nucleus. The repulsion causes the density to vary from a minimum value at the center of the nucleus to a maximum near the boundary.[14] The optimum single-particle potential well is pictured as a distorted mirror image of the particle density, being deepest where the density attains a maximum value and shallowest at the center where the minimum density occurs (Fig. 2B). It is postulated that levels with large particle density in the central region of the nucleus ($2s$, $2p$, and $2d$) are pushed up by the developing central elevation with sufficient rapidity to permit closed shells at 50, 82, and 126. Other levels are displaced relatively little because the wave functions are extremely small in the region of the elevation.

In light nuclei the particle density may be pictured as a bell-shaped curve. The corresponding optimum single-particle potential then resembles an inverted bell and may be approximated roughly by a rectangular well with a central depression (Fig. 2A). A sufficiently deep central depression pulls the $2s$ level below $1d$, thus permitting a closed shell at N or $Z=10$ and the closing of the $1d$ shell at N or $Z=20$. This explanation serves all the proposed schemes.

* Assisted by the Joint Program of the ONR and AEC.

† Based on two lectures at the symposium on modern physics sponsored by the Oak Ridge National Laboratory and the Oak Ridge Institute of Nuclear Studies, August, 1949.

[1] W. Elsasser, J. de phys. et rad. **5**, 625 (1934).
[2] M. G. Mayer, Phys. Rev. **74**, 235 (1948).
[3] W. D. Harkins, Phys. Rev. **76**, 1538 (1949).
[4] E. P. Wigner, Phys. Rev. **51**, 947 (1937).
[5] W. H. Barkas, Phys. Rev. **55**, 691 (1939).
[6] The notation is that proposed by M. G. Mayer. np, for example, denotes a state with one unit of orbital angular momentum and a radial wave function possessing $n-1$ nodes at finite values of the radial coordinate (excluding one at the origin).
[7] L. W. Nordheim, Phys. Rev. **75**, 1894 (1949).
[8] M. G. Mayer, Phys. Rev. **75**, 1969 (1949).
[9] Haxel, Jensen, and Suess, Phys. Rev. **75**, 1766 (1949). For obscure reasons these authors prefer the oscillator potential.
[10] D. R. Inglis, Phys. Rev. **50**, 783 (1936).
[11] L. Rosenfeld, *Nuclear Forces* (Interscience Publishers, Inc., New York, 1948).
[12] E. Feenberg, Phys. Rev. **76**, 1275 (1949).
[13] E. Feenberg and K. C. Hammack, Phys. Rev. **75**, 1877 (1949).
[14] E. Feenberg, Phys. Rev. **59**, 593 (1941).

The existence of alternative structures for the closed shells at N or $Z=50$, 82, and 126 may be a clue to the exceptional stability of these shells. In molecular theory the existence of alternative qualitative descriptions often provides an additional element of stability through the operation of the quantum-mechanical resonance effect. Similarly, in the nuclear problem, it is not unlikely that the optimum representation of the closed shell structure may be a linear combination of the various simple possibilities provided by the different schemes rather than exclusively one or the other.

In this connection it is interesting to consider the possibility that the dependence of level position on the variation of particle density within the nucleus may cause the order of levels to depend on whether certain orbits are occupied or empty. For example, eight particles in $2s$ and $2p$ orbits contribute materially to the particle density in the inner region of the nucleus, thus opposing the tendency toward the formation of a semihollow nucleus and the correlated development of a central elevation in the potential well. On the other hand, the transfer of eight particles from $2s$ and $2p$ into $1g$ orbits should materially reduce the central particle density and consequently accelerate the development of the central elevation in the potential well with the result that the unoccupied $2s$ and $2p$ levels are raised above the partially occupied $1g$ level. In the former situation, a closed shell may form at N or $Z=50$, utilizing only $G_{9/2}$ orbits in accordance with the postulates of the Mayer scheme. The latter situation produces a closed shell at N or $Z=50$ with $1g$ fully occupied. Similar conditions may prevail near N or $Z=82$ yielding two possible structures for a closed shell at 82, one with $2s$, $3s$, and $2p$ orbits fully occupied and only the $H_{11/2}$ subshell of $1h$ filled and a second with $2s$ and $2p$ empty and $1h$ completely filled.

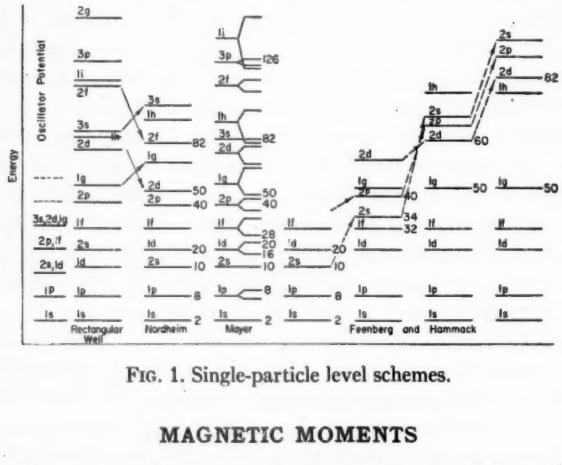

FIG. 1. Single-particle level schemes.

MAGNETIC MOMENTS

The magnetic moments[15] of odd nuclei are plotted in Fig. 3 (odd Z) and Fig. 4 (odd N). Large circles denote nuclei with closed ($\pm$) shells (one particle lacking to make a closed shell or one particle in excess of the number required for a closed shell). The theoretical interpretation of these diagrams is based on the study of simple limiting situations. Results of great value have been derived from the assumption that the nucleus possesses a definite orbital angular momentum and a total angular momentum $I=l+1/2$ or $I=l-1/2$ (Russel-Saunders coupling). The magnetic moment is given by the formula (in nuclear magneton units)

$$\mu=\tfrac{1}{2}\cdot I\left[g_l+g_s+(g_l-g_s)\frac{l(l+1)-\frac{3}{4}}{I(I+1)}\right]. \quad (1)$$

Here

$$\begin{aligned} g_s&=5.58 \text{ (odd proton)} \\ &=-3.82 \text{ (odd neutron)}, \end{aligned} \quad (2)$$

while g_l depends on special properties of the model. Two models have been employed in this connection.

(a) Extreme single-particle model. The odd nucleon moves in the spherically symmetric field of a core containing all the other particles. Even parity and zero angular momentum are assigned to the core in harmony with the empirical rule that even-even nuclei have always zero spin in the ground state. All angular momentum and parity properties are associated with the odd nucleon. Thus,

$$\begin{aligned} g_l&=1 \text{ (odd proton)} \\ &=0 \text{ (odd neutron)}. \end{aligned} \quad (3)$$

The dashed curves in Figs. 3 and 4 are the Schmidt limits[16] computed from Eqs. (1)–(3). It is not difficult to see that the experimental points on each diagram group themselves into two broad bands between the theoretical limits and paralleling them. This relation between theory and experiment has been interpreted as evidence for the substantial validity of the extreme single particle model and for the assumption that the orbital angular momentum l is a good quantum number (allowing, of course, notable exceptions). Inglis[17] presents theoretical arguments for this point of view. Paradoxically, the recognition of the magic numbers and the associated closed ($\pm$) shell systems weakens the case for the general validity of the extreme single-particle model. One expects somewhat closer conformity to the extreme single-particle model from closed ($\pm$) shell system than from other odd nuclei. Actually such

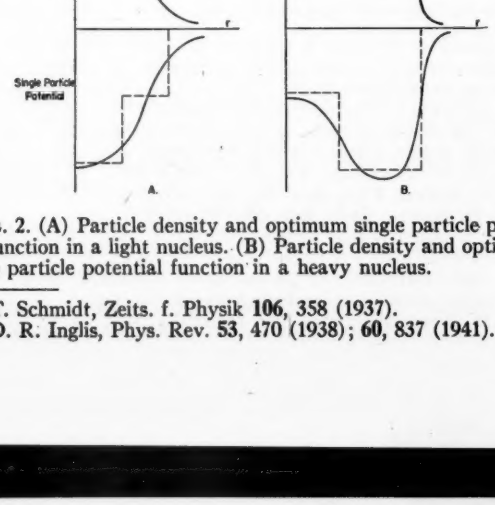

FIG. 2. (A) Particle density and optimum single particle potential function in a light nucleus. (B) Particle density and optimum single particle potential function in a heavy nucleus.

[15] (a) H. H. Goldsmith and D. R. Inglis, *The Properties of Atomic Nuclei I* (Information and Publications Division, Brookhaven National Laboratory, Upton, New York, October 1, 1948). (b) Livingston, Gilliam, and Gordy, Phys. Rev. **76**, 443 (1949). (c) L. Davis, Phys. Rev. **76**, 435 (1949).

[16] T. Schmidt, Zeits. f. Physik **106**, 358 (1937).

[17] D. R. Inglis, Phys. Rev. **53**, 470 (1938); **60**, 837 (1941).

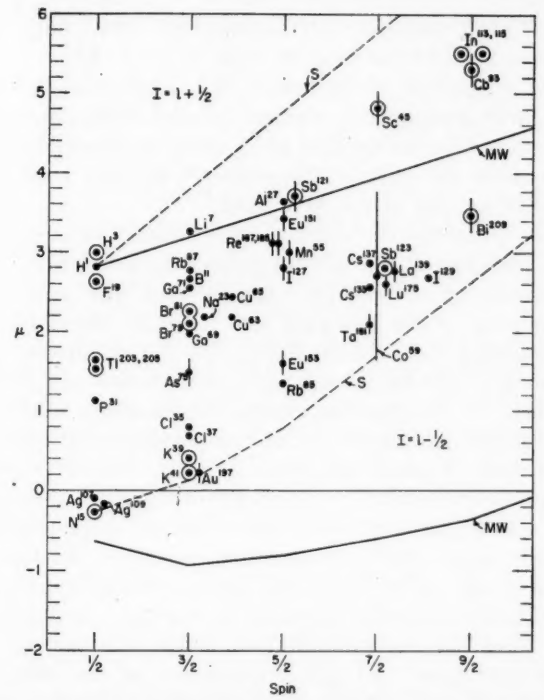

FIG. 3. Magnetic moments of the odd proton nuclei. S—Schmidt limits, MW—Margenau-Wigner limits. Circles ⊙ label nuclei containing closed (±) shells: one particle lacking to make a closed shell or one particle in addition to a closed shell.

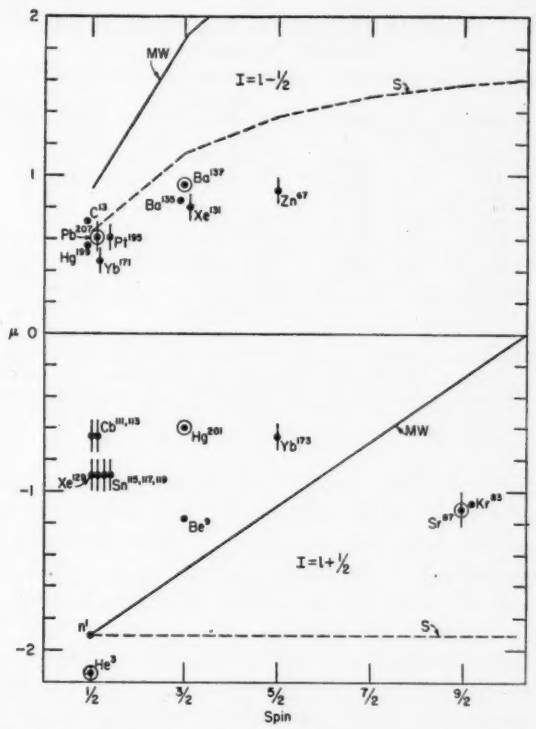

FIG. 4. Magnetic moments of the odd neutron nuclei. S—Schmidt limits, MW—Margenau-Wigner limits. Circles ⊙ label nuclei containing closed (±) shells: one particle lacking to make a closed shell or one particle in addition to a closed shell.

a distinction is not apparent relative to the Schmidt limits. The absence of a distinction puts in question the relevancy of the Schmidt limits for odd nuclei not of the closed (±) shell type.

Deviations from the Schmidt limits suggest a generalization of the single-particle model in which nuclear states are linear combinations of states with $l=I-1/2$ and $l=I+1/2$. The opposite parity of single-particle wave functions differing by one unit in l requires a corresponding ambivalence in the parity of the core.[7] In this form the model lacks plausibility. It seems preferable to admit that a single-particle model is not competent to deal with deviations from the Schmidt limits.[18]

The fact that all experimental magnetic moments lie close to or between the Schmidt limits supports the assumption of a predominantly doublet character for the low states of odd nuclei. It must be considered unlikely that a widespread occurrence of strong quartet components would never result in a breach of the limits.[18] Thus, for example, an odd proton nucleus in a state containing equal parts of $^4P_{5/2}$ and $^2D_{5/2}$ might have $\mu\sim 7.1$.

(b) Uniform model. This model, developed by Margenau and Wigner[18] from a suggestion of K. Way, distributes the orbital angular momentum uniformly over all the particles in the nucleus with the result

$$g_l \sim Z/A > 0.4 \qquad (4)$$

[18] H. Margenau and E. P. Wigner, Phys. Rev. 58, 103 (1939).

for both odd N and odd Z. The solid lines in Figs. 3 and 4 are the Margenau-Wigner limits computed from Eqs. (1), (2), and (4). Moments falling between the MW limits are interpreted as evidence that the orbital angular momentum is not a constant of motion. States with $l=I-1/2$ and $l=I+1/2$ may have the same parity in a many particle model and, consequently, may combine to produce intermediate values of the moments.

TABLE I. Possible doublet states for partially filled shells.[a] Number of linearly independent states.

Configuration	^1S	^3P	^3D	^3F	^3G	^3H	^3I	^3K	^3L	^3M	^3N	^3O
$(np)^{1,5}$		1										
$(np)^3$		1	1									
$(nd)^{1,9}$			1									
$(nd)^{3,7}$		1	2	1	1	1						
$(nd)^5$	1	1	3	2	2	1	1					
$(nf)^{1,13}$				1								
$(nf)^{3,11}$		1	2	2	2	2	1	1	1			
$(nf)^{5,9}$		4	5	7	6	7	5	5	3	2	1	1
$(nf)^7$	1	5	7	10	10	9	9	7	5	4	2	1
$(ng)^{1,17}$					1							
$(ng)^{3,15,b}$		1	2	2	3	3	2	2	2	1	1	1

[a] Gibbs, Wilbur, and White, Phys. Rev. 29, 790 (1927).
[b] Computed by the author.
The analysis of the g^n configurations has been completed by Mr. K. C. Hammack. In odd nuclei maximum degeneracy occurs always for ^3G states. Table I should be supplemented by a similar table for the degeneracy of singlet states in configurations containing an even number of equivalent orbits. The most significant property of the singlet table is a relatively high degeneracy of ^1S states. This circumstance is helpful in understanding the empirical rule that even-even nuclei have always zero spin in the ground state.

TABLE II. Three particles in *nd* orbits (central elevation level scheme).

Nucleus	Spin	Magnetic moment	Uniform model interpretation
$_{12}Mg^{25}$	5/2[a]	−0.96	$D_{5/2}$
$_{13}Al^{27}$	5/2	3.64	$D_{5/2}$
$_{42}Sr^{91}$	5/2[b]	——	——
$_{42}Mo^{95}$	5/2[b]	——	——
$_{53}I^{127}$	5/2	2.8	$D_{5/2}\gg F_{5/2}$
$_{75}Re^{185}$	5/2	3.3	$D_{5/2}\gg F_{5/2}$
$_{75}Re^{187}$	5/2	3.3	$D_{5/2}\gg F_{5/2}$
$_{54}Xe^{129}$	1/2	−0.9	$S_{1/2}\sim P_{1/2}$
$_{53}I^{129}$	7/2	2.74	$F_{7/2}\gg G_{7/2}$

[a] Crawford, Kelly, Shawlow, and Grey, Phys. Rev. **76**, 1423 (1949).
[b] Derived from the analysis of radioactivity and isomerism; reference 13 of this paper. *Added in proof:* Confirmed for Mo^{95} by hyperfine structure measurements (private communication from Prof. J. E. Mack).

Eight intermediate and heavy nuclei have moments falling outside of the MW limits.‡ It is noteworthy that six of the eight contain closed (±) shells for which the single-particle model might be expected to yield better results than the uniform model. Thus the exceptional cases occur where failures are not unexpected. The evidence is consistent with a composite interpretation based on (a) the approximate validity of the extreme single-particle model for nuclei containing closed (±) shells and (b) the approximate validity of the uniform model for all other odd nuclei. Under (a) l is generally a fairly good quantum number while under (b) admixtures of $l=I-1/2$ and $l=I+1/2$ in varying proportions are common.

No explanation has yet been advanced for the peculiar fact visible in both Figs. 3 and 4 that practically all moments (excluding the exceptional closed (±) shell systems) fall between the MW limit for $I=l+1/2$ and the Schmidt limit for $I=l-1/2$.

The question of the admixture of higher values of S (quartet components) already referred to becomes less pressing with recognition of an adequate interpetation, requiring no quartet component,[18] for the moments falling outside of the MW limits.

In summary the single-particle model, while not at all plausible on the basis of present notions concerning nuclear forces, receives support from the apparent grouping of the moments into irregular broad bands paralleling the Schmidt limits. No obvious distinction appears between closed (±) shell nuclei and other types. At the opposite extreme the uniform model is consistent with most of the data provided that l is not generally a good quantum number. Moreover, the failures are confined (with two exceptions) to the class of closed (±) shell nuclei for which the single-particle model is most likely to possess a useful degree of validity.

For odd nuclei not of the closed (±) shell-type configuration analysis provides a working compromise between the oversimplification of the extreme single-particle model and the intractability of the uniform model. The spherically symmetric core (of even parity) contains the even group of particles and the largest number of particles in the odd group forming a closed shell. The remaining particles or holes of the odd group are placed in appropriate single particle orbits. For example, $_{53}I^{127}$ is represented by a $(2d)^3$ configuration (three protons in $2d$ orbits) on a core containing 50 protons and 74 neutrons while $_{49}In^{115}$ requires a $1g$ orbit occupied by a proton hole on a core containing 50 protons and 66 neutrons.[19] In special cases a complete configuration for all particles outside of closed shells appears most plausible; $_{11}Na^{23}$ is an example. However, the $(1d)^1(1d)^2$ configuration contains no symmetrical ^2P state and fails, just as does the single-particle model, to account for the $P_{3/2}$ character of the ground state.

TABLE III. Three holes in *nd* orbits (central elevation level scheme).

Nucleus	Spin	Magnetic moment	Uniform model interpretation
$_{17}Cl^{35}$	3/2	0.82	$D_{3/2}>P_{3/2}$
$_{17}Cl^{37}$	3/2	0.68	$D_{3/2}>P_{3/2}$
$_{16}S^{33}$	3/2†	——	——
$_{56}Ba^{135}$	3/2	0.84	$D_{3/2}>P_{3/2}$
$_{79}Au^{197}$	3/2	0.195	$D_{3/2}>P_{3/2}$
$_{57}La^{139}$	7/2	2.76	$F_{7/2}>G_{7/2}$
$_{44}Ru^{101}$	——	——	——

† *Added in proof:* Confirmed by C. K. Jen, Bull. Am. Phys. Soc. **25**, No. 1, 35 (1950).

TABLE IV. Three particles or holes in $2p$ orbits (central elevation level scheme).

Nucleus	Spin	Magnetic moment	Uniform model interpretation
$_{37}Rb^{87}$	3/2	2.75	$P_{3/2}$
$_{37}Rb^{85}$	5/2	1.35	$D_{5/2}\sim F_{5/2}$
$_{30}Zn^{67}$	5/2	0.9	$F_{5/2}>D_{5/2}$
$_{63}Eu^{151}$	5/2	3.4	$D_{5/2}$
$_{63}Eu^{153}$	5/2	1.5	$D_{5/2}\sim F_{5/2}$

‡ $_{13}Al^{27}$ is not included among the exceptions because a more detailed treatment using exact values of Z/A in estimating g_l would place the magnetic moment of this nucleus between the accurate MW limits.

TABLE V. Shell structure of nuclei involved in beta-transitions showing the unique first-forbidden type of energy distribution.

Nucleus	Configuration	Parity	Spin
$_{17}Cl^{38}$	$(1d)^{-3}(1f)^1$	odd	..2...
$_{18}A^{38}$	$(1d)^{-2}$	even	0
$_{19}K^{42}$	$(1d)^{-1}(1f)^3$	odd	..2...
$_{20}Ca^{42}$	$(1f)^2$	even	0
$_{38}Sr_{89}$	$(1d)^1$	even	5/2
$_{39}Y_{89}$	$(2p)^{-1}$	odd	1/2
$_{38}Sr^{90}$	$(2p)^{-2}(2d)^2$	even	0
$_{39}Y^{90}$	$(2p)^{-1}(2d)^1$	odd	..2...
$_{40}Zr^{90}$	closed shells	even	0
$_{38}Sr^{91}$	$(2d)^3$	even	..5/2...
$_{39}Y^{91}$	$(2p)^{-1}$	odd	1/2
$_{40}Zr^{91}$	$(2d)^1$	even	5/2
$_{55}Cs^{137}$	$(2d)^5$	even	7/2[a]
$_{56}Ba^{137}$	$(1h)^{-1}$	odd	11/2
$_{56}Ba^{137}$	$(2d)^{-1}$	even	3/2[a]

[a] Experimental value.

[19] W. Heisenberg, Ann. d. Physik **10**, 888 (1931). The theory of holes is developed in this paper.

Table I contains the number of linearly independent doublet states generated by configurations of equivalent orbits. A certain tendency to simulate the results of the extreme single-particle model may be inferred from the fact that the smallest value of orbital angular momentum associated with maximum degeneracy is identical with that of a single orbit. Thus, for example, the $(1f)^7$ configuration with ten linearly independent ^2F states might be expected to favor $l=3$ for the ground state in agreement with the spin and magnetic moment of $_{27}Co^{59}$ (referred to the MW limits).

The threefold occurrence of *nd* orbits in the central elevation level scheme suggests a search for regularities based on repetitions of $(nd)^{3,5,7}$ configurations. Results, shown in Tables II and III, conform well to expectations based on the double degeneracy of ^2D states in the $(nd)^{\pm 3}$ configuration and the Breit-Inglis rule. In Mayer's level scheme $_{56}Ba^{135}$ and $_{79}Au^{197}$ are assigned $2d_{3/2}$ orbits.

No regularity is apparent in the $(nd)^5$ series. $_{15}P^{31}$ with $I=1/2$ and $\mu=1.13$ requires the interpretation $S_{1/2}+P_{1/2}$ (with approximately equal weights). Mayer assigns a $2s$ orbit to the odd proton, bracketing the $2s$ level between $1d_{5/2}$ and $1d_{3/2}$. This procedure requires both a splitting of the $1d$ level in the sense of the Breit-Inglis rule and an upward displacement of $2s$ relative to $1d$, thus combining features of the j–j coupling and central elevation level schemes. The occurrence of a large $P_{1/2}$ component is not explained. The partial configuration interpretation applied to the central elevation or Nordheim level schemes (identical in this region) provides two closely spaced configurations, $(2s)^2(1d)^5$ and $(2s)^1(1d)^6$ from which two ^2S and one ^2P states are derived.

The group of nuclei with $I=7/2$ in Fig. 3 all require the interpretation $G_{7/2}\gg F_{7/2}$ if the extreme single-particle model is favored.* However, only one nucleus in this group, $_{51}Sb^{123}$, contains a closed $(\pm)$ shell. For the others, the uniform model seems preferable, requiring the reversed inequality $F_{7/2}\gg G_{7/2}$.

The difficulties created by the uncritical application of the extreme single particle model are well illustrated by $_{27}Co^{59}$. All level schemes place the odd proton in a $1f$ orbit in contradiction with the $G_{7/2}$ interpretation derived from the Schmidt limits. On the other hand, the partial configuration $(1f)^7$ yields a wide range of possibilities with a predominant $F_{7/2}$ *a priori* most likely.

Nuclei containing half-filled $2p$ shells (according to the FH level scheme) provide material for Table IV. With theoretical possibilities limited to ^2P and ^2D (odd parity), the strong representation of $F_{5/2}$ components in three out of five examples is a serious difficulty for the level scheme, although less so now than earlier when the theoretical interpretation was based on the Schmidt limits. It is satisfactory that $_{37}Rb^{87}$ with a closed neutron shell ($N=50$) conforms to the theoretical possibilities of the $(2p)^3$ configuration. Mayer's scheme provides an $F_{5/2}$ component at N or $Z=37$, but no $D_{5/2}$, while at $Z=63$, the reverse is true. The two level schemes disagree regarding the parity of the europium isotopes, central elevation requiring odd and j–j coupling even parity.

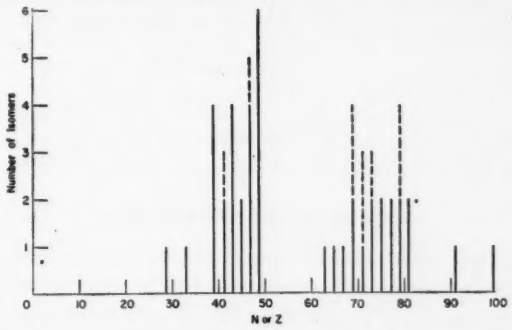

FIG. 5. Distribution of isomerism in odd nuclei. N or Z denotes the odd member of the N, Z pair.

The copper and gadolinium isotopes $_{29}Cu^{63,65}$ and $_{31}Ga^{69,71}$ form an interesting group with $P_{3/2}\gg D_{3/2}$ according to the MW limits. Mayer interpolates the $2p_{3/2}$ level between $1f_{7/2}$ and $1f_{5/2}$ to account for the properties of this group in terms of the extreme single-particle model. However, it is then necessary to assign the odd proton at $Z=35$ to an $f_{5/2}$ orbit in disagreement with the spins and moments of the bromine isotopes. A somewhat weaker interpretation is supplied by the partial configurations $(2s)^2(1f)^9$ for copper and $(2s)^2(1f)^{11}$ for gadolinium. The first with four linearly independent ^2P states is indeed quite plausible. Excited configurations of the types $(2s)^2(1f)^{2n}2p$ and $(1f)^{2n+1}$ may assist in stabilizing the $2P$ state. The bromine isotopes then mark the beginning of the $2p$ shell. The evidence is features of the j–j coupling and central elevation schemes: splitting of the $1f$ level and a rise of the $2p$ level with increasing Z (starting with $2p$ between $1f_{7/2}$ and $1f_{5/2}$ at $Z=29$).

A puzzling feature of the magnetic moment distribution is the large number of odd neutron nuclei with $I=1/2$ and magnetic moments requiring the interpretation $S_{1/2}>P_{1/2}$. The group contains $N=63$, 65, 67, 69, and 75,[20] while Z ranges from 48 to 54. It is evident from Table I that S states generated by configurations of equivalent orbits are extremely rare. Possibly configurations containing a singly occupied s orbit are required; however, it is not clear why the state of minimum angular momentum and even parity should be favored in so many cases.

The fact that the series begins at $Z=48$ suggests an interpretation consistent with the postulates of the central elevation scheme. In this scheme the $2s$ proton level crosses $1g$ and $2d$ just before $Z=48$. The simultaneous complete absence of neutrons from the $2s$

* The inequalities here and in Tables II–IV express relations between the statistical weights of the two Russel-Saunders components required for a complete description.

[20] $_{52}Te^{123}(N=71)$ and $_{52}Te^{125}(N=73)$ with $I=1/2$ are likely candidates for places on this list (G. R. Fowles, Phys. Rev. **76**, 571 (1949) and J. E. Mack and O. H. Arroe, Phys. Rev. **76**, 1002 (1949)).

neutron orbit may carry the system beyond the energy minimum resulting from the readjustment of particle density under the action of the Coulomb repulsion between protons. The experimental results permit the interpretation that the optimum distribution of nucleons when the $2s$ proton orbit is empty occurs with one neutron occupying a $2s$ orbit. One pictures the singly occupied $2s$ orbit constrained to lie just below the nearest level. When doubly occupied or completely empty it rises above the latter.

QUADRUPOLE MOMENTS

Nuclei with $I>1/2$ are expected to possess an electric quadrupole moment Q.[21] In the extreme single-particle model Q vanishes for odd N and takes negative values for odd Z (charge distribution flattened along axis of spin). Empirically quadrupole moments are more often positive (charge distribution elongated along axis of spin) than negative. The partial configuration method offers possibilities for obtaining positive values of Q through the operation of the hole mechanism since a hole in a proton shell behaves like a negatively charged particle.

One may hope to obtain a significant correlation between theory and experiment, at least as regards sign, for the closed ($\pm$) shell nuclei adjoining the magic numbers. Small negative Q's for $_{51}Sb^{121}$, $_{51}Sb^{123}$, and $_{83}Bi^{209}$ and a positive Q for $_{49}In^{115}$ are consistent with theory.[15a,22]

The bromine isotopes with positive values of Q are not in accord with theoretical expectations for a singly occupied $2p$ orbit. However, there is scarcely ground for a theoretical prediction where the shell structure does not make itself apparent in increased stability of the closed shell. Large positive values of Q, requiring a considerable elongation of the charge distribution along the axis of spin, occur in the region where the j–j coupling and central elevation level schemes place the filling of the $1h$ orbits. Several authors[23–25] have pointed out indications of a general correlation between quadrupole moments and shell structure. On this, judgment must be deferred until more experimental evidence is available. Caution is required in attempting to relate the large quadrupole moments to special schemes of shell structure. Generally a good wave function for the ground state can only be obtained as a sum of linearly independent elementary functions. The quadrupole moment is then a double sum involving both diagonal and non-diagonal matrix elements with respect to the linearly independent basis. Large values of the moment require suitable phase relations between the elementary functions making up the wave function and a sufficient number of large non-diagonal matrix elements.

ISOMERISM AND BETA-DECAY

Nuclear isomerism denotes long-lived (half-lives ranging from 10^{-7} second to 1 year) excited states decaying by the emission of electromagnetic radiation, the production of internal conversion electrons, pair production, or radioactive transitions.[26] Figure 5 shows the distribution of odd nuclei possessing isomeric states as a function of the odd member of the N, Z number pair. The existence of well-defined "islands" of isomerism points to a close connection with shell structure. Indeed, a plausible condition for isomerism is the occurrence of closely spaced single-particle levels, differing by several units in l, at the top of the filled level distribution. Possibilities for satisfying this condition occur in all three level schemes although the schemes differ in regard to the possible parity changes. In particular the j–j coupling scheme allows only isomeric transitions with change in parity when the spin change exceeds two units. The crossing of levels in the central elevation scheme provides a number of pairs of closely spaced configurations with the same and with opposite parity. Isomeric transitions with and without change in parity occur in each large island of isomerism indicating need for all the theoretical possibilities of the central elevation scheme.

The careful theoretical analysis by Axel and Dancoff[26] confirms the earlier deductions from a Wiedenbeck-type chart.[13] There is no change in parity at N or $Z=43$ (two examples), 45 (two examples), 47 (five examples), 63, 73, 79. A parity change occurs at N or $Z=39$ (three examples), 41 (two examples), 43, 49 (three examples), 69 (two examples), 71, 73, 75, 77 (two examples), 79, and 81 (two examples).

In relation to the theory of beta-decay, shell models assist in determining the order of allowed and forbidden transitions between ground states by fixing the parities and in some cases the spins of parent and daughter nuclei. The information derived from the models is particularly useful in an extended radioactive series involving two or more beta-transitions in cascade.

The recent discovery of the unique first forbidden distribution in the beta-decay $_{17}Cl^{38}$, $_{19}K^{42}$, $_{38}Sr^{89}$, $_{38}Sr^{90}$, $_{39}Y^{90}$, $_{39}Y^{91}$, and $_{55}Cs^{137}$ has verified a number of deductions based on shell structure, selection rules and observed half-lives and maximum energies.[13,27–34] These deductions from the central elevation level scheme are summarized in Table V; the results are also all compatible with the j–j coupling level scheme.

The high binding energies of two silicon isotopes,[35] inferred from radioactive decay energies, suggests the formation of a particularly stable structure at $Z=14$. The j–j coupling level scheme permits a closed subshell containing six like particles in $1d_{5/2}$ orbits; the reversal of the $2s$, $1d_{5/2}$ level order encountered earlier in the discussion of the $_{15}P^{31}$ spin places the closed structure at $Z=14$.

[21] See reference 10, p. 420.
[22] K. Murakawa and S. Suwa, Phys. Rev. **76**, 433 (1949).
[23] W. Gordy, Phys. Rev. **76**, 139 (1949).
[24] R. D. Hill, Phys. Rev. **76**, 1415 (1949).
[25] Townes, Foley, and Low, Phys. Rev. **76**, 1415 (1949).
[26] E. Segrè and A. C. Helmholtz, Rev. Mod. Phys. **21**, 271 (1949); P. Axel and S. M. Dancoff, Phys. Rev. **76**, 892 (1949).
[27] L. M. Langer and H. C. Price, Jr., Phys. Rev. **75**, 1109 (1949).
[28] A. C. G. Mitchell and C. L. Peacock, Phys. Rev. **75**, 1272 (1949).
[29] J. S. Osoba, Phys. Rev. **76**, 345 (1949).
[30] Braden, Slack, and Shull, Phys. Rev. **75**, 1964 (1949).
[31] Slack, Braden, and Shull, Phys. Rev. **75**, 1965 (1949).
[32] E. N. Jensen and L. J. Laslett, Phys. Rev. **75**, 1949 (1940).
[33] F. B. Shull and E. Feenberg, Phys. Rev. **75**, 1768 (1949). K. Siegbahn, Arkiv. f. Mat., Astr. o. Fys. **34B** No. 4 (1946).
[34] L. M. Langer, Phys. Rev. **77**, 50 (1950).
[35] Seidlitz, Bleuler, and Tendam, Phys. Rev. **76**, 861 (1949).

The East-West Asymmetry of Positive and of Negative Mesons and the Excess of the Positives as a Function of Zenith Angle and Altitude*

GERHART GROETZINGER AND GORDON W. MCCLURE**
Institute for Nuclear Studies, University of Chicago, Chicago, Illinois
(Received December 7, 1949)

The east-west asymmetry of positive and of negative mesons of energies around 800 Mev has been determined at altitudes of 260 and 4300 meters at a geomagnetic latitude of 50° north for zenith angles of 24 and 58 degrees. It is found that more positive mesons arrive from the west than from the east and more negative mesons arrive from the east than from the west, the asymmetries being equal but of opposite sign. From the magnitude of the asymmetries it can be concluded that the majority of the mesons observed under the above-mentioned conditions are produced in the top layer of the atmosphere. An increase of the positive excess for mesons of around 800 Mev is observed with an increase of the altitude from 260 to 4300 meters.

INTRODUCTION

THE east-west asymmetry of the hard component of the cosmic radiation which occurs at magnetic latitudes below 40 to 50 degrees (knee of the latitude effect) is interpreted as being mostly due to the deflection of the (at least preponderantly positive) primaries in the magnetic field of the earth. The secondaries (π-mesons) and the tertiaries (μ-mesons), which are eventually observed, preserve to a certain degree the direction of the primary producing them. This is due to the fact that the creation and the decay of the π-mesons take place at considerable energies so that little change of direction takes place in these events.

A much smaller asymmetry which is observed at higher latitudes, with which we will be concerned in this paper, is explained by Thomas H. Johnson[1] as being due to the magnetic deflection of the mesons after being produced by the symmetrically distributed primary radiation. This asymmetry is due to the energy loss of the mesons and would not exist were it not for an excess of the positives.

The following experimental results concerning the east-west asymmetry above the knee of the latitude effect and at higher altitudes were obtained on top of Mount Evans (49° geomagnetic latitude and 4300 meter height). J. C. Stearns and D. C. Froman[2] and T. H. Johnson[3] found, without any filter, asymmetries for zenith angles between 20° and 45° of somewhat below 0.02, and 0.005 for a zenith angle of 57°. On an airplane flight between 50° to 54° geomagnetic latitude at 9500 meter altitude, M. Schein, V. H. Yngve and H. L. Kraybill[4] found with a 22 cm lead filter an asymmetry of 0.13 for a zenith angle of 45°.

T. H. Johnson[1] calculated the high latitude asymmetries for sea level and an altitude of 4300 meters for a number of zenith angles under the assumption that the mesons are produced at the top of the atmosphere. First, the part of the deflection of either a positive or a negative meson in the magnetic field of the earth which leads to an asymmetry is calculated for various energies and zenith angles for both altitudes of the recorded mesons.[5] From these deflections the east-west asymmetry of the natural mixture of mesons of both signs is calculated for the case that mesons above a certain energy are recorded, that their energy-distribution at the two altitudes is of the form $N(E)dE = AE^{-3}dE$, and that the positive excess is 0.20 as determined by means of cloud chambers.[6] According to this theory the asymmetry on Mt. Evans should increase from 0.01 to 0.07 for an increase of the zenith angle from 20° to 57° if the E^{-3} distribution is cut off at 2.2×10^{8} electron volts.

All previous experiments concerned with asymmetries were performed with instruments recording mesons without regard to their sign. A much greater amount of information can be obtained from the asymmetries if they are determined for particles of one sign only with a small spread in energy. The results of such experiments can be compared with consequences of Johnson's theory which are not based on a knowledge of the positive excess and depend to a lesser degree on a knowledge of the meson energy distribution. Actually the only necessary information is the dependence of the intensity of the hard component on the zenith angle, which follows from the energy spectrum at the altitude at which the asymmetry is observed. The expected asymmetries should furthermore exceed approximately by a factor of five, the asymmetries of the natural mixture of positive and negative mesons, which is, as

* This research was assisted in part by the Joint Program of the ONR and AEC.
** Now at Bartol Research Foundation, Swarthmore, Pennsylvania.

[1] Thomas H. Johnson, Phys. Rev. **59**, 11 (1941); see also I. S. Bowen, Phys. Rev. **45**, 349 (1943), and B. Rossi, Rendi Lincei **15**, 62 (1932).
[2] J. C. Stearns and D. C. Froman, Phys. Rev. **46**, 535 (1934).
[3] T. H. Johnson, Phys. Rev. **48**, 287 (1935).
[4] Schein, Yngve, and Kraybill, Phys. Rev. **73**, 928 (1948).
[5] If the isotropically produced mesons would not lose energy in the atmosphere, their angular distribution would remain unchanged in spite of the deflection by the magnetic field, so that no asymmetry would result. The observed asymmetry is caused by the additional deflection due to energy loss. Johnson's argumentation is little affected by the discovery of the heavy mesons being intermediaries between primaries and μ-mesons.
[6] L. J. Hughes, Phys. Rev. **57**, 592 (1940); P. M. S. Blackett, Proc. Roy. Soc. **A159**, 1 (1937); L. Leprince-Ringuet and J. Crussard, J. de phys. et rad. **8**, 207 (1937).

explained before, due to the small difference in the number of positive and negative mesons.

We have performed an experiment using a magnetic lens type spectrometer focusing either positive or negative mesons with energies of approximately 800 Mev, but excluding protons, coming from the west and east respectively for two values of the zenith angle (24 and 58 degrees). The experiment was performed on Mt. Evans (altitude 4300 meters and geomagnetic latitude 49°) and in Chicago (altitude 260 meters and geomagnetic latitude 51°). Both locations are considered to be above the knee of the latitude effect.[7] If W_+, W_-, E_+, and E_- are the counting rates (corrected for background) where W_+, e.g., represents the rate for positive mesons arriving from the west, then the asymmetry for positive or for negative mesons is defined as

$$\alpha_\pm=\frac{2(W_\pm-E_\pm)}{W_\pm+E_\pm}.$$

These counting rates allow one to obtain, furthermore, an expression for the positive excess for the two altitudes and for different zenith angles. In order to eliminate the influence of the asymmetries, the following expression was used as a measure of the excess:

$$\beta=\frac{2(W_++E_+-W_--E_-)}{W_++E_++W_-+E_-}.$$

G. Bernardini *et al.*[8] found an average positive excess both at sea level and at an altitude of 3500 meters of 0.20 for energies between 500 Mev and 4 Bev using a counter telescope containing magnetized iron deflecting plates. With a similar instrument, I. F. Quercia, B. Rispoli, and S. Sciuti[9] found that a quantity called the "experimental effect," which is somewhat smaller than the excess and which depends to a certain extent also on the energy spectrum, increases from 0.07 at an altitude of 88 meters to 0.14 at an altitude of 5100 meters, and decreases to 0.12 at 7300 meters for meson energies higher than 460 Mev. All these experiments refer to mesons having approximately vertical directions. C. Ballario, M. Benini and G. Calamai[10] report a decrease of the above-mentioned "experimental effect" at sea level from 0.101 for vertical incidence to 0.035 by inclining the instrument 60° from the vertical in an unspecified direction. The decrease of the excess with altitude and increasing zenith angle is interpreted by both groups as possibly indicating an increase in the multiplicity of the production of mesons with the energy of the primaries.

P. Bassi *et al.*[11] observed an increase of the positive excess from 0.16 to 0.25 at sea level by increasing the thickness of a lead filter in their telescope, in which the magnetic deflection takes place in air, from 290 to 1150 g/cm². The high asymmetry for the large absorber thickness is in agreement with a result of R. B. Brode[12] who reports a positive excess of 0.30 for mesons with energies between 1.4 and 2 Bev at sea level.

The results of Bassi and co-workers seem to contradict the results of the two groups mentioned before wherein essentially the positive excess decreases with increasing air absorber.

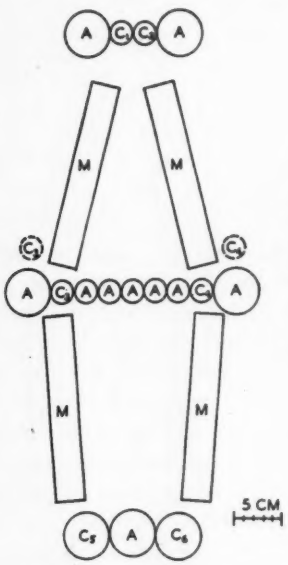

FIG. 1. Schematic diagram of the apparatus. (The two magnetic lens type telescopes consist of counters C_1, C_2 in parallel, with counters C_3 and C_5 in coincidence, and of counters C_1, C_2 in parallel, with counters C_4 and C_6 in coincidence.) During the experiment the apparatus is tilted either to the east or to the west.

A = Anticoincidence;
C = Coincidence;
M = Magnetic deflector.

APPARATUS

A schematic diagram of the apparatus is shown in Fig. 1. The two top counters C_1 and C_2, in parallel, form in coincidence with the counters C_3 and C_5, one telescope, and in coincidence with counters C_4 and C_6 a second telescope. The selection of the particles with respect to charge and energy is provided by their deflection in the magnetized iron plates M_1, M_2, M_3 and M_4 (height 20 cm, thickness 3 cm, and length 60 cm). The plates M_1 and M_2 and the plates M_3 and M_4 represent parts of two closed magnetic circuits. The field strength in the plates was approximately 18,500 gauss. Counters marked A are anticoincidence counters. All of the counters have an effective length of 50 cm and their diameter is either one or two inches as can be seen in the figure.

Each of the counter telescopes constitutes a kind of magnetic spectrograph which selects mesons having certain energies and charges of a particular sign (depending on the direction of the magnetic field). The resolving power depends on the geometry of the apparatus and is influenced by the multiple scattering of

[7] Preliminary results are published. G. Groetzinger and G. W. McClure, Phys. Rev. **75**, 349 (1949), and G. W. McClure and G. Groetzinger, Phys. Rev. **75**, 340 (1949).

[8] Bernardini, Conversi, Pancini, Serocco, and Wick, Phys. Rev. **68**, 109 (1945).

[9] Quercia, Rispoli, and Sciuti, Phys. Rev. **74**, 1728 (1948).

[10] Ballario, Benini, and Calamai, Phys. Rev. **74**, 1729 (1948).

[11] Bassi, Clementel, Filosofo, and Puppi, Phys. Rev. **76**, 854 (1949).

[12] R. B. Brode, Phys. Rev. **76**, 468 (1949).

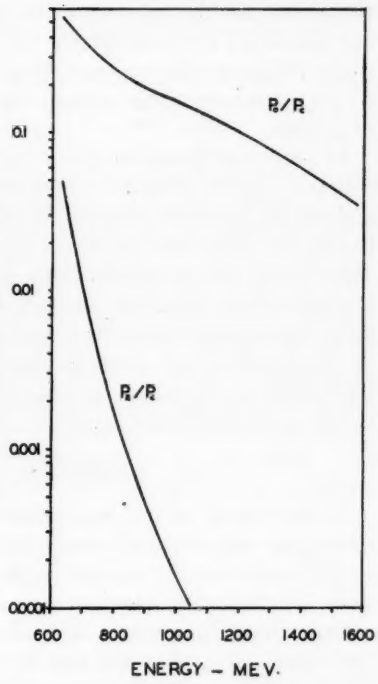

FIG. 2. Ratios of the probabilities of μ-mesons of the most favorable direction of incidence passing the telescope without being scattered out. P_e is the probability for the case of the magnetic field in a direction supporting the traversal, P_r for the case of the field rejecting the traversal, and P_0 for the case of no field.

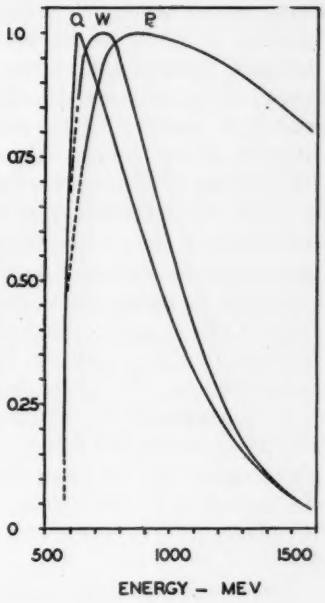

FIG. 3. Relative sensitivity, W, of the telescopes for particles of various energies. P_e is the relative probability for a μ-meson entering in the most favorable direction to traverse the telescope without being scattered out; Q is the relative probability for the traversal of unscattered μ-mesons of various energies. $W \approx P_e \times Q$.

the mesons in the deflecting plates. Due to the complicated geometry, a correct determination of the energy response is quite involved. For our purposes, however, the following rough estimate is sufficient.

We confine our attention to the projection of the trajectory of the particle onto a vertical plane perpendicular to the direction of the magnetic field in the deflecting plates. The condition that a particle traverse the telescope puts a lower limit on the magnitude of its momentum component in the direction of the magnetic field. Furthermore, the angular distribution of the incoming particles favors vertical incidence. Assuming an angular distribution of the recorded mesons proportional to $\cos^n\theta$, where θ is the zenith angle and n is a number between 2 and 3, it can be shown that, neglecting the scattering, the average energy, $\bar{E}$, of the particles passing through the telescope is only about 5 percent higher than the energy, E, corresponding to the momentum in the plane of projection considered here. The standard deviation about this mean is 8 percent which is small compared to the range of energies recorded by the telescope.

The curvature of a projected trajectory of a particle at a point in the deflecting plates can be considered as the sum of a "magnetic" and a "multiple scattering" curvature. Because of the appreciable energy loss in the iron parts of the telescope, the magnetic radius of curvature decreases along the trajectory. Using the well-known formula for energy loss by inelastic collisions, a "mean magnetic curvature," obtained as an average along the trajectory, was calculated for μ-mesons of various incident energies, assuming an effective magnetic field of 18,500 gauss. The multiple scattering of the mesons in the telescope was calculated according to the theory of Molière,[13] taking into account energy loss. The mean total curvature of the trajectory can be shown to be distributed approximately normally about the mean magnetic curvature with a standard deviation equal to the root mean square value of the multiple scattering curvature. By means of this distribution one can find the probability that the curvature of a meson incident with a certain energy will lie in that range—determined by the geometry of the telescope—which will allow passage. P_e is this probability for the magnetic field in the correct direction, P_r the probability for the field in reversed direction for the passage of the particle, and P_0 the probability in the absence of the field. The calculated ratios P_r/P_e and P_0/P_e are shown in Fig. 2 plotted against incident energy. It is seen that the probability that a particle of the wrong sign will pass the telescope is negligible. The relative number to pass in the absence of a magnetic field is considerable. It was found experimentally that the ratio of the counting rates (corrected for background, as will be described later) without a field and with the field collimating positive particles was about 20 percent, and the corresponding ratio for the case of the field collimating negative particles was about 15 percent. In order to compare these results with the curve for P_0/P_e it must be kept in mind that without a field the telescope is recording particles of both signs while P_0/P_e refers to the case where particles of only one sign are present.

The sensitivity of the telescope for mesons of a certain energy is approximately proportional to the probability P_e (correct field), which is a measure of the number of particles which traverse the telescope without

[13] G. Molière, Zeits. f. Naturforschung **3a**, 78 (1948).

being scattered out. P_e is shown in Fig. 3 (being normalized to unity at its maximum). The sensitivity depends, furthermore, upon the permissible angular spread of the projected direction of incidence which will lead to a traversal of the telescope. This spread is a function of the energy. The relative probabilities, Q, for particles of different energies, $\bar{E}$, which are assumed to suffer no deflections due to scattering, to traverse the telescope were determined by geometric construction assuming isotropic incidence and a path whose curvature increases due to energy-loss under the influence of the magnetic field. The probability, Q, as a function of the energy, $\bar{E}$, is shown in Fig. 3 (being normalized to unity at its maximum).

It is reasonable to assume that the (relative) sensitivity of the instrument for particles of various energies is given by the expression $W=P_e\times Q$ in spite of the fact that P_e and Q are not entirely independent. W, normalized to unity at its maximum, is shown in Fig. 3.

Due to the fact that the theory of multiple scattering is not applicable at very low energies, the curves P_e and W are dotted below $\bar{E}=600$ Mev. That the telescope is able to reject particles of improper charge even at the lowest energies which still allow a traversal of the iron deflecting plates is evident from the results of experiments in which a part of the mesons emerging from the telescopes were stopped in a lead plate. Twenty (delayed) neutron pulses were observed with the telescopes set for negative mesons, due to their capture in the lead while during an approximately equal time only one pulse was observed with the telescopes set for positive mesons.[14]

As can be seen from Fig. 3, the instrument records μ-mesons with an average energy of $\bar{E}_{av}=800$ Mev. For this energy the average angle of incidence is inclined 17° with respect to the axis of the instrument, so that with both telescopes intensities of mesons coming from two directions 34° apart can be measured simultaneously. It follows from an analysis of the work done using photographic emulsions that the number of π-mesons which are produced in the atmosphere above the telescope or in the deflecting plates of the telescope by a charged primary entering through the top counters is small compared to the number of μ-mesons present at this altitude. In an experiment to be described in another paper we have determined an upper limit of 10 percent for the ratio of π- to μ-mesons recorded in our telescopes by investigating the ratio of positive and negative decay electrons emerging from a carbon plate which stops part of the mesons emerging from the two telescopes.

In order to determine the number of counts in the course of the experiment which are due to showers or chance coincidences the two counters C_3 and C_4 were brought to a position indicated by the dotted circles in Fig. 1 and the counting rates recorded. They were approximately the same whether the deflecting plates were magnetized or not. The counting rates were found to be 1.6 ± 0.1 per hour on top of Mt. Evans and 0.28 ± 0.03 per hour in Chicago for each telescope. (All the errors are probable errors.)

RESULTS

In the course of the experiment the polarity of the telescopes was changed every 24 hours and the telescopes were turned around approximately every six days, so that they were facing east or west approximately the same amount of time. The counting rates (per hour) (W_+, W_-, E_+, and E_-) for zenith angles of 24° and 58°, corrected for background, are shown in Table I. Since one of the telescopes was used for the smaller and the other one for the larger angle throughout the experiment, the counting rates have to be corrected for a difference of the sensitivities of the telescopes in order to obtain the true angular dependence of the cosmic ray intensities in the energy interval recorded by the instrument.

From these data follow the positive excesses β and the asymmetries α_+ and α_- in Table II. The last two columns of this table refer to Johnson's theory and will be discussed later.

DISCUSSION

(a) Positive Excess

The dependence of the excess on altitude which we find is smaller than that found by Quercia and co-workers.[9] Our experiments do not confirm a decrease of the positive excess with zenith angle of the magnitude reported by Ballaria and co-workers.[10] A possible explanation for this discrepancy might be that Ballaria's arrangement did not record mesons in a vertical north-south plane. In this case their results would be due

TABLE I. The counting rates (per hour) for zenith angles of 24° and 58°, corrected for background.

Location	Zenith angle	W_+	W_-	E_+	E_-
Mt. Evans	24°	11.7±0.2	9.1±0.15	10.9±0.2	9.6±0.15
Mt. Evans	58°	6.4±0.25	3.7±0.2	4.4±0.15	5.4±0.2
Chicago	24°	4.60±0.075	3.78±0.07	4.29±0.075	3.93±0.07
Chicago	58°	1.50±0.05	1.13±0.045	1.32±0.05	1.37±0.045

[14] G. Groetzinger and G. W. McClure, Phys. Rev. **74**, 341 (1948), and G. W. McClure and G. Groetzinger, Phys. Rev. **75**, 340 (1949).

TABLE II. Positive excesses β and the asymmetries α_+ and α_-.

Location	Zenith angle	β	α_+	α_-	$\alpha_{\pm th}$	n
Mt. Evans	24°	0.180±0.015*	0.07±0.025	−0.055±0.02	±0.057	3
Mt. Evans	58°	0.17 ±0.035	0.37±0.055	−0.375±0.06	±0.329	3
Chicago	24°	0.135±0.011*	0.070±0.024	−0.039±0.024	±0.037	2
Chicago	58°	0.120±0.036	0.128±0.052	−0.192±0.057	±0.197	2

* This result is partly based on data obtained for a zenith angle of 17°.

to the combined effect of an angular dependence of the excess and the difference in the asymmetry of positive and negative mesons, as described in this paper.

According to a recent theory of Heisenberg[15] the positive excess is approximately proportional to the square root of the energy of the mesons at their point of creation. Under the assumption that π-mesons are created at an altitude of 35 km (this value is not critical for the considerations) and that the μ-mesons into which they decay enter our telescope with an energy of 800 Mev, we have calculated the initial energies of the π-mesons for the cases of an angle of incidence of 24° on top of Mt. Evans and in Chicago. (These are the only two cases for which the excess is determined with a sufficient accuracy.) The ratio of the excesses according to Heisenberg is 0.826 while our experiments give a ratio of 0.75±0.09.

(b) East-West Asymmetries

It can be seen from the results that more positive mesons arrive from the west than from the east, while more negative mesons arrive from the east than from the west, the asymmetries being approximately equal in magnitude but opposite in sign.

In order to compare the experimental results with the consequences of Johnson's theory[1] one has to keep in mind that his calculations refer to the case of particles in a vertical plane in the east-west direction only, while our telescope allows a small north-south component. As stated before, the average energy, $\bar{E}_{av}$, of the mesons recorded by our instrument is approximately 800 Mev. In order to make our data suitable for a comparison with the theory, the energy, E_{av}, of approximately 750 Mev, corresponding to the projection of the particles in a vertical east-west plane, will be substituted in the formulas. If the zenith-angle distribution is given by

$$j = j_0 \cos^n\theta,$$

where θ is the zenith-angle, then the east-west asymmetry $\alpha_{\pm th}$ for purely positive or purely negative radiation is, according to Johnson,

$$\alpha_{\pm th} = \pm 2\bar{\delta}(\theta) n \tan\theta,$$

where $\bar{\delta}(\theta)$ is the average increase of the deflection resulting from atmospheric energy loss. Johnson obtains $\bar{\delta}(\theta)$ by averaging over the meson energy spectrum above a certain cut-off given by the apparatus. Because of the energy selectivity of our telescope we have chosen $\delta(\theta)$ corresponding to the mean energy, $E_{av}=750$ Mev, recorded by our telescope. The value of the asymmetry is sensitive with respect to the choice of exponent n, which is taken by Johnson as being equal to two, for sea level and for the top of Mt. Evans. This value, to a good approximation, represents the zenith angle distribution of mesons of an inverse cube power law spectrum. Since our telescope selects mesons lying in a small energy range, one has to expect an exponent n somewhat smaller than three for such a spectrum. The values of n which gave good agreement with our experimental results were $n=3$ for Mt. Evans and $n=2$ for Chicago. The theoretical values for the asymmetries, and the exponents n on which they are based, are shown in the last two columns of Table II. A comparison of the sum of the counting rates W_+, W_-, E_+, and E_- at 24° and 58°, taking into account a slight difference in the sensitivity of the two telescopes leads to an exponent $n=2.2$ in the $\cos^n\theta$ distribution for the mesons recorded at Chicago, which is in good agreement with the exponent $n=2$ found from the asymmetries. No comparison of the sensitivities of the telescopes was made at Mt. Evans. The sensitivities are probably different from the ones at Chicago since the instrument was partly dismantled for transportation.

Since the exponent n on top of Mt. Evans can hardly exceed $n=3$, and the exponent $n=2$ is quite reasonable for Chicago, it follows from the observed asymmetries that the majority of mesons which are observed at altitudes up to 4 km at a geomagnetic latitude of 50° must be decay products of π-mesons (of both signs) produced in the top layer of the atmosphere by an isotropic primary radiation.

We are greatly indebted to Mr. Jack Aron for his help in constructing the equipment and performing the experiment, and to Dr. Byron E. Cohen and Dr. Mario Iona, Jr. of the Inter-University High Altitude Laboratory for their friendly support during our stay on Mt. Evans.

Note added in proof.—At the New York meeting of the American Physical Society (January 4, 1950) R. B. Brode presented (post-deadline paper) the results of an investigation of the east-west asymmetry in many respects similar to ours. With a magnetic lens type spectrometer collecting either positive or negative mesons of 2 Bev, he finds the asymmetries for the positive and for the negative mesons independent of the altitude up to approximately 4000 meters. The magnitude of the observed asymmetries are such that he is led to the conclusion that the recorded mesons are, in part, produced by negative primaries.

[15] Werner Heisenberg, Zeits. f. Physik 126, 569 (1949).

The Ionization in Argon and in Air by Single Alpha-Particles as a Function of Their Energy†

WILLIAM P. JESSE, HAROLD FORSTAT, AND JOHN SADAUSKIS
Argonne National Laboratory, Chicago, Illinois

(Received October 3, 1949)

An extended series of measurements has been made to determine the possible variation of W, the energy to make an ion pair in pure argon, with the energy of the ionizing alpha-particle. The ionization in argon relative to the ionization produced by a comparison polonium alpha has been measured for the alpha-emitters ThX, ThC, ThA, RaC′, ThC′. For alpha-particles in this energy region from 5 to 9 Mev, no deviation of W from the average W for the polonium alpha could be found amounting to as much as ½ percent. This is in marked contrast to the alpha-ionization in air from the work of Stetter. More indirect measurements in the region 1–5 Mev indicate no measurable change in W for alpha-particles in argon, while values derived from the Stetter curve for air show a marked increase of W as zero alpha-energy is approached. Evidence from direct measurements is given to show that the energy to make an ion pair in argon for the Li^{7*} ion emitted from the reaction $B^{10}(n,\alpha)Li^{7*}$ is apparently the same as the average for the polonium alpha-particle.

INTRODUCTION

FOR many years the ionization by alpha-particles in various gases has been studied both experimentally and theoretically, especially in regard to the relation between the total ionization produced by a single alpha-particle and its energy. The literature is too voluminous to allow here even a bibliography of individual papers pertaining to this subject. A good summary of the experimental results up to 1944 has been given by L. H. Gray,[1] and some of the theoretical aspects have been discussed in an older paper by Livingston and Bethe[2] and in a more recent paper by Bohr.[3] Certain phases of the subject have also been treated by Fano.[4] The general theory would indicate a somewhat greater energy to produce an ion pair by the alpha-particle as it approaches zero energy, but no satisfactory quantitative relations have as yet been derived. The theory seems even more inadequate to deal with the energy to make an ion pair in the similar case of recoil ions such as the Li^7 ion in the (n,α) reaction for B^{10}. On the experimental side the situation is somewhat more favorable, but even a casual reading of the reference cited brings out many fundamental contradictions between the work of various experimenters. Thus it seems probable that W, the average energy in electron volts to make an ion pair, is not constant in air for alpha-particles between 0 and 5 Mev, since relative ionization experiments show a marked difference in the behavior of air[1] as contrasted with a group comprising hydrogen and the noble gases. However, no very reliable work is available showing whether W is really constant with varying energy in the latter group of gases nor how W varies with the nature of the ionizing particle. Most measurements of this sort have been confined to air, and even in the older work with the noble gases, one is never sure that the extreme precautions now known to be necessary to insure the purity of the gas have been taken. Thus it seemed desirable to carry out a series of experiments to determine the variation of W with energy in the noble gases and the variation of W from particle to particle.

APPARATUS AND METHOD

The best region in which to work with alpha-particles would seem to be the range from 5 to 9 Mev, where there are a large number of natural alpha-emitters for which the alpha-energies have been determined with great precision by Briggs[5] and others. Our first measurements were therefore made in argon with these elements.

A brief description has already been given of the apparatus[6] and general method used together with a table of data showing the consistency obtainable. In general, an ion chamber, of which various types have been used, is connected to a vibrating reed electrometer,[7] which in turn feeds into a Brown recorder. An alpha-particle, usually from an active deposit on one of the electrodes, produces a number of ions in the very pure argon of the chamber. The sudden rise of potential of the floating insulated electrode from the collection of such a charge is amplified in the reed and causes a sharp jump of the pen of the recorder. The length of this jump is proportional to the change of potential and hence to the charge collected. These jumps are very reproducible and are quite large. At full instrumental sensitivity the length of such a jump for a polonium alpha in argon is well over 10 cm.

Perhaps the point which should be most emphasized is that this instrument is, in its operation, akin to an electrostatic electrometer, measuring the accumulated

† A summary of the preliminary work in this paper was given at the June, 1948, meeting of the American Physical Society. W. P. Jesse and H. Forstat, Phys. Rev. **74**, 1259(A) (1948).

[1] L. H. Gray, Proc. Camb. Phil. Soc. **40**, 95 (1944).

[2] M. S. Livingston and H. A. Bethe, Rev. Mod. Phys. **9**, 245 (1937).

[3] N. Bohr, Kgl. Danske Vid. Sels. Math.-Fys. Medd. **18**, 8 (1948).

[4] U. Fano, Phys. Rev. **70**, 44 (1946).

[5] G. H. Briggs, Proc. Roy. Soc. **157**, 183 (1936).

[6] W. P. Jesse and H. Forstat, Phys. Rev. **73**, 926 (1948).

[7] Palevsky, Swank, and Grenchik, Rev. Sci. Inst. **18**, 298 (1947).

charge by the potential rise induced rather than the height of a transient pulse. Since the time of response of the circuit is of the order of one second, both positive and negative ions are collected. The usual counting rate is of the order of 3 to 10 counts/min.

Most of the comparisons between the ionization produced by alpha-particles were carried out in a cylindrical chamber of 10-cm internal diameter and height 7 cm. The collecting electrode, a circular plate of 8 cm diameter, was $4\frac{1}{2}$ cm from the base plate of the chamber. Thus the field was that between two parallel plates, with a certain distortion at the edges due to the presence of the side walls. No apparent difficulty was experienced because of such inhomogeniety. In fact, the exact geometry of the chamber seemed relatively unimportant.

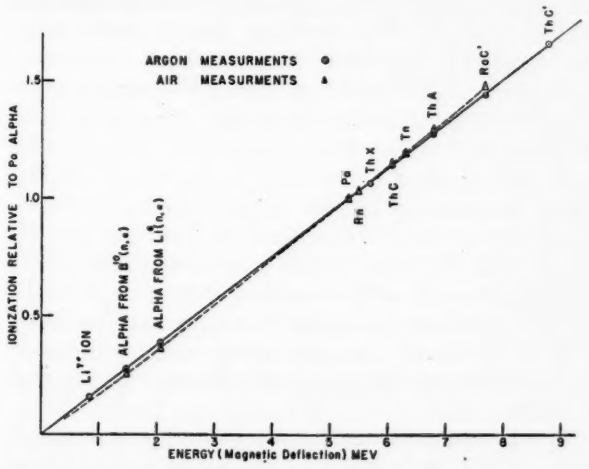

FIG. 1. The ionization of various alpha-particles in argon and in air, relative to that for the polonium alpha, plotted against alpha-particle energy.

The alpha-emitting elements were put on a highly polished button of nickel or stainless steel, inserted flush with the surface at the center of the circular electrode. The polonium was deposited from solution on the button by the usual method, and the other elements were deposited by the standard method of collecting recoil atoms.

The quantity of radioactive material to give five counts per minute is, of course, so small for any of the elements used that the normal sample absorption is completely negligible. However, one can never be sure that some sort of surface interaction between the deposited layer and the metal may not give a distorting effect such as has been recently reported.[8] In our work we could discover no evidence of any distortion of our plotted curves which could be attributed to such a phenomenon. Moreover, measurements with disks of nickel, stainless steel, and platinum all gave consistent results.

[8] Haissensky, Faraggi, Coche, and Avignon, Phys. Rev. **75**, 1963 (1949).

The argon used was of "spectroscopic purity" and was taken directly from glass breaker flasks. A calcium cell was used as a monitor, and a large number of runs were made with argon repeatedly circulated through the cell. Except in two doubtful cases, we could determine no marked change in the alpha-ratios after circulating the argon over the calcium. This is contrary to the general experience of those using pulse chambers with linear amplifiers. It must be remembered, however, that our instrument is probably much less sensitive to minute impurities than a linear amplifier system, where the time of flight of a collected ion or electron is an extremely important factor.

Great care was taken to insure voltage saturation in the chamber. Saturation curves of single alpha-jumps against voltage showed a rapid rise to a constant value. With further large increase of voltage no change in the length of the jumps could be observed within the limit of experimental statistical error. In a cylindrical chamber, with a polonium alpha-beam collimated parallel to the cylindrical electrode, we have obtained saturation with fields of approximately 15 volts/cm at an argon pressure of 60 cm. For uncollimated beams at the higher pressures used (up to 160 cm of mercury) one obtains correspondingly higher fields for saturation. In all cases the chamber voltage used was considerably higher than the voltage judged to give saturation.

Throughout the experiment only the ratio of the ionization of the alpha-particle in question to that of the comparison polonium alpha was determined. In finding this ratio, either of two methods could be used. Because of statistical fluctuations, the length L of successive jumps recorded for a given alpha-particle varied. To determine the most probable value of L, in the first method the conventional procedure was followed. From the recorded data the number of alphas was found lying between the limits L and $L+\Delta L$, as the length L was increased by successive increments ΔL. ΔL was an arbitrarily chosen small increment of length amounting to one or two tenths of a scale division. A plot, number of events within the interval against length of jump, gave an essentially Gaussian distribution, both for the alpha-particle in question, and for the reference polonium alpha. The ratio of the lengths corresponding

TABLE I. Relative ionization and energy for alpha-particles in argon.

Element	Ionization relative to Poα	Calculated energy for Po = 5.298$_4$ Mev	Energy by magnetic deflection Mev	Percent difference	Average slope I/E from origin
Po	1.0		5.298$_4$		0.1887
ThX	1.067	5.653	5.681$_3$	−0.5	0.1878
ThC(mean)	1.142	6.050	6.053$_7$	−0.1	0.1886
Tn	1.198	6.347	6.281$_8$	+1.0	0.1907
ThA	1.276	6.761	6.774$_4$	−0.2	0.1884
RaC′	1.444	7.653	7.680$_2$	−0.4	0.1881
ThC′	1.663	8.812	8.775$_9$	+0.4	0.1895

to the peak values for these two plots was taken as the value for the relative ionization for the two particles.

If the plots for the two alpha-particles have the same shape, as they do here, both being essentially Gaussian in character, and if they are well resolved so there is no overlap, then a second method is permissable. Here one takes the *average* length of the jumps included under each plot and determines the ratio. Where the above conditions are fulfilled, the two methods give very consistent results. The second method seems to have some advantage in runs of several hours, if the ratio is determined from groups of data chosen periodically, as within every half-hour. In this case, we are determining the ratio from data taken much more simultaneously; hence, any possible slow drift in the overall sensitivity of the apparatus is minimized.

RESULTS AND DISCUSSION

The results of our comparison of various alpha-emitters with polonium are shown in Fig. 1. Here the ordinate represents the ionization of each single alpha used relative to the ionization of a comparison polonium alpha in argon. On the horizontal axis are plotted the values of alpha-energies determined by magnetic deflection[9] methods. These energies in the region 5–9 Mev are supposed to be correct to within at least 1 part in 5000. On the scale as plotted, the experimental points seem to lie very well on a straight line through the origin. No accurate conclusion can be drawn as to minor deviations from such a line. Such can best be seen in Table I.

In the third vertical column of this table are shown the alpha-energies calculated from the ionization ratios of the second column on the assumption that the energy of the polonium alpha is 5.298_4 Mev. In column 4 are shown the true alpha-energies as determined by the magnetic deflection method. If a strict proportionality in the interval between 5 and 9 Mev exists between the energy of the alpha-particle and the ionization in argon produced by it, then the values in columns 3 and 4 should be the same. The difference in percent between these values is given in column 5. In column 6 we have indicated the slope I/E of an imaginary line drawn from the origin to the experimental point in question. The strict proportionality indicated above would be shown in a constant value for this slope.

The result for thoron is at once seen to be in disagreement with the other values. A plausible reason for such a discrepancy would seem to be as follows. Thoron, a gas derived from the decay of ThX on our plate, might well diffuse into the argon and decay there, following its 54-sec. half-life. If this occurs, the ionization due to the recoil atom would be included in the alpha-measurement, increasing it by the order of 2 percent. If the thoron on the average decayed about half the time in the gas, our value, high by about 1 percent, would seem to be explained.

If one accepts this explanation and omits the thoron point from further consideration, then the agreement, within the limits of experimental error, between columns 3 and 4 and the apparent constancy in column 6 would indicate a direct proportionality between ionization and alpha-energy in argon for alphas of energy 5 to 9 Mev.

One has only to compare these results with the results for alpha-particles in air to see the difference between the two gases. We have not carried out the same experiment for air, but apparently very careful measurements have been made in air by G. Stetter.[10] Instead of using the natural alpha-particles, as has been done here, he has obtained different ranges and energies by slowing down a collimated beam of ThC′ alpha-particles by passage through an absorbing column of air. A complete curve has been thus plotted relating the alpha-ionization with the extrapolated range of the alpha-particle. We have from this curve determined the relative air ionization corresponding to the same alpha-emitters used above. Here, except for ThC, we have used the tabulated extrapolated ranges given by Holloway and Livingston[9] for natural alpha-particles. It should be pointed out that these are not rigorously the ranges appropriate to Stetter's curve, since his experimental method gives a somewhat greater straggling than is characteristic of the alphas from the natural elements. It is not believed that any serious error is involved, especially for the alpha-particles of energy higher than polonium.

In Table II are given the results for air so obtained. The experimental points are also shown in the plot for air in Fig. 1. In the table a marked trend is seen in vertical columns 6 and 7 which was not apparent in the argon readings. This variation indicates a much steeper slope for energies larger than polonium for the ionization-energy curve for air compared with the *average* slope from the origin to the polonium point. This trend is shown clearly in the plot in Fig. 1.

Although we have evidence above of the constancy of W in argon within our experimental error for alpha-energies from 5 to 9 Mev, and that this value is the same as the *average* W from 0 to 5.3 Mev, we still have no knowledge as to possible minor variations of W below 5 Mev, especially in the region of the origin. Theory would predict a rise of W near the origin with a decreased slope of the ionization-energy curve. Any least-squares extrapolation from our data to determine an exact intercept on the energy axis with any real significance we must regard, after some trials, as futile, since the extrapolated value is extremely sensitive to even one or two slightly erratic experimental points.

Since there are no natural alpha-particles below 5 Mev with energies as well determined as the ones used, we have had to rely in this region on more indirect

[9] M. G. Holloway and M. S. Livingston, Phys. Rev. **54**, 18 (1938).

[10] G. Stetter, Zeits. f. Physik **120**, 639 (1943).

TABLE II. Relative ionization and energy for alpha-particles in air, computed from the work of Stetter.

Element	Extrapolated range (cm) at 15° and 76 cm	Ionization relative to Po α	Energy calculated for Po = 5.298$_4$ Mev	Energy by magnetic deflection Mev	Percent difference	Average slope I/E from origin
Po	3.870	1.0		5.298_4		0.1887
Rn	4.076	1.036	5.490	5.486_0	+0.1	0.1889
ThC	4.760	1.150	6.093	6.053_7	+0.6	0.1900
Tn	5.035	1.194	6.325	6.281_8	+0.7	0.1900
ThA	5.672	1.293	6.849	6.774_4	+1.1	0.1908
RaC′	6.953	1.478	7.833	7.680_2	+2.0	0.1925

methods. Fortunately some fairly accurate values of alpha-energies from nuclear reactions have recently been determined, which have been of great help.

For these indirect methods, the relations existing between ionization and alpha-energy derived from such available data are shown in Table III. Here, just as in Table II, the ionization in air relative to the polonium alpha was determined from Stetter's values from the extrapolated ranges. The latter were determined from the mean ranges by adding 0.028 cm, the difference between the mean and extrapolated range for the Po alpha, which value has been determined quite accurately by Holloway and Livingston. The earlier mentioned objection to this procedure applies also here, perhaps to an even greater degree. As has already been pointed out, the Holloway-Livingston range-energy curve,[9] derived between 0 and 5 Mev in essentially the same way as Stetter's, is likewise a range-ionization in air curve. Hence, from the mean ranges one can determine the ionization in air for the chosen particle relative to the Po alpha by simply taking the ratio of the "energies" as read from the H and L curve. The agreement between the Stetter and the H and L determination is seen in vertical columns 4 and 5 to be very good.

For the $Li^6(n,\alpha)H^3$ reaction the mean range is taken from the cloud-chamber result of Bøggild and Minnhagen;[11] for $B^{10}(n,\alpha)Li^{7*}$ a mean of the results of Bøggild,[12] 0.709 cm, O'Ceallaigh and Davies,[13] 0.715 cm and Bower, Bretscher and Gilbert,[14] 0.735 cm has been used. The last result has been corrected for the variation of stopping power with alpha-energy for the gases of the cloud chamber but not by as large an amount as has recently been suggested.[15] The other values already include such a correction.

Jesse and Sadauskis,[16] from a comparison of the relative ionization of samarium and polonium alpha-particles in argon and in air, have shown that the ratio of ionization $(Sm/Po)_{argon}$ is about 5 percent higher than the ionization ratio $(Sm/Po)_{air}$. An extension of this work with retarded alpha-particles has resulted in a fairly accurate curve relating the two ratios in argon and in air. Details of this curve will soon be published in another paper relating to other phases of this work. In vertical column 7 are given the multiplying factors to convert the ratio (Ionization for given alpha-particle/Ionization of Po alpha) in air to the corresponding ratio in argon. The latter ratio is given in column 8.

The energy release for each of these nuclear reactions‡ has been independently measured by a method involving the magnetic deflection of the emitted alpha-particle from closely associated reactions. The Q-values are 4.788 ± 0.023 Mev for the Li^6 reaction[17] and 2.316 ± 0.006 Mev for the B^{10} reaction[18] resulting in the excited state for Li^7. The corresponding energies for the alpha-particles are given in column 9, and the average slopes I/E are given for air and argon in the last two columns. Here again this slope for argon is seen to be in excellent agreement with the values in the last column

TABLE III. Ionization-energy relations for particles below 5 Mev.

Particle	Mean range cm	Extrapolated range cm	Corresponding relative ionization in air: Stetter	H and L	mean	Ratio rel. ion argon / rel. ion air	Ion. in argon relative to Po α	Direct meas. of particle energy Mev	Slope I/E from origin: Air	Argon
Alpha from $Li^6(n,\alpha)H^3$	1.04	1.068	0.363_6	0.369_9	0.366_8	1.05_7	0.387_7	2.060	0.1780	0.1882
Alpha from $B^{10}(n,\alpha)Li^{7*}$	0.720	0.748	0.255_7	0.256_7	0.256_2	1.08_3	0.277_5	1.474	0.1738	0.1883
Direct ionization measurements in argon of $B^{10}(n,\alpha)Li^{7*}$ reaction										
Alpha from $B^{10}(n,\alpha)Li^{7*}$					0.256_3	1.08_3	0.277_6	1.474	0.1739	0.1883
Li^{7*} ion from $B^{10}(n,\alpha)Li^{7*}$							0.158_3	0.841		0.1882

[11] J. K. Bøggild and L. Minnhagen, Phys. Rev. **75**, 782 (1949).
[12] J. K. Bøggild, Kgl. Danske Vid. Sels Math.-Fys. Medd. **23**, No. 4 (1945).
[13] C. O'Ceallaigh and W. T. Davies, Proc. Roy. Soc. (A) **167**, 81 (1938).
[14] Bower, Bretscher, and Gilbert, Proc. Camb. Phil. Soc. **34**, 290 (1938).
[15] C. W. Gilbert, Proc. Camb. Phil. Soc. **44**, 447 (1948).
[16] W. P. Jesse and J. Sadauskis, Phys. Rev. **75**, 1110 (1949); Phys. Rev. **76**, 163 (1949).
‡ We are indebted to Professor W. A. Fowler for a private communication giving us these values before their formal publication.
[17] Tollestrup, Fowler, and Lauritsen, Phys. Rev. **76**, 428 (1949).
[18] Chao, Lauritsen, and Tollestrup, Phys. Rev. **76**, 586 (1949).

of Table I, while for air a comparison of the slopes in Table III with those of Table II shows a falling off of the order of 10 percent.

In the last two horizontal rows in Table III are listed the results of direct measurements of the Q for the $B^{10}(n,\alpha)Li^{7*}$ reaction by an ionization chamber method. These measurements were made in this laboratory in a chamber similar to that described above. The runs were in argon to which had been added about 0.1 percent of enriched BF_3. The method was essentially that described above. A mean of six determinations at various pressures up to 160 cm of mercury gave for a total Q of the reaction 2.310 ± 0.010 Mev. The error here given was arbitrarily set from our past experience with such measurements. In this case it is about three times the standard deviation for the series of measurements and does not include any possible systematic errors. No corrections of any sort have been made to the data, such as a correction for the finite size of the chamber. This is believed to be very small but would tend to raise the values obtained. A comparison of our value with that of Chao, Lauritsen, and Tollestrup shows an excellent agreement, well within the combined experimental errors of the two determinations.

Unless we assume that the agreement here is the result of pure chance, i.e., a combination of experimental errors in both determinations forcing them into agreement, which of course may possibly be the case, we are forced to the conclusion that the average W for the combined ionization from Li^{7*} and the accompanying alpha is the same as for the average W for the polonium alpha. From this it would seem reasonable to assume the average W for Li^{7*} the same in argon as the average W for the polonium alpha. For comparison with the previous values from ranges, the appropriate values from these direct measurements have been calculated in Table III. The measured ionization has been partitioned in the same ratio as for the energies, and ionization values computed for air by now dividing by the ratio in vertical column 7. The applicability of this ratio, derived for alpha-particles, to the Li^7 ion is, of course, questionable. Hence, no values for the Li^{7*} ion in air were computed.

In the complete curves in Fig. 1 and from the tables there seems no evidence of a departure in argon, within the error of experiment, from a strict proportionality between ionization and particle energy. In air the plotted points between 2 and 6 Mev seem to fall fairly well on a straight line drawn from about $+0.175$ Mev on the energy axis through the polonium alpha-point. Numerically the values I/E', where $E'=E-0.175$ Mev, for the experimental values agree within $\frac{1}{2}$ percent inside this region. In the region 0–2 Mev and from 6–7.5 Mev the plotted points lie somewhat above this line, i.e., the curve is slightly concave upward. The values for RaC′ and for the B^{10} alpha are about 1 percent high in such a calculation.

In support of our present findings as to the essential constancy of W for alpha-particles in argon, it would seem worth while to mention two further pieces of evidence which, while not conclusive in themselves, at least support the above results.

1. It has been shown by Jesse and Sadauskis[16] that the alpha-range-energy curve of Holloway and Livingston on the basis of ionization measurements in air can be converted to a corresponding curve involving measurements in argon. The latter curve gives values in very good agreement with ranges and alpha-energies independently determined for a number of nuclear reactions. The agreement in a few cases has already been shown here indirectly in Table III. Furthermore, when the revised alpha-range-energy curve is used to determine the proton range-energy curve by Blackett's[2] transformation equation, the latter curve gives values in much better agreement with recently determined nuclear data. These revised range-energy curves are now consistent with other data, where the former curves were markedly inconsistent. This fact would seem a plausible argument for the fundamental assumption that in argon the value of W is at least approximately constant.

2. In recent experiments involving the measurement of the relative ionization of β-rays in argon, Curran, Angus, and Cockroft[19] have found that the energy to produce an ion pair in argon is nearly constant within the energy range 200 ev to 50 kev. This result is consistent with our findings above for alpha-ionization, since the latter ionization is made up in part of ionization from δ-rays with energies of a few kev. The fact, that in air for β-particles this direct proportion is no longer valid[20] but the energy to make an ion pair increases at low β-energies, is also consistent with the similar behavior for alpha-particles in air. The constancy of W for β-particles in argon would not seem, however, an entirely conclusive proof of the constancy for alpha-particles, since undoubtedly some ions are formed in the alpha-track by processes other than ionization by β-particles within the energy range investigated by Curran, Angus, and Cockroft.

ACKNOWLEDGMENTS

It is a pleasure to express our thanks to Professor H. A. Bethe, Professor Edward Teller, and Dr. Francis R. Shonka for many stimulating discussions of this general subject. Our thanks are due also to Mr. L. C. Ellsworth, whose painstaking skill in the construction of our ion chambers has added greatly to the success of this work.

[19] Curran, Angus, and Cockroft, Phil. Mag. **40**, 36 (1949).
[20] Reference 1, p. 91.

The $Cu^{63}(n,2n)Cu^{62}$ Cross Section as a Function of Neutron Energy near the Threshold*

J. L. Fowler and J. M. Slye, Jr.†
Los Alamos Scientific Laboratory, Los Alamos, New Mexico
(Received August 1, 1949)

Using the $D(d,n)He^3$ reaction produced by 10.5-Mev deuterons to give monoenergetic neutrons, the $Cu^{63}(n,2n)Cu^{62}$ reaction has been studied in the vicinity of the threshold. The product of the differential cross section of the former reaction and the activation cross section of the latter is obtained as a function of angle to the bombarding deuteron beam. By calibrating the Geiger counters with beta-particles from Cu^{66} produced by the thermal neutrons on Cu^{65}, the data are made absolute in terms of the known thermal capture cross section. Previous measurements of the differential cross section of the $D(d,n)He^3$ reaction allow the $Cu^{63}(n,2n)Cu^{62}$ cross section to be given as a function of energy. An extrapolation of the data gives the energy required to remove a neutron from Cu^{63} as 11.2±0.3 Mev.

I. INTRODUCTION

FOR some time it has been known that fast neutron bombardment of copper produces a beta-activity of 10-minute period. This activity has been identified as being due to the positron emitter, Cu^{62}, which is formed by the $Cu^{63}(n,2n)Cu^{62}$ reaction.[1–4] Since the energetic threshold is in the neighborhood of 12 Mev, this reaction has been used a number of times as a fast neutron detector.[5–7] Because of its convenience as such a detector, the $Cu^{63}(n,2n)Cu^{62}$ reaction has been studied with monoenergetic neutrons from the threshold up to 14 Mev.

II. EXPERIMENTAL APPARATUS

The neutrons in this experiment were produced by the $D(d,n)He^3$ reaction, where the bombarding deuterons were accelerated to 10.5 Mev by the cyclotron. The focused deuteron beam was used 15 feet away from the cyclotron with three feet of water and paraffin shielding between the cyclotron and the experimental area. The apparatus for focusing and monitoring the beam as well as for measuring the deuteron energy has been discussed previously.[8] Figure 1 is a diagram of the reaction chamber showing the arrangement of the deuteron gas target and the copper foil holder. The beam from the cyclotron was defined to ±0.6 deg. when it entered the mica window of the gas target. Rutherford scattering in this window effectively increased this spread to ±0.9 deg.[8] Both the side port for counting charged particle reaction products produced by bombarding deuterons and the exit port for the beam were also covered with mica windows. On emerging from the target the deuterons were monitored by a Faraday cage which was mounted in the center of the exit tube of the reaction chamber.

In order to mount the copper samples (5-mil foils 2.5 in.×one in.) as near to the forward direction as possible, it was found necessary to support them in holders which were placed inside the reaction chamber as shown in Fig. 1. The foils were sandwiched between $\frac{1}{16}$-in. sheets of cadmium to reduce the five-minute activity due to the $Cu^{65}(n,\gamma)Cu^{66}$ reaction which is produced mostly by thermal neutrons. The foils were mounted with their long dimension vertical and with their center in the horizontal plane which passes through the center of the gas target. The angular position of each foil in the horizontal plane and the distance of each foil from the center of the target was determined before an activation run was made. The foils subtended an angle of about ± three deg. in the horizontal plane.

III. EXPERIMENTAL PROCEDURE AND RESULTS

After a bombardment of 15 to 20 minutes, the foils were counted on thin glass-walled Geiger counters. Three such counters were used and the foils were interchanged for intercalibration purposes. The decay curves

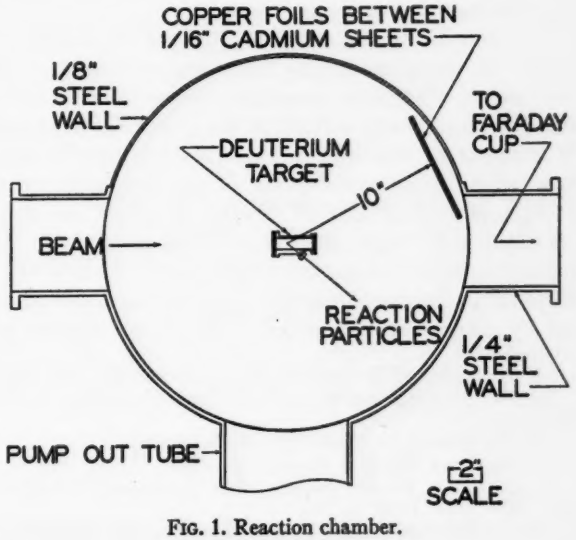

FIG. 1. Reaction chamber.

* This document is based on work performed at Los Alamos Scientific Laboratory of the University of California under Government Contract W-7405-eng-36.
† Now at the University of Texas, Austin, Texas.
[1] F. A. Heyn, Physica 4, 161 (1937).
[2] F. A. Heyn, Nature 138, 223 (1937).
[3] Pool, Cork, and Thornton, Phys. Rev. 51, 890 (1937).
[4] Chang, Goldhaber, and Sayane, Nature 139, 962 (1937).
[5] Salant, Roberts, and Wang, Phys. Rev. 55, 984 (1939).
[6] E. O. Salant and N. F. Ramsey, Phys. Rev. 57, 1075 (1940).
[7] Erickson, Fowler, and Stovall, Phys. Rev. 75, 894 (1949).
[8] Curtis, Fowler, and Rosen, Rev. Sci. Inst. 20, 388 (1949).

were found to be primarily due to 10-minute activity except for foils near the $(n,2n)$ threshold, where the five minute period due to Cu^{66} produced by the (n,γ) process began to show up. It was found possible to analyze all the decay curves in terms of the 10-minute and five-minute period. In correcting the data to initial activation 10 minutes has been used as the half-life of Cu^{62}, which is the average of several determinations reported in the literature[1,2,9–12] weighted according to their quoted accuracy.

For a measurement of the 10-minute activity in the direction of the deuteron beam the beam was stopped with a gold plate and monitored by counting He^3 particles emitted through the side port of the target (Fig. 1) into a proportional counter. This determination was carried out in connection with studies of the $D(d,n)He^3$ reaction.[7]

The 10-minute activity due to background fast neutrons was determined by runs in which hydrogen was substituted for deuterium in the gas target. These background neutrons produced 10-minute activity which amounted to about five percent of the activity produced by the $D(d,n)He^3$ neutrons at 11 deg. to the direction of the beam. The background was roughly constant with angle from seven deg. to 40 deg.

A convenient calibration of the Geiger counters was possible, since the positron emitted by the Cu^{62} nucleus has an end-point energy about equal to the end-point energy of the electron emitted by Cu^{66} which is produced with thermal neutrons by the $Cu^{65}(n,\gamma)Cu^{66}$ reaction.[13] After an irradiation for a known time in a known thermal flux of the Los Alamos standard graphite pile, the copper foils were counted for several half-lives. By use of runs in which the foils were covered with cadmium a correction was obtained for the activity produced by neutrons above the thermal region (about four percent). Since the thermal capture cross section for producing Cu^{66} has been determined (0.56 ± 20 percent barn in normal copper),[14] this enables us to determine the efficiency of the Geiger counters.

The results of the experiment were calculated in terms of the product of the cross section for the $Cu^{63}(n,2n)Cu^{62}$ reaction produced by fast neutrons and the differential cross section of the $D(d,n)He^3$ reaction. It is apparent that the $(n,2n)$ cross section discussed here refers to the production of positron activity of 10-minute period. If Cu^{62} decays by other processes (K-capture for example) this will not show up in the measurements. The efficiency of the Geiger counters was included in the calculations by dividing the above product by the cross section of the $Cu^{65}(n,\gamma)Cu^{66}$ reaction for thermal neutrons in normal copper. When this ratio was plotted as a function of the angle to the direction of the deuteron beam the points obtained lay on a smooth curve within the limits expected from the counting errors and the errors involved in determining the other factors measured. The average energy of the bombarding deuterons as determined by magnetic deflection of the beam[8] was 10.5 ± 0.25 Mev.

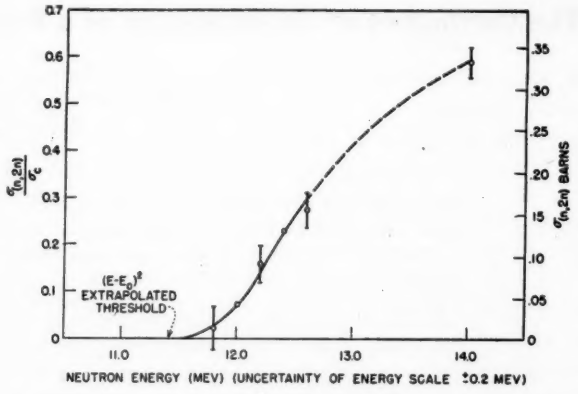

FIG. 2. Cross section of $Cu^{63}(n,2n)Cu^{62}$ reaction. For uncertainty of ordinate refer to left-hand scale which gives the ratio of the $Cu^{63}(n,2n)Cu^{62}$ cross section to the thermal capture cross section of the $Cu^{65}(n,\gamma)Cu^{66}$ reaction. Both cross sections are for activity produced in normal copper. The right-hand scale gives the $(n,2n)$ cross section directly and is based on 0.56 ± 20 percent barn (reference 14) as the thermal capture cross section.

Using data on elastic scattering of neutrons,[15–17] the results were corrected for the effect of the neutrons elastically scattered from the material of the reaction chamber behind the foils so that these neutrons pass through the foils more than once. The effect of neutrons absorbed by the material between the source and the foils was also estimated. Although these effects were small (the order of three percent) and were compensating over most of the angular region, at angles near the threshold of the $Cu^{63}(n,2n)Cu^{62}$ reaction the effect of the scattered neutrons predominated, so that the correction of about seven percent was applied to the data in this region. Over-all experimental checks of these correction factors were made which indicated the estimates were valid.

From the curves for the 10-minute activation as a function of angle and from the reported measurements of the differential cross section of the $D(d,n)He^3$ reaction,[7] the $Cu^{63}(n,2n)Cu^{62}$ cross section is plotted as a function of energy of the neutrons (Fig. 2). The uncertainty of the points as represented by the vertical lines refer to the ordinate scale on the left which gives the ratio of the $Cu^{63}(n,2n)Cu^{62}$ cross section to the $Cu^{65}(n,\gamma)Cu^{66}$ cross section. These uncertainties are estimated from the errors in the activation determina-

[9] V. W. Bothe and W. Gentner, Zeits. f. Physik **106**, 236 (1937).
[10] L. N. Ridenour and W. J. Henderson, Phys. Rev. **52**, 889 (1937).
[11] E. Crittenden, Jr., Phys. Rev. **56**, 709 (1939).
[12] Leith, Bratenahl, and Moyer, Phys. Rev. **72**, 732 (1947).
[13] J. Mattauch, *Nuclear Physics Tables* (Interscience Publishers, Inc., New York, 1946), p. 134.
[14] Seren, Friedlander, and Turkel, Phys. Rev. **72**, 888 (1947).
[15] H. H. Barschall and R. Ladenburg, Phys. Rev. **61**, 129 (1942).
[16] Manley, Agnew, Barschall, Bright, Coon, Graves, Jorgensen, and Waldman, Phys. Rev. **70**, 602 (1946).
[17] D. D. Phillips, Sr., doctoral dissertation, *Inelastic Collision Cross Section of Various Elements*, University of Texas (1949).

tion as well as errors in the differential cross section curve for the $D(d,n)He^3$ reaction.[7] The range of the measurements given here indicated by the solid line extend only over the region in which the $D(d,n)He^3$ reaction has been studied directly by counting He^3 particles.[7] The point at 14 Mev is an independent determination by D. D. Phillips and R. W. Davis.[17] This was obtained with a known flux of 14-Mev neutrons and by use of the same method of calibration of Geiger counters as is described in this report. The dotted portion of the curve in Fig. 2 is an extrapolation between this 14-Mev point and the part of the curve obtained at lower energies. The ordinate scale on the right in Fig. 2 which gives the cross section of the $Cu^{63}(n,2n)Cu^{62}$ reaction is based on the reported value of 0.56 barn for the production of Cu^{66} in normal copper. The uncertainty of this scale is ± 20 percent and is the reported uncertainty of the capture cross section.[14]

A linear extrapolation of the points in Fig. 2 gives an apparent threshold of 11.7 ± 0.3 Mev for the $Cu^{63}(n,2n)Cu^{62}$ reaction, where the error in the energy is estimated from the uncertainty of the energy scale and the uncertainty of the extrapolation of the points. In a number of runs in which only relative values of activation were measured, independent determination of this threshold in this manner gave an average value of 11.8 ± 0.2 Mev. Within the limits of error, this is in agreement with previously reported determinations of the threshold of about 12 Mev.[1, 6, 18]

One expects the extrapolation discussed above not to be valid in the case of the $(n,2n)$ reaction. Consideration of the volumes in phase space available for the products of the $(n,2n)$ reactions suggests that the cross sections of these reactions should go to zero as $(E-E_0)^2$, where E_0 is the threshold. The curve in Fig. 2 through the lower energy points is an $(E-E_0)^2$ extrapolation, which gives a threshold of 11.4 ± 0.3 Mev. Correcting this value for the recoil energy of the compound nucleus, one obtains 11.2 ± 0.3 Mev as a neutron binding energy. This agrees within the limits of error with the threshold of the $Cu^{63}(\gamma,n)Cu^{62}$ reaction which has been determined to be 10.9 ± 0.3 Mev by betatron activation.[19]

The authors wish to thank the members of the Los Alamos cyclotron group for their aid in this experiment. We wish to acknowledge the suggestion of Dr. J. H. Manley with regard to calibration of the Geiger counters. We are indebted to Dr. Edward Teller for the very helpful discussion of the behavior of cross sections near the threshold. We wish also to thank Dr. R. F. Taschek for his helpful criticism in preparing this report.

[18] R. Sagane, Phys. Rev. **53**, 492 (1938).
[19] G. C. Baldwin and H. W. Koch, Phys. Rev. **67**, 1 (1945).

PHYSICAL REVIEW VOLUME 77, NUMBER 6 MARCH 15, 1950

A Redetermination of the Relative Abundances of the Isotopes of Carbon, Nitrogen, Oxygen, Argon, and Potassium*

ALFRED O. NIER
Department of Physics, University of Minnesota, Minneapolis, Minnesota
(Received December 9, 1949)

Essentially pure samples of A^{36} and A^{40} have been produced by thermal diffusion and used for the preparation of synthetic argon isotope mixtures whose A^{36}/A^{40} isotope abundance ratios were very accurately determined. The mixtures were then employed for determining the mass discriminating effects in two mass spectrometers. Carbon, nitrogen, oxygen, argon, and potassium were investigated and new values given for the relative abundances of the isotopes. With atmospheric oxygen as a standard, the conversion factor between the physical and chemical atomic weight scales is 1.0002783 ± 5. The percentage abundance of K^{40} in potassium is found to be 0.0119 ± 0.0001 percent, a figure of special interest in geophysical problems, and approximately ten percent higher than the present accepted value.

THE general need for more precise information on nuclear constants suggests that a redetermination of isotope abundances in many of the elements may be of value. The existence of nearly pure samples of separated isotopes makes possible the preparation of artificial mixtures of isotopes whose relative abundances may be computed to a high degree of accuracy. The use of such standard isotopic mixtures together with mass spectrometers of modern design makes possible results in which both the accidental and systematic errors are reduced below those previously attainable. The present paper represents the beginning of a study of those elements where it appears redeterminations are of value and can profitably be made.

* This research was supported by a joint ONR and AEC grant.

APPARATUS

Two mass spectrometers of the 60° type were used in the present investigation. One of these has already been described in detail.[1] During the past two years numerous minor modifications have been made in this instrument. The only one of interest here concerns the ion source. Plate J_3 has been eliminated, the space

[1] A. O. Nier, Rev. Sci. Inst. **18**, 398 (1947).

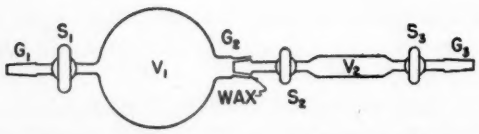

FIG. 1. Mixing bulb for making argon isotope mixtures. G_1 and G_3, standard tapers 10/30; G_2, 14/20; S_1 3-mm bore stopcock, S_2 and S_3 2-mm bore stopcocks. The bulb is made in two pieces for ease in measuring the volumes. Both parts were measured by weighing, water being employed for the larger, mercury for the smaller. Corrections for temperature and for buoyancy of the atmosphere were made. V_1 (measured between S_1 and S_2) was 1012.7 cc for Samples A I and A IV and 1013.5 cc for Samples A V and A VI. V_2 (including bore of S_3) was 9.9982 for A I and 11.6991 for A IV, A V, and A VI.

between S and J_1, J_2 increased to 2 mm and that between J_1, J_2, and G, decreased to 2 mm. In the present work the instrument was used with the single collector No. 2. Mass spectra were obtained by varying the voltage on the left grid of V_4 (reference 1, Fig. 6) with a motor-driven potentiometer. Records were taken on a Brown Electronik 4.5-second recording potentiometer. For purposes of identification, the mass spectrometer just discussed will be known as MS1.

The second instrument (to be called MS2) was that employed in the helium and argon work[2] of the past few years. In the present work the source employed was essentially the same as that used in MS1. The greatest difference was that it contained a small furnace very similar to one employed in some earlier work.[3] This permits the study of substances not volatile at room temperature. A further difference was that the gas was led directly into the spectrometer housing rather than into the shield can as in MS1. Perhaps the most important difference between MS1 and MS2 was the fact that MS2 employed a molecular flow gas leak[4] consisting of a hole 0.001 in. diameter in an aluminum sheet 0.001 in. thick. The reservoir behind this leak had a volume of 5000 cc. Thus in MS2 the gas composition in the ionization region should be the same as in the sample reservoir whereas in MS1 where a viscous-type leak is employed it should be distorted according to the square root of the ratio of the pair of masses

TABLE I. Composition of isotopically separated samples used for making standards.

Standard No.	Pressure cm oil	Temp. °K	Gas	Composition (%) A^{36}	A^{40}	Impurities
A I	63.40	——	A^{40}	0.00	99.85	0.15
	62.95	——	A^{36}	97.17	1.69	0.45
A IV	65.83	299.90	A^{40}	0.00	99.71	0.29
	65.83	300.16	A^{36}	94.78	3.44	0.78
A V	44.52	299.41	A^{40}	0.00	99.32	0.68
	44.14	299.31	A^{36}	95.21	3.46	0.33
A VI	59.50	298.76	A^{40}	0.00	99.80	0.20
	59.50	298.66	A^{36}	94.99	3.45	0.57

[2] L. T. Aldrich and A. O. Nier, Phys. Rev. **74**, 876 (1948); **74**, 1590 (1948).
[3] A. O. Nier, Phys. Rev. **53**, 282 (1938).
[4] R. E. Honig, J. App. Phys. **16**, 646 (1945).

TABLE II. A^{36}/A^{40} ratios ($\times 10^6$) for standards.

	Calc. from Table I	Measured with MS Run 1	Run 2	Calc./av. meas.	Recalculated adopted values
A I	953.8	953.7	957.1	0.9983	949±1.9
A IV	1098.6	1108.6	1114.9	0.9882	1105±2.4
A V	1097.0	1103.2	1102.1	0.9949	1096±1.5
A VI	1100.4	1108.8	1106.9	0.9932	1101±1.6
				Av. 0.9937±0.0014	

under consideration. These assumptions were made in computing the measured A^{36}/A^{40} ratios in Tables III–VII before applying the correction for the "true" isotopic composition of the argon standards. The fact that the subsequent corrections were relatively small in all cases shows that not only did the instruments have small mass discriminating effects but moreover the assumption made for the gas composition in the instruments was very nearly correct if not completely so.

The electrometer tube grid resistors had a resistance of 10^{11} ohms in each case and as nearly as could be determined were completely ohmic in their performance. Since inverse feed-back amplifiers and self-balancing recording potentiometers were used for measuring and recording the ion currents, linearity problems do not occur in the measuring system.

Argon was chosen as the reference gas for all the measurements reported here. By means of thermal diffusion columns described elsewhere,[5] some nearly pure A^{36} and nearly pure A^{40} were obtained. These were mixed in known proportions to give an accurately determined ratio A^{36}/A^{40} near to 0.01. The gas so obtained was then used as a standard for calibrating the mass

TABLE III. Comparison of mass spectrometer readings for standard argon and argon from several sources.

Data taken with MS2 $A^{36}/A^{40}\times10^6$ Stand. A V	$A^{36}/A^{40}\times10^6$ Airco	Atmos.	$A^{38}/A^{40}\times10^6$ Airco	Atmos.
1085	3290	3368	669	681
1090	3326	3341	634	695
1096				
1090	3315	3356	627	699
1090				
Av. 1090±1.2	3310.3±7.3	3355.0±5.3	643.3±8.8	691.7±3.7
Corr. 1096±1.5	3328 ±9	3373 ±8	645 ±9	694 ±4
Data taken with MS1 Stand. A I				
937	3333	3361	626	633
939				
943	3319	3342	625	631
942				
940				
940	3327	3355	630	
940				
Av. 940.1±0.6	3326.3±2.8	3352.7±3.8	627.0±1.0	632.0±0.7
Corr. 949 ±1.9	3358 ±8	3384 ±8	630 ±1	635 ±1
Weighted grand mean of data taken with MS1 and MS2	3346 ±6	3378 ±6	630 ±1*	635 ±1*

* Data from MS2 discarded.

[5] McInteer, Aldrich, and Nier, Phys. Rev. **74**, 946 (1948).

TABLE IV. Comparison of mass spectrometer readings for atmospheric nitrogen and standard argon.

Data taken with MS2 $36/40\times10^5$ Stand. A I	$(N^{15}N^{15}/N^{14}N^{14})\times10^6$ Atmos. N_2
939	739
941	
942	738
938	736
939	
Av. 939.8±0.5	737.7±0.5
Corr. 949 ±1.9	735.3±0.7
Data taken with MS1 Stand. A I	
942	737
940	
940	725
943	729
944	
Av. 941.8±0.5	729.7±2.9
Corr. 949 ±1.9	728 ±3
Weighted grand mean of data taken with MS1 and MS2	735 ±1
Unweighted average of MS1 and MS2 data	732 ±2*

* The large difference in the P.E. in the two instruments and an examination of the data suggest systematic errors may have been present. It seems safer to assume the data to be inconsistent and adopt the average value disregarding the P.E. in the data from the individual instruments.

spectrometers for systematic errors which depend upon the relative masses of the ions studied.

Figure 1 shows the bulb employed for making the argon isotope mixtures. The following procedure was employed in making gas mixtures: After evacuating the bulb, including the stopcock bores, V_1 was filled with A^{40} to a given pressure carefully measured on an oil manometer. V_2 was filled with A^{36} to approximately the same pressure (the exact value being carefully measured) through G_3, the temperatures being carefully noted in both cases except in A I where they were assumed to be the same. Mixing is accomplished by attaching G_3 to a Toeppler pump. Since the bore of S_3 is included in the measurement of V_2, no errors are caused by gases trapped in stopcocks.

Table I gives essential data for computing the composition of the standards made. The purity of the gases was measured with a mass spectrometer, known mixtures of pure argon and air being employed to calibrate the mass spectrometer for making the gas analyses. Since highly enriched A^{36} and A^{40} were employed, it was not necessary to know the isotopic compositions to an extremely high accuracy. Nevertheless, any systematic spectrometer errors which existed while measuring the original enriched samples were reduced to negligible proportions by subsequent calibration of the instrument with the standard samples.

The four standard samples were actually made at different times, three different persons being involved. Table II gives the results of the calculations based on the data in Table I. As a check on the reliability of the mixing and calibrating procedures all four of the samples were run on the mass spectrometer MS2 within a period of a few hours, two sets of ten ratios being obtained for each sample. The calculated-to-measured ratios were tabulated and averaged as noted. The difference between 1.0000 and 0.9937 is believed to be due to a mass discriminating effect in the spectrometer. It was gratifying to see the close agreement between the individual calc./meas. ratios. Deviations in these were attributed to errors in the data in Table I and accordingly the original calculated values were recalculated to give the recalculated adopted values used in all of the work which follows. Although all samples were weighted equally in the averaging, extreme care was exercised in preparing and measuring A V and A VI and these may be slightly more accurate than

TABLE V. Comparison of mass spectrometer readings for standard argon and for oxygen from several sources.

Data taken with MS2 $36/40\times10^5$ Stand. A V	$34/32\times10^5$ Tank	$34/32\times10^5$ Air	$33/32\times10^6$ Tank	$33/32\times10^6$ Air
1083	415.3	417.5	754	761
1090	415.7	409.6	754	757
	411.4	407.9	760	764
1068				
Av. 1080.3±4.4	414.1±1.8	411.7±2.0	756.0±1.3	760.7±1.3
Corr. 1096 ±1.5	410.7±2.0	408.2±2.2	752.8±1.6	757.5±1.6
Data taken with MS1 Stand A I				
942	411.3	410.7	757	742
943	412.3	410.1	755	743
945	411.1	409.4	757	742
946				
Av. 944.0±0.6	411.6±0.3	410.1±0.2	756.3±0.5	742.3±0.3
Corr. 949 ±1.9	410.3±0.5	408.8±0.5	755.1±0.7	741.1±0.6
Weighted grand mean of data taken with MS1 and MS2	410.3±0.5	408.8±0.5	755 ±1	749 ±5*

* Data from two instruments assumed inconsistent. Final result unweighted.

TABLE VI. Comparison of mass spectrometer readings for standard argon and carbon dioxide from several sources.

Data taken with MS2 $A^{36}/A^{40}\times10^5$ Stand. A I	$45/44\times10^5$ C No. 2*	$45/44\times10^5$ C No. 3**	$46/44\times10^5$ C No. 2	$46/44\times10^5$ C No. 3
938	1190	1207	412	412
938	1206	1196	416	414
944	1194	1199	412	418
941				
Av. 940.0±1	1197±3	1201±2	413.3±0.9	414.7±1.2
Corr. 949 ±1.9	1194±3	1198±2	411.7±1.0	413.1±1.3
Data taken with MS1				
939	1186	1193	410	418
940	1197	1223	417	416
942	1196	1194	414	417
944				
Av. 941.2±0.9	1193±2.4	1203±7	413.7±1.3	417.0±0.4
Corr. 949 ±1.9	1191±3	1201±7	412.3±1.4	415.5±0.6
Weighted grand mean of data taken with MS1 and MS2	1192±2	1199±2	412 ±1	415 ±1

* Pre-Cambrian limestone, Champlain Valley, Adirondacks, New York.
** Jurassic limestone, Solenhofen, Bavaria.

the others. All errors given here and elsewhere in this paper are probable errors unless otherwise noted.

RESULTS

Argon

The synthetic argon isotope mixtures were employed to determine the isotopic composition of naturally occurring argon. Two sources of gas were studied. One was atmospheric argon obtained by passing air over hot lithium metal until essentially all the oxygen and nitrogen were removed. The second consisted of spectroscopically pure argon purchased from the Air Reduction Sales Corporation. In making analyses the procedure was to run the standard followed by each of the unknowns repeating this process at least three times. In each series of runs an extra run was made at the end on the standard. Each of the numbers given is the average of ten determinations, scanning of the spectrum being first in one direction and then in the other to eliminate effect of drift in intensity.

Table III gives the results obtained together with their probable errors. It appears that Airco argon contains slightly less A^{36} and A^{38} than atmospheric argon. The data on A^{38}/A^{40} taken on MS2 is discarded in the final computation. The machine was known to have a residual impurity mass 38 peak and although correction was made for it, one can never be certain that the size of a residual peak in an instrument does not change when a gas is introduced. The final adopted values for atmospheric argon correspond to percentage abundances of 99.600, 0.063, and 0.337 for A^{40}, A^{38}, and A^{36}, respectively. In earlier investigation the following values have been given for the percentage abundances: Vaughan, Williams, and Tate,[6] 99.67, $\cdots$, 0.33; Nier,[7] 99.633, 0.060, 0.307; Dibeler, Mohler, and Reese,[8] 99.57, 0.08, 0.35.

If one assumes the masses of A^{36} and A^{38} to be approximately the same as that of A^{40}, which has been given as 39.9751 ± 3,[9] and uses a conversion factor of 1.000278 in going from the physical to the chemical scale, one computes an atomic weight of 39.9493 ± 3 where the probable error is due entirely to the uncertainty in the atomic mass determination. The present International value is given as 39.944.

Nitrogen

In this case, room air was admitted directly into the mass spectrometer, no attempt being made to remove the oxygen. Table IV gives the results obtained. The N^{14}/N^{15} ratio found here, 273 ± 1, is to be compared with 274.5, computed from data of Urey and Murphy[10] on assumption $O^{16}/O^{18}=500$, 265 ± 8 given by Vaughan, Williams, and Tate,[6] and 265, given by Wahl, Huffman, and Hipple.[11] With an atomic mass of 14.00754 ± 2 [9] for N^{14}, and the conversion factor 1.000278 for going from the physical to the chemical scale, one computes an atomic weight of 14.00730 ± 2 for nitrogen. This is to be compared with the international value of 14.008.

Oxygen

As in the case of nitrogen, room air was admitted to the mass spectrometer. No effort was made to remove the nitrogen. Tank oxygen was also investigated. The results are shown in Table V. The close agreement between the 34/32 ratios found in the instruments suggests that the slight difference between atmospheric and "tank" oxygen is real. It is interesting to note that Thode[12] reports a difference of almost exactly the same magnitude and direction. The values 0.004088 and 0.000749 for the $O^{16}/O^{18}/O^{16}O^{16}$ and $O^{16}O^{17}/O^{16}O^{16}$ abundance ratios, respectively, yield the following percentage abundances for atmospheric oxygen isotopes: O^{16}, 99.759; O^{17}, 0.0374; O^{18}, 0.2039. The mean mass number is 16.004452 ± 7 and the conversion factor between the physical and chemical atomic weight scales (if atmospheric oxygen is used as a reference) is 1.0002783 ± 5. Due to the fact that the O^{18}/O^{16} oxygen isotope abundance ratio is known to vary in nature by some four percent,[13,14] care must be exercised in applying the factor given here. If the oxygen from limestone is considered, the factor given here should be nearly correct. On the other hand, if the oxygen from water or iron ores were employed, the O^{18} content may be almost four percent lower[13] and the conversion factor would be only about 1.000268. This computation takes no account of possible variations in O^{17} as yet unstudied. It is clear, however, in this example, and others, that the accuracy of measurement has now reached the stage where it is meaningless to speak of precise atomic weights unless the source of material is clearly defined. Recent results of other investigations on the oxygen isotope abundances include, for O^{16}/O^{18}: Mecke and Childs,[15] 630; Smythe[16] for oxygen prepared from PbO_2, 503 ± 10; Bleakney and Hipple[17] for over 100 samples, average is 500; Murphey[18] for tank oxygen, 500 ± 15; for O^{18}/O^{17}: Mecke and Childs,[15] 5; Murphey[18] for tank oxygen, 4.9 ± 0.2.

[6] Vaughan, Williams, and Tate, Phys. Rev. **46**, 327 (1934).
[7] A. O. Nier, Phys. Rev. **50**, 1041 (1936).
[8] Dibeler, Mohler, and Reese, J. Research Nat. Bur. Stand. **38**, 617 (1947).
[9] K. T. Bainbridge, National Research Council Preliminary Report No. 1, Nuclear Science Series (1948).
[10] H. C. Urey and G. M. Murphy, Phys. Rev. **38**, 575 (1931).
[11] Wahl, Huffman, and Hipple, J. Chem. Phys. **3**, 434 (1935).
[12] H. G. Thode, Report No. MC-57 National Research Council, McMaster University, Hamilton, Ontario (April 29, 1944). Results also reported by K. T. Bainbridge in Abstracts of Proceedings of Seventh Solvay Congress, Brussels (September 22–27, 1947).
[13] M. Dole and R. L. Slobod, J. Am. Chem. Soc. **62**, 471 (1940).
[14] H. G. Thode, Research **2**, 154 (1949).
[15] R. Mecke and W. H. J. Childs, Zeits. f. Physik **68**, 362 (1931).
[16] W. R. Smythe, Phys. Rev. **45**, 299 (1934).
[17] W. Bleakney and J. A. Hipple, Phys. Rev. **47**, 800 (1935).
[18] B. F. Murphey, Phys. Rev. **59**, 320 (1941).

TABLE VII. Comparison of mass spectrometer readings for potassium (Sylvite, New Mexico) and standard argon.

All data taken with MS2	$36/40\times10^5$ Stand. A I	K^{39}/K^{41}	K^{41}/K^{40}
Collector slit 0.025 in.	966	13.39	592
	949	13.40	587
		13.50	579
Av.	958±6	13.43±0.03	586±3
Corr.	949±1.9	13.37±0.06	587±4
Collector slit 0.015 in.	945±4	13.50	570
		13.59	572
Av.	945±4	13.55±0.03	571±1
Corr.	949±1.9	13.58±0.04	570±1
Unweighted average of two sets of data assuming inconsistency in data		13.48±0.07	578±6

Carbon

Two of the limestone samples studied earlier by Murphey and Nier[19] were used in the present work. The results are given in Table VI. Due to the fact that the molecule $C^{12}O^{16}O^{17}$ contributes to the mass 45 ion current, a correction must be made before the C^{13}/C^{12} abundance ratio can be found. The largest variation reported for the O^{18}/O^{16} ratio in nature has been four percent.[13] However, this ratio appears to be about the same in limestones and the atmosphere. Thus, it may be reasonable to arbitrarily assume that the O^{17} in the limestone studied here should not differ by as much as two percent from the value found for it in Table V. Thus, subtracting 0.00075±1.5 from each of the 45/44 ratios, one obtains $C^{13}/C^{12}=0.01117\pm3$ and 0.01124 ± 3 for samples No. 2 and No. 3, respectively. The average percentage C^{13} abundance for the two samples is then 1.108±4. The close agreement between the present results and the earlier ones of Murphey and Nier[19] indicates that any systematic errors present earlier, affecting the absolute answers, must not have exceeded one-half percent. With an atomic mass of 12.003856±19 for C^{12} [9] and a conversion factor of 1.000278 for going from the physical to the chemical scale, one computes an atomic weight of 12.01160±5 for carbon from limestone. A change of one percent in the C^{13}/C^{12} ratio will change this value by 0.0001. Thus, the greatest uncertainty in the atomic weight of carbon can be attributed to the uncertainty in the isotope abundance ratio in the particular substance under investigation. The present International value is given as 12.010.

Table VI gives also the 46/44 ratio (this is just twice the O^{18}/O^{16}) for the CO_2 analyzed. Since the CO_2 was released from the carbonate by treatment with acid in water and conditions were not under control so far as oxygen equilibrium is concerned no particular significance should be attached to the exact value found for the 46/44 ratio beyond the fact that it is approximately correct.

Potassium

In this case a sample of potassium metal prepared from New Mexico Sylvite was introduced in the small furnace of instrument MS2. For calibration purposes argon was allowed to leak into the instrument through a molecular leak. Whereas 75-volt electrons were employed for producing ions in all of the other work reported here, it was found necessary to use 7.5-volt electrons in the potassium study in order to be certain that possible impurities such as A^{40} did not contribute to the very rare K^{40}. The K^{39}/K^{41} ratio was found to be the same for 52.5- and 7.5-volt electrons. The calibration of the instrument with the standard argon sample was made with 52.5-volt electrons. Since the resolution of the K^{40} peak was not quite complete with the 0.025-in. final collector slit used in the spectrometer, a second set of data were accumulated with a slit 0.015 in. wide. The agreement appears satisfactory and the final values adopted for the isotope ratios are shown at the bottom of Table VII. These values correspond to percentage abundances of 6.91±0.04, 0.0119±0.0001, and 93.08 ±0.04 for K^{41}, K^{40}, and K^{39}, respectively. The most significant thing about the present study is that K^{40} appears to be about ten percent more abundant than previously[7,20–22] believed to be the case. This change will alter the half-life of K^{40} correspondingly. The K^{39}/K^{41} ratio agrees reasonably well with the recent value 13.66±0.1 given by White and Cameron.[23] Since these authors list in their paper all of the previous values given for this ratio, the reader is referred to their Table IV for details. Because of the uncertainty in the exact atomic masses of the isotopes an accurate atomic weight computation does not appear practical at this time.

The writer wishes to express his appreciation to Mrs. R. C. Boe and Mr. Craige Schensted for the assistance given in making the many careful measurements and computations required in this work. The separated argon isotopes were produced by E. G. Franklin and B. B. McInteer. The construction of the apparatus was aided materially by grants from the Graduate School and the Minnesota Technical Research Fund subscribed to by General Mills, Inc., *Minneapolis Star-Journal and Tribune*, Minnesota Mining and Manufacturing Company, Northern States Power Company, and Minneapolis Honeywell Regulator Company.

[19] B. F. Murphey and A. O. Nier, Phys. Rev. **59**, 771 (1941).

[20] A. O. Nier, Phys. Rev. **48**, 283 (1935).

[21] A. K. Brewer, Phys. Rev. **48**, 640 (1935).

[22] M. B. Sampson and W. Bleakney, Phys. Rev. **50**, 456 (1936).

[23] J. R. White and A. E. Cameron, Phys. Rev. **74**, 991 (1948).

Nuclear Energy Levels in Isotopes of Potassium

VANCE L. SAILOR*
*Sloane Physics Laboratory, Yale University,** New Haven, Connecticut*
(Received November 25, 1949)

Targets made from the separated isotopes K^{39} and K^{41} were bombarded by 3.90-Mev deuterons, and protons from the nuclear reactions $K^{39}(d,p)K^{40}$ and $K^{41}(d,p)K^{42}$ were observed. The energy distribution of the protons emitted in each reaction was obtained by measuring the proton yield as a function of range. The ground state Q-value for $K^{39}(d,p)K^{40}$ was found to be 5.48 ± 0.08 Mev, giving the mass difference $K^{40}-K^{39}=1.00070\pm0.00007$ mass units. Excited states of K^{40} were found at 0.81, 2.01, 2.56, 3.3, 3.7, 4.2, and 4.8 Mev. The ground state Q-value for $K^{41}(d,p)K^{42}$ was 5.12 ± 0.10 Mev, giving the mass difference $K^{42}-K^{41}=1.00109\pm0.00010$ mass units. Excited states of K^{42} were found at 0.62, 1.18, 1.97, and 2.29 Mev.

INTRODUCTION

NUCLEAR energy level schemes for K^{40} and K^{42} can be obtained by measuring the Q-values of the reactions $K^{39}(d,p)K^{40}$ and $K^{41}(d,p)K^{42}$. In 1940, Pollard[1] bombarded natural potassium with deuterons and observed three groups of protons giving Q-values of 5.6, 4.5, and 3.4 Mev. All three of these were attributed to the reaction $K^{39}(d,p)K^{40}$, because K^{39} is the most abundant of the potassium isotopes.

Natural potassium contains three isotopes in the following abundances:[2] $K^{39}=93.3$ percent, $K^{40}=0.01$ percent, and $K^{41}=6.7$ percent. It would be expected that d,p type reactions would result from each of the three isotopes in the target, because d,p reactions are generally exoergic and have reasonably large cross sections. It is possible to prove that a nuclear reaction occurs by observing the half-life of the activity produced in the target provided that the product nucleus is radioactive. In this manner the reaction $K^{41}(d,p)K^{42}$ has been identified[3] and measurements have been made of the total yield of K^{42} from deuteron bombardment of thick targets of natural potassium.[4,5] No such proof of the occurrence of $K^{39}(d,p)K^{40}$ can be obtained because the increased target activity due to the production of K^{40} is negligible. Likewise, $K^{40}(d,p)K^{41}$ cannot be detected by this method because K^{41} is stable.

Another method which has many advantages for detecting the occurrence of d,p reactions consists of studying the proton yield from targets enriched in the isotope in question. Comparison of the proton yield from the enriched target with the yield from a natural target usually shows at once whether or not the reaction occurs with appreciable cross section. The use of an enriched target also permits the assignment of the various observed Q-values to the proper isotope.

This paper is a report on the reactions $K^{39}(d,p)K^{40}$ and $K^{41}(d,p)K^{42}$ which were studied with the assistance of enriched targets.

APPARATUS AND PROCEDURE

Various targets of potassium were bombarded by the 3.90-Mev deuteron beam of the Yale cyclotron and the protons emerging from the target were observed with a proportional counter. The counter was placed at 90° from the direction of the deuteron beam. Protons from the target passed through several calibrated aluminum absorbers, a short air gap, then entered the counter. The aluminum absorbers could be changed by remote control so that the total absorption in the proton path was variable.

The energy of the deuteron beam was determined by measuring its range in an air absorption cell and converting the range into energy by means of the Cornell 1937 range-energy curves. The apparatus for observing the protons and measuring the beam range has been described previously.[6]

Curves of proton yield as a function of total absorption were obtained by varying the aluminum absorption in steps of 1-cm air-equivalent and observing the number of protons at each absorption. The cyclotron beam current was collected by the target and integrated. The counting interval was chosen to be the time required to accumulate a standard amount of beam current. Two types of yield curves were obtained: (A) "Integral Curves" obtained by counting all protons entering the counter (i.e., all pulses above noise); and (B) "Peaked Curves" obtained by counting only those protons giving the largest pulses (i.e., those protons which were very near the end of their range).

TABLE I. Isotopic abundance of natural potassium and enriched samples in percent.

	Natural potassium	Sample #346(a)†	Sample #348(a)†
K^{39}	93.3	96.5 ± 2.0	13.3 ± 0.5
K^{40}	0.01	$0.6^{+0.1}_{-0.6}$	$0.2^{+0.1}_{-0.2}$
K^{41}	6.7	3.0 ± 0.5	86.6 ± 1.0

† Sample number as designated by the Carbide and Carbon Chemicals Corporation.

* Now at Brookhaven National Laboratory, Upton, Long Island, New York.
** Assisted by the Joint Program of the ONR and the AEC.
[1] E. C. Pollard, Phys. Rev. **57**, 1086 (1940).
[2] W. Paul and M. Pahl, Naturwiss. **32**, 228 (1944).
[3] D. G. Hurst and H. Walke, Phys. Rev. **51**, 1033 (1937).
[4] E. C. Barker, MDDC-7, May, 1946.
[5] Clarke and Irvine, Phys. Rev. **70**, 893 (1946).
[6] V. L. Sailor, Phys. Rev. **75**, 1836 (1949).

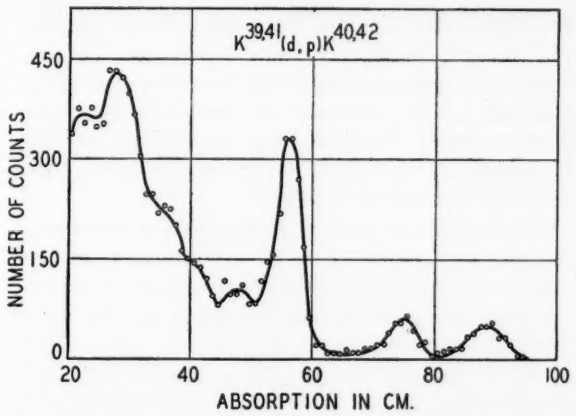

FIG. 1. The proton yield from a target of natural potassium bombarded by 3.90-Mev deuterons. Counting statistics are given approximately by the square root of the ordinate. The absorption is in cm air-equivalent.

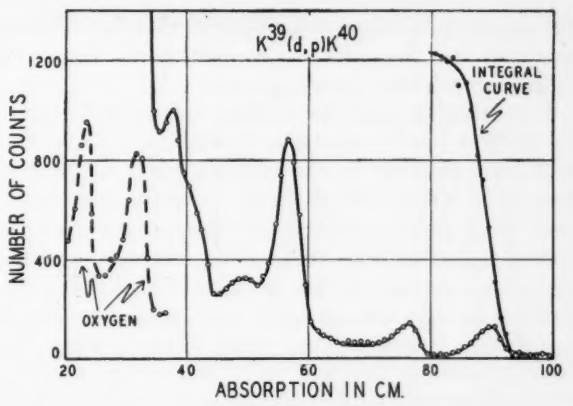

FIG. 2. The proton yield from a target enriched to 96.5 percent in K^{39}. The integral curve was used to calculate Q_0 for $K^{39}(d,p)K^{40}$. The dashed curve is due to oxygen contamination and has been reduced by a factor of ten relative to the solid curve.

Integral curves (type A) were used to determine the Q-value of the longest range group of each reaction, and therefore to calculate the mass difference between the target and residual nucleus. Peaked curves (type B) were used for determining the group structure of the shorter range protons, and hence to obtain the energy level schemes.

The extrapolated range of each proton group was determined graphically and this range was used to compute the Q-value according to the procedure outlined by Livingston and Bethe.[7] The computations take into account the variation in the stopping power of aluminum with energy, proton straggling, and the effect of observing over a finite solid angle for the case of "good geometry." In addition a small correction was applied for the effect of the proton range of the inhomogeneity of the deuteron beam, according to the method developed recently by H. T. Motz and R. F. Humphreys.[8]

PREPARATION OF TARGETS

The quality of the target is a primary factor in determining the results of the study of a nuclear reaction. The target should be uniform and thin so as to permit maximum resolution, but must be thick enough to give usable counting rates. It is important of course to keep the target free of contaminations. For these studies the targets were prepared by depositing thin layers of potassium metal or potassium iodide on gold foil by evaporation in high vacuum.

Three types of potassium were used: Natural potassium, potassium enriched in K^{39}, and potassium enriched in K^{41}. The relative concentrations of the isotopes in these three types are listed in Table I.

The targets of natural potassium were prepared from several different samples of the metal, the iodide and the chloride. The use of a variety of samples from independent sources reduced the possibility of the presence of some unsuspected impurity which might give large proton yields. The proton yield curves from all the targets of natural potassium were identical with the exception of those made from the metal, which always contained large amounts of oxygen. Target thicknesses varied from 0.5 to 2.0 mg/cm^2.

Two samples of enriched isotopes were supplied by the Carbide and Carbon Chemicals Corporation and obtained on allocation from the Stable Isotopes Division, AEC. The mass spectroscopic analysis furnished with the samples is given in Table I. Both of the enriched samples were in the form of KCl, which is not suitable for use as a target because of the copious yield of protons from chlorine. A method was devised for preparing targets from the KCl which eliminated the chlorine and in the same step gave thin uniform deposits of potassium or potassium iodide. The KCl was mixed in stoichiometrical proportions with calcium metal filings and placed in a small glass oven in a vacuum chamber. A nichrome filament was sealed in the walls of the oven to permit the contents to be heated without allowing contaminations from the filament to reach the target. When the mixture in the oven was heated to about 400°C in high vacuum, potassium vapor was released through a $\frac{1}{4}$-inch opening at the top of the oven and condensed on the gold target foil placed about 2 cm above. The gold foil was cooled from behind by a brass block through which water circulated. A baffle system surrounded the oven and target to trap any of the valuable potassium sample which failed to condense on the target. After the potassium had condensed on the target a small amount of iodine vapor was admitted to the chamber and served to convert the thin potassium deposit on the target to potassium iodide. The potassium iodide targets could be exposed to air without damage while transferring the target from the evapora-

[7] M. S. Livingston and H. A. Bethe, Rev. Mod. Phys. 9, 245 (1937).

[8] H. T. Motz and R. F. Humphreys (to be published).

tion apparatus to the cyclotron target chamber. Targets produced in this manner contained no detectable chlorine or calcium contamination.

The gold foil used for making the targets was of the highest purity available commercially. 3.90-Mev deuterons produce no appreciable yield of protons from gold. Experimental studies were made to determine what proton yield could be expected from the surface contaminations of the gold which was processed in the same way as the targets. It was found that at 90° observation the proton yield was negligible. At 0° observation, however, two long range groups were present but with very low yield. These were found to be due to nitrogen contamination on the front and back surfaces of the gold foil. Also at 0° small yields from the $O^{16}(d,p)O^{17}$, $C^{12}(d,p)C^{13}$, and $D^2(d,p)T^3$ reactions were located.

The yield from a PbI_2 target was observed and found to be negligible indicating that iodine contributed nothing to the proton yield from KI targets.

PROTON YIELD FROM NATURAL POTASSIUM

A typical proton yield curve taken at 90° with a target of natural potassium iodide is shown in Fig. 1. Several unsuccessful attempts were made to obtain better resolution of the group structure at ranges less than 40 cm by using thinner targets and a more homogeneous beam. It appears that many groups from both K^{39} and K^{41} isotopes lie in this region with small spacing and much better resolution will be necessary to separate them.

Several factors limit the resolution in range measurements; the most important being the straggling of the protons, the inhomogeneity of the deuteron beam and the thickness of the targets. These factors cause a proton group to have a half-width of about 3 cm at 30 cm range increasing to about 4 cm at 100 cm range. The half-width is the group width at one-half the maximum. If the resolution is defined as being the half-width in cm air-equivalent divided by the range, then the resolution is about 4 percent at 100 cm and 10 percent at 30 cm.

Several runs were taken at 0° observation and the relative intensities of some of the shorter range groups were sufficiently different from the relative intensities at 90° to assist in the location of the groups. Targets of several different specimens of potassium metal and potassium iodide were used for these observations and the same group structure was consistently obtained. The groups with peaks at 88, 75, and 56 cm are those previously reported by Pollard.[1]

Some early data taken at 0° observation indicated the presence of two long range groups having Q-values of 8.2 and 7.6 Mev. These values were incorrectly reported in a previous abstract[9] as belonging to one of the potassium d,p reactions. Subsequent data showed however that these two groups are due to the nitrogen contamination on the front and back surfaces of the gold foil as mentioned above and are not due to potassium.

PROTON YIELD FROM K^{39}

The proton yield from the $K^{39}(d,p)K^{40}$ reaction is shown in Fig. 2. The target for this curve was prepared from sample #346(a) (Table I) enriched to 96.5 percent in K^{39}. Comparison with Fig. 1 shows that the three most prominent long range groups belong to $K^{39}(d,p)K^{40}$ as previously assigned by Pollard.[1] An extensive search was made at longer ranges for additional groups but none were found, so the group with a peak at 88 cm is apparently due to the formation of K^{40} in the ground state. The Q-value corresponding to this group was calculated from the integral curve in Fig. 2. From this Q-value the mass difference between K^{40} and K^{39} may be calculated giving: $K^{40}-K^{39}=1.00070\pm0.00007$ mass units.

Excited states in the K^{40} nucleus were obtained from the several groups in the peaked curve (Fig. 2, solid curve), because the groups at ranges shorter than 88 cm correspond to the formation of K^{40} in excited states. The excitation energy and the Q-values of each level are listed in Table II.

In Fig. 2 the group structure at ranges less than 40 cm is badly distorted by the presence of oxygen. The potassium target used for this curve was allowed to oxidize. The two peaks due to $O^{16}(d,p)O^{17}$ are shown in Fig. 2 as the dashed curve and have been reduced by a

TABLE II. Q-values from $K^{39}(d,p)K^{40}$ and energy levels in K^{40}. The proton yield relative to the longest range group is given in the last column. The assignment of Q_6 to this reaction is uncertain.

	Q	Energy levels in K^{40}	Relative proton yield
Q_0	5.48±0.08 Mev	0 Mev	1.0
Q_1	4.67±0.09	0.81±0.03	1.1
Q_2	3.47±0.09	2.01±0.03	6.7
Q_3	2.92±0.10	2.56±0.05	2.4
Q_4	2.2 ±0.1	3.3 ±0.1	2.4
Q_5	1.8 ±0.1	3.7 ±0.1	3.8
Q_6	*1.3 ±0.1*	*4.2 ±0.1*	*7.4*
Q_7	0.7 ±0.1	4.8 ±0.1	6.5

TABLE III. Q-values of $O^{16}(d,p)O^{17}$ obtained from oxidized K^{39} target. Q_1 is probably too high because Q_7 of $K^{39}(d,p)K^{40}$ falls at approximately the same range and was not resolved.

	Q	Energy levels in O^{17}	Relative proton yield
	This report		
Q_0	1.94±0.08 Mev	0 Mev	1.0
Q_1	1.13±0.10	0.81	1.14
	Heydenburg *et al.*[10]		
Q_0	1.90 Mev	0 Mev	
Q_1	0.99	0.90	

[9] V. L. Sailor, Phys. Rev. **75**, 1292 (1949).

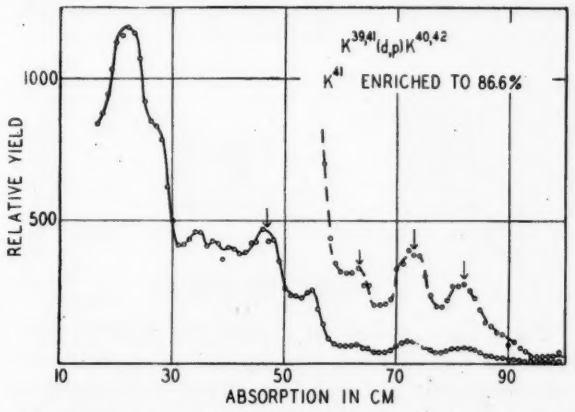

FIG. 3. The proton yield from a target enriched in K^{41} to 86.6 percent but containing also 13.3 percent of K^{39}. The arrows indicate the peaks of proton groups attributed to $K^{41}(d,p)K^{42}$. The dashed curve has been magnified by a factor of four.

factor of ten relative to the rest of the curve. The shorter range oxygen peak almost coincides with the potassium group Q_7 and is therefore somewhat distorted toward longer ranges. The $O^{16}(d,p)O^{17}$ reaction can be used as a reference reaction because it has been observed in many different experiments at many laboratories. Table III lists the Q-values calculated for the oxygen reaction from Fig. 2 and compares them with the results of Heydenburg *et al.*,[10] which are probably the most reliable values at present.

The energy level spacing in K^{40} is similar to the spacing found for other nuclei of odd Z and even A. For example Al^{28} obtained from $Al^{27}(d,p)Al^{28}$, and Cl^{38} from $Cl^{37}(d,p)Cl^{38}$ show spacings of approximately 1 Mev between the lowest levels with the spacing between levels decreasing rapidly with increasing excitation.[11,12]

The most striking feature of the proton yield curve is the relative intensity of the four longest range groups. The ratios of the proton yields for the groups are: Q_0 (88 cm):Q_1(75 cm):Q_2 (56 cm):Q_3 (48 cm)=1:1.1:6.7:2.4. If the requirements for the conservation of angular momentum are considered for the *ground* state it is seen that the incident deuterons or the emerging protons (or both) must have large orbital angular momentum, because the spin of K^{39} is $\frac{3}{2}$ and the spin of K^{40} ground state is 4. Thus the cross section for the production of K^{40} in the ground state is reduced. This suggests that the level Q_2 has a spin such that the conservation of angular momentum is most easily satisfied; i.e., a spin of 2, which would permit an s-deuteron to produce an s-proton. Similar reasoning indicates that the spin of the level Q_1 is 3, and of Q_3 is 1.

PROTON YIELD FROM $K^{40}(d,p)K^{41}$

The mass difference between K^{40} and K^{41} computed from several related nuclear reactions[6] is about 0.9981 mass units, indicating that the most energetic protons from the $K^{40}(d,p)K^{41}$ reaction would have a range between 120 and 150 cm for bombarding deuterons of 3.9 Mev. Because of the absence of other protons at such a long range the presence of the $K^{40}(d,p)K^{41}$ protons could be detected with this apparatus if as much as 0.1 percent of K^{40} were in the target (assuming that the cross section for the reaction is of the same order of magnitude as for the $K^{39}(d,p)K^{40}$ reaction). A careful search for the long range protons was made using a target prepared from sample #346(a) which contained $0.6\,^{+0.2}_{-0.6}$ percent K^{40}. No protons were found. It appears that a target with greater enrichment of K^{40} will be necessary to verify the reaction.

PROTON YIELD FROM $K^{41}(d,p)K^{42}$

The occurrence of the $K^{41}(d,p)K^{42}$ reaction has been verified many times by the presence of the radioactivity of K^{42} in the irradiated target. Q-values from this reaction have not been obtained previously because of the low abundance of K^{41} in targets of natural potassium. Sample #348(a) enriched in K^{41} to 86.6 percent was used as a target to obtain the Q-values. The proton yield resulting from this target is shown in Fig. 3. Because the target contained 13.3 percent of K^{39} it was necessary to subtract out the yield due to this isotope. This operation was performed by normalizing Fig. 2 to fit the 56-cm peak in Fig. 3 and then subtracting.

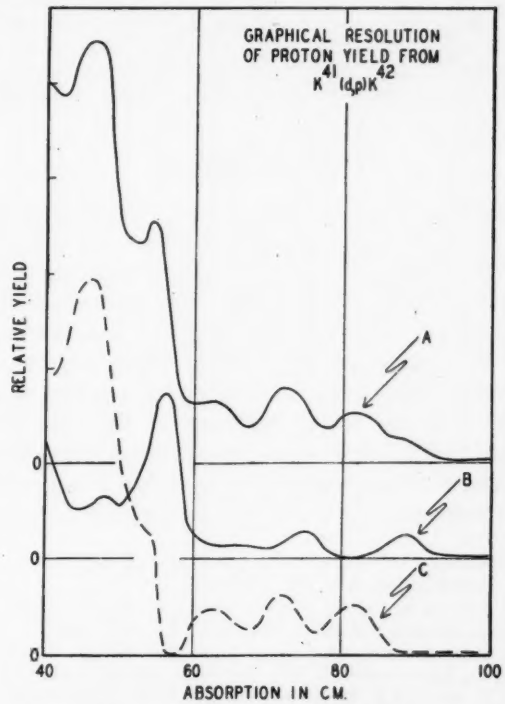

FIG. 4. Graphical resolution to about $K^{41}(d,p)K^{42}$ proton yield. Curve B (from Fig. 2) was subtracted from curve A (from Fig. 3) to obtain curve C, which is the proton yield of $K^{41}(d,p)K^{42}$. Curve B was normalized to A at the peak occurring at 56 cm.

[10] Heydenburg, Inglis, Whitehead, and Hafner, Phys. Rev. **75**, 1147 (1949).
[11] Pollard, Sailor, and Wyly, Phys. Rev. **75**, 725 (1949).
[12] E. F. Schrader and E. C. Pollard, Phys. Rev. **59**, 277 (1941).

The resultant curve is shown in Fig. 4 (curve *C*) and is the proton yield attributed to $K^{41}(d,p)K^{42}$. The *Q*-values calculated from this curve are less accurate because of the graphical subtraction. An additional curve of the $K^{41}(d,p)K^{42}$ spectrum of protons was obtained by comparing the yield from a target of natural KCl with the yield from a KCl target enriched in K^{41}. This curve verified the results shown in Fig. 4, curve *C*.

The *Q*-values from $K^{41}(d,p)K^{42}$ are listed in Table IV. The mass difference between K^{42} and K^{41} computed from Q_0 is $K^{42}-K^{41}=1.00109\pm0.00010$ mass units.

The spacings between the levels in K^{42} are similar to those in K^{40} and the relative yields of the proton groups show similar variations. Many more levels in K^{42} exist above Q_3 but the proton spectrum was so complicated that they could not be accurately located with the available resolution.

TABLE IV. *Q*-values from $K^{41}(d,p)K^{42}$ and energy levels in K^{42}.

	Q	Excitation of K^{42}	Relative proton yield
Q_0	5.12±0.10 Mev	0 Mev	1
Q_1	4.50±0.12	0.62±0.07	1.2
Q_2	3.94±0.12	1.18±0.07	0.9
Q_3	3.15±0.18	1.97±0.15	0.9
Q_4	2.83±0.12	2.29±0.07	7.5

ACKNOWLEDGMENTS

The author wishes to express his appreciation to Professor E. C. Pollard who suggested this problem and who constantly assisted with valuable discussion and advice. Professor R. F. Humphreys and H. T. Motz also contributed much valuable information the treatment of data.

Low Energy Beta-Ray Spectra: Pm^{147} S^{35} *

L. M. LANGER, J. W. MOTZ, AND H. C. PRICE, JR.
Department of Physics, Indiana University, Bloomington, Indiana
(Received November 7, 1949)

The beta-spectra of S^{35} and $_{61}Pm^{147}$ have been measured in order to study further the nature of any low energy deviation from the Fermi theory of beta-decay. Measurements were made with thin, relatively uniform sources in both the 40-cm radius of curvature spectrometer and also in a small 180 degree focusing Helmholtz coil spectrometer designed specifically for low energy spectra. The thinnest sources were less than 10 micrograms/cm². Using Zapon counter windows ranging from 15 to 3 micrograms/cm² and also a windowless counter technique, Fermi plots were obtained which showed how the measured distribution of particles at low energy depends on both source and counter window thickness.

Favorable experimental conditions yielded a straight line Fermi plot for Pm^{147} above 8 kev. Less favorable conditions resulted in a straight line plot for S^{35} down to at least 50 kev. Thus, S^{35}, which is allowed, and Pm^{147}, which is probably once forbidden, are found to have spectra of the allowed shape. It is concluded that under very favorable experimental conditions there is probably no real disagreement between the observed momentum distribution and that predicted for an allowed transition by the Fermi theory. On the basis of an improved calibration, the following end points are obtained: Pm^{147}, 223.2±0.5 kev and S^{35}, 167.0±0.5 kev.

I. INTRODUCTION

RECENT experimental investigations,[1–4] particularly of the beta-ray spectra of Cu^{64}, Cu^{61}, N^{13}, and S^{35}, have suggested possible deviations from the Fermi theory in the low energy region. Some experiments[3, 5–7] indicated that this excess of low energy particles might be a function of source thickness. Other experiments showed no observable increase in the number of low energy particles as the thickness of the source was varied.[2] Still other investigations[8–10] resulted in straight line Fermi plots extending to quite low energies even when extremely thick sources were employed.

Further studies in the low energy region were undertaken in order to clarify this question and in order to try to determine the extent to which instrumentation may distort the shape of a spectrum. Some instrumental effects which may influence the shape of a spectrum at low energies are: source thickness and uniformity, source backing, scattering from the residual gas and walls of the spectrometer chamber, distortion of the analyzing field by saturation or remanence, counter window thickness, and counter response as a function of particle energy. In the present investigation, thin and relatively uniform sources deposited on extremely thin backings were employed, and the experiments were designed so as to make the other possible distortion factors negligible. Detailed measurements were made on the spectra of the allowed S^{35} transition (87 day) and the empirically once forbidden Pm^{147} transition (3.7 year) under favorable experimental conditions in both the 40-cm radius of curvature spectrometer[11] and in a small Helmholtz coil spectrometer designed specifically for low energy measurements.

* Assisted by the Joint Program of ONR and AEC.
[1] J. Backus, Phys. Rev. **68**, 59 (1945).
[2] C. S. Cook and L. M. Langer, Phys. Rev. **73**, 601 (1948).
[3] Cook, Langer, and Price, Phys. Rev. **74**, 548 (1948).
[4] C. S. Cook and L. M. Langer, Phys. Rev. **74**, 227 (1948).
[5] R. D. Albert and C. S. Wu, Phys. Rev. **74**, 847 (1948).
[6] C. S. Wu and R. D. Albert, Phys. Rev. **75**, 1107 (1948).
[7] L. Feldman and C. S. Wu, Phys. Rev. **76**, 697 (1949).
[8] P. W. Levy, Phys. Rev. **72**, 248 (1947).
[9] D. Saxon, Phys. Rev. **74**, 849 (1948).
[10] D. E. Alburger, Phys. Rev. **75**, 1442 (1949).
[11] L. M. Langer and C. S. Cook, Rev. Sci. Inst. **19**, 257 (1948).

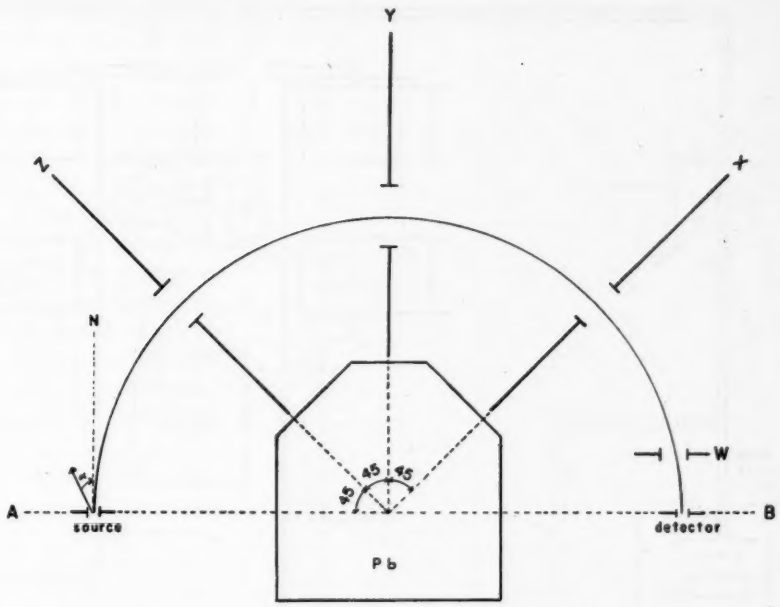

FIG. 1. Schematic arrangement of baffles and slits in small Helmholtz coil spectrometer.

II. EXPERIMENTAL METHOD

A. The Helmholtz Coil Spectrometer

The feasibility of using a windowless Geiger counter in a spectrometer to measure low energy spectra was first investigated. This necessitates a constant supply of gas to the counter and rapid pumping to remove the diffusing gas from the spectrometer proper. To this end, ethyl alcohol at 20-mm Hg pressure was used as the counting medium. This was supplied by evaporation from a constant temperature bath controlled at 23°C at which the vapor pressure of alcohol is 45 mm. The adjustment to a dynamic pressure of 20 mm was made with a Hoke valve and monitered with a manometer.

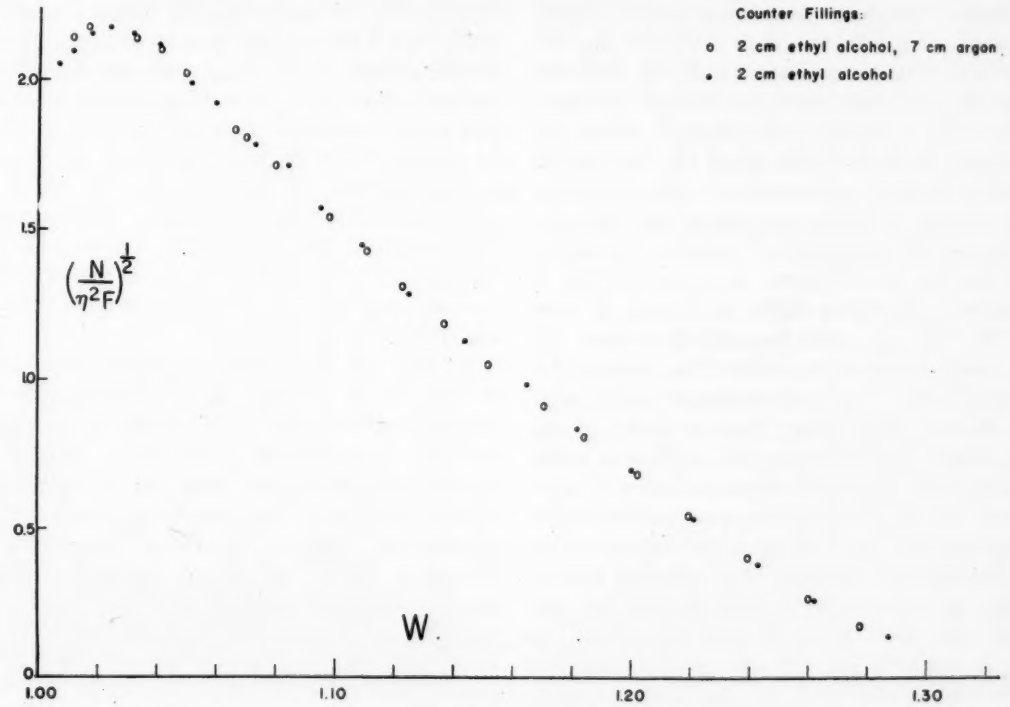

FIG. 2. Fermi plot of momentum distribution of C^{14} electrons. The open circles are for data recorded with a counter filled with a normal mixture of 2-cm alcohol plus 7-cm argon. The closed circles are for data obtained under identical conditions except that the counter filling was 2-cm alcohol only.

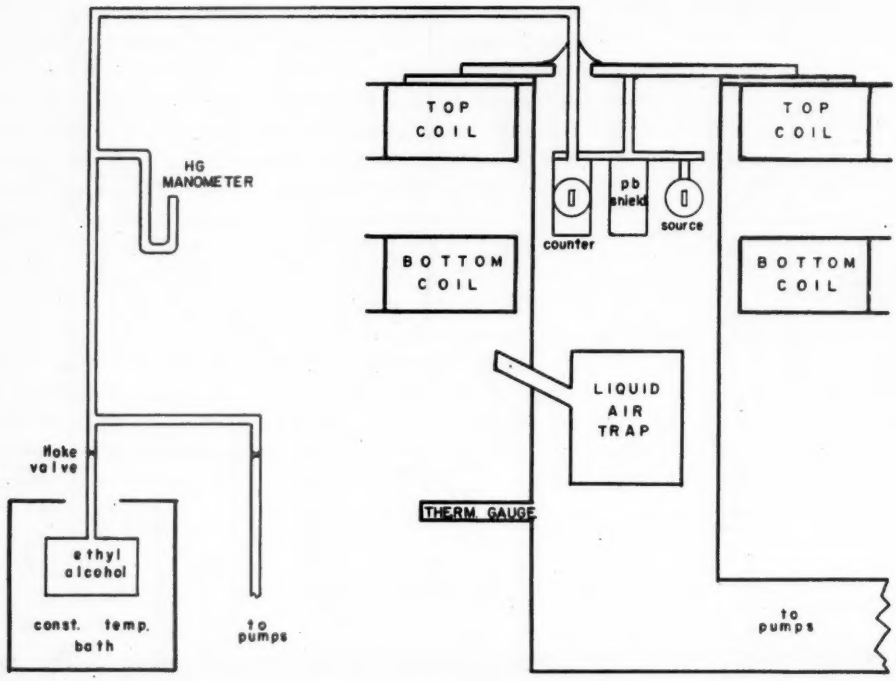

FIG. 3. Schematic arrangement of components in Helmholtz coil spectrometer.

Instead of a window, a detector slit 0.5 mm×10 mm located in the side of the counter separated it from the main spectrometer chamber. Pumping continuously with a liquid air trap and an oil diffusion pump, the pressure gradient was measured to be such that the constant pressure of 20-mm Hg in the counter dropped to 0.1-mm Hg at a distance 0.8 mm away and to a fairly constant value somewhat less than 0.01-mm Hg for distances greater than 20 mm from the slit. An approximate integration indicated that this pressure gradient was equivalent to a window thickness of about 1.5 micrograms/cm². A mean radius of 5.0 cm was chosen for the electron path so as to avoid excessive scattering of the beam by gas molecules. At this radius, electrons with an energy of 230 kev can be focused by the maximum available field of 360 gauss. As shown in Fig. 1, aquadag coated polystyrene baffles Z, Y, and X were placed at 45°, 90°, and 135° respectively to line AB joining the source and detector slits. The defining slit is contained in baffle Y, while the baffles Z and X, with slit widths about $\frac{1}{32}$ inch larger than the width of the beam, help reduce wall scattering. An additional baffle W was located near the counter slit to reduce wall scattering further. The fact that the top and bottom of the spectrometer are far removed from the beam is also helpful in minimizing scattering. Other possible sources of scattering in a conventional spectrometer are the edges of the slits and baffles. In this case, since the instrument is designed for use only at low energies, these edges could be restricted to a thickness of $\frac{1}{8}$ inch. With a 2-mm wide source, the resolution was calculated to be 2.5 percent. The experimental resolution of the thorium B line, which was used for calibration, was 2.6 percent for the full width at half-maximum. The transmission of the spectrometer was calculated at 0.1 percent.

Helmholtz coils were used to produce the field since they avoid the effect of residual ferromagnetism at the weak fields employed. Each coil was layer wound with 15,600 turns of round No. 22 Formex wire on brass spools with a rectangular cross section 3.25 inches×3.84 inches. Optimum coil separation was found to be 125 mm between coil centers. Under these conditions the field in the median plane showed a variation of less than 0.1 percent in the 20-mm range about the 50-mm mean radius, and no measurable variation within 10 mm above and below the median plane. The current for the Helmholtz coils was provided by an electronic constant current supply such that the coil current could be held constant over a period of at least an hour to better than one part in ten thousand.

It was calculated that counters filled with ethyl alcohol at 20-mm Hg should count with constant efficiency all electrons with energies up to at least 200 kev. In a preliminary experiment, an end window counter with its window removed was placed directly above a C^{14} source in a small vacuum chamber. The counter was tested with alcohol fillings ranging from 10-mm to 40-mm Hg, all of which gave satisfactory results. The counter plateau ranged from 50 to 100 volts depending on the pressure and purity of the alcohol vapor. For a high enough operating voltage and pure alcohol vapor the pulses were clean and of uniform height. The operating voltage for an alcohol filling of 20 mm was 1100 volts. Total efficiency was first checked in the above arrangement by establishing that the

same total number of counts was recorded in a given time by the counter filled with alcohol vapor (at 20 mm) and by the counter filled with the normal mixture of 20-mm alcohol and 70-mm argon. A check on the counter efficiency as a function of energy over the range up to 150 kev was accomplished by comparing the beta-spectra of C^{14} obtained in the Helmholtz coil spectrometer with its side window counter filled to the same pressures as used above in the end window counter.

A Fermi plot of the C^{14} spectrum for each case is shown in Fig. 2. It is apparent from the close agreement of the two curves (no adjustments were made) that the alcohol counter may be considered 100 percent efficient up to at least 150 kev. The shape of the Fermi plot in this case has no absolute significance since the source used was thick.

The counters used in the spectrometer were cylindrical side window counters with an inside diameter of 1 inch and a length of 3.625 inches. The central wire was 0.005-inch diameter tungsten. Side window counters offer a more positive detection of low energy particles than end window counters because of the finite distance particles must travel past an end window to feel the full electric field. For the windowless counter the slit was 0.5 mm by 10 mm covered by copper Lektromesh[12] grid, 0.004 inch thick having 0.006 inch openings which yields a transmission of 23 percent. Similar counters were used with Zapon windows down to 3 micrograms/cm²; however, in this case the slit was 10 mm by 2.0 mm.

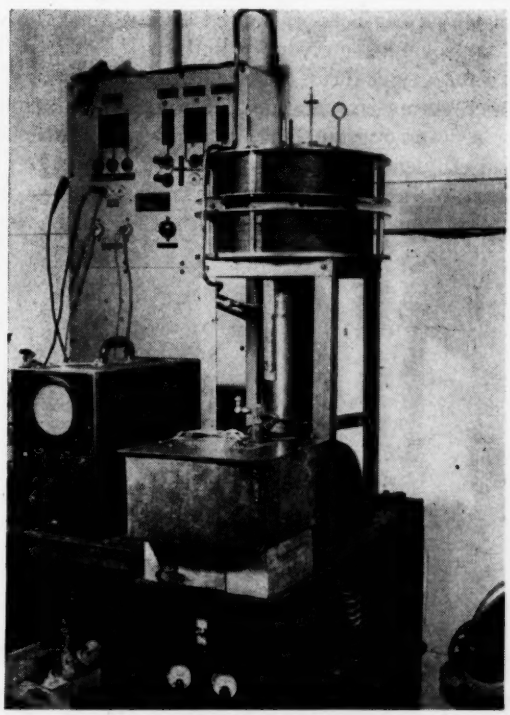

FIG. 4. Helmholtz coil spectrometer.

[12] Obtainable from C. O. Jelliff Manufacturing Corporation, Southport, Connecticut.

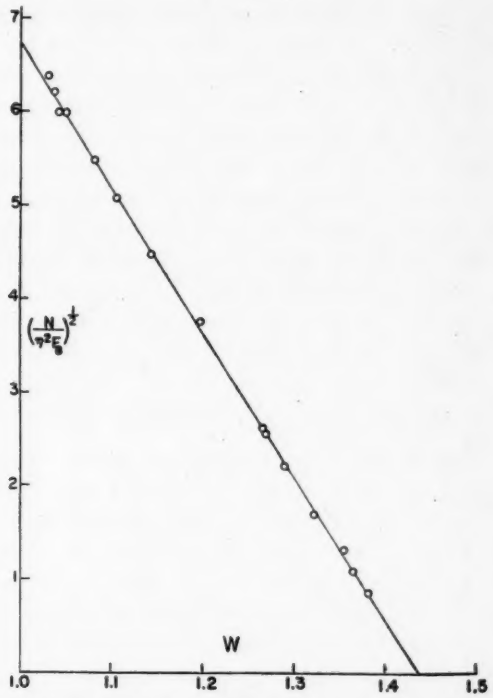

FIG. 5. Fermi plot of data for Pm^{147} spectrum obtained with the large shaped field spectrometer using a 6-microgram/cm² window supported on a Lektromesh grid. The source was about 10 micrograms/cm² thick.

It was possible to make counters with Zapon windows as thin as 1.5 micrograms/cm². However, the excessive rate of diffusion through such windows makes the counters inconvenient to use unless special means are taken to keep the pressure constant.[13] Figure 3 shows a schematic drawing of the experimental arrangement. Figure 4 shows a photograph of this spectrometer.

B. The 40-Cm Radius of Curvature Spectrometer

This spectrometer was adjusted for a resolution of 0.5 percent.[11] Spectra were recorded with counters having Zapon windows of 6 micrograms/cm² and 3 micrograms/cm² supported by a Lektromesh[12] grid or a Lucite-tantalum combination of a type described elsewhere.[11] The counters with the thinner windows were filled with a mixture of 20-mm ethylene and 10-mm argon, and the others at higher pressures.

In addition to its high resolution, this spectrometer is particularly suited for low energy measurements because of negligible wall scattering and a large source area (4 mm×25 mm at the above resolution) which makes it possible for a source of given intensity to be spread relatively thin.

[13] Ter-Pogossian, Robinson, and Townsend, Rev. Sci. Inst. 20, 289 (1949).

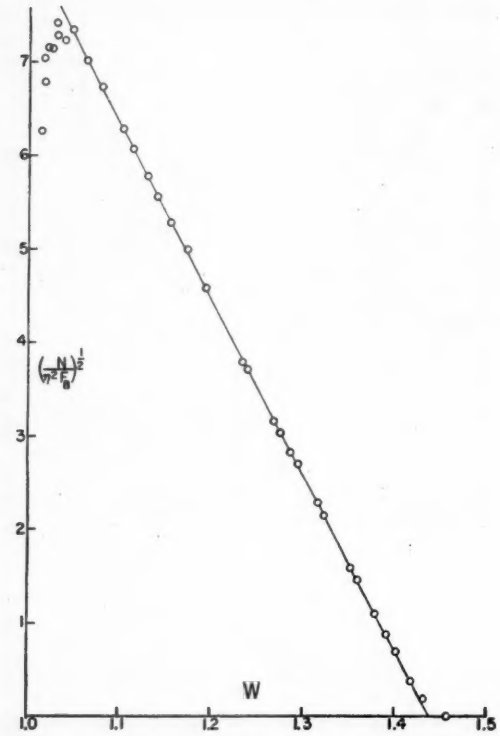

FIG. 6. Fermi plot of the Pm^{147} spectrum obtained with the large shaped field spectrometer using a tantalum grid and a 6-microgram/cm² Zapon window. The source was about 10 micrograms/cm² thick.

C. Preparation of Sources

In view of the conflicting reports in the literature on the effect of source thickness, we made a study of autoradiographs of sources prepared from chemical solutions. By this technique it was found that in general such sources, though appearing uniform, may in many cases have variations of intensity of as much as one hundred-fold. Under these circumstances the *average* source thickness as reported by various investigators does not have much meaning. We are not as yet able to deposit completely uniform sources from chemical solution. Our best technique consists of wetting the portion of the backing foil on which the source is to be placed with one drop of 5 percent solution of Lilly Insulin (40 units per cc) in water. A drop of radioactive solution applied any place in this area will spread over the entire region defined by the insulin. In the case of water solutions, it seems to be of no consequence whether or not the insulin layer is first dried. However, after the application of the radioactive material we find it best to quickly dry the source under an infra-red lamp, preferably while gently agitating (rocking) the liquid sample in order to prevent the formation of large crystals. Calibration of the medium Eastman Kodak lantern slide plates used for obtaining autoradiographs showed that sources could be made in this manner which were uniform to within a factor of four. In every case a narrow strip of 0.18 milligram/cm² grounded aluminum leaf was placed near the end of the deposit to minimize electrostatic effects of the source's charging on the dielectric film.

In the case of the narrow 1-mm and 2-mm sources for the Helmholtz coil spectrometer the width was controlled by applying full strength insulin from a stainless steel stylus. With the aid of a ruling jig, the stylus was placed directly above the Zapon film so that a suspended drop of insulin just touched the film, and finally, by moving the stylus across the film a narrow insulin line was obtained. A small drop of the liquid source was then applied and dried as before. Fairly uniform sources are easily made on larger areas by covering the region with narrow insulin lines and putting a small drop of liquid source on each. Extremely uniform sources can, if the activity permits, be successfully prepared by thermal evaporation in vacuum.

III. RESULTS

A. The 40-Cm Radius of Curvature Shaped Field Spectrometer

Figure 5 shows the Fermi plot for the spectrum of Pm^{147}. N is the number of particle per minute per unit momentum interval normalized to constant detector slit acceptance by dividing the actual number detected at any magnetic field strength by the value of the field. η is the electron momentum in units of m_0c and W is the electron energy in units of m_0c^2. F_B is the Coulomb factor which has been evaluated by means of the very good approximation given by Bethe and Bacher.[14] This data is for a typical run obtained with a source of about 10 micrograms/cm² and a Lektromesh grid counter with a 6-microgram/cm² window and filled with 20-mm ethylene and 10-mm argon.

Figure 6 shows data from the same source recorded in a tantalum grid counter with the same window

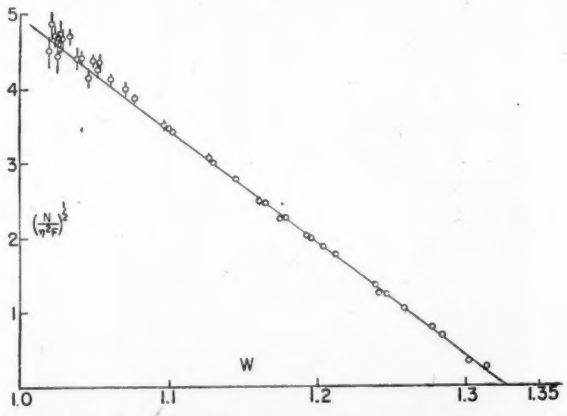

FIG. 7. Fermi plot of the S^{35} spectrum obtained with the large shaped field spectrometer using a tantalum grid and a 6-microgram/cm² window. The source was about 10 micrograms/cm² thick.

[14] H. A. Bethe and R. F. Bacher, Rev. Mod. Phys. 8, 194 (1936).

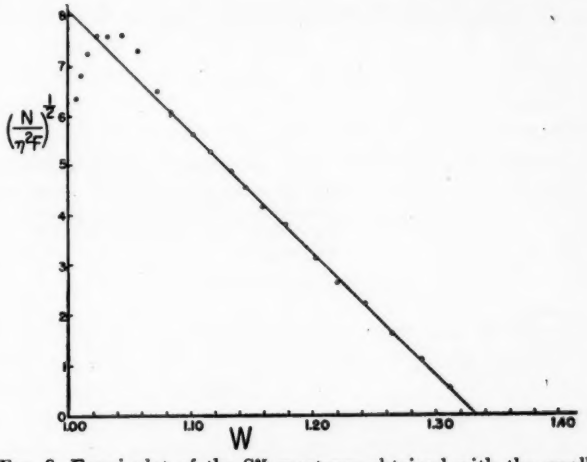

FIG. 8. Fermi plot of the S^{35} spectrum obtained with the small Helmholtz coil spectrometer.

thickness but filled to a higher pressure. The Fermi plot is certainly straight back to at least 20 kev and the end point is well determined at 223.2±0.5 kev (both verified by several other runs not shown). This may be compared with the 223 kev reported by Levy.[15]

Figure 7 shows the Fermi plot of the data for S^{35} obtained with a source of 10 micrograms/cm². One sees this plot is straight in agreement with the Fermi theory from the end point to energies at least as low as 50 kev, a lower value than was obtained with thicker sources.[3] Wu and Albert[5] report a rise at 100 kev for a source of 5 micrograms/cm² which may occur because of the difficulty of preparing uniform sources from chemical solutions as previously discussed in this paper. The new value of the end point of 167.0±0.5 kev is based on an improved calibration of the instrument. This may be compared with the 166 kev found by Wu and Albert.[5]

B. The Helmholtz Coil Spectrometer

Figure 8 shows the Fermi plot for the S^{35} spectrum obtained with a source of about 50 micrograms/cm² and a Zapon counter window of 3 micrograms/cm². The end point obtained with the large instrument is confirmed and the plot appears straight back to 40 kev.

Figure 9 shows Fermi plots obtained with the above counter for various thicknesses of Pm^{147} sources. The

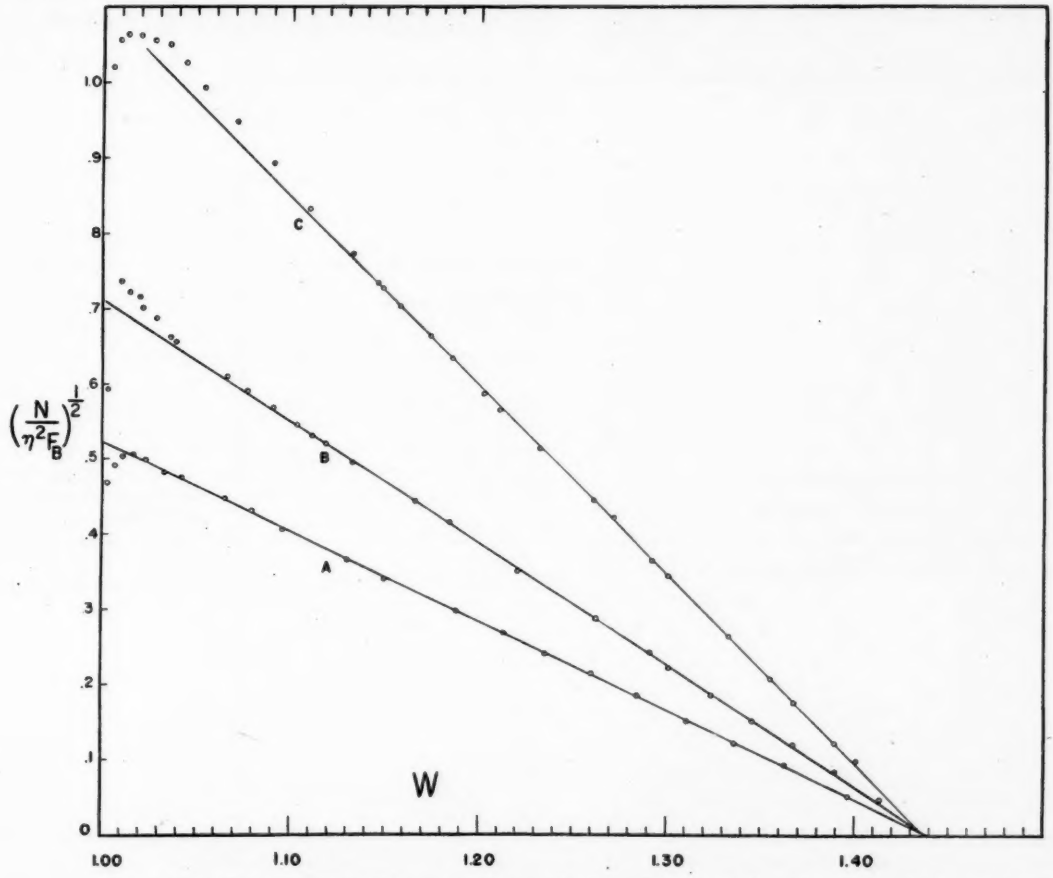

FIG. 9. Fermi plots of the Pm^{147} spectra obtained in the small Helmholtz coil spectrometer from sources of different thickness. Curve *A* is for a source somewhat less than 11 micrograms/cm². Curve *B* is for a source of about 43 micrograms/cm². Curve *C* is for a source somewhat thicker than 50 micrograms/cm².

[15] P. W. Levy, Plutonium Project Report, Mon. P-228, p. 29 (December, 1946).

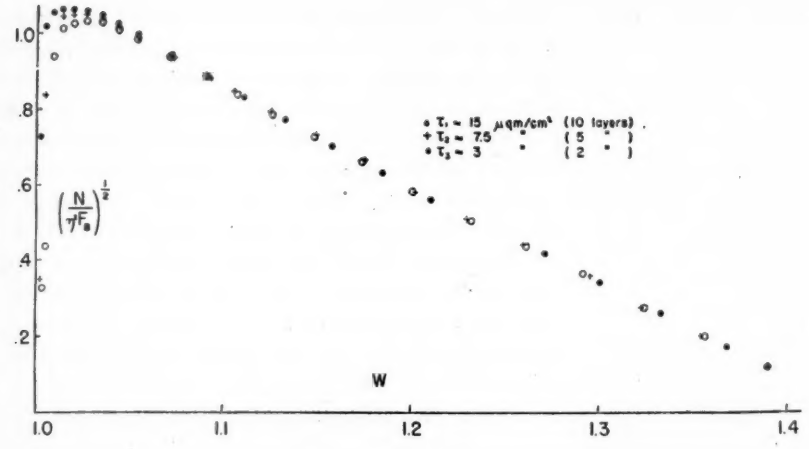

FIG. 10. Fermi plot of Pm^{147} spectra obtained in the small Helmholtz coil spectrometer showing effect of counter window thickness.

backings were all 1.5 micrograms/cm² Zapon. For the thinnest source, less than 11 micrograms/cm², there is no deviation from the straight line allowed shape above 8 kev. As the source thickness is increased the energy at which a deviation occurs also rises. The value of the end point is well confirmed.

Figure 10 shows the effect of window thickness on the measured spectral distribution of Pm^{147}. These data were taken with the thickest source (somewhat thicker than 50 micrograms/cm²) shown in Fig. 9. One sees clearly the expected effect of increased particle absorption at low energies for increasing counter window thickness.

For the same source, Fig. 11 compares the observed distribution with and without counter window. The Fermi plot of the data taken with a 3-microgram/cm²

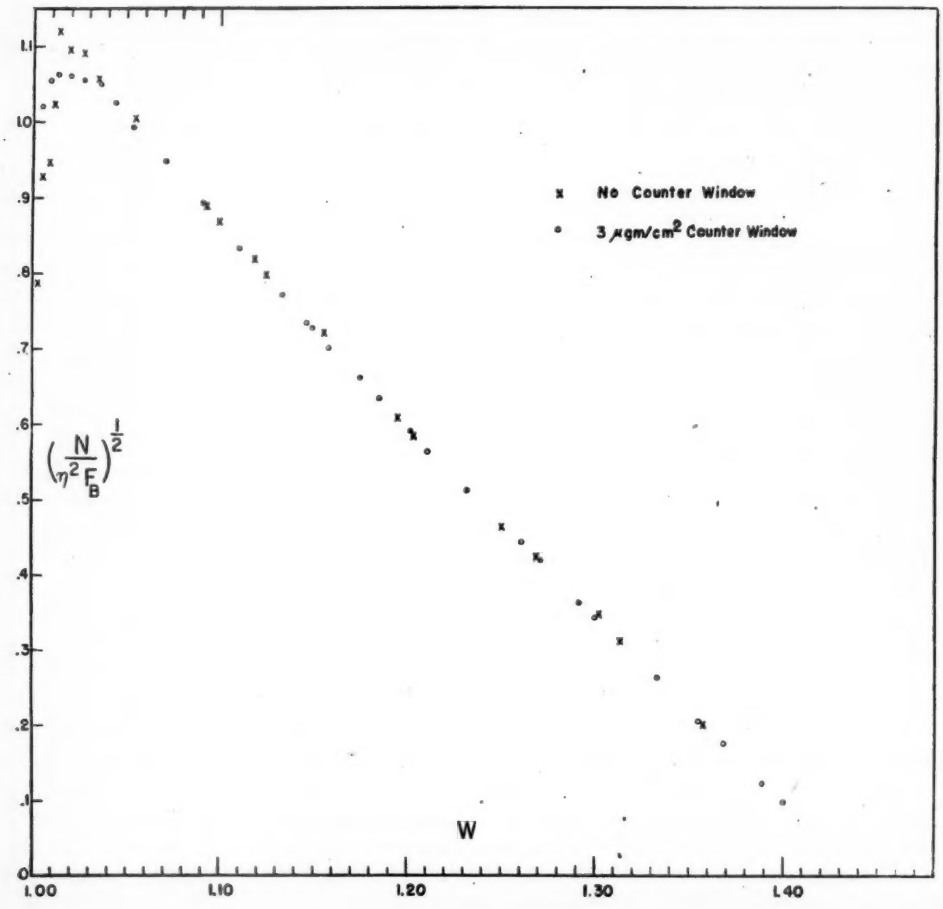

FIG. 11. Fermi plot of Pm^{147} spectra obtained in small Helmholtz coil spectrometer with a 3-microgram/cm² window and with the windowless counter.

window is in good agreement with that obtained with no window down to about 8 kev, where noticeable window absorption apparently sets in. The windowless counter continues to accept most electrons down to about 6 kev where the diffusing gas seems to become effective as a "window." The crossing of the curves at extremely low energy is probably not real but arises from poor statistics at the lowest energies.

IV. CONCLUSIONS

Fermi plots of the beta-spectra of S^{35} and Pm^{147} yield extrapolated end points of 167.0±0.5 kev, and 223.2 ±0.5 kev, respectively.

The S^{35} spectrum is in agreement with the Fermi theory for an allowed transition at least for energies above 50 kev. Wu and Albert[5] found the excess of particles at low energies to be a function of source thickness. For an average source thickness reported at 1 microgram/cm² their curve appears straight back to at least 20 kev. Coupled with the present findings on the effect of source thickness, S^{35} appears to offer no contradiction to the Fermi theory.[16]

The Pm^{147} Fermi plot is indistinguishable from a straight line for all energies above 8 kev. Empirically forbidden with a $ft=4.3\times10^7$, it is probably at most once forbidden since an allowed shape is highly improbable for higher forbidden transitions.[17] An allowed shape for a once forbidden transition may be taken to infer that the spin change is not two units which would be expected to lead to the unique first forbidden shape found recently.[18]

According to the nuclear shell scheme of M. G. Mayer,[19] the disintegration of $_{61}Pm^{147}$ into $_{62}Sm^{147}$ may be described as a transition from a $g_{7/2}$ to a $h_{9/2}$ state involving a change of parity. This is consistent with a once forbidden transition involving a spin change of one unit.

Thin uniform sources are difficult to prepare, and their attainment can be most reliably confirmed by some measurement of the relative activities of the various parts of the source, such as the autoradiographs described, coupled with a mass determination. Reasonably uniform sources can be made by the method described and extremely uniform sources result from thermal evaporation in vacuum.[16] Inasmuch as sources prepared by chemical deposit may in general be extremely non-uniform, the *average* thickness as reported in different laboratories does not have much absolute meaning. This undoubtedly accounts for the different results found at low energy by different observers working with sources which were reported to be of comparable *average* thickness.

Counters filled with ethyl alcohol at a pressure of 20-mm Hg can detect electrons up to at least 220 kev with 100 percent efficiency. This filling may be used with Zapon counter windows of 3 micrograms/cm² without excessive diffusion. Windowless counters of 100 percent efficiency may be used under the conditions of our experiment with an "effective window" of as little as 1.5 micrograms/cm². Some electrons with energies less than 1 kev are detected by both methods.

Thickness of counter window has the qualitatively expected effect at low energies of increasingly absorbing more particles as the window is made thicker. A 1.5-microgram/cm² "effective window" shows no indication of spectral disturbance above 6 kev; a 3-microgram/cm² Zapon window, none above 10 kev; a 6-microgram/cm², none above 20 kev; a 7.5-microgram/cm², none above 30 kev; a 15-microgram/cm², none above 80 kev. It is interesting to note that under certain conditions a thick counter window can just cancel the excess of low energy particles which arises because of source thickness. Partial transmission through the corners of a counter window supporting grid may have the same effect.

This work was partially supported by a grant from the Frederick Gardner Cottrell fund of the Research Corporation and by the Joint Program of ONR and AEC. The radioactive S^{35} and Pm^{147} were obtained from Oak Ridge.

[16] Since the completion of the work reported in this paper, measurements made on Cu^{64} with extremely thin and uniform sources prepared by evaporation of metallic copper in vacuum show no disagreement with the Fermi theory. Langer, Moffat, and Price, Phys. Rev. **76**, 1725 (1949); G. E. Owen and C. S. Cook, Phys. Rev. **76**, 1726 (1949).

[17] E. J. Konopinski and G. E. Uhlenbeck, Phys. Rev. **60**, 308 (1941).

[18] L. M. Langer and H. C. Price, Jr., Phys. Rev. **76**, 641 (1949).

[19] M. G. Mayer, Phys. Rev. **75**, 1969 (1949).

Yields and Angular Distributions of Some Gamma-Neutron Processes*

G. A. PRICE AND D. W. KERST
University of Illinois, Urbana, Illinois
(Received December 14, 1949)

Measurements of $\gamma-n$ yields for 53 elements have been made using betatron bremsstrahlung with maximum energies of 18 Mev and 22 Mev. The neutron flux was observed by a rhodium detector and compared with a standard Ra-Be neutron source. In the region from $Z=22$ to $Z=83$ the $\gamma-n$ yield in neutrons per mole per r of radiation is observed to be 2270. $Z^{2.1}$ when the bremsstrahlung spectrum has a 22-Mev maximum energy. The regularity of neutron yield as a function of atomic number indicates a definite similarity in the $\gamma-n$ cross-section curves for neighboring heavy elements. The trend of the observed yields is in rough agreement with the yields predicted by Goldhaber and Teller. Estimates are made of the fractions of thorium and uranium atoms which undergo photo-fission.

Angular distributions of photo-neutrons using bremsstrahlung with a 19.7-Mev maximum energy show no spherical asymmetry greater than the probable error for iron and lead whereas deuterium and beryllium have maxima at 90°.

MOST measurements of $\gamma-n$ cross sections have required the detection of a beta-activity following the emission of a neutron. Previous experiments can be classified according to the type of gamma-rays used. Wäffler and Hirzel[1] have measured the relative $\gamma-n$ cross section for 35 isotopes using the 17.5-Mev gamma-ray from the lithium (p,γ) reaction. High energy bremsstrahlung from betatrons have been used by McElhinney[2] and by Friedlander and Perlman.[3] These cross-section measurements have been restricted to those isotopes which have a detectable beta-decay following the $\gamma-n$ reaction.

An alternate method for cross-section measurements is to measure the number of neutrons emitted in the $\gamma-n$ process. This has been done at low gamma-energies in measuring the angular distribution of neutrons[4] from light elements. A similar method is described below for measuring the absolute neutron yields and angular distributions.

Bremsstrahlung from the betatron with maximum energies of 18 Mev and 22 Mev were used for the absolute $\gamma-n$ yields and 19.7 Mev for angular distributions. Samples consisted of natural isotopic mixtures, usually of a single element. The only enriched sample was deuterium oxide. Some of the samples were chemical compounds in which cases corrections were made for the presence of undesired elements. Most of the samples were chemical reagents with a high degree of purity. Sample weights varied from 54.5 grams to 567 grams.

The detector was a rhodium foil in a large paraffin block placed in a double wall Lucite box. The $\frac{1}{4}$-in. space between the walls was filled with B_4C. Fast neutrons from the irradiated sample pass through the B_4C, are moderated by the paraffin, and as slow neutrons are captured by the rhodium (Fig. 1). The 44-second beta-activity in rhodium is observed with a Geiger counter. The standard procedure was to irradiate the sample for three minutes, wait 30 seconds, and measure the Rh beta-activity for three minutes. Slow neutrons from the room were absorbed by the boron shield. Large paraffin blocks shielded the detector on all sides except the side facing the sample. A 24-inch concrete wall in front of the betatron shielded the detector from x-rays and also helped moderate the fast neutrons from the betatron.

A rhodium foil placed in a cavity of the concrete wall served as the x-ray monitor. The wall moderates fast neutrons from the betatron. Since the number of neutrons generated in the betatron is proportional to the x-ray intensity and is much greater than the number produced in the sample, the beta-activity of the monitor Rh foil is a good measure of the x-ray intensity. Since the detector and monitor integrate the neutron intensities with the same 44-second decay period, fluctuations in x-ray intensity do not have to be considered.

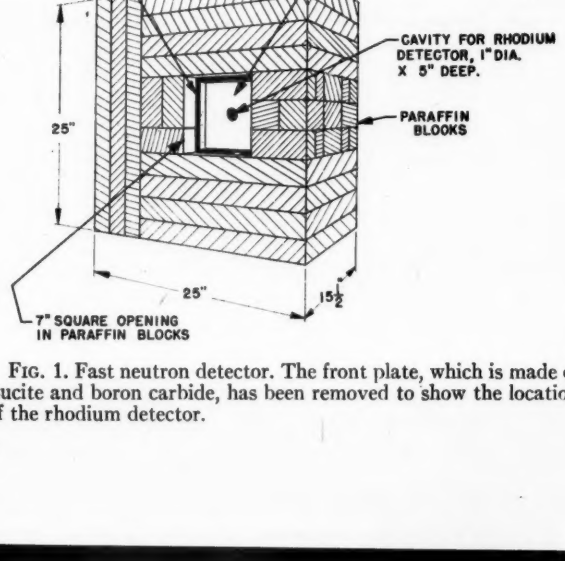

FIG. 1. Fast neutron detector. The front plate, which is made of Lucite and boron carbide, has been removed to show the location of the rhodium detector.

* This work was supported by the Joint Program of ONR and AEC.

[1] Wäffler and Hirzel, Helv. Phys. Acta, **21**, 200 (1948).
[2] J. McElhinney *et al.* (not published).
[3] G. Friedlander and M. L. Perlman, Phys. Rev. **74**, 442 (1948); Phys. Rev. **75**, 988 (1949).
[4] Hammermesh, Hammermesh, and Wattenberg, Phys. Rev. **76**, 611 (1949).

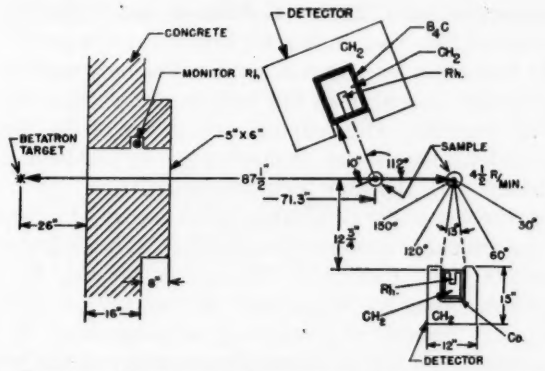

FIG. 2. Schematic diagram of apparatus. During measurements only one detector was in position at any time.

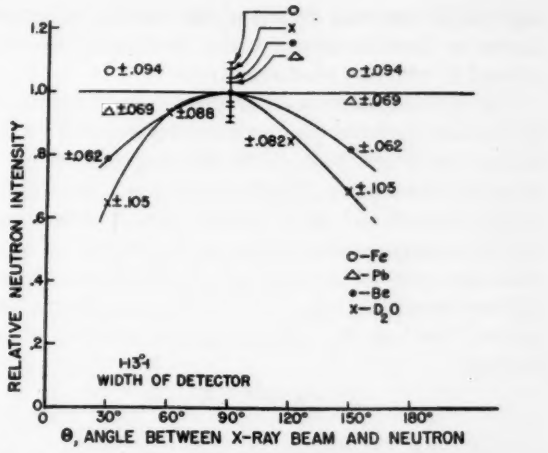

FIG. 3. Angular distributions of photo-neutrons for bremsstrahlung spectrum with maximum energy of 19.7 Mev. Intensities are normalized at 90° and probable errors are given for each point.

A 25-mg standard radium-beryllium neutron source was used to calibrate the neutron detector by placing it at the normal sample position. The x-ray monitor was calibrated by putting a thick walled Victoreen ionization chamber at the normal sample position.

Neutron background was measured by removing the sample completely from the x-ray beam. The sample was supported by fine wires to minimize the background.

Corrections for x-ray absorption in the sample were made assuming monochromatic x-rays for 13.73 Mev, using absorption coefficients by Adams.[5] Interpolations were made for those elements whose absorption coefficients had not been measured. The absorption correction factors varied from 1.00 to 1.97. This is the factor by which the observed neutron yield was multiplied to get the true neutron yield. If the absorption coefficient for 19.1 Mev is used instead, the corrected yields are changed by $5\frac{1}{2}$ percent for Hg and Mo which are the extreme cases but generally the change is less than 2 percent.

Probable errors were calculated on the basis of the counts registered by the Geiger counters. Each sample was tested at least twice and the variation in the neutron yields was generally within the statistical fluctuations to be expected on the basis of total counts.

There had been some indication that the neutron distribution from $\gamma-n$ processes was not spherically symmetrical. A rough test of this distribution was made for lead, iron, beryllium, and deuterium. The deuterium test with a 100-gram sample of heavy water was merely for the purpose of proving that asymmetries could be observed.

Neutron intensities were measured at various angles relative to the x-ray beam by a smaller detector which could be moved around. The detector subtended an angle of 13° from the sample, and could be moved from 30° to 150° with respect to the x-ray beam (Fig. 2). The probable error in the angular distribution values is relatively high because the small detector gave less activity in the rhodium foil and a lower sample to background ratio. The small detector had cadmium shielding, whereas the large detector had boron carbide shielding.

Neutron intensity distributions from deuterium and beryllium have a definite asymmetry with a maximum at 90°. In the cases of iron and lead any asymmetry is less than the probable error of the measurements. Figure 3 shows the angular distributions of neutrons from the four samples where they have been normalized at 90°. The probable error for each sample is also shown.

Figure 4 shows the absolute neutron yield expressed in neutrons per mole per r of radiation plotted against atomic number. The two sets of points represent measurements with the betatron operating at a maximum energy of 18 Mev and 22 Mev. The solid curves in the range from Z equals 22 to 92 show the best fit of the function aZ^b to the data. Between 82 and 92 the solid curves are supplemented by dotted curves which pass through the thorium and uranium yields. Below $Z=20$ curves have been drawn to indicate general trends only. In the region of low atomic number it appears that elements of odd and even atomic number behave quite differently. Probable errors are indicated by a vertical line through each point.

Figure 5 shows the gamma-neutron yields which have been obtained by McElhinney, Wäffler, and Hirzel, and Friedlander and Perlman. Neutron yields by McElhinney are absolute, whereas the other yields are relative and have been normalized at silver. These yields are due only to one isotope in each element, or in the cases where two isotopes of an element were used a weighted average was taken.

DISCUSSION

Two of the deviations of neutron yield from the general trend are for thorium and uranium. In each case the neutron yield seems to be much higher than the yield one would expect by extrapolating the curve found at lower atomic numbers. From these abnormally

[5] G. D. Adams, Phys. Rev. **74**, 1707 (1948).

high yields one can estimate the fraction of uranium atoms or thorium atoms which undergo photo-fission instead of emitting photo-neutrons.

The ratio, R, of the actual neutron yield for uranium to the extrapolated photo-neutron yield is 1.76 at 22 million volts and 1.64 at 18 million volts; while this ratio for thorium at 22 million volts is 1.36, and at 18 million volts it is 1.26. If the fraction of excited nuclei which undergo photo-fissions is K, and if we assume that the number of neutrons produced per fission is between two and three, say 2.5, then taking the extrapolated yield as the measure of the number of nuclei excited,

$$2.5\times K+(1-K)=R.$$

Solving for K, we obtain

$$K=(R-1)/1.5.$$

This branching ratio, K, is 0.51 for uranium bombarded by 22-million volt x-rays, 0.43 for uranium bombarded by 18-Mev x-rays, 0.24 for thorium bombarded by 22-million volt x-rays, and 0.17 for thorium bombarded by 18-million volt x-rays. Thus, about one-half of the disintegrating uranium atoms disintegrate by photo-fission and about one-fourth of the thorium atoms disintegrate by photo-fission.

The observed photo-neutron yields show such regularity as a function of Z that it is possible to make a comparison with theory. Goldhaber and Teller have estimated the cross section for excitation of a nucleus.[6] The excitation by γ-rays is supposed to be a resonance absorption in which all the protons are set into oscillation together. The resonance character of the γ-ray excitation process was demonstrated by Baldwin and Klaiber[7] with 100-Mev bremsstrahlung.

According to the Goldhaber-Teller theory, the energy of the resonance is proportional to $A^{-1/6}$. The theory also predicts that $\int\sigma dE\propto A$, the atomic weight. If the bremsstrahlung spectrum from the betatron contained the same number of photons at all frequencies up to the maximum, and if the maximum energy of the betatron exceeded the energies at which the excitation of the nuclei occurred, then the photo-neutron yields observed by an experiment such as ours would be expected to be proportional to $\int\sigma dE$. A rough test of the theory can be made by allowing for the real shape of the spectrum and by allowing for the fact that the upper energy limit of the bremsstrahlung spectrum is not high enough to include all of the resonance curves for all the nuclei tested. Since the *intensity* spectrum from the betatron decreases approximately linearly by a factor of three between zero energy photons and maximum energy photons, the *number* spectrum is

$$N\propto 3(E/h\nu)-2.$$

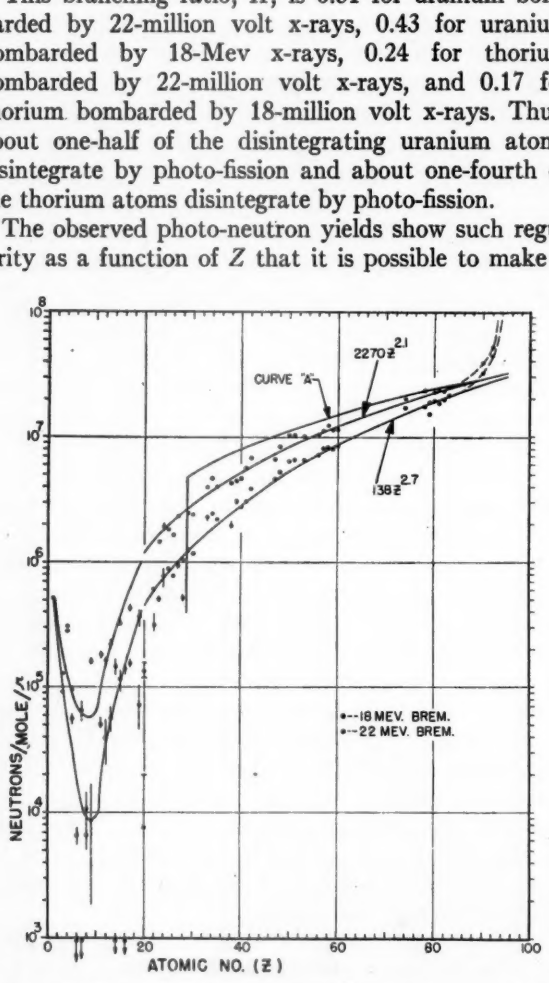

FIG. 4. Yields of photo-neutron sources for two bremsstrahlung spectra. Probable errors are shown by vertical lines through each point. Curve A is the yield predicted by Goldhaber and Teller which has been corrected for the 22-Mev bremsstrahlung spectrum and normalized at $Z=90$. The observed yield at $Z=29$ is about half the predicted yield because approximately half of the resonance is below 22 Mev.

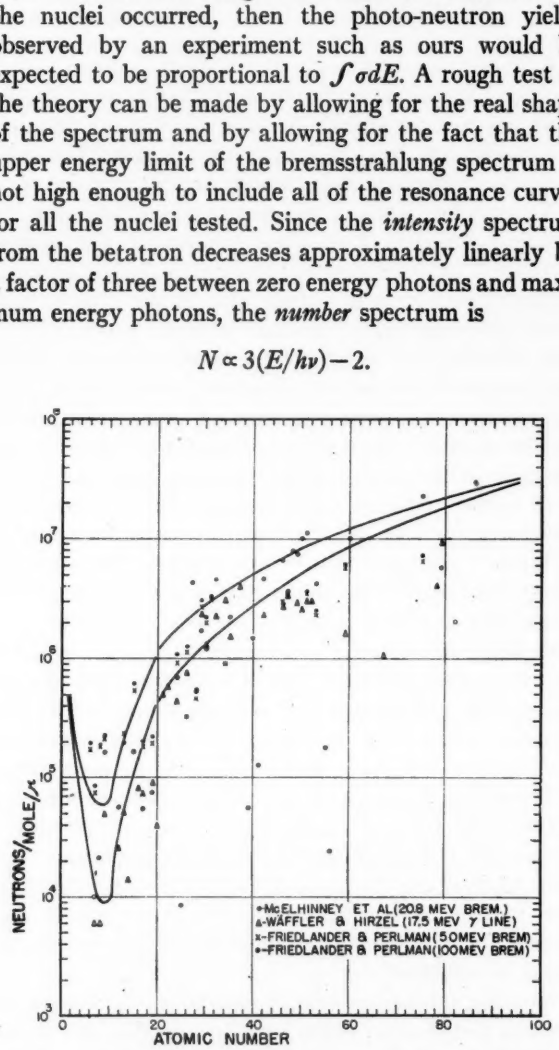

FIG. 5. Comparison of photo-neutron yields. Solid curves indicate results by Kerst and Price. The yields measured by McElhinney *et al.* are absolute whereas those measured by Wäffler and Hirzel, and Friedlander and Perlman are relative and have been normalized at $Z=47$.

[6] M. Goldhaber and E. Teller, Phys. Rev. **74**, 1046 (1948).

[7] G. C. Baldwin and G. C. Klaiber, Phys. Rev. **71**, 3 (1947); Phys. Rev. **73**, 1156 (1948). See also McElhinney, Hanson, Becker, Duffield and Diven, Phys. Rev. **75**, 552 (1949).

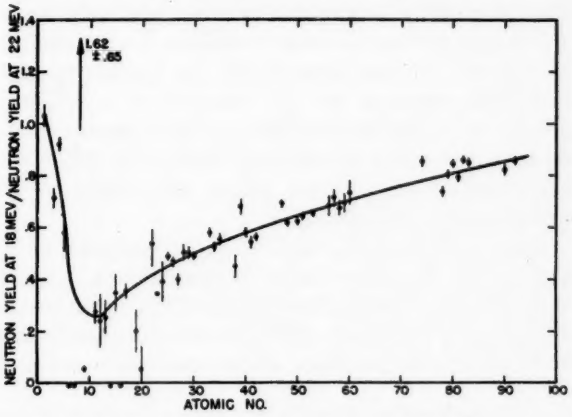

FIG. 6. Ratio of photo-neutron yields with 18-Mev and 22-Mev bremsstrahlung spectra.

For the sake of simplicity we now assume that the resonance is narrow. Then the yield $Y \propto N_{RES} \int \sigma dE \propto N_{RES} A$ but $N_{RES} \propto 3(A/A_0)^{1/6} - 2$, where A_0 is the atomic number for which the resonant energy, $h\nu_{RES}$, is equal to the upper limit of the bremsstrahlung spectrum, E. Then $Y \propto [3(A/A_0)^{1/6} - 2]A$.

Figure 4, curve A, shows this calculated yield with $Z_0 = 29$ for 22 Mev as is observed.[7] This curve has been made coincident with the extrapolated yield at $Z = 90$ assuming that all of the thorium resonance curve is below 22 Mev. One sees that at $Z = 29$, for copper, the calculated yield is 1.75 times the observed yield. This is approximately what is expected if half of the resonance curve for copper exceeds the upper limit of the bremsstrahlung spectrum. Thus to the rough approximation of these estimates the Goldhaber-Teller theory is in agreement with the observed yield. Levinger and Bethe[8] find $\int \sigma dE \propto ZN/A$. This gives approximately the same curve A.

It has not been possible to fit the yield curve by assuming Breit-Wigner resonance curves of widths 0 to 8 Mev and by assuming the threshold energy to be one-half of the resonance energy. The integrated cross section was kept proportional to A. The results follow the narrow resonance curve except in the vicinity $Z = 29$. Although the energy dependence of our neutron detector is not tested, it ought to be similar to the dependence for the "long counter."[9]

The ratio of yield for 18 Mev to the yield for 22 Mev, Fig. 6, shows that the resonance curves must have gradually varying shapes as a function of Z, because (above $Z = 20$) the ratio changes slowly with atomic number. Below $Z = 20$ the yields, and consequently the ratio of yields is strongly influenced by high thresholds.

Nickel yields for 18 Mev and for 22-Mev bremsstrahlung are each about 45 percent of the general trend. Chemical analysis shows 98.45 percent Ni, 0.86 percent Fe and traces of Sn and Sb. Thus impurities cannot be responsible for the low yields. The fact that the ratio for nickel (Fig. 6) is nearly the same as the ratio for neighboring elements suggests that the shape of the cross-section curve is not radically different for nickel, but it is possible to have a normal ratio with low yields as a result of high neutron binding energy and unusually large (γ,γ) or (γ,p) competition. It would be valuable to know the thresholds and the shapes of cross-section curves for nickel.

[8] J. S. Levinger and H. A. Bethe, Phys. Rev. **77**, 756 (1950).
[9] A. O. Hanson and J. L. McKibben, Phys. Rev. **72**, 673 (1947).

PHYSICAL REVIEW VOLUME 77, NUMBER 6 MARCH 15, 1950

Correlation of Geiger Counter and Hall Effect Measurements in Alloys Containing Germanium and Radioactive Antimony 124

G. L. PEARSON, J. D. STRUTHERS, AND H. C. THEUERER
Bell Telephone Laboratories, Murray Hill, New Jersey
(Received November 7, 1949)

The distribution of the solute atoms in ingots of germanium antimony alloys which were prepared according to a prescribed cooling cycle have been measured. The solute was Sb^{124} and its distribution was measured with a Geiger counter. In addition, Hall measurements were made which show that in the impurity saturation range each antimony atom contributes one conduction electron. This makes it possible to determine the solute distribution in non-radioactive samples by the Hall method.

I. INTRODUCTION

THE electric properties of germanium containing small amounts of antimony depend on the concentration of antimony present. In preparing the ingots they are slowly cooled to control the antimony separation which occurs on solidifying a binary alloy. Because of the small concentrations of the antimony, 10^{-2} to 10^{-6} percent by weight, it is impossible to determine quantitatively its distribution in the ingot by ordinary chemical or spectrochemical methods. The availability of a radioactive isotope of antimony (Sb^{124}) offers a solution to this problem.[1]

[1] A preliminary account of this work was presented by the authors at the American Physical Society meeting in Chicago (November, 1948); Phys. Rev. **75**, 344 (1949).

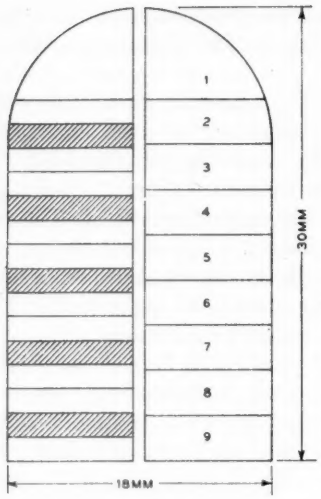

FIG. 1. Dimensions of germanium antimony ingots and method of cutting samples.

It is possible to determine the density of conduction electrons in semiconducting alloys such as these by means of the Hall effect. At low temperatures very few of the impurity antimony atoms are ionized and the density of conduction electrons is low. Raising the temperature increases the ionization and the density until a saturation value is reached around room temperature. A further increase in temperature has no effect on the electron density until one approaches the intrinsic range after which there is a rapid increase due to germanium atom ionization. Our measurements show that in the saturation range the antimony atom density is equal to the conduction electron density. We conclude that in this saturation range every antimony atom is ionized and each atom contributes one conduction electron.[2] Accurate quantitative analyses can therefore be made on germanium containing extremely small concentrations of antimony by either method.

II. PREPARATION OF SAMPLES[3]

The source of the germanium used in this study was germanium dioxide obtained from the Eagle-Pitcher Company, Joplin, Missouri. Reduction to the element was accomplished by heating in hydrogen. The Sb^{124} was obtained from the Isotopes Division, AEC, Oak Ridge, Tennessee, and was prepared by irradiating 0.2 gram of antimony metal in the pile. Such treatment gives a product containing approximately 4 millicuries of Sb^{124} having a half-life of 60 days and 55 millicuries of Sb^{122} having a half-life of 2.8 days. The irradiated material was stored for several weeks before using to allow the Sb^{122} activity to become relatively weak. Sb^{124} decays by two beta-ray emissions having energies of 0.53 and 2.25 Mev respectively, the low energy beta-emission is followed by the emission of a 1.72-Mev gamma-ray. The concentration of Sb^{124} present in the irradiated material as received from Oak Ridge was approximately one part per million with respect to the stable isotopes Sb^{121} and Sb^{123}.

Figure 1 shows the details of the preparation of the samples. A 50-gram charge of germanium, coarsely powdered, was thoroughly mixed with a given weight of powdered antimony (100 percent irradiated antimony for the more dilute alloys and irradiated antimony plus non-radioactive antimony for the more concentrated alloys). This charge was placed in a graphite crucible having an internal diameter of 18 mm and heated by an induction furnace in an atmosphere of helium. The furnace temperature was raised above the melting point of germanium and allowed to remain for 15 minutes after which the ingot was solidified by slowly raising the induction coil with the power applied. As a result solidification started at the bottom of the ingot and proceeded slowly upward, the total time of solidification being about 30 minutes. Since germanium expands on solidification a round dome was formed at the top. Melts containing 0.00078, 0.0081, 0.0086, and

TABLE I. Radioactive counts on top surface of slabs cut from germanium ingot H-308 to which 0.0086 percent antimony had been added.

Slab No.	Counts/minute
1	59,000
2	308
3	106
4	80
5	70
6	67
7	64
8	59
9	60

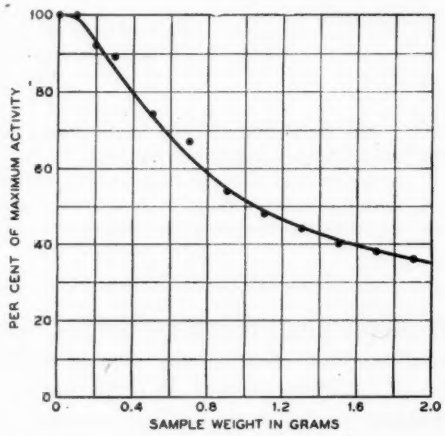

FIG. 2. Self-absorption correction for Sb^{124} in germanium antimony alloys.

[2] A similar conclusion has been drawn regarding silicon-boron and silicon-phosphorus alloys, G. L. Pearson and J. Bardeen, Phys. Rev. 75, 865 (1949).

[3] For a more detailed description of the preparation of germanium ingots see J. H. Scaff and H. C. Theuerer, "Preparation of high back voltage germanium rectifiers," N.D.R.C. 14-555 (October 24, 1945).

TABLE II. Distribution of antimony in germanium antimony alloy ingots.

Slab No.	7.8×10^{-4}% Sb added 2.09×10^{17} Sb atoms/cc			8.1×10^{-3} %Sb added 2.17×10^{18} Sb atoms/cc			5.39×10^{-2}% Sb added 1.44×10^{19} Sb atoms/cc		
	% Sb	Sb atoms per cc	% Sb added / % Sb present	% Sb	Sb atoms per cc	% Sb added / % Sb present	% Sb	Sb atoms per cc	% Sb added / % Sb present
1	6.18×10^{-3}	1.66×10^{18}	7.93	4.58×10^{-2}	1.23×10^{19}	5.66	6.56×10^{-1}	1.76×10^{20}	12.2
2	6.20×10^{-5}	1.66×10^{16}	0.0795	5.42×10^{-4}	1.45×10^{17}	0.0670	1.61×10^{-2}	4.32×10^{18}	0.300
3	2.28×10^{-5}	6.10×10^{15}	0.0292	2.54×10^{-4}	6.80×10^{16}	0.0314	1.47×10^{-3}	3.94×10^{17}	0.0272
4	1.49×10^{-5}	3.96×10^{15}	0.0192	1.56×10^{-4}	4.18×10^{16}	0.0193	9.68×10^{-4}	2.59×10^{17}	0.0180
5	1.21×10^{-5}	3.22×10^{15}	0.0156	1.15×10^{-4}	3.08×10^{16}	0.0142	8.63×10^{-4}	2.31×10^{17}	0.0160
6	7.7×10^{-6}	2.06×10^{15}	0.0101	8.37×10^{-5}	2.24×10^{16}	0.0103	5.07×10^{-4}	1.36×10^{17}	0.00942
7	5.2×10^{-6}	1.40×10^{15}	0.00666	6.01×10^{-5}	1.61×10^{16}	0.00745	4.12×10^{-4}	1.10×10^{17}	0.00765
8	4.6×10^{-6}	1.23×10^{15}	0.00590	5.79×10^{-5}	1.55×10^{16}	0.00714	3.39×10^{-4}	9.9×10^{16}	0.00630
9	8.2×10^{-6}	2.20×10^{15}	0.0106	1.07×10^{-4}	2.89×10^{16}	0.0132	5.05×10^{-4}	1.35×10^{17}	0.00936

0.054 percent antimony by weight were prepared in this manner. These were designated melts H-309, H-308, H-310 and H-311, respectively. A sample of the antimony used in each ingot was kept for calibrating the subsequent G-M counter measurements.

Each of the ingots was cut in half parallel to its long dimension with a diamond wheel. Nine semicircular slices were cut from right-hand sections and sixteen similar slices were cut from the left-hand sections as shown in Fig. 1.

III. RADIOACTIVITY MEASUREMENTS

A preliminary qualitative determination of the relative antimony distribution in the 0.0086 percent antimony ingot was obtained by the radioautograph technique. For this purpose the flat surface of a half-melt section (previous to slicing) was placed in contact with Ansco No-Screen x-ray film for 5.5 hours. The resulting radioautograph showed that a major portion of the antimony had concentrated near the top of the ingot, that is, in the last material to solidify. There was also indication of a slight concentration of antimony over the entire surface, particularly on the bottom surface of the ingot.

Additional data on the relative distribution of the antimony in the 0.0086 percent antimony ingot were obtained by making radioactive counts on each of the nine semicircular slabs after they had been cut as shown on the right of Fig. 1. Table I gives the number of counts per minute on each slab with the upper surface facing the G-M tube. It can be seen that more than 98 percent of the antimony is in the top section and that there is a marked decrease with depth. In the slabs nearest the top of the ingot there was a considerable difference in the count, and hence in the antimony concentration, from the top and bottom surfaces. For example, slab number 2 gave 308 counts per minute from the top surface and 163 counts per minute from the bottom surface. Slab number 9 gave 60 counts per minute from the top and 100 counts per minute from the bottom, thus substantiating the evidence obtained from the radioautograph that the antimony content tended to be higher at the surface than within the ingot.

It should be emphasized that these results give the relative distribution of antimony in the ingot. In order to obtain quantitative data on the antimony content at any given position in the ingot it was necessary to work out a technique for correlating the counts per minute with the antimony concentration. The method used was to powder the slab under analysis, make a radioactive count on a weighed quantity of the powder which had been placed in a small counting dish, and compare this count with that taken under similar conditions on a weighed amount of the 100 percent antimony sample which had been set aside when the ingot was prepared. All samples were ground to pass a 100 mesh screen, and glass counting dishes of uniform diameter were used.

The above counting method automatically corrects for the decrease in radioactivity with time. The sample size taken, however, was sufficiently large in most cases to make it necessary to correct for the absorption of the beta-particles by the germanium present. To determine this correction 2.5 grams of germanium, powdered to pass a 100-mesh screen, was thoroughly mixed with 2.5 ml of standard Sb^{124} solution. This solution was prepared by dissolving 1.126 mg of Sb^{124} in a small amount of *aqua regia* and diluting to 100 ml with water in a volumetric flask. 0.1 ml, equivalent to 1.126 μg of

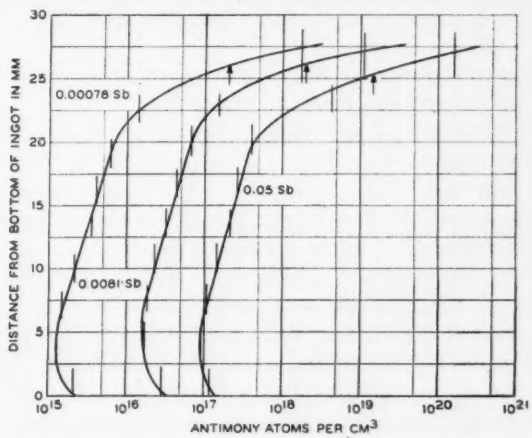

FIG. 3. Distribution of antimony atoms in ingots of germanium antimony alloy ingots.

antimony, gave approximately 600 counts per minute. This mixture was then dried and thoroughly mixed by grinding in an agate mortar. Counts were made on weighed amounts of the mixture from 0.3 to 2.0 grams. The percent maximum activity per unit weight of sample, in this case 0.1 gram is given by the following:

$$\text{Percent maximum activity} = \frac{\text{sample count} \times 0.1 \text{ gram}/(\text{sample wt.} \times 100)}{\text{zero weight count}}.$$

The zero weight count is obtained by counting 0.1 ml of the standard Sb^{124} solution, under the same conditions as the sample; this being equivalent to the amount of antimony present in 0.1 gram of sample. Plotting the

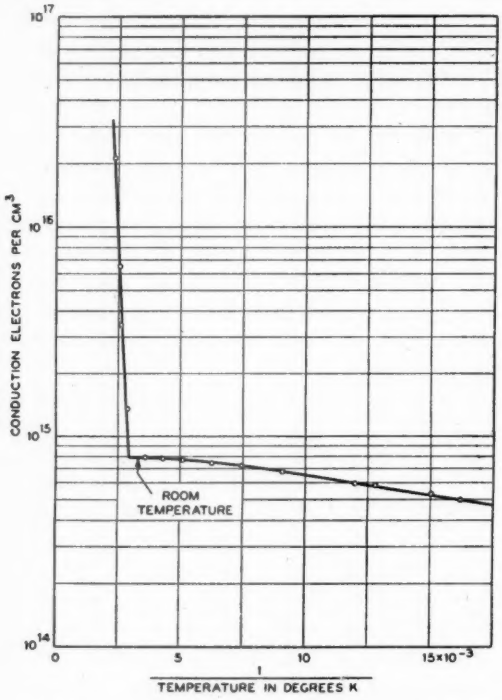

FIG. 4. Conduction electrons in a high purity germanium sample *versus* the reciprocal of the absolute temperature.

percent maximum activity against sample weight gives the self-absorption curve shown in Fig. 2.

A summary of the data obtained on three ingots in the manner described is given in Table II. The results for each of the nine slices in each ingot are given in terms of: (1) The weight percent of the antimony, (2) the number of antimony atoms per cm^3, and (3) the ratio of the antimony added to the melt to the amount present. The number of antimony atoms per cm^3 as a function of the distance from the bottom of the melt is plotted in Fig. 3. The length of the experimental lines in this figure indicate the width of the slice before powdering. The arrows show the average concentration of solute atoms which were placed in the charge before melting. Notice that the concentrations in the dome slices are about 10 times the amount added, whereas the concentrations in the lower half of the ingot are less than one percent of this amount. The observed changes in antimony concentration with location in the ingot are to be expected from the basic nature of the freezing process. When a germanium antimony alloy freezes over a range of temperatures, the first material to solidify contains less antimony than the last material to freeze. This effect is known as coring and the resulting concentration differences persist in the solid material unless they are eliminated by diffusion.[4] Coring normally manifests itself as a gradient in concentration between the center and periphery of dendritic grains, but in this case since the growth process is from the bottom of the ingot upward the differences in concentration occur gradually from bottom to top in the ingot. Microscopic examination reveals the presence of second phase material at the extreme tips of these ingots which suggests that for these locations the concentrations of antimony were above the solid solubility limit.

IV. HALL MEASUREMENTS

In a semiconductor such as germanium the number of conduction electrons per unit volume can be obtained from Hall effect measurements. In the low temperature or impurity range where the charge carriers arise solely from the impurity centers, the antimony atoms in the present study, the relation is

$$n = \pm(3\pi/8eR) = \pm 7.4 \times 10^{18}/R, \qquad (1)$$

where n is the number of charge carriers per cc and R is the Hall coefficient in cm^3/coulomb. The plus sign applies to p-type impurities which furnish holes and the negative sign to n-type impurities which furnish electrons. Antimony is an n-type impurity and the conduction charges are electrons.

Figure 4 gives conduction electrons per cm^3 *versus* the reciprocal of the absolute temperature for a typical

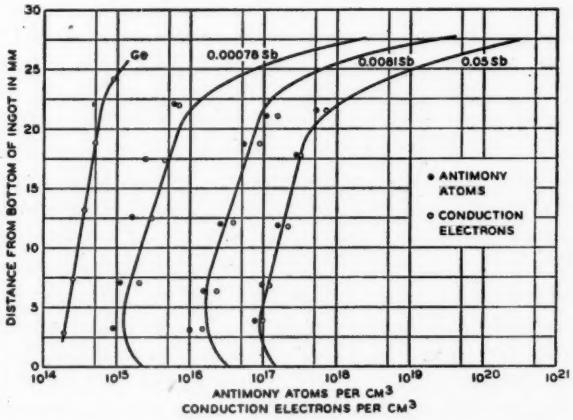

FIG. 5. Correlation of antimony atoms and conduction electrons in germanium antimony ingots at room temperature.

[4] R. M. Brick, Trans. A.I.M.E. **161**, 65 (1945).

high purity n-type germanium sample. The straight line portion on the left is the intrinsic range and the portion to the right of the break in the curve is the impurity range. At low temperatures very few of the impurity atoms are thermally ionized and the number of conduction electrons is low. As the temperature is raised ionization increases, thus causing an increase in the number of conduction electrons. Near room temperature a saturation region is attained in which all the impurity atoms become ionized and the number of conduction electrons is constant. It is in this saturation region that we find one conduction electron for each antimony atom as will be shown by comparing the G-M counter and Hall measurements on identical samples.

The left half of the ingots were cut into thin rectangular wafers approximately 0.5 mm in thickness. Measurements were made on the cross-hatched samples as shown in Fig. 1. First the density of conduction electrons in the saturation range was determined from Hall measurements, then the wafers were powdered and the density of antimony atoms was determined from radioactive measurements on the identical material. The results are plotted in Fig. 5 as a function of the position in the melt. The open circles represent conduction electrons per cc and the solid circles antimony atoms per cc. The solid lines are reproduced from Fig. 3 and give the antimony distribution in the other half of the melt as determined from radioactivity measurements. There is a close agreement between the conduction electron and antimony atom densities with the former usually being a little larger.[5] Within the experimental error these results show that when ionized each impurity atom produces one conduction electron.

Having obtained this result, impurity atom densities can now be determined from Hall measurements alone either on radioactive or non-radioactive samples. As an example, such measurements have been made on a high purity germanium melt to which no impurity had been deliberately added. The results are given by the curve on the left of Fig. 5 which shows about 2×10^{14} donor atoms per cc at the bottom of the melt and 1×10^{15} per cc near the top. It should be pointed out that if both donor and acceptor atoms are present, Hall measurements give only the excess of one over the other. As a method of quantitative analysis, Hall measurements are very sensitive. Since there are 4.5×10^{22} germanium atoms per cc, impurities present to only one part in two hundred million have been detected.

[5] Recent measurements by J. R. Haynes (private communication) using pulse techniques give conduction electron densities 30 percent lower than those determined by Hall measurements and therefore check the impurity atom densities even better.

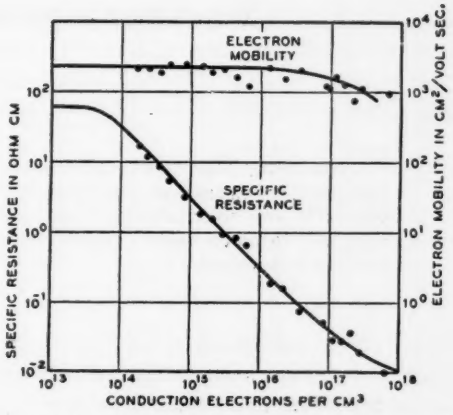

FIG. 6. Specific resistance and electron mobility as a function of electron density in germanium antimony alloys at room temperature.

V. RESISTIVITY AND ELECTRON MOBILITY *VERSUS* ANTIMONY CONTENT

Electrical resistivity measurements at room temperature were made on the twenty-five rectangular shaped samples which had been prepared for Hall measurements. These are shown in Fig. 6 where specific resistance in ohm cm is plotted *versus* the number of conduction electrons per cc. Over a major portion of the curve the resistivity is inversely proportional to the electron density. The constant value of 60 ohm cm at low impurity content arises from thermally ionized germanium atoms and is obtained by extrapolating the intrinsic resistivity *versus* temperature characteristic to room temperature.[6]

The electron mobility is defined by the fundamental relation

$$\sigma=1/\rho=ne\mu, \tag{2}$$

where ρ is the specific resistance in ohm cm (σ=conductivity), n is the density of conduction electrons, $e(=1.6\times10^{-19}$ coulomb) is the electronic charge, and μ is the mobility in cm² per volt sec. Mobility has been calculated from the measured values of ρ and n and plotted as a function of n in Fig. 7. It can be seen that μ is constant for values of n up to about 5×10^{16} after which it decreases with further increase in n.[7] This characteristic is expected from theory[2] since the constant value is due to scattering by the germanium lattice while the decrease at high impurity concentration arises from the added scattering of the antimony atoms.

The linear relationship between resistivity and the density of conduction electrons at room temperature (equal to the density of antimony atoms) suggests resistivity measurements at room temperature as a simple analytical method for determining the quantity of antimony in germanium alloys.

[6] G. L. Pearson, Phys. Rev. **76**, 179 (1949).

[7] Similar curves have been given for germanium copper alloys by W. Ringer and H. Welke, Zeits. f. Naturforschung **1**, 20 (1948).

Interaction between Elementary Particles. Part II.

ALFRED LANDÉ
Ohio State University, Columbus, Ohio
(Received October 19, 1949)

A particle described by an exact δ-function with shift of origin, rather than by a structural smoothed-out δ-function, has equations of motion derivable from Fokker's least action principle, in analogy to Feynman's work. The two objections of arbitrariness of the structure function, and of violation of the linear field equations within the particle radius, are thereby avoided. The relation to Born's new theory of elementary particles is discussed.

IN Part I[1] we considered a particle whose point center produces the surrounding field through communication according to a "signal equation"

$$r^2-c^2t^2+\mathfrak{a}^2=0 (\text{or } R^2+\mathfrak{a}^2=S^2=0). \quad (1)$$

The length $\mathfrak{a}$ thereby becomes the radius of the particle without further structural assumptions. In this Part II we proceed to the equations of motion under self and mutual forces derived from a *least action principal*, discarding former speculations (Part I, §5) about these forces. We rather proceed in close analogy to the method applied by Feynman[2] to a general class of particles whose finite radius is obtained by replacing the exact δ-function of a point source by a smoothed-out structural function $f(R^2)$, a favorite choice being an exponentially shading-off function. The drawback of this method is (A) the arbitrary selection of a structure function, and (B) the violation of the linear field equations within the range of $f(R^2)$. Both objections are avoided in the present theory[3] which replaces $\delta(R^2)$ by $\delta(S^2)$.

(A) the finite radius is introduced by Eq. (1) which is "reciprocal" to the energy equation $p^2-(E/c)^2+\mathfrak{b}^2=0$ with $\mathfrak{b}=mc$, so that there is hardly a way to tamper with this equation; (B) using an exact δ-function although with shift of origin leaves the linear field equations valid in the whole space. In the following discussion we closely follow Feynman's method and notation; we also refer to his quotations of the literature.

Equations of Motion.—First we quote Fokker's unified principle of stationary action for the case of point particles $a, b\cdots$ at world distances R_{ab} with coordinate increments da_μ, db_μ, and proper time increments $d\tau_a=(da_\mu da_\mu)^{\frac{1}{2}}$:

$$\sum_a m_a c^2\int d\tau_a+\tfrac{1}{2}\sum_a\sum_b e_a e_b\int\int\delta(R_{ab}^2)da_\mu db_\mu = \text{Extr.} \quad (2)$$

The terms $a=b$ in the double sum yield infinite field masses.

Therefore one may replace $\delta(R^2)$ by various trial functions $f(R^2)$ with consequences discussed by Feynman. We propose instead to modify Eq. (2) to

$$\sum_a m_a c^2\int d\tau_a+\tfrac{1}{2}\sum_a\sum_b e_a e_b\int\int\delta(S_{ab}^2)da_\mu db_\mu = \text{Extr.} \quad (3)$$

Field quantities F resulting from (2) are indicated by F, those from (3) by $\bar{F}$. Dots indicate derivatives with respect to proper time. The equations of motion resulting from the variation problem (3) are

$$m_a\ddot{a}_\nu=e_a\dot{a}_\mu\{\textstyle\sum_{b\neq a}\bar{F}_{\mu\nu}{}^b(a)+\bar{F}_{\mu\nu}{}^a(a)\}, \quad (4)$$

where

$$\bar{F}_{\mu\nu}{}^b(x)=\partial\bar{A}_\mu{}^b(x)/\partial x_\nu-\partial\bar{A}_\nu{}^b(x)/\partial x_\mu \quad (5)$$

and

$$\bar{A}_\mu{}^b(x)=e_b\int\delta(S_{bx}^2)db_\mu. \quad (6)$$

From $d(S^2)=d(R^2)=2(R\cdot dR)=2d\tau(R\cdot U)$ follows

$$db_\mu=\frac{db_\mu}{d\tau}\frac{d\tau}{d(S^2)}d(S^2)=\frac{1}{2}\frac{U_\mu}{(R\cdot U)}d(S^2).$$

Therefore (6) is identical with the 4-vector potential given in Part I, namely

$$\bar{A}_\mu{}^b(x)=-e_b\{U_\mu{}^b/(R_{bx}\cdot U^b)\}_{S=0}. \quad (6')$$

This is the Liénard-Wiechert potential except for the communication law $S=0$ rather than $R=0$. The Lorentz condition Div $\bar{A}=0$ is satisfied in the whole space; therefore, the linear Maxwell scheme holds everywhere without exception. However, (6) leads to (6′) only when the latter is understood as half the sum of an advanced and a retarded potential. (Part I left this question unsettled.)

The following considerations are almost identical with those of Feynman,[2] except that our

$$\bar{A}=\tfrac{1}{2}(\bar{A}_{\text{ret}}+\bar{A}_{\text{adv}})$$

is defined in (6) with $\delta(S^2)$ replacing the arbitrary structure function $f(R^2)$. When defining

$$\langle F\rangle_{\text{ret}}=\bar{F}+\tfrac{1}{2}F_{\text{ret}}-\tfrac{1}{2}F_{\text{adv}}=\tfrac{1}{2}(\bar{F}_{\text{ret}}+F_{\text{ret}})+\tfrac{1}{2}(\bar{F}_{\text{adv}}-F_{\text{adv}}).$$

[1] A. Landé, Phys. Rev. **76**, 1176 (1949).
[2] R. P. Feynman, Phys. Rev. **74**, 939 (1948).
[3] It was pointed out to me by Dr. Belinfante that a similar classical theory was developed by H. J. Groenewold, Physica, **6**, 115 (1939), coincident with the author's introduction of the signal equation in Phys. Rev. **56**, 482 (1939).

$\langle F\rangle_{\text{ret}}$ approaches the *retarded* field of a point charge outside the range **a**. Similar to Feynman's Eq. (12) the equation of motion of a particle can now be written in the form

$$m_a\ddot{a}_\nu = e_a\dot{a}_\mu\{\textstyle\sum_{b\neq a}\langle F\rangle_{\mu\nu}{}^{b}{}_{\text{ret}} + \frac{1}{2}\sum_{\text{all } b}[F_{\mu\nu}{}^{b}{}_{\text{adv}} - F_{\mu\nu}{}^{b}{}_{\text{ret}}] + \tfrac{1}{2}[F_{\mu\nu}{}^{a}{}_{\text{ret}} - F_{\mu\nu}{}^{a}{}_{\text{adv}}] + \bar{F}_{\mu\nu}{}^{a}\}. \quad (7)$$

The first term approaches the *retarded* field of all other particles outside the range **a**. The second term vanishes in a Wheeler-Feynman world in which all light is eventually absorbed. The third term depends only on the motion of the particle a and represents the force of radiative damping. The fourth term is the inertial force of the particle on itself. Its value corresponds to a mass $e^2/2ac^2$, refer to Groenewold.[3] The third and fourth term contract, according to the above definition, to the one symbol $\langle F\rangle_{\text{ret}}{}^{a}$ so that (7) reduces to

$$m_a\ddot{a}_\nu = e_a\dot{a}_\mu \sum_{\text{all } b} \langle F\rangle_{\mu\nu}{}^{b}{}_{\text{ret}}. \quad (8)$$

Except for the removal of the objections (A) and (B) this result conforms with Feynman's. The above equations represent a *unitary theory* of interaction between point centers. The field plays only the part of an intermediary mathematical scheme. Simultaneous action and reaction between distant points is abandoned since simultaneity is not a covariant concept. A following Part III will discuss the particle-field dynamics in case of a dualistic theory.

Relation to Born's Reciprocity.—The length **a** in (1) which leads to the field mass $m_0=\frac{1}{2}e^2/\mathbf{a}c^2$ takes the place of the electrostatic radius in structure functions $f(R^2)$ and removes classical infinities. Quantum theory predicts new phenomena beginning at the much larger Compton length $\lambda_C=h/mc=h/\mathbf{b}$. Whereas the Compton length depends on the mass of the individual particle, the length **a** in the communication law (1) ought to be considered as universal. This contention is supported by considerations of *reciprocity* in conjunction with the fact that there are elementary particles of many different masses, but with one universal charge only. The argument of reciprocity may be presented here in the purely formal and unphysical fashion proposed in 1940 and meant only as a preliminary exploration of a formal character. Let $\psi(r)$ and $\chi(p)$ be two functions pertaining to a free particle in space v and in momentum space w. Let ψ and χ be Fourier transforms of one another. According to non-relativistic quantum theory this would mean:

$$\chi(p)=h^{-\frac{1}{2}}\int\psi(r)\exp(ip\cdot r/\hbar)dv, \qquad \psi(r)=h^{-\frac{1}{2}}\int\chi(p)\exp(-ip\cdot r/\hbar)dw, \quad (9)$$

where $h=h/2\pi$ is a certain constant of action (we think, of course, of Planck's constant). When generalizing to four-dimensional spaces (r, ct) and $(p, E/c)$, the energy E is determined by the momentum p according to

$$E/c=\pm(p^2+\mathbf{b}^2)^{\frac{1}{2}} \text{ with } \mathbf{b}=mc. \quad (10)$$

Formal reasons of reciprocity then suggest that the parameter t is determined by r according to the equation

$$ct=\pm(r^2+\mathbf{a}^2)^{\frac{1}{2}}. \quad (10')$$

an equation interpreted physically at the beginning of Part I. Introducing reduced quantities $R=r/\mathbf{a}$, $T=ct/\mathbf{a}$, $P=p/\mathbf{b}$, $E=E/\mathbf{b}c$, together with $dv_0=dv(1+R^2)^{-\frac{1}{2}}\mathbf{a}^{-3}$ and $dw_0=dw(1+P^2)^{-\frac{1}{2}}\mathbf{b}^{-3}$, the relativistically revised Eqs. (9) read

$$\chi(P)=(\kappa/2\pi)^{\frac{1}{2}}\int\psi(R)\exp[i\kappa(PR+ET)]dV_0, \qquad \psi(R)=(\kappa/2\pi)^{\frac{1}{2}}\int\chi(P)\exp[-i\kappa(PR+ET)]dW_0, \quad (11)$$

where κ stands for

$$\kappa=\mathbf{ab}/h. \quad (12)$$

In contrast to the Eqs. (9) which for all functions $\psi(r)$ are identical inversions of one another, the new Eqs. (11) are compatible with one another only under certain conditions. In particular, when resorting once more to reciprocity and requiring that $|\psi|^2$ and $|\chi|^2$ are the same functions of their respective arguments, that is, when considering either $\psi=\pm\chi$, or $\psi=\pm i\chi$, then (11) is satisfied[4] only when the parameter κ satisfies the transcendental equation

$$2\pi\kappa[J_0(\kappa)]^2=1, \quad (13)$$

solved by an infinite set of values

$$\kappa=0.157,\ \sim1.8,\ \sim3.0,\ \text{etc.}, \quad (13')$$

or when κ satisfies

$$2\pi\kappa[Y_0(\kappa)]^2=1, \quad (14)$$

solved by the set

$$\kappa=0.03,\ \sim1.38,\ \sim3.44,\ \text{etc.} \quad (14')$$

There are two possible interpretations of these results. In 1940 we assumed *one* value $\mathbf{b}=m_0c$ and a variety of values of $\mathbf{a}=\frac{1}{2}e^2/m_0c^2$, i.e., a variety of charges $e=(2\kappa\hbar c)^{\frac{1}{2}}$, namely a smallest charge, $e\sim10^{-9}$ e.s.u. from the smallest $\kappa=0.03$, and larger charges which might be considered as unstable.

It seems more appropriate now to assume that there is *one* universal value of **a** $(=\frac{1}{2}e^2/m_0c^2$ with $m_0=$ electron field mass) and a variety of values $\mathbf{b}=mc$ belonging to

[4] M. Born, Proc. Roy. Soc. Edinburgh, 49, 219 (1939); A. Landé, J. Franklin Inst. 229, 767 (1940).

particles of total masses $m=\kappa\hbar/ac=2\kappa\cdot 137m_0$. This purely formal calculation is related to the physically meaningful investigation of Born and Green.[5] These authors obtain for the field mass of the electron $(3/2\pi^4)e^2/ac^2$, and they derive the eigenvalues of κ from the transcendental equation $\kappa^k L_n^{k+1}(\kappa^2)=0$ where L_n^{k+1} is the $(k+1)^{st}$ derivative of the Laguerre polynomial L_n.

[5] M. Born and H. S. Green, Proc. Roy. Soc. Edinburgh 62, 470 (1949); M. Born, Rev. Mod. Phys. 21, 463 (1949).

PHYSICAL REVIEW VOLUME 77, NUMBER 6 MARCH 15, 1950

Electron Bombardment Conductivity in Diamond. Part II*

KENNETH G. McKAY
Bell Telephone Laboratories, Murray Hill, New Jersey
(Received November 21, 1949)

Previously published results of a study of electron bombardment conductivity in diamond have been revised by the use of an improved alternating field method of internal space-charge neutralization. In addition lower limits are set for the mobilities of electrons and positive holes at room temperature. Measurements have also been made of the decay of current due to internal space-charge fields which are in reasonable agreement with theory. Finally, a double-pulsing technique is used to provide a novel method to study the rates of release of positive holes and electrons from traps.

1. INTRODUCTION

RECENTLY the results were published of work on electron bombardment conductivity in diamond[1] in which two principal effects were observed:

(1) In a crystal which is free of space charge, some or all of the the internal charge carriers produced by the bombardment are trapped before traversing the crystal so that the initial observed current is a function of the field applied across the crystal.
(2) The trapped charges build up an internal space-charge field such as to oppose the applied field. This causes the observed current to vary with time with constant applied field.

Part I described a neutralization technique by which the two effects could be separated and it reported an analysis of the motion of electrons through a space charge free crystal. It is the purpose of the present paper to present:

(1) An analysis of the positive hole current as well as a reinvestigation of the electron current through the space-charge free crystal in the light of an improved technique for eliminating the effect of space charge on the measurement, Section 2.
(2) An analysis of the transient behavior of the current as affected by internal space charge, Section 3.
(3) A new method of studying the release of electrons or positive holes from traps, Section 4.

In Part I, the theory, based on work by Hecht[2] for photo-conductivity, was developed for the configuration shown in Fig. 1. A pulsed beam of electrons bombards a diamond crystal through a thin electrode mounted directly on the surface of the material and to which a current indicating device is connected. On the other face of the crystal is mounted a second electrode maintained at an elevated potential.

If now a step function bombarding current strikes a space-charge free crystal, the initial peak current passing through the crystal represents the current we would obtain if we could neglect the internal field set up by trapped electrons and positive holes. Under such conditions and with the assumptions listed, the voltage-current characteristic of the bombarded crystal could be described by an equation of the form:

$$\Delta=\Omega[1-\exp(-\Omega^{-1})], \qquad (1)$$

where $\Delta=\delta/\delta_\infty$ is the normalized yield; δ is the observed current passing through the crystal divided by the bombarding current; δ_∞ is the yield δ for infinite applied crystal field; $\Omega=\omega/l$ is the normalized range; l is the thickness of the crystal; $\omega=vFT$ is the probable electron range; v is the electron mobility; F is the applied field across the crystal; and T is the probable time an electron would spend in a semi-infinite crystal before being trapped.

The principal assumptions involved in formulating the theory are that the traps are distributed homogeneously throughout the crystal and that the effects of internal space-charge fields are negligible. The other assumptions discussed in Part I are all reasonably well met in the present applications of the theory. Calculations have been made which indicate that a fairly wide distribution of trap densities can be tolerated without introducing an appreciable error in the use of this theory.

2. THE SPACE-CHARGE FREE CRYSTAL

2.1 Determination of Yield

The experimental arrangement was similar to that described in Part I with an important difference. One difficulty that arose in the earlier work was that of

* A report of this work was given at the Congress of the Canadian Association of Physicists on June 1, 1949.
[1] K. G. McKay, Phys. Rev. 74, 1606 (1948) herein designated as Part I.
[2] K. Hecht, Zeits. f. Physik 77, 235 (1932).

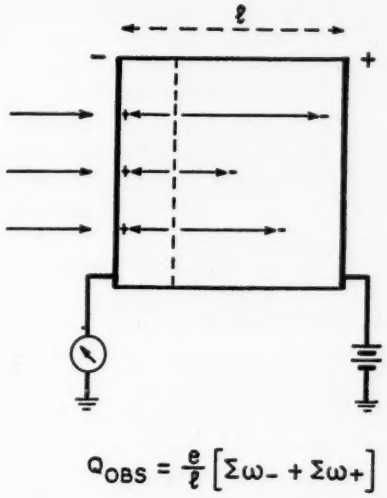

FIG. 1. Illustration of principle of bombardment-induced conductivity.

determining whether or not there was really no net space charge in the crystal just before the occurrence of the current pulse we wished to examine.† This difficulty was overcome as follows: A 60-cycle sine wave was operated on so that the field applied across the crystal had the shape of the upper curve in Fig. 2. The middle line shows the relative position in time of the pulsed primary beam and the lowest line shows the corresponding current flow through the crystal as seen on the oscilloscope. The bombarding current was zero except during the pulses shown on Fig. 2. Starting on the left-hand side with a space-charge free crystal, the primary beam bombards the crystal for a few microseconds at the peak of the positive half-cycle of the crystal field. This causes electrons to travel through the crystal with the circuit arranged as in Fig. 1. At the end of the pulse the current through the crystal is somewhat reduced owing to the formation of an internal negative space charge due to trapped electrons. The crystal field is then reversed and at the peak of the negative half-cycle, a second or neutralizing pulse, possibly different both in length and amplitude from the first pulse, bombards the crystal. The positive holes produced by this pulse travel through the crystal initially under the influence of the applied field aided by the negative space-charge field. This current decreases as the space-charge field is neutralized by trapped positive holes. However, at the end of the second pulse, we do not know whether the crystal has been left with a net space-charge field or not. Consequently, we now reduce the applied field accurately to zero and, having established this condition, a third or test pulse bombards the crystal. If, as a result of the test pulse bombardment, there is any current flow through the crystal it will be due to an internal field. The general procedure was to observe the current flow through the crystal resulting from the test pulse and adjust the length of the neutralizing pulse until the observed current flow was reduced to zero. This was the condition in which only the primary pulse itself was seen since the amplifier is connected to the bombarded face of the crystal. Having established this condition, we can proceed to the next pulse that occurs at the peak of the positive half-cycle of the crystal field and be reasonably confident that the first wave of conduction electrons resulting from this pulse travels through a crystal which has no net space-charge field. By reversing the order of bombardment following the test pulse at zero field, the motion of positive holes rather than electrons can be studied for the "space-charge free" crystal.

A block diagram of the equipment used is shown in Fig. 3. The amplifier, pulsers, and experimental tube are as described in Part I. To provide a comparison with previously measured values, the same area of the same diamond was bombarded. Measurements were made by recording all bombarding and resulting induced current pulses photographically. These were subsequently measured with the aid of a special coordinate scale which eliminated effects of oscilloscope distortion such as keystone effect, etc.

2.2 Analysis of Results

Before considering the actual results we must notice that the neutralizing procedure adopted establishes the condition for zero net space-charge in the crystal; it is still possible that even with this condition there are trapped in the crystal equal numbers of electrons and positive holes (assuming plane parallel geometry). If these are thermally released in the interval between the test pulse and the next pulse to be observed, and if the rate of escape for electrons is different from that for holes, it is possible that the crystal may acquire a net space-charge field by the time the principal pulse occurs. This was tested in several ways. First, the time between the test pulse and the principal pulse was varied from 4 to 16 msec. This was done for a crystal field well below saturation where any change in field would result in a pronounced change in yield. No difference could be observed in the amplitude or shape of

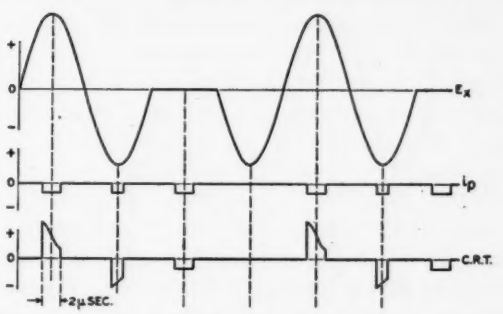

FIG. 2. Time relations between crystal field, bombarding current pulses, and induced conductivity pulses.

† Reference 1, Section 57.

the current resulting from the principal pulse. Second, two test pulses were used separated by 12 msec. In the interval between the test pulses, the crystal field was raised to a high value so that any electrons or holes which were released from traps would have a probability of greater than 0.5 of leaving the crystal. The second test pulse showed no trace of induced current nor was there any departure in the amplitude or shape of the principal pulse from its appearance when only one test pulse was used. From this we can conclude that once the crystal has been neutralized it remains neutralized as well as can be detected by this type of experiment.

If after neutralization, the crystal does contain large equal numbers of trapped electrons and holes, it is possible that owing to their different ranges, the holes

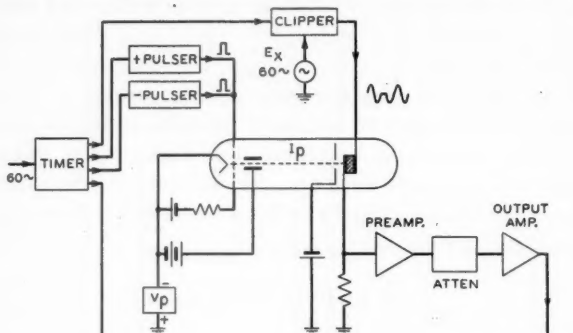

FIG. 3. Block diagram of experimental equipment.

will not be trapped at the same depths as the electrons. In that case sizable fields might exist inside the crystal although no space-charge field could be detected externally. Such a situation would probably affect the yield measurements. To test this, a d.c. source was incorporated into the circuit which generated the crystal field so that the principal pulse occurred at the same positive peak value each time but the neutralizing pulse could occur at different negative peak values. The test pulse, of course, always occurred with zero applied field. For a fixed positive voltage of 300 volts, the negative peak voltage was varied from 100 to 1200 volts. In each case, the pulse occurring at the negative peak voltage—the neutralizing pulse—was adjusted for proper neutralization. Under these circumstances there was no observable change in the amplitude or shape of the principal pulse representing electron flow through the crystal. This experiment was repeated with a reversal of the order of bombardment so that the principal pulse represented positive holes traversing the crystal. Again, no change in the principal pulse could be detected as the voltage at which the neutralizing pulse occurred was varied over the same range as that described above. The conclusion is that these experiments are completely insensitive to any effects due to a possible displacement of the center of gravity of trapped positive holes from the center of gravity of trapped electrons. This may be accounted for by an effective mobility of trapped charges through thermal release and subsequent retrapping or by the possibility that the neutralization process consists primarily of actual recombination between a positive hole and a trapped electron or vice versa rather than merely a trapping of both carriers in the same region.

In view of this insensitiveness to the crystal voltage at the onset of the neutralizing pulse, the investigation was extended to neutralization at zero applied field. Now we had simply a principal pulse at a positive applied crystal voltage followed by a neutralizing pulse at zero applied crystal voltage. It was found that if the neutralizing pulse was at least equal in duration and intensity to the principal bombarding pulse, the current wave form induced by the principal pulse was indistinguishable from that obtained by the conventional neutralizing procedure. These measurements were carried out for the full range of crystal fields that have been used (2000 to 20,000 volts/cm) and for several different pulse lengths.

We have established by the above experiments that the neutralization procedure does indeed result in not only a space charge neutral crystal but also a crystal with a residual internal space charge which is too small to effect our measurements. Consequently we are now in a position to analyze the results obtained by the conventional neutralizing procedure described in Section 2.1. Measurements were made of the peak yield as a function of applied crystal field for bombarding voltages, V_p, of 5, 7, 10, and 14 kv with both electrons and positive holes as carriers. Throughout this series of measurements the primary bombarding current during both the principal and neutralizing pulse was held constant at 1.25×10^{-4} amp./cm^2. Some typical wave forms for electron carriers are shown in Fig. 4 and the corresponding wave forms for positive holes are shown in Fig. 5. The procedure followed was to measure all the values of peak yield, for, say electrons, and plot these as a function of applied field for each value of V_p. Each curve was then fitted as well as possible to the theoretical curve given by Eq. (1) by scaling the coordinates. It was found that only one scaling factor for the abscissas was needed to provide a best fit for each of the four curves obtained at different values of V_p, which is as it should be since the product (vT) is independent of the conduction current. A typical correlation between theory and experiment is shown in Fig. 6 for $V_p=10$ kv. Those for the other values of V_p were comparable to this although some showed a somewhat greater scatter in experimental points. Having established the scaling factor for the abscissas, the experimental values of applied voltage were transformed to Ω-values, and, by Eq. (1) to equivalent Δ-values. These values of Δ were plotted against the experimentally determined values of δ and the best

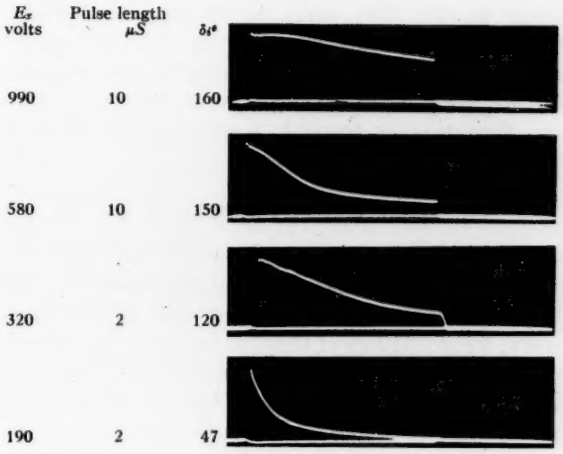

FIG. 4. Variation of δ_i^e with crystal voltage. $V_p = 10$ kv.

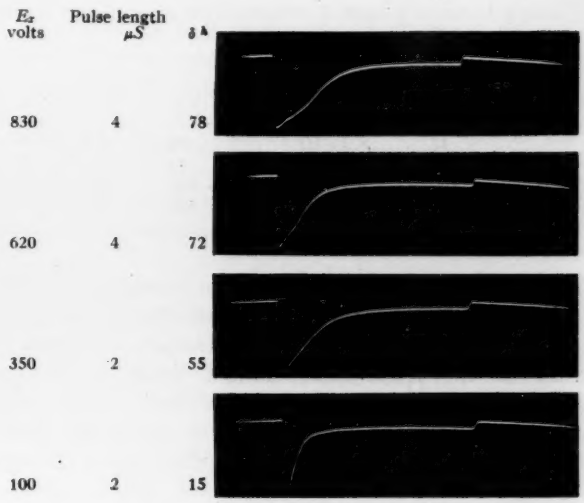

FIG. 5. Variation of δ_i^h with crystal voltage. $V_p = 10$ kv.

straight line fit used to determine the ordinate scaling factor, i.e., δ_∞, for each value of V_p.

The same procedure was carried out for the measurements on positive holes as carriers. Again, one abscissa scaling factor was adequate to give a best fit between theory and experiment for bombarding voltages of 5, 7, 10, and 14 kv. However, the product vT for positive holes was 55 percent of that for electrons signifying a difference in mobility or in probable free time before trapping or both. Experimentally, the approach to saturation for positive hole current was somewhat slower as a function of applied field. Approximately the same upper limit of applied field was used in both sets of measurements so that the largest values of Ω achieved for positive holes were less than those for electrons with a possible loss of accuracy in fitting the experimental points to the theoretical curve. A typical correlation is shown in Fig. 7, for $V_p = 10$ kv. Table I gives a summary of the results obtained from the values of the scaling factors for both electrons and positive holes.

If our picture of what is occurring is correct, there is another method of measuring the peak yield. Having established the proper condition for neutralization, the height of the trailing edge of the neutralizing pulse should represent current flow through a space-charge free crystal since the following test pulse tells us that the crystal is neutral. Actually this will only be true if there is no appreciable release of the neutralizing carriers from traps. Moreover, the trailing edge of the pulse is not quite as fast as the leading edge so that there is more experimental error in making the measurement than by the conventional method. Actual measurements of the yield were made in this manner and were found to agree within about 10 percent with those described. However, there was considerably more scatter and the data for electrons were worse than those for positive holes. This is to be expected in view of the data on release of carriers from traps to be presented in Section 4.

The wave forms of the type shown in Figs. 4 and 5 also supply information about the pulse rise time. If, for the moment, we neglect instrumental limitations, this rise time is essentially the time required to establish equality between the number of carriers being created by the primary electrons and the number being removed either by trapping or by arrival at the unbombarded electrode. It is assumed that such a condition can be achieved before the internal space charge field has become appreciable. If the rise time, T_R, is defined as the time taken for the pulse to rise from 10 to 90 percent of its final value, it can be shown for small values of Ω, where practically all of the carriers are ultimately trapped in the crystal with a probable trapping time equal to T, that $T_R/T \simeq 2 \cdot 2$. As the applied field is increased this ratio decreases until T_R approaches a value determined by the transit time across the crystal. To use the rise time to determine T, it is desirable to use low field strengths such that $\Omega \ll 1$ and this is the region in which space-charge limitation becomes important. Owing to the finite rise time and the fact that the period of observation is limited by the onset of space-charge build-up, it is conceivable that the observed peak value may not represent the true yield as given by Eq. (1), but may be somewhat smaller. This means that the current begins to be reduced by the effect of the internal space-charge field before the current has reached its full value. This would be particularly true at low field strengths where the rate of build-up of trapped space charge is high and the rise time T_R is large. However, Wannier[3] has pointed out that if such a situation could be set up, it is probable that the current would be limited primarily by the space charge of the conduction current in the crystal itself so that these rise time considerations would not necessarily apply. It should be noted that if the space-

[3] G. H. Wannier (private communication).

TABLE I. Values of δ_∞ and vT obtained from correlation of theory and experimental points.

V_p (kv)	Electrons δ_∞[a]	Electrons (vT)[a] (cm² volt⁻¹)	Positive holes δ_∞[b]	Positive holes (vT)[b] (cm² volt⁻¹)
5	31	8.3×10^{-6}	19	4.6×10^{-6}
7	76	8.3×10^{-6}	49	4.6×10^{-6}
10	190	8.3×10^{-6}	108	4.6×10^{-6}
14	480	8.3×10^{-6}	320	4.6×10^{-6}

charge field of the charges in motion were providing the principal limitation to the rise time for low values of applied field, we would have a situation analogous to that of the space-charge-limited diode where the current is dependent only on the field and is independent of the cathode temperature. We would therefore expect that for low fields the peak current through the crystal should be a function only of the field and should be independent of the bombarding voltage V_p. This is not observed to be the case. Even for very low applied fields, the peak current through the crystal increases as the bombarding current or the bombarding voltage increases although the relation is not linear over the region covered by the experimental data. It is conceivable that under these conditions, the current in the center of the bombarded region is actually space-charge-limited but the current around the periphery is not. This would result in a partially space-charge-limited current. However, the rise time would be characteristic of the current flow around the periphery and therefore it seems reasonable that the rise time measurements can be used to determine the magnitude of T. In the actual experiments, the input RC constant ranged from 5×10^{-10} sec. to 2×10^{-9} sec. which provides a negligible limitation to the rise time in comparison with the band width of the amplifier together with the finite rise time of the primary pulse itself. The observed rise time as set by all these factors was about 0.05 μsec. and was the same for all values of Ω and also the same for positive holes and electrons. Since a 40 percent change in rise time could be readily detected, it is probable that $T<0.02$ μsec. We can also conclude that the peak yields for low field strengths are suspect as they are likely to be too small, either through a transit time limitation or through a space-charge limitation of the conduction current itself.

2.3 Derived Constants

One rather surprising result, shown in Table I, is that δ_∞ for electrons is considerably greater than that for positive holes, while, on the basis of our simple theory, we would expect them to be equal. One possible explanation of this is that the trap distribution is such that part of the bombarded area has perhaps ten times the trap density for positive holes as the rest of the area. Over the range in field with which we have dealt, such an area would be almost opaque to positive holes and thus the holes would be trapped before they could move a sufficient distance to contribute appreciably to the observed current. This is a much more radical inhomogeneity in trap distribution than was considered in Section 1. The scatter in the experimental points and the relatively narrow range of Ω over which the measurements were made do not warrant fitting the points to a composite yield curve covering such inhomogeneities in trap density. Further evidence in support of this explanation of the disparity in the δ_∞ for electrons and that for positive holes will be presented in Section 3.

One important result that can be derived from the values of δ_∞ is the number of electron volts energy, φ, required to produce one internal secondary electron. The energy per primary electron which is dissipated in the diamond is equal to V_p minus the energy lost in penetrating the gold electrode. One method of obtaining φ is to plot V_p/δ_∞ against V_p, and extrapolate to large values of V_p. A more sensitive method is to plot $dV_p/d\delta_\infty$ against V_p. It is true that taking the slope of a curve with only four determining points is markedly dependent on the form of the smoothing and consequently

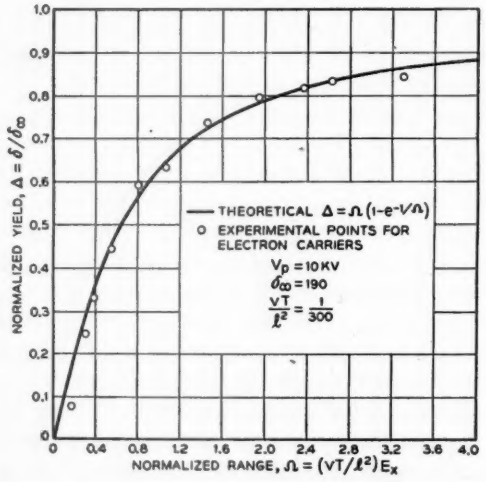
NORMALIZED YIELD, Δ = δ/δ∞
NORMALIZED RANGE, Ω = (vT/ℓ²)Ex
THEORETICAL Δ = Ω(1-e^-1/Ω)
EXPERIMENTAL POINTS FOR ELECTRON CARRIERS
Vp = 10 KV
δ∞ = 190
vT/ℓ² = 1/300

FIG. 6. Electron yield as a function of normalized range.

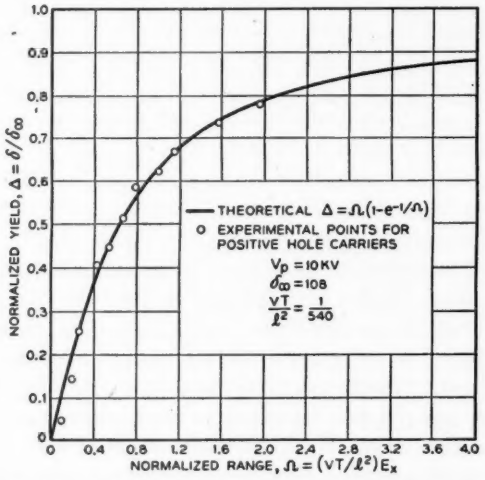
NORMALIZED YIELD, Δ = δ/δ∞
NORMALIZED RANGE, Ω = (vT/ℓ²)Ex
THEORETICAL Δ = Ω(1-e^-1/Ω)
EXPERIMENTAL POINTS FOR POSITIVE HOLE CARRIERS
Vp = 10 KV
δ∞ = 108
vT/ℓ² = 1/540

FIG. 7. Positive hole yield as a function of normalized range.

the results should be regarded with some caution. Figure 8 shows the result of such a plot. The lower curve is for electrons and the upper curve for positive holes. From this it can be concluded that φ is less than 13 volts and probably greater than 7 volts. The mean value of $\varphi=10$ volts is the same as the value determined by Ahearn on experiments with alpha-particles.[4] It will also be observed that in spite of the difference between δ_∞ for electrons and for positive holes, this plot suggests that they both extrapolate to approximately the same value of φ. It is tempting to speculate

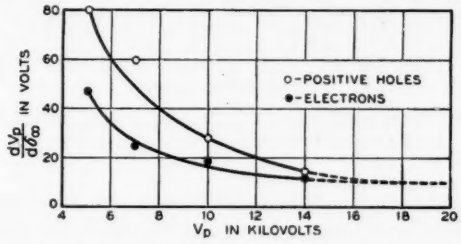

FIG. 8. Determination of primary energy required to produce one free electron or positive hole.

that this implies that the sections of the bombarded area which are "opaque" to positive holes lie very close to the surface but more accurate data are required before this could be concluded with any certainty.

The abscissa scaling factors may also be used to determine some other solid state properties of the diamond. It was shown that $T\leq 2\times 10^{-8}$ sec. for both electrons and positive holes. Thus from vT in Table I we can conclude that the mobility for electrons must be greater than 400 cm²/volt-sec. and for positive holes must be greater than 200 cm²/volt-sec. On the other hand, Klick and Maurer[5] have recently concluded from Hall effect measurements that the electronic mobility in diamond at room temperature is 900 cm²/volt-sec. which is not contradicted by the result derived above. If we use Klick and Maurer's value, we obtain for the electrons $T\simeq 10^{-8}$ sec. Now the trap density N_t is given by

$$N_t=1/T\sigma u,$$

where u is the thermal velocity of the electrons and σ is the trapping cross section.

If we assume a trapping cross section of 10^{-16} cm², we obtain a trap density of 10^{17}/cm³ or somewhat less than one trap per million atoms.

In comparing these results with the preliminary data published in Part I, we see that the values of (vT) are now more consistent and slightly higher. It was necessary in the earlier paper to use values of vT which varied by a factor of two to obtain a reasonable fit to Eq. (1) for electron carriers produced by the different bombarding voltages. The earlier value of δ_∞ for $V_p=14$ kv was considerably higher than that now obtained and much of that may be ascribed to the earlier method of neutralization together with the relatively few points used to define the yield curve. However, actual yields were observed for $V_p=14$ kv which were slightly in excess of the value of δ_∞ now obtained. This may have been due to inaccurate attenuator calibration (a complete recalibration accompanied the present measurements) or it is possible that there had been a change in the surface structure of the crystal, either in the electrode or in the diamond itself, in the elapsed time interval between the two sets of measurements.

3. BOMBARDMENT CONDUCTIVITY UNDER SPACE-CHARGE CONDITIONS

In a recent paper,[6] R. R. Newton set up the equations governing the flow of current through the crystal as a function of time, in which he included the build-up of internal space-charge fields due to trapped electrons and the subsequent release of trapped electrons, but neglected diffusion terms and space-charge effects due to the charges in motion. Newton defines the region in which free electrons and positive holes are being produced in equal numbers as the plasma layer. In this paper it was concluded that if the applied field was sufficiently high, all of the electrons produced in the plasma layer would initially be drawn out into the body of the crystal and the current would then fall off due to a reduction in the range of these electrons owing to the build-up of the opposing internal space-charge field. In this time region the current, as a function of time, must fall off more rapidly than an exponential and probably the second derivative of the current is negative for small times. Using a power series method, Newton developed approximate solutions for small time and could thus predict the initial rate of decay of the current. However, when the field across the plasma layer becomes sufficiently low, trapping and recombination in the plasma layer become important and the current of electrons leaving the plasma layer is no longer a constant. The subsequent current flow will then be determined primarily by conditions in the plasma layer and by the thermal release of trapped electrons. Newton concluded that the current-time curve should have an inflection point when the field across the plasma layer becomes very small. By assuming that the inflection point should occur when the field across the plasma layer equals zero, the time for the appearance of the inflection point was also calculated. The only parameters used in these calculations are derived from experimental data obtained solely from the space-charge free crystal.

It is evident that if there is no appreciable release of trapped electrons within the time of 1 μsec. or less, the initial slope will not be influenced appreciably by the release of trapped electrons. Consequently, Newton's theory can be tested by neglecting release of trapped

[4] A. J. Ahearn, Phys. Rev. **73**, 1113 (1948).
[5] C. C. Klick and R. J. Maurer, Phys. Rev. **76**, 179 (1949).
[6] R. R. Newton, Phys. Rev. **75**, 234 (1949).

electrons and calculating $-(1/\delta_\infty^2)(di/dt)_{t=0}$ as a function of Ω where i is the observed current. This was done using the values of δ_∞, (vT) and bombarding current density given in Section 2.2. The dielectric constant was taken as $K=5.68$. The result, plotted as a function of Ω ($\Omega=\lambda^{-1}$ in Newton's paper), is shown as the solid curve in Fig. 9. The experimental points for $V_p=5$, 7, 10, and 14 kv are also plotted and the agreement both as to the shape of the curve and its absolute magnitude is quite satisfactory particularly since the expression for the theoretical curve contains no adjustable parameters.

The experimental curves for higher field strengths clearly show an inflection point, e.g., see the upper two traces in Fig. 4. Figure 10 shows a comparison between the calculated time τ_i, to reach the inflection point and the experimentally determined values for different values of V_p. The calculated curve again neglects release of trapped electrons and in this case the product $\delta_\infty\tau_i$ should be a unique function of δ_∞. It will be seen that the theory predicts the proper form of the variation of $\tau_i\delta_\infty$ with field strength but is too low in absolute magnitude by a factor of approximately two. The only cause that Newton postulates for the existence of an inflection point, as opposed to an abrupt fall of current to zero, is the release of trapped electrons and the inclusion of this factor will indeed increase the magnitude of the calculated values bringing them more in agreement with the experimental points. However, in this case $\delta_\infty\tau_i$ is no longer a unique function of Ω because, for a given value of Ω, when δ_∞ is small, τ_i is

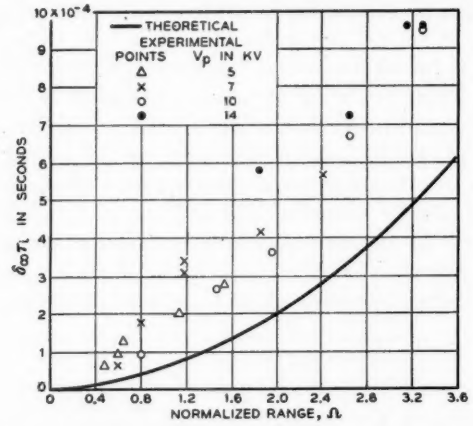

FIG. 10. τ_i, the time to reach the inflection point for electron carriers as a function of normalized range.

large and thus would be considerably affected by release of trapped electrons. On the other hand, for large δ_∞, τ_i is small and should be relatively independent of such a release of trapped electrons. On examining the experimental points there does not appear any consistent trend in the discrepancy between theory and experiment of the values of $\delta_\infty\tau_i$ as a function of V_p. From this we can conclude that release from traps does not play a significant role in determining the position of the inflection point in these experiments. The relatively minor disagreement between the absolute values may be due merely to the approximations involved such as the assumption of plane parallel geometry, homogeneous trap distribution, etc., or it may be necessary to examine

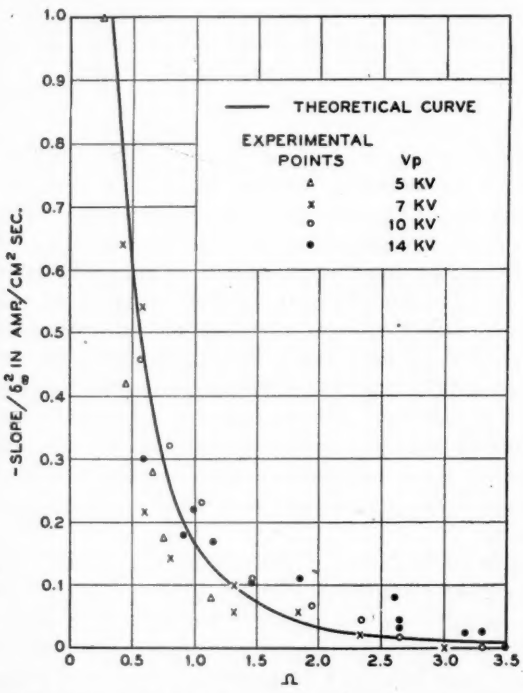

FIG. 9. Initial rate of decay of electron current through crystal as a function of normalized range.

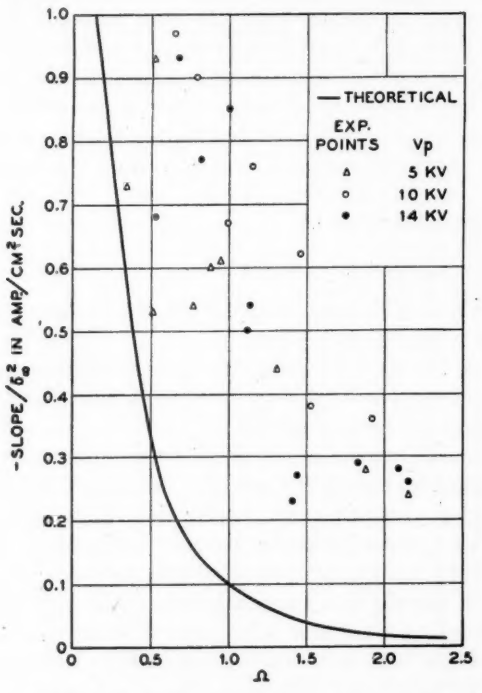

FIG. 11. Initial rate of decay of positive hole current through crystal as a function of normalized range.

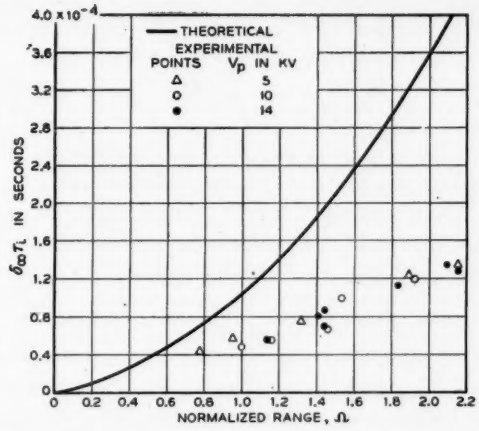

FIG. 12. τ_i, the time to reach the inflection point for positive hole carriers as a function of normalized range.

the behavior of the plasma layer in detail before resolving this difference.

The same type of comparison between theory and experiment can be carried out for positive holes merely by recalculating the theoretical curves using the appropriate data for positive holes as determined in Section 2.2. Figure 11 shows the comparison between theory and experiment for the initial rate of decay of current divided by δ_∞^2 as a function of Ω. In spite of the rather large scatter in the experimental points, it is evident that the correlation between theory and experiment is not nearly as good as the corresponding correlation for electrons. However, we are using the value of δ_∞ for positive holes that was derived in Section 2.2 for the space-charge free crystal and it was suggested there that the value was too low because of some high trap density regions in the bombarded area. A positive hole which cannot move appreciably before being trapped will not contribute to the value of δ_∞ but it will contribute to the space-charge field. Consequently we should use a much larger value of δ_∞ in this comparison. If in Fig. 11 we use the value of δ_∞ determined for electrons, we find that the agreement between theory and experiment is good for low values of Ω. For larger values of Ω the theoretical curve would have to be modified to include regions coexisting with different values of Ω. As stated in Section 2.2 the accuracy of the data does not warrant such a modification although various plausible arrangements have been set up which correlate the theory and experiment within the experimental error.

Further evidence to support this thesis is shown in Fig. 12 where the calculated curve for $\delta_\infty\tau_i$ is compared with the experimentally determined points for positive holes. Again, release from traps have been neglected. Here the experimental points lie below the theoretical curve but if we put in the value of δ_∞ for electrons rather than that for holes, the agreement is fairly good for low Ω while the same modified theory considered above will produce fairly good agreement for high Ω.

4. MULTIPLE PULSE BOMBARDMENT

An extension of the pulsing technique described in Section 2.1 has been made which is a novel approach to the problem of thermal release from traps. Starting with a space-charge neutralized crystal, a positive voltage is applied and an "initial" pulse of current bombards the crystal just as before. The trailing edge of the observed pulse represents the current which flows through the crystal under the combined influence of the applied field and the internal space-charge field which exists at that instant. If the applied field is held constant and, after a few microseconds the crystal is again bombarded with a primary current pulse equal in magnitude to the first pulse, the height of the leading edge of the current resulting from the second or "test" pulse‡ should be exactly the same as the height of the trailing edge of the "initial" pulse provided there has been no change in the internal space-charge field during the intervening time interval Δt. Presumably the only way in which this field could change during the unbombarded interval is through the thermal release of trapped electrons and their subsequent removal from the crystal under the influence of the existing field. If this process does take place, the negative space-charge field will decrease in magnitude during the unbombarded interval and the peak test pulse current will be greater than the height of the trailing edge of the initial pulse. The extent of the difference will be a function of the length of the unbombarded time interval.

Figure 13 is a composite photograph showing a series of such pulses. In each case we have started with a neutralized crystal; the initial pulse which is 6 μsec. long is produced and then, a certain time later, the test pulse occurs. The complete experiment is then repeated with a different time interval between the end of the initial pulse and the onset of the test pulse. In Fig. 13 the different unbombarded time intervals Δt expressed in microseconds are: 0.05, 5, 10, 15, 20, 25, and 30. The first interval which is barely resolved produces no appreciable change but in all subsequent intervals the

FIG. 13. Release of trapped electrons. Initial pulse length = 6 μsec. Test pulse length = 4 μsec. at 5 μsec. intervals.

peak test pulse current increases regularly with increasing time interval. These measurements were all made with $V_p = 14$ kv and an applied field which corresponded to $\Omega = 1.84$. A set of similar measurements was made for initial pulse lengths of 2 and 10 μsec. Let ψ be the ratio of the peak current in the test pulse

‡ Note that the term "test pulse" as used here does not have the same connotation as in Section 2.

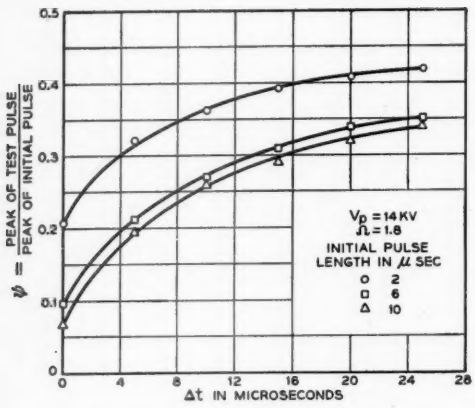

FIG. 14. ψ=peak of test pulse divided by peak of initial pulse as a function of Δt, the time interval after the end of the initial pulse.

to the peak current in the initial pulse. (The peak current in the initial pulse cannot be determined directly from Fig. 13 owing to amplifier compression.) The results of these measurements expressed in terms of ψ are shown in Fig. 14. It is evident that the interpretation of these curves in terms of a quantitative determination of the actual number of traps present of a given trap depth is rather complicated. The motion of released electrons changes the space-charge field which in turn alters the observed current but the region in which we are working is one in which the field across the plasma layer is important and, lacking information about the current-field characteristics of the plasma layer, we cannot make a direct quantitative analysis of the data. However, we can make a crude calculation which is applicable to small values of the effective field where the yield varies approximately linearly with the field.

Let n_s equal the number of electrons initially trapped in shallow traps, i.e., at the end of the initial pulse; n_d equal the number of electrons initially trapped in deep traps; and $n_e(t)$ equal the number of electrons initially trapped which have escaped from the crystal. Then $\psi=[F_0-K_1(n_s+n_d-n_e(t))]/F_0$, where F_0 is the applied field and K_1 is a constant.

Let the probability of release of a trapped electron from a shallow trap be $1-e^{-t/\tau}$ and the probability of that electron then escaping from the crystal be P. Then the total number of electrons which have escaped from the crystal at time t is

$$n_e(t)=Pn_s(1-e^{-t/\tau}),$$

where we neglect the effect of electrons which, having been released, are retrapped in shallow traps and subsequently are released and escape from the crystal. Then

$$\psi=1-(K_1/F_0)[n_s+n_d-Pn_s(1-e^{-t/\tau})].$$

If we assume that P is essentially independent of t, at least in comparison with $e^{-t/\tau}$, we have that

$$\ln(d\psi/dt)=K_2-(t/\tau).$$

Although in these experiments we begin with a high value of Ω, the effective value of the field when operating in the space-charge-controlled region is small so that even such a crude calculation may be a fair approximation. Figure 15 shows a semilog plot of $d\psi/dt$ as a function of t for various initial pulse lengths. We expect some variation from linearity near $t=0$ since we have neglected the finite length of the initial pulse. Nevertheless, the data do indicate that the main contribution to the increased height of the leading edge of the test pulses comes from traps with a $\tau\simeq 10$ μsec. Mott and Gurney[7] give an approximate relation between the half-life and the trap depth which gives for τ,

$$\tau=\frac{h^3e^{E/kT}}{1.386\pi m\sigma(kT)^2(6\pi)^{\frac{1}{2}}},$$

where E is the depth of the trap below the conduction band and σ is the capture cross section of the trap for thermal electrons. Assuming that $\sigma\sim 10^{-16}$ cm^2, we find that for $\tau=10$ μsec., $E\simeq 0.28$ ev at room temperature. If we assume that this trap consists of a hydrogenic orbit, the ionization energy will be approximately $10\kappa^{-2}\simeq 0.3$ ev where κ is the dielectric constant. This may be merely a coincidence but it does suggest a possible mechanism for this type of trap.

Measurements have been made with longer intervals between the initial and test pulses. Owing to instrumental limitations, the results were rather qualitative. However, it was demonstrated that electrons were being released from traps many milliseconds after the initial pulse. It seems unlikely that this can be accounted for by successive retrapping in shallow traps

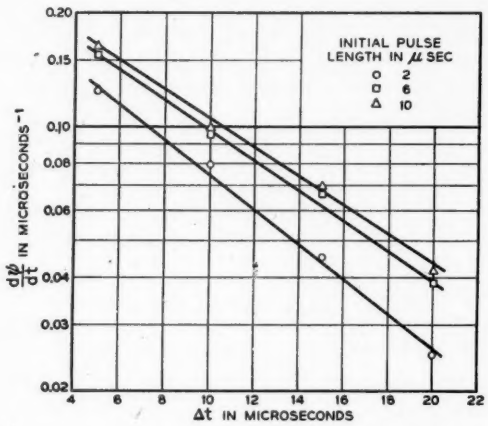

FIG. 15. $d\psi/dt$ as a function of Δt to determine rate of thermal release from traps.

[7] N. F. Mott and R. W. Gurney, *Electronic Processes of Ionic Crystals* (Oxford University Press, London, 1940), p. 108.

and suggests that we are dealing with at least two types of traps and possibly more.

The same experiments have been repeated for positive holes. Within the experimental error, no release of positive holes can be observed in times up to 16 msec., which is as far as the measurements were carried. The value of the crystal field between initial and test pulses did not affect this although in some cases it was negative for all of the Δt and in some cases positive for most of the time. We could probably detect a 10 percent release of trapped holes. Consequently, the release time constant for these traps must be greater than 100 msec. This confirms our expectation that the traps for electrons and traps for positive holes should exhibit quite different behavior.

All of the double-pulsing experiments have been performed at room temperature. It would certainly be of great interest to study this as a function of temperature. Nevertheless, the results obtained so far are of considerable interest. Newton[6] suggested that the current-time curves of Section 3 would have a negative second time derivative as long as the thermal release rate from traps was zero, i.e., there would be no inflection point. However, we have shown that the thermal release rate for positive holes is completely negligible on any microsecond time scale at room temperature. We have also shown in the previous section that the positive hole current has a well-defined inflection point which occurs over quite a wide range of experimental conditions and evidently occurs when the field across the plasma layer is very small. Moreover, the measurements of the time to reach the inflection point, τ_i, for electrons show that, for a given crystal field, $\delta_\infty \tau_i$ is independent of δ_∞ over a range of more than 10:1. This would not be so if the release of electrons from traps played a significant role in determining the inflection point.

We may conclude that the thermal release of trapped charges is not necessary to produce an inflection point although its position undoubtedly should be influenced by any significant release of trapped charges. Two other possibilities may account for the existence of a current following the inflection point: An inhomogeneous trap distribution could result in the current being cut off in some sections but still persisting in others in a process analogous to the operation of a variable μ-vacuum tube. The other possibility is that as the internal field approaches its final value, edge effects begin to play a role and some of the electrons move through regions of the crystal which are not subtended by the bombarded area. Either or both of these mechanisms could account for the observed behavior and further experiments are required to distinguish between them.

5. CONCLUSIONS

This investigation has clearly demonstrated that it is possible to make quantitative measurements of the behavior of mobile electrons and positive holes, produced by electron bombardment, in an insulating crystal and to fit the results into the framework of a simple theory for the space-charge free crystal. The theory does not attempt to describe the processes involved in detail but predicts merely the over-all current-voltage characteristic of the crystal under certain specific conditions. The experimental results are reasonably consistent and nowhere contradict the theory except for cases where the restrictions pertaining to the theory have been violated. This should not be interpreted as ruling out the existence of more complex processes than have been considered here.

The studies of the bombardment conduction current flowing under internal space charge conditions enable us to deal with the specific behavior in more detail. Here certain postulates are made concerning the nature of the internal fields and the behavior of the charge carriers in those fields. The good agreement between theory and experiment serves not only to specify more completely the actual mechanism but also to point up the fact that this establishes at least a sound beginning to the understanding of current flow through an insulator under the influence of space-charge fields.

The measurements of release of trapped electrons demonstrate a new method of studying this aspect of electron-solid interaction. The method is, at present, rather crude but it has a big advantage over studies of this process by the decay of luminescence in that the released electron does not have to emit light subsequent to its release in order to be detected. Moreover, the measurements serve to present in further detail the processes involved in bombardment conductivity.

I wish to express my thanks to Addison H. White for his constant encouragement during the course of the work and for his constructive criticism of the manuscript.

Effect of the Type of Support on the Photoelectric Work Function of Silver Films

L. L. BLACKMER*,** AND H. E. FARNSWORTH
Brown University, Providence, Rhode Island
(Received November 25, 1949)

Silver was doubly and fractionally distilled with the middle fraction deposited on previously outgassed bulk silver, on smooth fused quartz, and on outgassed molybdenum sheet in a sealed-off, gettered tube. Photoelectric measurements were made using the Fowler method. Deposit of a film of silver on bulk silver caused φ to decrease by varying amounts as great as 0.25 ev to 4.50±0.02 ev. Subsequent heating estimated at below 100°C caused ϕ to increase to the original value. φ for a silver film on smooth fused quartz and on outgassed molybdenum sheet is 4.41 ev. The results are unaffected by residual gas pressure in the tube. The low values of φ for the film appear to be due to a surface structure composed of microcrystals which are much smaller than those of the bulk silver. The variations in the observed values of φ for films on different supports is attributed to a dependence of the sizes of the microcrystals on the structure of the support. Information is given regarding the effect of the equilibrium conditions between volume and surface gas on the value of φ during the outgassing period of bulk silver.

INTRODUCTION

PREVIOUS experiments on thin films deposited on various bases have been carried out by means of electron diffraction,[1–3] contact potential,[4–6] and photoelectric[6] measurements. This interest in metal films is largely due to the fact that a specimen properly prepared by deposition from the vapor state in a high vacuum should present a surface nearly free of gas. The results obtained have led various experimenters[6,7] to suggest that the work function of such a metal film is greatly influenced by the underlying structure, although no detailed study of the problem has been made. Such an influence is expected if a particular crystal face predominates at the surface and is related to the support on which the film is deposited, since the work function of a single crystal is known to be a function of the crystal face which forms the surface. Observations by Farnsworth[1] on low speed electron diffraction indicate that a film which is deposited by evaporation at a low rate forms in a single lattice on the surface of a crystal of the same metal with an orientation which is the same as that of the underlying crystal face. Furthermore, it seems probable that any preferred orientation of a lattice in the film may also depend on the roughness[8] and temperature[3,9] of the condensing surface.

The primary purpose of this investigation was to determine the effect of the type of support and of its condition prior to deposition on the photoelectric work function of silver films deposited from the vapor state in high vacuum. Observations were also made on the effect of elapsed time after deposition, of heat treatment of the film after deposition, and of exposure to gas pressure.

APPARATUS AND PROCEDURE

A double evaporation procedure was employed in order to obtain films as nearly gas free as possible. The experimental arrangement was such that the silver source A, Fig. 1, could be heated by electron bombardment from the filament F_2 while the supports B were withdrawn into the side tube T_1. The U-shaped molybdenum filament F_1, which received some silver from A, could in turn be heated by conduction to deposit silver on the supports after they had been moved into the proper forward positions. Before making deposits, the source A and filament F_1 were outgassed at red heat for several hundred hours. The first few deposits on F_1 were driven off before exposing the supports, and it was thereafter kept coated with a heavy layer of silver. Usually one support was placed directly in front of the opening in F_1 during the evaporation from F_1 so that readings could be taken on the film immediately after deposition.

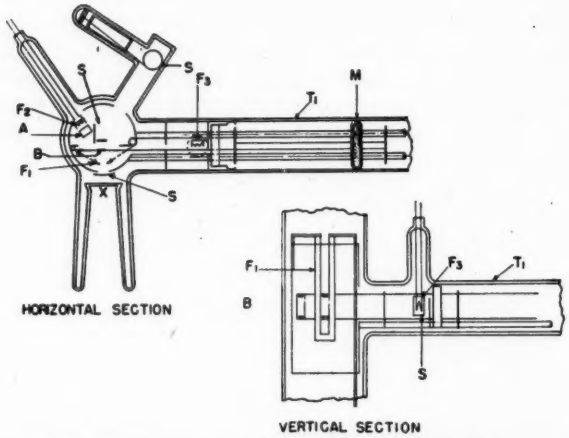

FIG. 1. Diagrammatic sketch of experimental tube.

* The experimental results presented here are taken from a thesis submitted in partial fulfillment of the requirements for the degree of Doctor of Philosophy in Brown University.
** Now with Eastman Kodak Company, Rochester, New York.
[1] H. E. Farnsworth, Phys. Rev. **43**, 904 (1933).
[2] H. E. Farnsworth, Phys. Rev. **49**, 605 (1936).
[3] O. Goche and H. Wilman, Proc. Phys. Soc. London **51**, 625 (1939).
[4] P. A. Anderson, Phys. Rev. **56**, 850A (1939); **49**, 320 (1936).
[5] P. A. Anderson, Phys. Rev. **59**, 1034 (1941).
[6] H. E. Farnsworth and R. P. Winch, Phys. Rev. **58**, 812 (1940).
[7] R. S. Cashman, Phys. Rev. **57**, 971 (1938).
[8] P. A. Anderson, Phys. Rev. **54**, 753 (1938).
[9] O. Rudiger, Ann. d. Physik **30**, 6 (1937).

Three supports for the films were used, one of polycrystalline silver 1.5 mm thick, one of smooth fused quartz, and one of molybdenum sheet. The silver support was cut from the same sample as the primary source used for the deposited films. It was of the same purity as that used by Farnsworth and Winch[6] in their determination of the work functions of silver crystal faces. Each support presented a surface 5×12 mm, and was mounted in a molybdenum frame held between molybdenum rods which were fastened to a sliding mechanism.

The specimens could be withdrawn into the side tube T_1 opposite the filament F_3 by an external electromagnet acting on the iron armature M. Magnetically controlled shutters S were provided to prevent condensation of metal on the windows, and other shields were placed at appropriate places. The bombarding filaments were surrounded by molybdenum shields on all sides except that facing the element to be heated. All iron armatures were enclosed in Pyrex glass. The collector of photo-electrons consisted of a molybdenum cylinder with suitable apertures to permit entrance of filaments. Ultraviolet light entered through the fused quartz window X, attached to the Pyrex envelope by a graded seal.

Before final assembly all parts were cleaned chemically. The assembly was made in a dust-free, dry room and parts were touched only with clean tools. Immediately thereafter, the tube was sealed directly to a vacuum system with two large traps in series separating the tube from the oil diffusion pumps, and a third trap separating the diffusion and backing pumps. The traps were cooled by solid carbon dioxide in acetone.

The gas pressure in the tube was measured with an ionization gauge. After the second baking of the experimental tube in an electric furnace, outgassing of the elements was conducted at a rate such that the pressure did not exceed 5×10^{-7} mm Hg. After the third baking, outgassing was continued until all elements could be heated to the desired temperatures at a pressure not in excess of 5×10^{-8} mm Hg. At this point the tube was gettered by two sets of six RCA getters[10] in series and sealed from the vacuum system. The getters were located in a side tube to prevent contamination of the surfaces under investigation. During the deposition process the pressure was below 5×10^{-8} mm Hg.

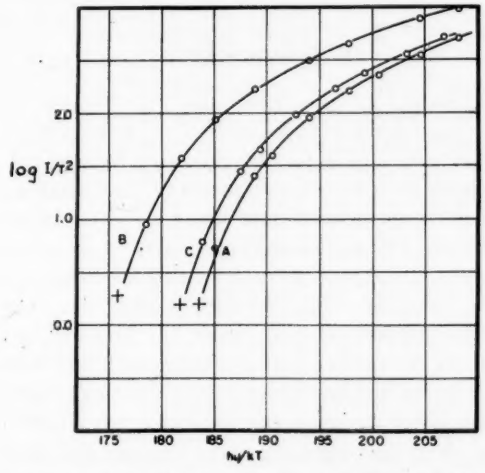

FIG. 2. Typical Fowler plots. Curve A is for a freshly heated surface, curve B is for the same surface some time after heating, curve C is for this surface subsequent to low temperature heating.

TABLE I. Values of the work function after depositions and at various stages of outgassing of the bulk sample.

Total time of outgassing after seal-off	φ immediately after heating	φ prior to deposit	Time between heating and deposition	φ after deposition	$\Delta\varphi$
27 hr.	4.60				
30	4.61	4.55	7 hr.	4.46	0.09
30+	4.62	4.58	3	4.44	0.14
	4.62	4.55	7	4.47	0.08
	4.62	4.56	3.5	4.50	0.06
	4.61	4.46	19.5	4.39	0.07
	4.62		0.25	4.50	0.12
	4.65		0.25	4.51	0.14
	4.64		0.25	4.50	0.14
	4.64		0.25	4.52	0.12
31	4.69				
47	4.66				
57	4.76				
159	4.76			4.64	0.12
198	4.74		0.25	4.49	0.25
222	4.76		0.25	4.51	0.25
232	4.68				
247	4.67				
265	4.68				

The monochromator, light source for photoelectric readings, and procedure have been described in a previous paper.[6] The Fowler method of analysis was used to determine work functions.

RESULTS AND DISCUSSION[11]

A. Polycrystalline Bulk Silver

φ for polycrystalline bulk silver, following a total heating of 250 hours after seal-off with frequent flashing to the evaporation point, was found to increase to 4.68±0.01 ev. Before this value was reached, numerous deposits were made. However, the sample was heated at temperatures high enough to evaporate deposited layers, and later heating at still higher temperatures produced no change from the above value.

No change of φ with time was observed during intervals of less than one hour after heating was discontinued. Over longer periods, φ decreased with time after heating. In the early stages of outgassing a decrease of 0.25 ev was observed in 700 hours. There is evidence that the rate of decrease is less after more outgassing, although the data on this point are not complete. At the end of the experiment the pressure was

[10] E. A. Lederer, RCA Rev. 4, 310 (1939).

[11] The constants h and k used in determining the experimental values of φ reported here are those given by Raymond T. Birge, Rev. Mod. Phys. 13, 233 (1941). Use of these constants results in a φ which is about 0.05 ev greater than that obtained with the constants accepted previously. No corrections have been applied to published results determined with the old constants.

increased to 10^{-6} mm Hg for five minutes by heating one of the side tubes. After this treatment the pressure dropped rapidly to 10^{-7} mm Hg and then continued to fall more slowly. Within the experimental error no change in φ for the freshly heated surface was observed within one hour. Subsequent to a decrease of φ with time after heating, it was found that only a small increase of temperature (to a value estimated to be considerably less than 100°C) for times as short as one minute was required to cause φ to return to the higher value obtained by high temperature heating.

B. Deposition of Silver on Polycrystalline Silver

Deposition of silver on the bulk sample soon after heating and at various stages of outgassing of the bulk sample[12] caused a sharp decrease in φ as shown in Table I. The results of six runs indicate a value for φ of 4.50 ± 0.02 ev for the film. Prior to seal-off, deposits were made on the freshly heated surface without taking intermediate readings and φ was 4.48 ev. The film thickness is not known, but it must have been of the order of several hundred atoms. Readings were taken as a function of time, starting within 30 seconds after deposition, but in no case was there a rapid increase such as that observed by Farnsworth and Winch[6] for a single crystal face. Even after periods as long as 18 hours no change in φ greater than 0.05 ev was observed and this was always a decrease.

When the time between end of heating of bulk metal and beginning of deposition of the film was several hours, the observed value of φ following deposition was lower than that given above. In some cases the difference between the two values is very nearly the decrease in φ for the bulk silver which occurred following heating and prior to deposition. However, the data are too limited to draw a definite conclusion on this point.

As in the case of the bulk silver subsequent to remaining at room temperature for some time after heating, a small rise in temperature caused an increase in φ for the film to nearly the same high value obtained for the freshly heated surface. Typical Fowler plots for this cycle are given in Fig. 2. As indicated by the data in Table I, the value of φ, which is obtained when deposition is made on the freshly heated surface, is independent of the outgassing time and of the value of φ before deposit.

The decrease of 0.12 to 0.25 ev brought about by deposition may be compared to a decrease of 0.09 ev observed by Farnsworth and Winch[6] in the case of the (100) crystal face of silver and a decrease of several tenths of a volt in the case of the (111) face of the same metal.

[12] In each case φ was measured immediately after heating was discontinued. This procedure usually required about fifteen minutes. A deposit was then made and a set of readings to determine φ of the film was taken immediately.

C. Deposition of Silver on Clear Fused Quartz

In the early stages of the investigation, before seal-off of tube from the vacuum system, deposition resulted from heating the adjacent bulk silver specimen. The film thus formed was clearly visible, but transparent. At this time φ was 4.68 ev. After subsequent heatings of the adjacent bulk silver, φ decreased to 4.52. Deposits, using the doubly distilled source, resulted in further decreases of φ to the equilibrium value of 4.41 ev after the fourth deposit. At the time of seal-off the surface was opaque. Later depositions in the gettered tube caused no further change in φ.

Raising the temperature of the film on quartz by heating the adjacent bulk silver to a temperature just below red heat caused an increase of φ to 4.48 ev. There was no change of this value with time, but deposition always decreased φ to 4.41 ± 0.01 ev. This value may be compared with 4.47 ev obtained by Anderson[5] for a silver film on glass.

The precision of the observations was not sufficient to make an accurate comparison of the minimum temperature required to increase φ for bulk silver with the minimum temperature required to increase φ for a silver film on bulk silver. However, it was estimated that they are approximately the same.

D. Deposition of Silver on Molybdenum Sheet

Deposition of silver on polycrystalline molybdenum caused φ to decrease from the value of 4.78 ev, obtained after outgassing at red heat for 150 hours. After the fourth deposit the value of φ was 4.41 ev, the same as that for silver or quartz, and did not change with further deposition. No noticeable change of φ for the silver film occurred with time after deposit when the molybdenum had been thoroughly outgassed. A low temperature heating (less than 100°C) of the silver film on molybdenum caused an increase in φ of 0.1 to 0.2 ev.

E. Interpretations

The residual gas pressures maintained in the experimental tube appear to have had no influence on the observed values of φ for the following reasons: (1) An intentional increase of gas pressure produced no observed decrease in φ of bulk silver. (2) The value of φ for a film of silver deposited on quartz or on outgassed molybdenum did not decrease with time after deposit. A slight decrease with time after deposit was observed for a film of silver on bulk silver. (3) Although φ for a silver film on quartz and on outgassed molybdenum was increased by low temperature heating, there was no subsequent decrease of this value with time after heating as in the case for a silver film on bulk silver.

Two other possible causes for the decrease of φ of bulk silver and of a silver film on bulk silver, with time after heating or after deposit may be considered: (1)

During the heating process gas from the interior of the bulk metal diffuses to the surface and evaporates. Because of the relatively long time required to obtain equilibrium between the surface and volume gas at the elevated temperature, the amount of gas on the surface at any instant at the high temperature is less than the equilibrium value which exists after the metal is later cooled to room temperature. Hence a slow increase in the amount of surface gas is expected later at room temperature as a result of diffusion from the interior. This interpretation requires that this equilibrium condition is disturbed by the low temperature heating and that surface gas is removed to the same extent that existed immediately following the higher temperature heating. (2) At the highest temperature of heating a surface arrangement of atoms occurs which is not the most stable at room temperature. Subsequent to high temperature heating a slow rearrangement would then occur at room temperature. We know of no experimental evidence for this second assumption and therefore tentatively conclude that only the first assumption regarding gas diffusion deserves serious consideration.

We interpret the relatively low values of 4.41 ev for a silver film on quartz and on outgassed molybdenum, and 4.50 ev for a silver film on bulk silver as due to a structure of the film which differs from that of bulk silver. Electron diffraction patterns from evaporated films on fused quartz indicate a micro crystalline structure[9] and we tentatively associate the low value of φ with the minute size of the crystals. The increase of φ for the film caused by low temperature heating is attributed to crystal growth. The fact that the same values of φ were obtained for the film on quartz and on molybdenum suggests that the film structure is the same in these cases. Molybdenum has a body-centered lattice of 3.14A compared to 4.08A for face-centered silver and it is expected that there would be little or no tendency for the silver to conform to the molybdenum lattice. In the case of the silver support, the higher value of φ for the film suggests a partial alignment with the underlying structure under similar conditions of rate and temperature of deposition. This would also be expected with other metal supports having suitable lattice constants. For example, the lattice constant of gold differs from that of silver by less than 0.5 percent.

The decrease of φ with increase of film thickness on quartz may also be associated with a structure change, but before considering this result in detail a repetition of the observation should be made with better control of conditions.

The observations of Farnsworth and Winch[6] now appear to require some changes in interpretations. They found, after depositing a silver film on two bulk silver single crystals with (111) and (100) faces, respectively, that the sudden decrease in φ due to the film deposition was followed by a spontaneous increase extending over a period of an hour or two. In many cases the value of φ after the increase coincided with that for the bulk crystal before the deposit. At that time the increase was attributed to adsorption from the residual gas in the tube. That interpretation requires that the values of φ for the two crystal faces after thorough outgassing are characteristic of gas contaminated faces. On the basis of the present observations, it now appears that the spontaneous increase in φ, following the decrease due to film deposition, corresponds to the increase in the present observations induced by slight heating of the film on bulk silver above room temperature. The reason for the spontaneous increase of φ in the observations of Farnsworth and Winch may be due to a greater mobility on the single crystal surface, a different rate of deposition, or a higher ambient temperature during these observations. This interpretation indicates the values of $\varphi_{100}=4.81$ ev and $\varphi_{111}=4.75$ ev obtained by Farnsworth and Winch for the two crystal faces after thorough outgassing are those for *gas-free faces*.

With the above values of φ for the low index faces which are found to predominate in a polycrystal it is clear that the low value of 4.41 ev cannot result from a random arrangement of low index faces, but must be characteristic of the structure of the film composed of exceedingly minute elementary crystals.

Although some evidence has been obtained previously by Anderson[8] that φ for a microcrystalline film of magnesium is less than that for a surface composed of "equilibrium crystal faces," no observations were made on the dependence of φ (for a film) on the type of support.

The Increase in the Primary Cosmic-Ray Intensity at High Latitudes, and the Non-Existence of a Detectable Permanent Solar Magnetic Field*

MARTIN A. POMERANTZ
Bartol Research Foundation of The Franklin Institute, Swarthmore, Pennsylvania

(Received December 7, 1949)

The primary cosmic-ray intensity at Churchill, Manitoba (geomagnetic latitude 69° N) has been compared directly with that at Swarthmore, Pennsylvania (geomagnetic latitude 52° N). The measurements, obtained with identical vertical quadruple-coincidence counter trains, have revealed an increase at the more northern station caused by the presence in the primary radiation of particles having energies below that which would have been permitted had the sun's magnetic field been effective to the extent previously assumed. The ratio of intensities is $I_T(0, 69°)/I_T(0, 52°)=1.46$. *Intensity vs. altitude* curves were obtained with several different thicknesses of absorber interposed in the counter trains.

These experiments have revealed the absence of a sharp cut-off at the low energy end of the spectrum, imposed by a permanent solar dipole-moment having a magnitude consistent with certain controversial astrophysical determinations. Such a dipole-moment would have produced a knee in the latitude effect at about 50° N geomagnetic latitude. Furthermore, there is no indication of any diurnal variation which could be in conformity with the existence of a permanent dipole-moment at the sun.

The differential energy distribution at the low energy end of the primary cosmic-ray spectrum cannot be evaluated exactly because of absorption considerations, but it is doubtful that the exponent in an inverse power-law representation is as large as has usually been assumed heretofore.

Alternative explanations of the observed increase in counting rates, by invoking trapped orbit or re-entrant particle hypotheses, have been considered and rejected. It is concluded that the sun possesses no detectable permanent magnetic field and, on the basis of the present experiments, an upper limit of 0.6×10^{33} gauss-cm^3, as compared with the previously quoted value of 10^{34} gauss-cm^3, may be assigned as a maximum possible value of the dipole-moment, if indeed it exists at all.

I. INTRODUCTION

THAT the magnetic field of the sun imposes a sharp cut-off at the low energy end of the spectrum of primary cosmic rays, and hence precludes the presence near the earth of any such particles having momenta below that required for entrance at a geomagnetic latitude of about 50°, has become generally accepted as a well-established fact. This almost universal agreement among physicists as regards the magnitude of the effect is paradoxical indeed in view of the fact that even the very existence of a permanent solar magnetic dipole-moment is a controversial issue among astronomers.

Discordant results have been reported by different investigators as a consequence of the extremely difficult nature of the observations. The only method available to the astrophysicist for detecting a magnetic field at the sun involves a search for a splitting of spectral lines arising from the Zeeman effect. The measurements, just on the fringe of feasibility, involve displacements as small as one-thousandth of the line width.

The original determinations of Hale *et al.*[1] were reported as being consistent with a value of field strength of 50 gauss at the poles. However, the results apparently depended upon which point on the sun served as source, and the measured field dropped rapidly in the outer regions of the solar atmosphere. Factors such as the grain of the photographic plates, distortions, local magnetic fields, and other technical difficulties complicated the problem. Of a group of independent measurements, three yielded confirmation of the polarity and magnitude of the field, whereas three indicated zero results. Subsequent remeasurements by Hale[2] indicated no shift. Evershed,[3] following a different procedure in the analysis of Hale's plates, independently concluded that no field exists, whereas Thiessen[4*] applied an interferometric method which presumably confirms the maximum value originally quoted by Hale.

It had been realized for more than a decade that the knee of the latitude effect at sea level would be expected where the minimum energy required for penetration of the atmosphere is equal to the low energy limit permitted by the earth's magnetic field. However, Cosyns,[5] who operated an ionization chamber in a balloon which was floating over Europe between $\lambda=47°$ and $\lambda=51°$, reported that the position of the knee was independent of altitude up to a height corresponding to a pressure of 70 mm of Hg. This prompted the suggestion by Janossy[6] and by Vallarta,[7] later extended by Epstein,[8] that a permanent solar magnetic dipole-moment of the magnitude cited earlier could cut off rays of energy less than 3×10^9 ev. This appeared to be consistent with the aforementioned constancy of intensity at

* Assisted by the Joint Program of the ONR and the AEC.

[1] Hale, Seares, Van Maanen, and Ellerman, Astrophys. J. **47**, 206 (1918).

[2] Carnegie Institution Year Book **34**, 157 (1935); **35**, 173 (1936).

[3] Evershed, M.N.R.A.S. **99**, 438 (1939).

[4] G. Thiessen, Ann. Astrophys. **9**, 101 (1946); Himmelswelt **55**, 22 (1947).

[4*] *Note added in proof:* Subsequent investigations by Thiessen revealed that the earlier result was too high because of an insufficient number of observations. G. Thiessen, Zeits. f. Astrophys. **26**, 16 (1949). Very recent measurements with modified apparatus yielded a value for the polar field strength of -1.5 ± 0.5 gauss. G. Thiessen, Observatory **69**, 228 (1949).

[5] M. Cosyns, Nature **137**, 616 (1936).

[6] L. Janossy, Zeits. f. Physik **104**, 430 (1937).

[7] M. S. Vallarta, Nature **139**, 839 (1937).

[8] P. S. Epstein, Phys. Rev. **53**, 862 (1938).

latitudes north of $\lambda = 50°$ where the lowest permitted energy was also 3×10^9 ev.

Experimental verification of this hypothesis was sought simultaneously by Carmichael and Dymond[9] and by Johnson.[10] The conclusion regarding the imposition by a solar magnetic field of a low energy limit in the cosmic-ray spectrum appeared inescapable in the light of the results obtained by the former with ionization chambers, and with coincidence counters which yielded an *intensity vs. altitude* curve near the north magnetic pole of the same general shape as that of Pfotzer[11] at $\lambda = 49°$. Inasmuch as an enormous difference between the appearance of these curves was anticipated (on the basis of shower production considerations) in accordance with the concepts then prevalent regarding the nature and properties of the primary cosmic radiation, the comparison from this point of view was regarded as meaningful. In the light of the present state of our knowledge concerning the composition of the primaries, it seemed probable that the net effect of the entrance of lower energies at latitudes north of the knee might be considerably smaller than had been expected earlier on the basis of an exclusively electronic primary radiation, and hence could have remained undetected as a consequence of the rather gross procedures which had seemed warranted previously.

Various factors had precluded the discovery of an increase at high latitudes of a magnitude which would seem reasonable now. First, for reasons stressed previously[12,13] the comparison between the results of different observers on the basis of an arbitrary normalization could easily mask an appreciable effect. Secondly, inasmuch as the measurements involved the total intensity, considerable ambiguity is introduced by differences in the effect of thicknesses of counter walls, as pointed out earlier.[13] Furthermore, fluctuations produced by variations in the softer radiation from one day to another could be important. As a matter of fact, the conclusion that there is no sharp cut-off at an altitude corresponding to 1.5 m of H_2O as far north as 60° geomagnetic latitude was vitiated somewhat by such considerations.[14] In the third place, coincidence data were available from only a single flight at $\lambda = 88°$, and it was necessary to compare these with averages obtained by Pfotzer in a number of flights yielding widely varying results and requiring instrumental corrections comparable with the recorded counting rates. These separate measurements were then fitted to a common scale at ground level. Finally, a period of several years had elapsed between the experiments of Pfotzer and of Carmichael and Dymond.

Although the electroscope measurements of Bowen, Millikan, and Neher[15] showed an increase in ionization between Omaha, Nebraska (geomagnetic latitude 51° N) and Saskatoon, Saskatchewan (geomagnetic latitude 60° N) this was not interpreted until very recently[16] as evidence against the existence of a sharp cut-off. However, the situation in this instance is beclouded by an uncertainty in the net contribution to the integrated ionization measurements arising from small geomagnetic directional effects.

It was therefore deemed important to seek independent confirmation of these results, particularly in view of their rather fundamental significance in cosmic-ray physics as well as in astrophysics. Techniques which have been subjected to repeated tests during the course of an extensive program of investigations at very high altitudes were well adapted to this purpose.

II. EXPERIMENTAL PROCEDURE

The experiment essentially comprised a direct comparison by identical instruments of the vertical cosmic-ray intensity near the "top of the atmosphere" at Swarthmore, Pennsylvania (geomagnetic latitude 52° N) with that at Fort Churchill, Manitoba (geomagnetic latitude 69° N). The necessary data were obtained with standard quadruple-coincidence counter trains similar to those utilized previously.[12] Radio signals indicating atmospheric pressure, temperature within the gondola, and cosmic-ray events were continuously transmitted to the ground receiving station installed inside a house-trailer equipped as a mobile laboratory. Here the information was recorded on a paper tape by means of a high speed direct-inking recording oscillograph arrangement.[17]

TABLE I. Summary of ground runs of instruments prepared for this series of flights. No interposed absorber.

Flight number	Ground counting rate
1*C*	0.886±0.010
2*C*	0.906±0.013
3*C*	0.918±0.017
4*C*	0.914±0.010
5*C*	0.910±0.012
6*C*	0.900±0.012
7*C*	0.899±0.009
8*C*	0.910±0.014
9*C*	0.915±0.011
10*C*	0.911±0.009
11*C*	0.915±0.011
12*C*	0.897±0.011
13*C*	0.895±0.012
15*C*	0.920±0.014
16*C*	0.894±0.009
17*C*	0.915±0.010
18*C*	0.889±0.015
19*C*	0.895±0.012
20*C*	See 17*C*
21*C*	0.906±0.008
Average	0.905±0.003

[9] H. Carmichael and E. G. Dymond, Nature **141**, 910 (1938); Proc. Roy. Soc. **171**, 321 (1939).
[10] T. H. Johnson, Phys. Rev. **54**, 151 (1938).
[11] G. Pfotzer, Zeits. f. Physik **102**, 23 (1936).
[12] M. A. Pomerantz, Phys. Rev. **75**, 69 (1949).
[13] M. A. Pomerantz, Phys. Rev. **75**, 1721 (1949).
[14] Biehl, Montgomery, Neher, Pickering, and Roesch, Rev. Mod. Phys. **20**, 360 (1948).
[15] Bowen, Millikan, and Neher, Phys. Rev. **53**, 855 (1938).
[16] Biehl, Neher, and Roesch, Phys. Rev. **76**, 914 (1949).
[17] M. A. Pomerantz and R. C. Pfeiffer, J. Franklin Inst. **248**, 305 (1949).

TABLE II. Comparison of counting rates on the ground at Churchill, Manitoba, and Swarthmore, Pennsylvania. Flight 15C with no interposed absorber. The stated uncertainties are statistical standard deviations. The rate at Churchill would be expected to be slightly lower owing to the difference in altitudes.

Station	Average counting rate	Average station pressure, mm of Hg	Altitude above sea-level, feet
Swarthmore	0.920±0.014	758	296
Churchill	0.890±0.013	762	0

In accordance with the philosophy formulated during the early stages of development of the experimental techniques utilized in this program, the policy of confining the observations to a single type of measurement per flight was adopted; many simple flights are preferred over a few complicated ones. Numerous practical advantages accrue from this approach.

The desirability of reducing the complexity of an individual instrument to an absolute minimum need hardly be stressed. Furthermore, the accompanying reduction in weight simplifies the launching procedure to an extent far out of proportion to the load. It becomes feasible to conduct repeated flights with identical arrangements, thereby providing independent checks which experience has dictated must be regarded as indispensable in view of the unique conditions prevailing in radiosonde operation. Complications associated with telemetering various types of information simultaneously are avoided, and the receiving and recording systems are readily adaptable to field operation. It is also possible to follow the progress of a flight without analyzing a photographic record, and audibly to determine counting rates as frequently as necessary to facilitate immediate preliminary plotting of the results. Thus, the flight program during the course of a field expedition may be modified in a manner which is most advantageous in the light of the actual results. This feature was especially important during the Fort Churchill expedition.

Finally, the consequences of failure of any essential component are far less serious. Particularly valuable, moreover, is the "hedging" thereby afforded against inevitable premature bursting of balloons. A flight which does not attain an altitude sufficiently high to provide all of the desired data need not be discounted as a total loss. On the contrary, the data may nevertheless serve quite satisfactorily as a confirmation of results obtained in another higher ascent.

Each apparatus was operated on the ground for a long period during which the internal consistency of the runs was continuously checked. As may be seen in Table I, the average counting rates with no interposed

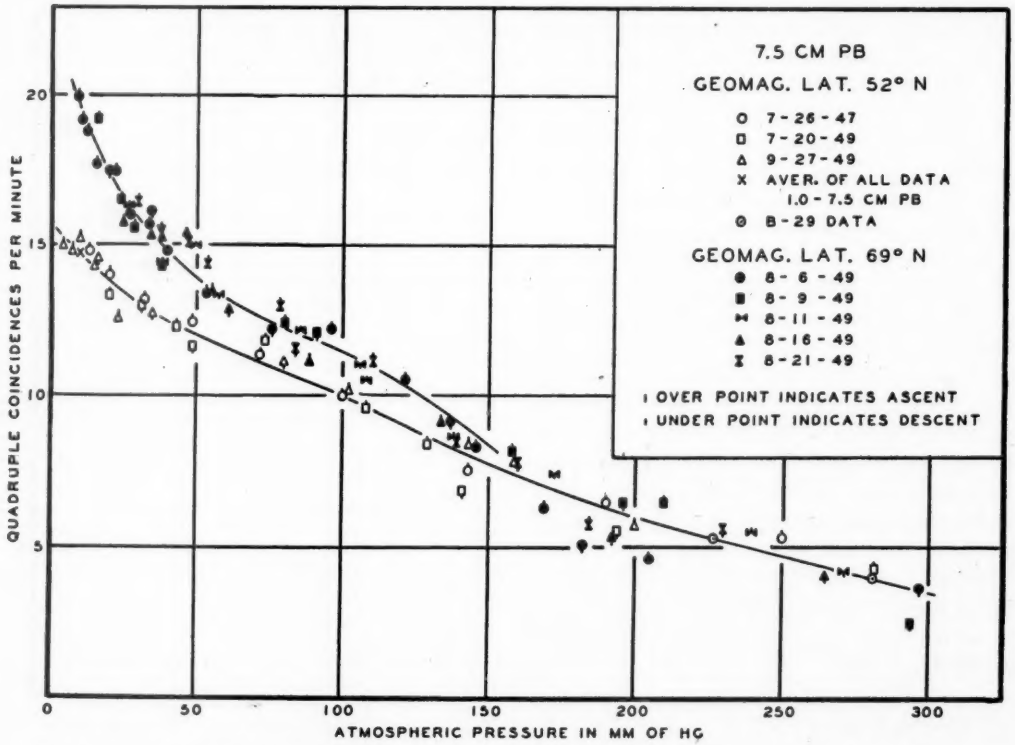

FIG. 1. *Intensity vs. altitude* curves for cosmic rays arriving vertically, and having a minimum residual range of 7.5 cm Pb, at $\lambda = 52°$ N and at $\lambda = 69°$ N. The increase in the intensity at high altitudes is clearly evident. The point × previously obtained with similar instruments does not include the present data, and the points ⊙ were obtained during B-29 flights (see reference 13). The reproducibility of the data from flight to flight, and year to year, should be noted.

absorber agreed within a statistical uncertainty of approximately 1 percent.

Although a detailed description of instrumental techniques will be omitted for the present, it is perhaps worthwhile mentioning by way of example one of the precautionary measures to which good reproducibility from flight to flight and the extremely small shrinkage rate are attributable. Vacuum tubes which are entirely satisfactory and uniform according to the standards established for commercial test instruments may be very dissimilar as regards performance in specialized equipment of the type designed for operation in free-balloon flights. Rather severe tests are therefore conducted on all tubes under the circuit conditions actually encountered in the specific application. Among other requirements, characteristics must remain constant during the final portion of an aging process, and subsequently throughout the long period of pre-flight operation in an apparatus. Furthermore, the characteristics of tubes incorporated in a particular set must be closely matched. Tests of the various tubes as well as of the complete instruments prior to release reveal their ability to operate satisfactorily over a range of battery voltages down to values much lower than the minima which could prevail during a flight. The enforcement of such severe requirements results in the rejection of a very large percentage of stock tubes, but assures reliability and stability of components throughout the course of a flight, of extremely short duration in comparison with the entire period of operation of a set.

It was most expedient for the present purposes to utilize ballooning techniques which cause the flights to rise relatively rapidly (approximately 800 feet per minute) through the lower regions of the atmosphere, and then more slowly from about 40,000 feet to the ceiling altitude. Rates of rise between 200 and 500 feet per minute in the upper regions, considerably smaller than have been customary, reduce statistical uncertainties. It is evident that the number of counts recorded by a given instrument is inversely proportional to the ascent rate. It was also advantageous for the descent to commence immediately after the ceiling was reached, so that the original curve could be retraced.

In order to minimize any possible complications which might have been introduced by the frequently-cited non-reproducibility in the results obtained at different times[14,18] with coincidence-counter trains containing no absorber other than the counter walls, the initial flights were conducted with 7.5 cm of interposed lead. This would certainly preclude the observation of particles in the lower portion of the new band of energies which would be permitted at 69° N in the absence of a solar dipole-moment. In any event, even the small amount of residual atmosphere above the apparatus (approximately 11 g/cm² at the highest altitudes attained) would absorb such low energy primaries. However, the absence at the "top of the atmosphere" of absorption in small thicknesses of lead, observed in earlier experiments,[12] had indicated that if particles having less than the geomagnetic cut-off energy at Swarthmore were in fact entering at higher latitudes, their presence would be detected by this arrangement.

III. RESULTS

The results of flights in which an absorber of 7.5 cm of Pb was interposed in the coincidence train are plotted in Fig. 1. It is clear that near the "top of the atmosphere" a real increase of about 40 percent occurs in the intensity of particles having the aforementioned residual range. In the lower atmosphere, points recorded over Swarthmore and Fort Churchill overlap within rather large statistical uncertainties.[19] On the ground, the counting rate was the same at the two stations as is shown for a typical instrument in Table II. At an altitude corresponding to somewhat less than 150 mm of Hg the departure becomes quite unambiguous.

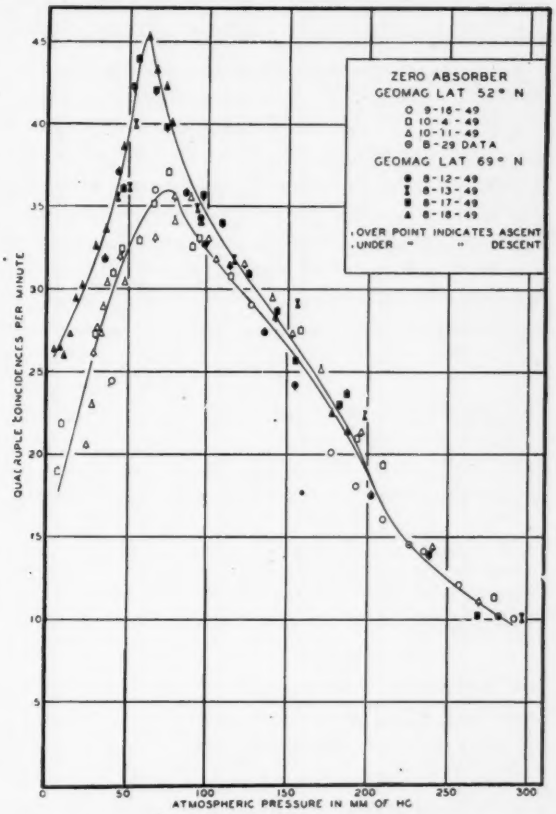

FIG. 2. *Intensity vs. altitude* curves, obtained with no interposed absorber other than the counter walls (mean thickness 4.4 g/cm²), for cosmic-rays arriving vertically at λ=52° N and λ=69° N. (Correction: The first line in the box in the upper right-hand corner of the figure should read: 0 9-16-47.)

[18] D. J. Montgomery, *Cosmic Ray Physics* (Princeton University Press, Princeton 1949), p. 164.

[19] See reference 13 for the causes of large statistical uncertainties in data obtained in the lower atmosphere.

The point × at 52° N represents an average (standard deviation ±2 percent) of all previous data obtained at altitudes exceeding 90,000 feet with vertical coincidence counter trains.[12] It is based upon the results of 9 flights containing different amounts of interposed material (1.0–7.5 cm Pb). The data obtained in 1949 have not been incorporated in this value. A considerable body of data accumulated in another series of measurements at small zenith angles and correspondingly higher altitudes also confirms this value of the primary relative intensity[20] near Swarthmore.

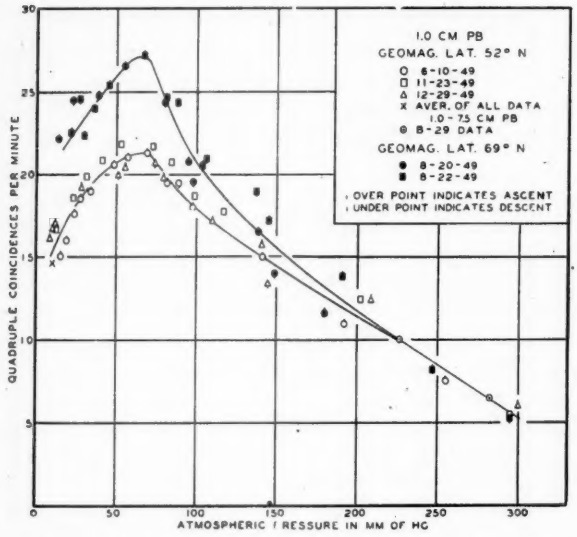

FIG. 3. *Intensity vs. altitude* curves, obtained with 1 cm of Pb interposed in the coincidence-counter train, for cosmic rays arriving vertically at λ = 52° N and λ=69° N. (Correction: The first line in the box in the upper right-hand corner of the figure should read: 0 16–10–48.)

The agreement between ascent and descent and between individual flights is satisfactory. It should be noted that flights immediately preceeding departure and following the return of the expedition yielded results in good accord with those obtained two years earlier.

Following verification of the results of the initial flight, which had revealed the presence in the primary radiation of particles having energies below that which would have been permitted had the sun's magnetic field been effective to the extent previously assumed, the program was extended to include flights with no interposed absorber as well as with intermediate thicknesses. In every case, the increase with latitude of the intensity at very high altitudes is clearly evident.

Figure 2 shows the results for the so-called "total" intensity, i.e., for all particles which can penetrate the counter walls (4.4 g/cm²=1.8 g/cm² Cu+2.6 g/cm² glass, mean thickness between sensitive volumes of extreme counters). The shape of the *intensity vs. altitude* curves has also been altered, with a sharper peak occurring at about 60 mm of Hg for the more northern latitude.

Data obtained with 1 cm of Pb interposed in the counter train are plotted in Fig. 3. Because the maxima are relatively broad, it is not clear whether a shift has occurred in this case.

Although the detection of a very small diurnal variation was not specifically attempted, the data may be examined for evidence of such an effect. Despite the fact that flights were conducted at different times of the day, there is no indication of any marked differences which could be attributable to a diurnal effect. Table III is a summary of the flights at Churchill showing the time of day at which the maximum altitude was attained in each case.

Additional verification of the absence of an appreciable diurnal variation was provided by data obtained in a flight which fortuitously leveled off at about 35 mm of Hg, and remained here for 7 hours. During this period, owing to the presence of a strategically situated hole in one of the balloons, the flight oscillated above and below a pressure reference point. Counts were recorded continuously between contacts. The counting rates averaged over the individual intervals between pressure signals are listed in Table IV. It is seen that the average intensity remained constant within statistical uncertainties of less than 3 percent.

There is little doubt that the diurnal variation predicted for the top of the atmosphere (and exceeding the aforementioned statistical uncertainty) should propagate itself to this depth, and, in fact, undergo amplification. Furthermore, even though data are available from only one flight, there are no grounds for doubting the validity of the negative conclusion. If a variation following a particular trend had been indicated, the single result could have been challenged on the basis of possible systematic instrumental changes. The observed constancy, on the contrary, is not vulnerable to such potential criticism.

IV. DISCUSSIONS

A. Solar Dipole-Moment

In view of the fact that the Störmer cone created at the earth by a permanent solar magnetic field would not move with respect to a coordinate system fixed on the sun, the rotation of the earth would produce an apparent motion of the forbidden regions past a particular point of observation. Thus, particles having certain energies would be excluded during some portions of the day and permitted at others, giving rise to a diurnal effect. Calculations by Dwight[21] have already been discussed,[22] and quantitative considerations have led to the conclusion that it is not possible to account for

[20] Geometrical factors for computing absolute intensities are given in reference 13.

[21] K. Dwight, Princeton University thesis (1949), unpublished.

[22] M. A. Pomerantz and M. S. Vallarta, Phys. Rev. **76**, 1889 (1949).

TABLE III. Resume of flights conducted at Churchill. As may be seen from a comparison of points plotted in Figs. 1–3, no dependence upon time is indicated within the limits of the present experiments.

Flight No.	Time of arrival at ceiling altitude, local solar time	Date
1C	9:31 a.m.	Aug. 23
2C	4:24 p.m.	Aug. 11
3C	9:56 a.m.	Aug. 20
4C	4:55 p.m.	Aug. 18
5C	10:13 a.m.	Aug. 21
6C	10:17 a.m.	Aug. 16
9C	8:40 a.m.	Aug. 9
10C	8:23 a.m.	Aug. 12
11C	10:32 a.m.	Aug. 6
12C	8:42 a.m.–3:42 p.m.	Aug. 13
13C	9:31 a.m.	Aug. 22
15C	7:19 a.m.	Aug. 17

TABLE IV. Summary of data recorded during Flight 12C after leveling-off at an altitude corresponding to approximately 38 mm of Hg. Counting rates have been averaged over the entire intervals between successive pressure signals, about the mean local solar times indicated. The stated uncertainties are statistical standard deviations.

Pressure range*	Mean local solar time	Average counting rate
Above pressure contact—Average pressure approx. 34 mm of Hg	10:27 a.m. 2:17 p.m.	33.3±0.3 33.8±0.6
Below pressure contact—Average pressure approx. 42 mm of Hg	8:52 a.m. 11:42 a.m. 12:42 p.m.	35.2±1.1 36.2±1.2 35.2±1.1

* The pressure signal was transmitted continuously while the instrument was in the pressure interval 40 mm–36 mm, and no counts were recorded during these periods.

these results by a shift in the latitude of the knee caused by a diurnal variation of the vertical intensity. Actually, according to these computations, the vertical intensity at 69° N should be 7 percent *less* than that at 52° N in the early morning.

It is possible to assign an upper limit to the magnetic dipole-moment of the sun, if indeed it exists at all, on the basis of the present data. The value of 0.6×10^{33} gauss-cm^3 replaces, as a maximum possible value, that previously assumed of 10^{34} gauss-cm^3. This limit in turn pushes a possible knee of the latitude effect to 75° N. geomagnetic latitude.

Unfortunately, considerations which will be discussed later probably preclude any further reduction in this upper limit by a repetition of measurements of this type at more northerly latitudes. Particles with energies below the geomagnetic cut-off at Churchill would in fact be absorbed before reaching balloon-borne instruments.

B. Low Energy Spectrum

The total measureable unidirectional primary cosmic-ray intensity is given by:

$$I_T(\theta,\lambda)=\sum_1^n\int_{\epsilon_n(t,\lambda)}^{\infty} i_n(\epsilon)d\epsilon, \qquad (1)$$

where $i_n(\epsilon)$ is the spectral intensity, the index n represents a particular type of particle, t is the thickness of the atmosphere above the detecting apparatus plus the counter walls which must be penetrated to record a coincidence, θ is the zenith angle, and λ is the geomagnetic latitude.

Ideally, at a point sufficiently near the top of the atmosphere so that multiplicative effects are relatively small, the lower limit $\epsilon_n(t,\lambda)$ of the above integral will be either the geomagnetic cut-off energy at latitude λ *or* the minimum energy required by a primary particle (or its progeny) to penetrate the thickness t. The larger of these two quantities is the governing factor. At 52° N the minimum energy for entrance of protons in the vertical direction is 1.6 Bev, and experiments have revealed[12] that this exceeds the energy required to penetrate the absorbing layer. At Churchill, however, even though the geomagnetic cut-off energy is only 0.1 Bev, lower energy-primaries could not be detected. Considering ionization losses alone, 0.09 Bev would be required for a primary proton to reach 110,000 feet. Obviously, penetration of the counter walls further increases the requisite energy, and other modes of energy loss raise $\epsilon_n(t,69°)$ to an extent which cannot now be specified because of the lack of information regarding the primary interaction.

In principle, the nature of the spectral energy distribution may be determined from a comparison of the primary intensities at two different latitudes. Following earlier practice, this would be accomplished by assuming an inverse power function of the energy:

$$i_n(\epsilon)d\epsilon=k\epsilon^{-\gamma}d\epsilon. \qquad (2)$$

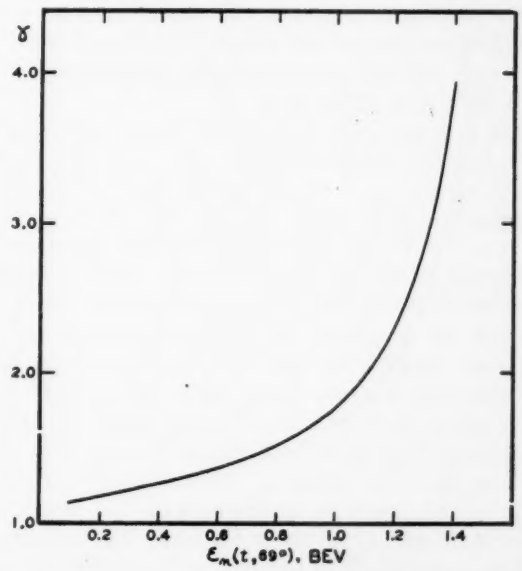

FIG. 4. The power γ, in the differential energy distribution, $i_n(\epsilon)d\epsilon=k\epsilon^{-\gamma}d\epsilon$, plotted as a function of $\epsilon_n(t,69°)$ for the case of the experimentally-determined ratio of primary intensities at Churchill, Manitoba, and Swarthmore, Pennsylvania, $I_T(0,69°)/I_T(0,52°)=1.46$. Here, $\epsilon_n(t,69°)$ is determined by the thickness, t, of air above the ceiling altitude plus the counter walls.

Integration of Eq. (1) then leads to the result:

$$I_n(\theta, \lambda) = k[\epsilon_n(t, \lambda)]^{1-\gamma}/(\gamma - 1). \quad (3)$$

From this the ratio of intensities of a particular primary component at two different latitudes is:

$$[I_n(\theta, \lambda_1)]/[I_n(\theta, \lambda_2)] = [\epsilon_n(t, \lambda_2)/\epsilon_n(t, \lambda_1)]^{\gamma-1}. \quad (4)$$

Actually the measurements yield values of the ratio $I_T(0, 69°)/I_T(0, 52°)$. Determination of the energy distribution of the different components at latitudes south of 50° where $\epsilon_n(t, \lambda)$ is well defined presupposes a knowledge of the relative composition of the primary radiation at the two different locations. Even if it were assumed quite arbitrarily that the energy distribution of the various components were initially the same at very large distances from the earth, the sorting effect of the terrestrial magnetic field for rays below the lower limit would alter the percentage composition of the primary beam as a function of latitude, inasmuch as the geomagnetic effects depend fundamentally upon magnetic-rigidity. Thus, strictly speaking, ratios of total intensities can only provide a magnetic-rigidity distribution.

It has been demonstrated by means of particle-discriminating counter trains[23] and by photographic emulsion techniques[24] that at 52° N approximately one-third of the incoming cosmic rays are alpha-particles, and the remainder are predominantly protons. To a first approximation, it can be assumed that this does not change appreciably at 69° N. As a matter of fact, the ratio of cut-off energies is $\epsilon_p(0, 52°)/\epsilon_p(0, 69°) = 16$ for protons and $\epsilon_\alpha(0, 52°)/\epsilon_\alpha(0, 69°) = 19$ for α-particles. Hence $I_T(0, 69°)/I_T(0, 52°) \approx I_n(0, 69°)/I_n(0, 52°)$. Figure 4 shows the power γ in the differential energy distribution plotted as a function of $\epsilon_n(t, 69°)$, for the case of the experimentally determined value $I_T(0, 69°)/I_T(0, 52°) = 1.46$.

The extreme value of 1.14 for γ would apply if all of the primaries incident at the top of the atmosphere would register an event. Although the correct value is necessarily higher, it is unlikely that the power is as great as 3. Although this had previously appeared to be consistent with observation[25] on the basis of assumptions which are no longer tenable, it has been propagated through the literature and more or less accepted as a law even though the failure at the low energy end of the spectrum was recognized. As a matter of fact, there is no reason to expect that the distribution function is a constant independent of energy. Furthermore, it is obvious that the validity of a law of this form down to zero energy leads to a divergence, and implies an infinite amount of energy in the form of cosmic-rays.

The correct value of $\epsilon_n(t, 69°)$ at Churchill is actually quite difficult to predict. The range of a primary particle could conceivably be either reduced or enhanced by conversion into secondaries. A mesotron may have considerably greater range than the proton which produces it. The net result depends of course upon the multiplicity, the division of energy among secondaries, and similar considerations. A knowledge of the spectrum and its rate of change just south of Swarthmore would conversely permit an approximate evaluation of $\epsilon_n(t, 69°)$ on the basis of Fig. 4.*

C. Intensity vs. Altitude Curves

Various features of the *intensity vs. altitude* curves may be commented upon at least qualitatively, pending detailed theoretical analysis. The pronounced alterations in the shapes of the curves are all indicative of the addition of a group of low energy particles at the more northerly location.

It is not surprising that, in Fig. 1, the shape of the Churchill curve in the upper portion of the atmosphere becomes steeper than that representing the Swarthmore results. The low energy particles which contribute to the higher intensity at 69° N are rapidly absorbed. Furthermore, the maximum for the "total intensity" (Fig. 2) is displaced toward higher altitudes because of the combination of this factor together with lower average secondary energies and correspondingly diminished mean-free-paths. Finally, absorption is observed to occur in small thicknesses of material at the highest altitudes attained over Churchill but not over Swarthmore.

D. Trapped Orbit Hypotheses and Similar Considerations

It might be suggested that the increase in cosmic-ray intensity observed at high latitudes is produced by the presence of particles deflected to directions forbidden by the sun's magnetic field. For example, Alfven[26] has pointed out that particles coming in from infinity on unbounded orbits may be scattered by the earth's magnetic field into bound orbits. This occurs when they approach the earth so closely that the radius of curvature in the terrestrial magnetic field is of the same order as the distance to the earth's magnetic dipole. Here they are trapped, and circulate until they eventually (about 5,000 years) are absorbed by interplanetary matter or by striking some heavenly body or the earth, in the latter case from a normally forbidden region. In this manner, it is supposed that the intensity in forbidden directions may be appreciable in comparison with that in allowed directions. This idea was subsequently carefully investigated quantitatively by Kane, Shanley, and Wheeler.[27]

[23] M. A. Pomerantz and F. L. Hereford, Phys. Rev. **76**, 997 (1949).
[24] Goldfarb, Bradt, and Peters, Bull. Am. Phys. Soc. **24**, No. 7, 19 (1949); Phys. Rev. **77**, 54 (1949).
[25] T. H. Johnson, Phys. Rev. **53**, 499 (1938).

* *Note added in proof:* The Princeton group has recently obtained very important pertinent data which is in good accord with the above considerations. K. Dwight, R. Sabin, T. Stix, J. R. Winckler, Bull. Am. Phys. Soc. **25**, No. 1. (1950), p. 17.
[26] H. Alfven, Phys. Rev. **72**, 88 (1947).
[27] Kane, Shanley, and Wheeler, Rev. Mod. Phys. **21**, 51 (1949).

It is not the purpose of the present paper to discuss the assumptions underlying these hypotheses, which initially had their inception in an attempt to account for the absence of the large diurnal effect in the cosmic-ray intensity expected previously on the basis of the value of the solar magnetic moment heretofore assumed. Actually, the theoretical conclusion about rough equality of intensity incident from allowed and forbidden directions was inferred solely from the absence of an observable diurnal variation in the cosmic-ray intensity. A powerful argument against invoking this type of explanation of the present experimental results is based upon the observation of low energy particles in the primary beam at Churchill, as has been pointed out in the preceding section. A solar magnetic moment of 10^{34} gauss-cm^3 permits no particles having momenta less than 2.3×10^9 ev/c to reach the region where scattering by the earth's field could occur under any circumstances. The particles deflected into forbidden directions can have energies only between this lower limit and $p_{\max}=[(2)^{\frac{1}{3}}+1]^2\times p_{\min}=13.5\times10^9$ ev/c. The absorption in small thickness of lead at Churchill and not at Swarthmore indicates the presence of primary particles below this range at the more northern location. It need hardly be mentioned that the present conclusions directly explain the absence of such diurnal variations.

Another alternative explanation of the increase at high latitudes might, in principle, be sought in a contribution to the counting rate by either primaries or secondaries which initially pass outside the solid angle of the coincidence-counter train, suffer energy loss in the atmosphere, and are subsequently bent around by the earth's magnetic field so that they enter the telescope from below. It can be seen on the basis of some pertinent theorems by Swann[28] that no pencils of either protons or mesotrons which have undergone large angular deviation can be expected with any appreciable intensity. As a matter of fact, this effect would be in the wrong direction to account for the increase at high latitudes even qualitatively, inasmuch as a decrease in H actually reduces the fraction of the rays surviving along the deflected path.

E. The Sun as a Source of Cosmic-Rays

The sudden worldwide increases in the intensity of cosmic radiation accompanying solar flares, originally reported by Forbush,[29] indicated that the sun might be the source of at least some cosmic-ray particles. The sun's magnetic field was invoked to account for the fact that only relatively few flares produced such an increase.[30] According to Vallarta[31] a permanent dipole moment of 10^{32} gauss-cm^3 would suffice from this point of view.

Reference has already been made to the possibility that a variable solar magnetic field† could account for the acceleration of cosmic rays in the neighborhood of the sun. Should this be substantiated by future experiments, the sun may eventually be regarded as the source of practically all of the cosmic-radiation reaching the earth. This would indeed alleviate the difficulties regarding the total energy associated with a uniform distribution of cosmic rays throughout space.

V. ACKNOWLEDGMENTS

Grateful appreciation is expressed to the National Geographic Society for sponsoring the 1949 Expedition to Hudson Bay, and especially to Dr. Lyman J. Briggs, Chairman of the Committee on Research, for his continued encouragement. It is a pleasure to acknowledge the cordial cooperation accorded by the Canadian government, through the wholehearted support of the Defence Research Board; thanks are due many individuals including Dr. Guy Marier, Superintendent of Defence Research Northern Laboratories, and Donald Hiles, OIC of the Radiosonde Station at Churchill, for their hospitality; and G. W. Rowley of DRB for facilitating the numerous arrangements. Valuable assistance in every phase of this expedition was rendered by R. J. Kerr and R. C. Pfeiffer. Dr. E. Pickup and Dr. L. Voyvodic of the National Research Council of Canada helped immeasurably in the field work at Churchill; D. W. Watson, E. T. Kurtzner, and A. Viele assisted in the preparations, and A. G. Nester was in charge of G-M counter production. Finally, the author is indebted to Dr. W. F. G. Swann for helpful discussions and constant interest in this work.

[28] W. F. G. Swann, Phys. Rev. **76**, 157 (1949). Analogous considerations have subsequently been applied to protons, and lead to similar conclusions.

[29] S. E. Forbush, Phys. Rev. **70**, 771 (1946).

[30] Forbush, Gill, and Vallarta, Rev. Mod. Phys. **21**, 44 (1949).

[31] M. S. Vallarta, private communication.

† *Note added in proof:* Babcock has reported that of 42 sets of lines measured, including spectrograms in 1940, 1941, 1943, 1946, and 1947, 18 support Hale's conclusions, with intensity at the pole ranging from 6 to 60 gauss, whereas the remaining 24 show either no field or small negative values. H. D. Babcock, P.A.S.P. **60**, 224 (1948). Owing to difficulties associated with sunspots, there is no information regarding the possibility of a periodic variation. Although the value of 50 gauss has become imbedded in the literature by repetition, the mean of several lines was actually about 20 gauss. The author is indebted to Dr. H. W. Babcock for enlightening discussions of this subject.

Letters to the Editor

PUBLICATION of brief reports of important discoveries in physics may be secured by addressing them to this department. The closing date for this department is five weeks prior to the date of issue. No proof will be sent to the authors. The Board of Editors does not hold itself responsible for the opinions expressed by the correspondents. Communications should not exceed 600 words in length.

Electric Resistivity of Polycrystalline Graphite and Carbons

S. MROZOWSKI
Department of Physics, University of Buffalo, Buffalo, New York
January 23, 1950

SINGLE graphite crystals are known to be good conductors along the graphite planes and very poor ones across (ratio of resistivities 10^4 or higher.[1]) Coulson[2] and Wallace[3] have shown that a graphite crystal along the planes is a semiconductor with zero activation energy, the only difference with a metal consisting in a decrease of the density of states to zero for both the filled and unfilled bands as one approaches their common limit. Although the tight binding approximation does not yield a completely satisfactory description of all the properties of a graphite crystal, the result mentioned seems well established. The theory is, however, developed only for the case of infinitely large crystals.

For the artificial carbons with width of graphitic crystallites varies from 25A (calcined cokes) up to 1000A or more (highly graphitized specimens), we have therefore a continuous transition from small crystals down to the realm of large aromatic molecules. In studying the change of the electric resistivity ρ with temperature T, information is obtained only concerning the flow of electric current along the molecular planes, due to the high anisotropy of the crystallites. The curves ρ *versus* T reveal each a minimum, the position of the minimum shifting toward lower temperatures as the size of crystallites increases. The existence of the minimum is a direct consequence of an intrinsic semiconductivity of crystallites of graphite. In distinction to the infinitely large crystal it may be assumed that they possess a finite energy gap between the full and empty bands, the activation energy ΔE increasing with decrease of the crystallite size. The existence of an energy gap at the boundary of the Brillouin zone was found necessary for the explanation of the quantitative relations found in absorption spectra of aromatic molecules.[4] For each carbon a negative temperature coefficient of resistance typical for semiconductors is observed at lower temperatures; for temperatures $T \gg \Delta E/k$ the presence of the gap becomes immaterial and a typical metallic behavior is obtained (linear increase). For commercial graphites an activation energy of about 25×10^{-3} ev is calculated from the position of the minimum (500°C).

For calcined cokes the effective energy gap is probably at least as large as 0.1 ev or greater, and the small crystals should consequently be very poorly conducting at room temperature. The relatively low electric resistivity of such carbons (five to seven times that of graphitized material at room temperature) must be due therefore to an extrinsic semiconductivity. The existence of such a semiconductivity is revealed by an analysis of the resistivity curves even for commercial graphite in the region 600°–150°K. The curves can be explained by assuming the presence of a constant number of free electrons in the conduction band in addition to the variable number of electrons activated from the lower band. Since in highly graphitized specimens there are practically no impurities present, the excess electrons must be due to the carbon atoms themselves. In the polycrystalline graphite some carbons on the periphery of the crystals are bound by valence forces to carbons belonging to neighboring crystallites. A great number, however, of peripheral carbons (and also carbons around lattice imperfections) have free valence electrons which drop down from their energy states into the bottom of the conduction band (at very low temperatures into bound states around their original atoms with low activation energies ϵ), thus becoming the free excess electrons required for the conduction.

In conclusion, the polycrystalline carbons are true semiconductors with an activation energy depending on the size of crystallites. They show a metallic conductivity for $kT \gg \Delta E$, an intrinsic semiconductivity for $kT \sim \Delta E$ gradually changing as the temperature is lowered into a free electron excess semiconductivity. Finally, a fourth region should be reached at the lowest temperatures ($kT \sim \epsilon$) where a sharp increase in the resistivity is expected. A paper containing a more complete discussion of the problem and of all the experimental evidence available at present is in preparation. Experimental studies of the resistivity and Hall effect to check further the proposed explanation are in preparation.

Recently Bowen[5] succeeded in reproducing the shape of the resistivity curve for the polycrystalline graphite by simply adding the scattering due to crystal boundaries to the temperature scattering for infinite crystals. It is believed, however, that Bowen overestimated the magnitude of the boundary effect.

[1] K. S. Krishman and N. Ganguli, Nature **144**, 667 (1939).
[2] C. A. Coulson, Nature **159**, 265 (1947).
[3] R. P. Wallace, Phys. Rev. **71**, 622 (1947).
[4] H. Kuhn, J. Chem. Phys. **16**, 840 (1948). J. R. Platt, J. Chem. Phys. **17**, 484 (1949).
[5] D. Bowen, Phys. Rev. **76**, 1878 (1949).

Element 97*

S. G. THOMPSON, A. GHIORSO, AND G. T. SEABORG
Radiation Laboratory and Department of Chemistry, University of California, Berkeley, California
January 23, 1950

GOOD evidence has been obtained for the identification of an isotope of the element with atomic number 97 through the irradiation of americium-241 with helium ions in the Berkeley 60-inch cyclotron. The particular isotope discovered is thought to be 97^{243}, or possibly 97^{244}, decaying with a 4.8-hour half-life by electron capture with approximately 0.1 percent alpha-decay branching. There seem to be three alpha-particle groups associated with the activity, the highest energy being 6.72 Mev.

The chemical separation of element 97 from the target material and other reaction products was made by combinations of precipitation and ion exchange adsorption methods making use of its anticipated properties of having III and IV oxidation states and its position as a member of the actinide transition series. The distinctive chemical properties made use of in its separation and the equally distinctive decay properties of the particular isotope constitute the principal evidence for the new element.

It is suggested that element 97 be given the name berkelium (symbol Bk), after the city of Berkeley, in a manner similar to that used in naming its chemical homologue terbium (atomic number 65) whose name was derived from the town of Ytterby, Sweden, where the rare earth minerals were first found.

We wish to acknowledge the assistance in the early phases of the problem and the continuous advice of Professor B. B. Cunningham, whose help contributed greatly to the success of the work.

It is a pleasure to acknowledge the special help in the bombardment of the americium samples of Professor J. G. Hamilton, G. B. Rossi, T. M. Putnam, Jr., M. T. Webb, and the operating crew of the 60-inch cyclotron in the Crocker Laboratory. The successful handling in a safe manner of the radioactivity involved was made possible through the use of the excellent protective equipment provided by Nelson Garden and the members of his Health Chemistry Group, particularly C. M. Gordon, W. G. Ruehle, and J. M. Davis. We wish also to thank E. K. Hulet and G. H. Higgins for their assistance in some of the experiments and to express our appreciation to Dr. Kenneth Street, Jr., for valuable

suggestions and for the development of methods which were useful in the chemical separations.

* This work was performed under the auspices of the U. S. AEC.

A Lower Bound on the Range of Neutron-Proton Interaction

A. A. Broyles and B. Kivel
University of Florida, Gainesville, Florida
January 30, 1950

THE electric quadrupole moment of the deuteron is given by the expression

$$Q=(2\tfrac{1}{2}/10)\int_0^\infty r^2w(u-w/8\tfrac{1}{2})dr \Big/ \int_0^\infty (u^2+w^2)dr \qquad (1)$$

when the ordinary and tensor forces are assumed to exist. It will be shown here that this formula will not yield a value of Q as large as the experimental value unless the largest range of interaction r_0 is greater than 0.39 e^2/mc^2 regardless of the shapes and relative sizes of u and w for $r<r_0$ provided they are required to be real. In this formula, u and w are, respectively, r times the S and D radial wave functions for the bound state of the deuteron.[1]

Beyond r_0, u and w have the forms

$$\begin{aligned} u&=C\exp(\alpha r_0-\alpha r)\\ w&=D(\alpha r)^{-2}(\alpha^2r^2+3\alpha r+3)\exp(\alpha r_0-\alpha r), \end{aligned} \qquad (2)$$

where $\alpha=|E_0|^{\frac{1}{2}}$, E_0 is the binding energy of the deuteron, and C and D are arbitrary constants. The functions from $r=0$ to r_0 (as yet undetermined) may be represented by step functions of step widths Δr. The integrals employed in Eq. (1) will now be represented by the following symbols:

$$\begin{aligned} A&=\int_{r_0}^\infty r^2w(u-w/8\tfrac{1}{2})dr\\ B&=\int_{r_0}^\infty (u^2+w^2)dr\\ a_i&=\int_{r_i-\Delta r}^{r_i} r^2w(u-w/8\tfrac{1}{2})dr\approx r_i^2w_i(u_i-w_i/8\tfrac{1}{2})\Delta r\\ b_i&=\int_{r_i-\Delta r}^{r_i}(u^2+w^2)dr\approx(u_i^2+w_i^2)\Delta r. \end{aligned} \qquad (3)$$

It is now desired to find the maximum possible value of the expression,

$$Q=\frac{2\tfrac{1}{2}}{10}\,\frac{\sum_{i=1}^{n} a_i+A}{\sum_{i=1}^{n} b_i+B}, \qquad (4)$$

where n is the number of intervals of width Δr from $r=0$ to $r=r_0$. Consider the contribution to Q from any interval, say the jth interval. The contributions of the integrals over this interval will increase or decrease Q depending upon whether or not a_j/b_j is greater than or less than the remainder of Q as given by Eq. (4) with the jth interval omitted from the sums. If the contribution of the jth interval decreases Q, it may be eliminated by setting u_j and w_j equal to zero. Thus an upper bound for Q may be obtained by setting u and w equal to zero in all intervals except the one with the largest value of a_i/b_i or A/B (since the interval from r_0 to ∞ may be included in the argument).

The value of a_i/b_i may be obtained from Eq. (3) and it is seen that a_i/b_i may be maximized by varying u_i/w_i. The maximum occurs when $u_i/w_i=2\tfrac{1}{2}$ and is $r_i^2/8\tfrac{1}{2}$. Thus, the largest value of a_i/b_i occurs for $r_i=r_0$ and is $r_0^2/8\tfrac{1}{2}$. It is also clear from Eq. (2) that A/B is a function of C/D, r_0, and α. Choosing C/D to give a maximum value for A/B makes it possible to obtain an upper bound for $Q=(2\tfrac{1}{2}/10)(A/B)$ equal to the experimental value[2] of Q, which is 2.73×10^{-27} cm² when r_0 is 0.39 e^2/mc^2 and E_0 is 2.17 Mev. For this value of r_0, $(2\tfrac{1}{2}/10)(r_0^2/8\tfrac{1}{2})=0.49\times10^{-27}$ cm² so that (A/B) is greater than (a/b). For smaller values of r_0 the maximum value of $(2\tfrac{1}{2}/10)(A/B)$ is less than 2.73×10^{-27} cm² so that it is certain that if Eq. (1) is correct for Q and if u and w are real, then the experimental value of Q requires that the neutron-proton interaction be appreciable at a distance of separation of at least 0.39 e^2/mc^2.

It is interesting to note that the minimum value of r_0 obtained by Hu and Massey,[3] using square wells and assuming equal range for the tensor and ordinary forces, was about 0.46 e^2/mc^2; and the minimum value obtained by Schwinger,[4] again assuming equal ranges for the tensor and ordinary forces and, further, that not more than five percent D wave is present, was about 0.93 e^2/mc^2.

Recent changes in the experimental values of E_0 and Q are not large enough to alter these conclusions significantly.

The authors are greatly indebted to Professor G. Breit for helpful suggestions in connection with this problem and to Mr. M. H. Hull for checking the calculations.

[1] W. Rarita and J. Schwinger, Phys. Rev. **59**, 436 (1941).
[2] A. Nordseik, Phys. Rev. **58**, 310 (1940); Kellog, Rabi, Ramsey, and Zacharias, Phys. Rev. **57**, 677 (1940).
[3] T. M. Hu and H. S. W. Massey, Proc. Roy. Soc. **A196**, 135 (1949).
[4] J. Schwinger, Phys. Rev. **60**, 164A (1941).

Theory of Magnetic Properties and Nucleation in Alnico V

C. Kittel, E. A. Nesbitt, and W. Shockley
Bell Telephone Laboratories, Murray Hill, New Jersey
January 30, 1950

ALNICO V is a permanent magnet alloy containing by weight 8Al, 14Ni, 24Co, 3Cu and 51Fe, with the unique property among conventional magnet alloys that the energy product $(BH)_{max}$ is increased by heat treatment in a magnetic field from 1.8×10^6 ergs/cc with $H_t=0$ to 5×10^6 ergs/cc after treatment with $H_t\sim1000$ oersteds. After treatment, the remanence, coercivity, magnetostriction, loop shape, and approach to saturation are all characteristic[1,2] of anisotropic materials, and the anisotropy of the electrical resistivity[3] establishes that the treatment affects other than purely magnetic properties. A means whereby magnetic effects may control nucleation and produce the observed anisotropy and other properties is proposed below.

Alnico V is cooled from 1300°C, at which it is stable as a single phase, at about 2 to 5°C/sec. to 600°C with $H_t\sim1000$ oersteds; H_t is effective in the range from 900°C to 800°C. We have found that if the alloy is quenched from 800°C the anisotropic properties are already fully developed, although the coercivity H_c is only 10 oersteds. Further aging at 600°C increases H_c to 600 oersteds. H_t has no effect during the 600°C treatment.

We propose that at 800°–900°C thermal nucleation[4] occurs in the form of plate-like precipitates with a lattice coherent with the matrix, an assumption supported by the small difference 0.10 percent of precipitate and matrix lattice constants.[5] The good coherence means that the surface free energy of the nucleus is unusually small, perhaps equal to the energy of an order-disorder transformation in a layer 2A thick or about 10 ergs/cm² (as compared to approximately 1000 ergs/cm² for a grain boundary). Estimating equally roughly the energy barrier for a critical nucleus as 5×10^{-12} erg from the slope of log (optimum treatment time at fixed temperatures between 800 and 900°C) *vs.* $1/T$, we obtain a diameter of about 100A for a disk-shaped nucleus leading to a volume of approximately 10^{-19} cm³ for a 10A thickness.

If the precipitate, whose exact nature is unknown, is magnetically different at 800–900°C from the matrix so that $\Delta I_s=500$ gauss, then a nucleus with H_t perpendicular to its plane will have a demagnetizing energy of $(\Delta I_s)^2NV/2\approx1.5\times10^{-13}$ erg and will be suppressed by a factor of e^{-1} compared to nuclei with H_t in their planes. This rough estimate shows that demagnetization energy could control nucleation so that only those nuclei with planes $\|\Delta I_s\|H_t$ would form, consistent with results on the sample quenched from 800°.

At 600°C elastic energy and concentration gradients will continue the growth of the nuclei on the predetermined planes

independent of H_i. Maximum magnetic hardness apparently corresponds to initiation of an optimum number of nuclei between 800° and 900°C and growth of the precipitate in plates at 600°C which divide the matrix into plate and rod-like units whose shortest dimensions may be 100 to 1000A, so that they will behave as single ferromagnetic domains.

The coercive force presumably may be accounted for by the crystalline and magnetostatic anisotropy energy of the matrix units: the plate-like part of the volume will have $H_c=2K/I_s$, requiring a K of only $\sim 5\times 10^5$ ergs/cc, which is not unreasonable; additional coercivity of $\sim 2\pi p\Delta I_s$(20°C) from the rods may be important for reasonable values of ΔI_s and p, the fractional volume of precipitate.

The above theory does not require internal strains to have an important effect on the coercive force, and is in keeping with the fact that the disregistry strain of the transition lattice[5] is unusually small in Alnico V as compared with other permanent magnet alloys; further, on geometrical grounds it seems likely that the plate-like portion of the volume should be under large loading with symmetry axis normal to the plates. This gives no contribution to the coercive force if the magnetostriction is isotropic; if the magnetostriction is anisotropic, as in Ni, a strain of 0.1 percent (the disregistry strain) will give a small directional anisotropy in the plane of the plate, but in Ni this would only be about 2×10^4 ergs/cc, and it seems unreasonable to suppose a 25 times larger value in Alnico V.

We are indebted to J. H. Hollomon for general education on nucleation theory, to R. M. Bozorth under whose stimulus the experimental part of this investigation was undertaken, and to W. P. Mason, R. D. Heidenreich, and J. K. Galt for discussions on particular points.

[1] E. A. Nesbitt, J. App. Phys. (to be submitted).
[2] K. Hoselitz and M. McCaig, Proc. Phys. Soc. **B62**, 163 (1949).
[3] V. I. Drozhjina, M. G. Luzhinskaya, and Y. S. Shur, J. Tech. Phys. U.S.S.R. **19**, 95–99 (1949).
[4] J. C. Fisher, J. H. Hollomon, and D. Turnbull, J. App. Phys. **19**, 775 (1948).
[5] A. H. Geisler, Elec. Eng. **69**, 32–34 (1950).

The Thermal Neutron-Capture Cross Section of A^{36}

G. E. McMurtrie and D. P. Crawford*
Chalk River Laboratories, National Research Council of Canada, Chalk River, Ontario, Canada
January 16, 1950

THE thermal neutron-capture cross section of A^{36} has been measured as 6.5 ± 1.0 barns. Approximately 500 cc (N.T.P.) of commercial argon were sealed in a boron-free glass flask and irradiated in the thermal column of the N.R.X. pile for one hour. The neutron flux through the gas was measured with manganese foils and found to be 8.6×10^9 neutrons/cm²/sec. These foils had been calibrated[1] by irradiating them in a neutron flux, the value of which was measured by means of a small pulse ion chamber filled with a known amount of BF_3. The neutron flux through the argon was thus based on the neutron-capture cross section of boron, the number of boron atoms in the ion chamber and the counting rate. The experimental error is given as 3.5 percent.

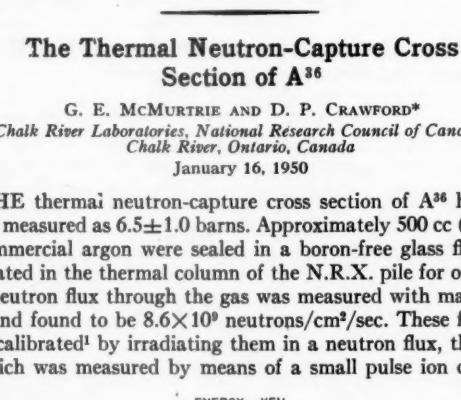

FIG. 1. Activity caused by K-capture in A^{37}.

It was found by comparing foils irradiated inside and outside of a similar glass flask that neutron absorption in this glass was negligible.

After removal of the flask from the reactor, the 110-minute A^{41} activity was allowed to decay through forty half-lives before introducing an accurately measured pressure (10.58 cm) of the irradiated gas into a proportional counter[2] preparatory to counting the A^{37} activity. The pulses from the counter were suitably amplified and fed to a thirty-channel pulse analyzer in parallel with a commercial scaler. (The latter served as a check on the total number of counts.)

The operation of the counter and the location of the 2.8 kev K-capture peak of A^{37} were checked by comparing the amplitude of the argon pulses with those produced by a beam of 17.4 kev x-rays (Mo $K\alpha$ line, selected by a crystal spectrometer). A typical run is shown in Fig. 1. The fraction of K-capture radiation which escapes from the counter must be allowed for, and has been estimated as 4.5 percent. Moreover, there is a low energy tail associated with the K-capture peak due to the reduced field strength at the ends of the counter. This tail must be extrapolated down to zero pulse size and its contribution added to the counting rate. The active volume of the counter (130.2 cc) was taken as the volume enclosed by the cylindrical cathode. It should be noted that the measurements do not extend below 1.2 kev and thus the L-capture radiation was not included. The contribution from L-capture has been measured by Pontecorvo, Kirkwood, and Hanna[2] as between 8 and 9 percent and calculated by Rose and Jackson[3] as 8.2 percent. A correction of 8.5 percent is applied.

The activity thus determined was corrected back to zero decay time using a half-life value of 34.1 days[4] for A^{37}. The calculation of the cross section was based on an isotopic abundance of 0.307 percent for A^{36}. The error shown in the value of the cross section 6.5 ± 1.0 barns is the standard error. We thank Mr. G. C. Hanna for putting his apparatus at our disposal and for valuable help with the experiment.

* Now at Mount Allison University, Sackville, New Brunswick, Canada.
[1] F. W. Fenning, Montreal Report MP-252 (1946), National Research Council of Canada.
[2] This was the counter used by Pontecorvo, Kirkwood, and Hanna, Phys. Rev. **75**, 982 (1949).
[3] M. E. Rose and J. L. Jackson, Phys. Rev. **76**, 1540 (1949).
[4] Weimar, Kurbatov, and Pool, Phys. Rev. **66**, 209 (1944).

Temperature Dependence of Microwave Line Widths*

Raydeen Howard and William V. Smith
Department of Physics, Duke University, Durham, North Carolina
February 2, 1950

IN their pioneering work on the pressure broadening of the ammonia inversion spectrum, Bleaney and Penrose[1] assumed that the cross section σ for collisions interrupting the microwave radiation or absorption was independent of the average velocity of impact $\bar{v}$. Although the agreement between their data and theory is actually independent of any possible variation of σ with $\bar{v}$, their assumption has crept into many estimates of microwave intensities, by way of the assumed dependence of the line width parameter $\Delta\nu=(n\bar{v}\sigma)/(2\pi)$ on temperature. Thus the above "hard sphere" theory predicts a line width at constant pressure proportional to $T^{-\frac{1}{2}}(V\simeq T^{\frac{1}{2}}; n\simeq P/T)$.

Recent theories proposed by Anderson[2] and Margenau,[3] while differing in their basic assumptions, both predict a line width independent of the impact velocity, with σ inversely proportional to $\bar{v}$. These theories, too, are in agreement with Bleaney and Penrose's data, although Anderson's theory alone includes an explanation of observed saturation effect.[4]

We have performed the simple experiment of measuring $\Delta\nu$ for the ammonia 3,3 line as a function of temperature. The results

TABLE I. Temperature dependence of line widths.

Temperature Kelvin	$\bar{\mu}/\mu$	$P/\Delta\nu$ arbitrary	$(T\Delta\nu_\mu)/(\bar{\mu}P)$	$(T^{\frac{1}{2}}\Delta\nu_\mu)/\bar{\mu}P$
300	0.54	1±0.02	556±10	32.1±0.6
195	0.516	0.66±0.02	574±15	41.0±1.0

are summarized in Table I. In interpreting the data, it is assumed that the line width is also proportional to the average component of dipole moment $\bar{\mu}$ of the colliding molecules along the angular momentum axis.[2,3] As $\bar{\mu}$ varies slightly with temperature, its ratio to the static dipole moment μ is also tabulated.

The experiment clearly shows that $\Delta\nu$ is inversely proportional to the temperature and hence σ is inversely proportional to the impact velocity, confirming Anderson's theory. These results however should not be extrapolated indiscriminately to all types of microwave collision broadening. They may be expected to hold rigorously only for an inverse cube dependence of interaction energy on molecular separation—exemplified by the above symmetric top dipole-dipole interactions. Experimental and theoretical papers on these and other interactions are now in preparation.

* The research reported in this document has been made possible through support and sponsorship extended by the Geophysical Research Directorate of the Air Force Cambridge Research Laboratories under Contract No. W19-122-ac-35. It is published for technical information only and does not represent recommendations or conclusions of the sponsoring agency.

[1] B. Bleaney and R. P. Penrose, Proc. Phys. Soc. London **LX**, 540 (1948).
[2] P. W. Anderson, Phys. Rev. **76**, 647 (1949).
[3] Henry Margenau, Phys. Rev. **76**, 121 (1949).
[4] B. Bleaney and R. P. Penrose, Proc. Phys. Soc London **LX**, 83 (1948); Robert L. Carter and William V. Smith, Phys. Rev. **73**, 1053 (1948); Robert Karplus, Phys. Rev. **73**, 1120 (1948); Robert Karplus and Julian Schwinger, Phys. Rev. **73**, 1020 (1948).

Recoil Electron Spectrum of the K^{40} Gamma-Ray

R. W. PRINGLE, S. STANDIL, AND K. I. ROULSTON
Physics Department, University of Manitoba, Winnipeg, Canada
January 26, 1950

THE observation that the ratio of positron emission to electron capture in the decay of K^{40} is $\lambda^{\beta+}/\lambda^{c}<0.005$, leads to the conclusion that the $A^{40}-K^{40}$ mass difference must be less than 1.6 Mev, if expressions for either third or fourth forbidden beta-transitions and axial vector or tensor interactions are used.[1] As considerations of the K^{40} β^- energy end point[2] seem to indicate that the gamma-ray from K^{40} be placed on the A^{40} side of the decay scheme, it is remarkable that the energy which has been observed[3] for the gamma-ray of 1.55±0.05 Mev should be so close to the maximum possible $A^{40}-K^{40}$ mass difference. It was therefore thought of interest to measure the energy of the gamma-ray more accurately, using the new scintillation spectrometer which we have developed.[4]

The crystal element of activated NaI, $1''\times1''\times1''$, was surrounded by approximately 90 g of KF, and the recoil electron spectrum which was obtained after filtering of the radiation by 4 mm of Al is shown in Fig. 1. The shape of the spectrum was later confirmed using another source of KCl. The pulse height distribution for the background is given and also the recoil electron spectrum of an uncollimated beam of Co^{60} gamma-rays for purposes of comparison and calibration. The Co^{60} scale is greatly reduced and ordinates refer only to the K^{40} and background spectra. In these experiments the spectrometer was enclosed in a three-inch wall lead castle. The photo-cell noise becomes apparent only below 20 kev on the pulse scale and the rise in the recoil electron spectra at low energies is attributed to degenerate radiation entering the crystal, as well as to the loss of recoil electrons from the surfaces and possible low energy gamma-rays in the case of $K^{40}\rightarrow Ca^{40}$. Any differences in the form of the two spectra are due, in addition, to the nature of the extended source in the case of K^{40}, and to the existence of two Co^{60} gamma-rays. It would not be possible from these results to draw any conclusions

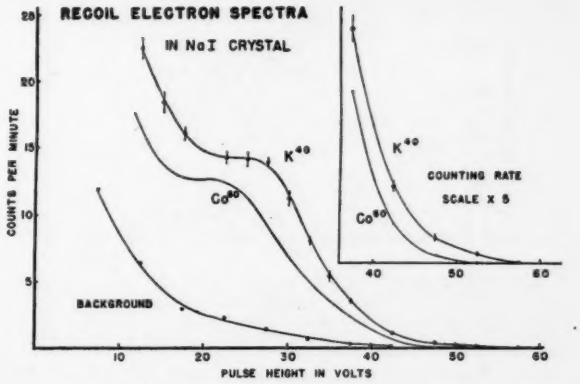

FIG. 1. Differential pulse height distributions obtained with scintillation spectrometer. The curves for K^{40} and Co^{60} have been corrected for background.

regarding a possible complexity of the K^{40} gamma-radiation. Careful consideration has been given to the manner of approach to the axis of the two spectra near the end point (Fig. 1) and, due account being taken of resolving power, the form of the Compton distribution, etc., a value has been estimated for the gamma-ray energy for K^{40} of 1.47±0.03 Mev in terms of the 1.33 Mev Co^{60} gamma-ray. This means that the energy available for electron capture to the excited state of A^{40} is less than 0.13±0.03 Mev. Coincidence experiments are being carried out to elucidate further the decay scheme.

The scintillation spectrometer has been used to measure the possible gamma-activity of certain members of the isobaric pairs of nuclei of neighboring Z. In some cases (notably cerium) activity has been observed but measurements with the spectrometer have indicated these activities to be due in the main to minute traces of thorium. Attempts are being made to have the purest possible materials prepared for this work.

[1] E. L. Fireman, Phys. Rev. **75**, 1447 (1949).
[2] D. E. Alburger, Phys. Rev. **75**, 1442 (1949).
[3] E. Gleditsch and T. Graf, Phys. Rev. **72**, 640 (1947).
[4] R. W. Pringle, K. I. Roulston, and H. W. Taylor, Rev. Sci. Inst. (in press).

The Cation Distribution in Ferrites with Spinel Structure

FRANK G. BROCKMAN
Philips Laboratories, Inc., Irvington-on-Hudson, New York
January 23, 1950

FROM studies of the cation distribution in spinels it was concluded by Verwey and co-workers[1] that, for the ferrites with this structure, zinc ferrite and cadmium ferrite are normal spinels while nickel-, copper-, magnesium-, ferrous- and manganese-ferrite are inverse spinels.[2] In the normal spinel the divalent ions (zinc or cadmium) occupy the tetrahedral position while the trivalent iron occupies the octahedral position. In the inverse spinel the tetrahedral position is occupied by one-half of the trivalent iron ions while the octahedral positions are occupied by a random distribution of the remainder of the iron ions together with the divalent cations (e.g., Cu^{+2}). In addition, it was indicated that a solid solution of a normal-spinel ferrite with an inverse-spinel ferrite (for instance, zinc ferrite in solid solution with copper ferrite) had a structure in which, in the example taken, the tetrahedral positions were occupied preferentially by Zn^{+2}, the remainder of these positions being filled by Fe^{+3}; the octahedral positions were occupied by the remaining Fe^{+3} and the Cu^{+2}.

Néel,[3] however, from a consideration of the magnetic properties of the ferrites concludes that the cation distribution is not as "ordered" as in the description given. The distribution according to Néel may vary so that, for instance, the distribution in copper ferrite is not simply $Fe\,[FeCu]O_4$ but may be $Fe_{0.82}Cu_{0.18}$

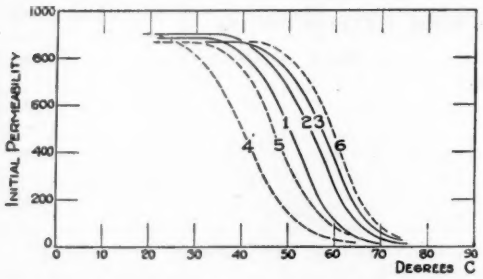

FIG. 1. Effect of quenching of copper-zinc ferrite on permeability *vs.* temperature curves. Curve 1. Quenched in air from 550°C. Curve 2. Quenched in air from 600°C. Curve 3. Quenched in air from 650°C. Curve 4. Slow-cooled from 650°C to room temperature. Curve 5. Quenched in air from 500°C. Curve 6. Quenched in air from 750°C.

$[Fe_{1.18}Cu_{0.82}]O_4$ for slowly cooled copper ferrite and even approximate the most random distribution, $Fe_{2/3}Cu_{1/3}\,[Fe_{4/3}Cu_{2/3}]O_4$, when quenched, i.e., when neither Fe^{+3} nor Cu^{+2} is located preferentially in tetrahedral or octahedral positions.

This encourages us to report some experiments which were performed prior to Néel's publication and which led to similar conclusions as regards both single ferrites and mixed ferrites.

The experiments were conducted in order to establish whether or not any kind of ordering occurred in ferrites. In mixed ferrites, in particular, it is conceivable that several different kinds of ordering could occur. Accordingly, test pieces of a copper-zinc-ferrite (40 mole percent copper ferrite and 60 mole percent zinc ferrite) were prepared and these were soaked for periods of eight or more hours at elevated temperatures and then quenched quickly in air to room temperature. The initial permeability of the sample so treated was measured as a function of temperature from room temperature to above the ferromagnetic Curie point. The results for different quenching temperatures are shown in Fig. 1. The numbers for each curve indicate the order in which the experiment was performed; that is, the sample was quenched from 650°C as the third treatment to which it was subjected and then for the fourth treatment it was heated to 650°C and slowly cooled to room temperature. After this it was subjected to the fifth and then the sixth treatment. It will be noted that the phenomenon is a reversible one.

It has been demonstrated by Snoek[4] that the Curie temperature of a mixed crystal of a ferromagnetic ferrite with zinc ferrite decreases with increasing zinc ferrite concentration. This fact, together with the results given, suggested that quenching from high temperatures brought about a condition which was equivalent to a reduction of the zinc cation concentration. Since, as described, the zinc ion was assumed to be in the tetrahedral position, it appeared reasonable that the phenomenon was to be attributed to a migration of zinc ions to the octahedral position with replacement of these ions by ferric ions. This is consistent with the fact that the higher the quenching temperature the higher the Curie point became, because it is to be expected that the most random arrangement will occur at the highest temperature.

That no separation of phases occurred in this heat treating was demonstrated by x-ray diffraction, and observation on the weight of the test piece after each heating showed that no loss of material was associated with the treatment.

In discussing these results and this interpretation with Professor G. E. Uhlenbeck and Dr. O. S. Duffendack they pointed out that, if the interpretation is correct, then it should be possible to render zinc ferrite and cadmium ferrite ferromagnetic by suitable heat treatment. Such experiments were carried out and it was found that if zinc ferrite is quenched from 1400°C it becomes slightly ferromagnetic as indicated by its attraction to a permanent magnet. Cadmium ferrite appears to be somewhat more magnetic under the same treatment.

More extensive work along this line has been carried out in the Eindhoven, Holland, laboratories of the Philips Company. A communication by E. W. Gorter of that laboratory will appear in the near future and will describe in more detail the phenomena and their interpretation.

[1] Verwey, Haayman, and Heilmann, Philips Tech. Rev. **9**, 185 (1947); Verwey and Heilmann, J. Chem. Phys. **15**, 174 (1947).
[2] Barth and Posnjak, Zeits. f. Krist. **82**, 325 (1932).
[3] L. Néel, Ann. de Physique (12) **3**, 137 (1948).
[4] J. L. Snoek, *New Developments in Ferromagnetic Materials* (Elsevier Publishing Company, Inc., New York, 1947).

Note on the Coefficient of Eddy Viscosity in Isotropic Turbulence

T. D. LEE
Yerkes Observatory, University of Chicago, Williams Bay, Wisconsin
February 2, 1950

IT has been suggested by Heisenberg[1] that the inertial transfer of energy by eddies with wave number less than a particular k can be pictured in terms of an eddy viscosity, ν_k, due to the eddies with wave numbers greater than k; he writes

$$\nu_k=\kappa\int_k^\infty [F(k)]^{\frac{1}{2}}k^{-\frac{1}{2}}dk \tag{1}$$

where $F(k)$ denotes the spectrum of turbulence and κ is a numerical constant. From a comparison with the experimental results on decay of turbulence, Heisenberg obtained for κ the value 0.85. This determination depends chiefly on the region of the spectrum where the ordinary kinematic viscosity ν plays no role.

An alternative determination of κ that depends sensitively on the behavior of $F(k)$ in the region of large k can be made by using the experimental results on vorticity by Batchelor and Townsend.[2] They found that

$$S\equiv-\langle(\partial v_x/\partial x)^3\rangle_{Av}/\langle(\partial v_x/\partial x)^2\rangle_{Av}^{\frac{3}{2}}=0.39 \tag{2}$$

where v_x is the x component of the velocity of turbulent motion. Now, from the Karman-Howarth equation[3] the vorticity equation can be written as

$$-\frac{1}{2}\frac{d}{dt}\langle(\partial v_x/\partial x)^2\rangle_{Av}-\frac{7}{3}\nu\langle(\partial^2 v_x/\partial x^2)^2\rangle_{Av}=\frac{7}{6}\langle(\partial v_x/\partial x)^3\rangle_{Av}. \tag{3}$$

In terms of the spectrum of turbulence, we have[4]

$$\langle(\partial v_x/\partial x)^2\rangle_{Av}=(2/15)\int_0^\infty F(k)k^2dk \tag{4}$$

and (3) can be rewritten as

$$\langle(\partial v_x/\partial x)^3\rangle_{Av}=-\frac{4}{35}\nu\int_0^\infty F(k)k^4dk-\frac{2}{35}\int_0^\infty\frac{\partial F}{\partial t}k^2dk. \tag{5}$$

Since S remains constant during the decay of turbulence, we can use the equilibrium spectrum for stationary turbulence derived from Heisenberg's theory, namely[5]

$$F(k)=F_0\left(\frac{k_0}{k}\right)^{5/3}\frac{1}{[1+(k/k_s)^4]^{4/3}};\qquad\frac{k_s^{4/3}}{(F_0k_0^{5/3})^{\frac{1}{2}}}=\frac{3}{4}\frac{\kappa}{\nu}. \tag{6}$$

Using (4), (5), (6) and neglecting the second member of the right side of (5), we can evaluate S. Thus

$$S=\frac{9}{14}\left(\frac{15}{2}\right)^{\frac{1}{2}}\frac{\int_0^\infty[x^{7/3}dx/(1+x^4)^{4/3}]}{\left\{\int_0^\infty[x^4dx/(1+x^4)^{4/3}]\right\}^{\frac{1}{2}}}\kappa=1.52\kappa. \tag{7}$$

From (2), we obtain for κ the value 0.26. This differs from Heisenberg's determination $\kappa=0.85$. However, since the principal contribution to S comes from the transition region where $F(k)$ changes from the $k^{-5/3}$ to the k^{-7} law, the difference must be traced to the inadequacy of the expression (1) for ν_k for all k and can perhaps be interpreted in the following way: For a given k it is to be expected that only those eddies with wave numbers appreciably greater than k say $\alpha k(\alpha>1)$ can effectively contribute to the eddy viscosity. We may expect α to be a function of k but it must always be greater than one. If one neglects completely the contribution by those eddies with wave numbers

between k and αk, then ν_k can be written as

$$\nu_k = \kappa \int_{\alpha k}^{\infty} [F(k)]^{\frac{1}{2}} k^{-\frac{1}{2}} dk;$$

or, in the approximate forms:

$$\nu_k \cong \kappa [\alpha(k)]^{-4/3} \int_k^{\infty} [F(k)]^{\frac{1}{2}} k^{-\frac{1}{2}} dk \quad \text{for} \quad k_0 \ll k \ll k_s \qquad (8a)$$

$$\nu_k \cong \kappa [\alpha(k)]^{-4} \int_k^{\infty} [F(k)]^{\frac{1}{2}} k^{-\frac{1}{2}} dk \quad \text{for} \quad k \gg k_s. \qquad (8b)$$

The further assumption that α is a numerical constant will lead one to suppose that in the comparison made by Heisenberg, (8a) is appropriate, while for our present comparison based on S (8b) will be more appropriate. Thus

$$\kappa\alpha^{-4} \cong 0.26 \quad \text{and} \quad \kappa\alpha^{-4/3} \cong 0.85. \qquad (9)$$

The corresponding values of κ and α are 1.5 and 1.6 approximately.

The author is much indebted to Professor S. Chandrasekhar for many invaluable discussions.

[1] W. Heisenberg, Zeits. f. Physik **124**, 628 (1948).
[2] G. Batchelor and A. Townsend, Proc. Roy. Soc. A**190**, 534 (1947).
[3] T. von Karman and L. Howarth, Proc. Roy. Soc. A**164**, 192 (1938).
[4] G. I. Taylor, Proc. Roy. Soc. A**151**, 421 (1935).
[5] S. Chandrasekhar, Proc. Roy. Soc. A**200**, 20 (1949).

Radioactivity in Platinum by Neutron Capture*

J. M. Cork, A. E. Stoddard, W. C. Rutledge, C. E. Branyan, and J. M. LeBlanc
Department of Physics, University of Michigan, Ann Arbor, Michigan
February 6, 1950

THE stable isotopes of platinum, shown in Fig. 1, will by neutron capture produce radioactive atoms of mass 193, 197, and 199. Previous studies[1] have assigned half-lives of 4.33 days, 18 hr., and 31 min., respectively, to these activities. Specimens of supposedly chemically pure platinum irradiated in the Oak Ridge and Argonne piles yield a complex decay curve as shown in Fig. 2. This curve resolves quite completely into three components, as shown, whose half-lives are 82 days, 3.4 days, and 17.4 hr.

The 82-day activity previously unreported, is found by absorption in aluminum to have beta-radiation with an upper limit of about 0.54 Mev and by absorption in lead, a gamma-ray of energy about 0.6 Mev. That the activity is in platinum was shown by a chemical separation. This emitter is thus isomeric with one of the previously reported radioactive isotopes of mass 197 or 199, probably the former.

Exposures in beta-spectrometers under varying conditions showed that the radioactive platinum emitted more than 20 electron lines, whose energies are shown in Table I. The K–L–M differences, where observable, are in every case characteristic of mercury, and the activity producing the lines decayed with the half-life of 3.4 days. It is thus clear that this activity is due to radioactive gold 199, derived from platinum 199, whose half-life is 31 min., and is formed by neutron capture in platinum 198. The suggested interpretation of each electron line is shown in column 2 of Table I and a summary of the gamma-rays in the final mercury 199 nucleus is given in Table II. The K/L ratio can be roughly estimated from the relative line blackness and is approximately unity for lines arbitrarily numbered 4 and 9 and is much less than unity, indicating a high degree of forbiddenness, for lines 5, 6, and 8.

TABLE I. Electron energies from radioactive platinum.

Electron energy kev		Interpretation	Energy sum kev	Electron energy kev		Interpretation	Energy sum kev
20.4		K^4	103.3	114.8		$L_{1,2}{}^5$	129.3
45.9		K^5	128.8	117.0		$L_3{}^5$	129.2
48.5		K^6	131.4	—	or	$L_{1,2}{}^6$	131.5
50.7		$L_{1,2}{}^1$	65.2	119.2		$L_3{}^6$	131.4
—	or	K^7	133.6	—	or	$L_{1,2}{}^7$	133.7
52.4		$L_3{}^1$	64.6	124.0		$L_{1,2}{}^8$	138.5
56.2		K^8	139.1	125.8		M^5	129.4
62.4		$L_{1,2}{}^2$	76.9	—	or	$L_3{}^8$	138.0
64.3		$L_3{}^2$	76.5	128.0		N^5	128.8
74.7		K^9	157.6	—	or	M^6	131.6
84.2		$L_{1,2}{}^3$	98.7	143.0		$L_{1,2}{}^9$	157.5
88.0		$L_{1,2}{}^4$	102.5	145.0		$L_3{}^9$	157.2
94.5		M^3	98.1	154.1		M^9	157.7
				156.2		N^9	157.0

ELEMENT	MASS NUMBER							
	192	193	194	195	196	197	198	199
77 IR		61.5 % (4.3 K)						
78 PT	0.78 %	4.33 D	32.8 %	33.7 %	25.4 %	17.4 H (82 D)	7.23 %	31 M
79 AU						100 %	2.7 D	3.4 D
80 HG					0.15 %		10.1 %	17.0 %

FIG. 1. Isotopic distribution in platinum and neighboring elements.

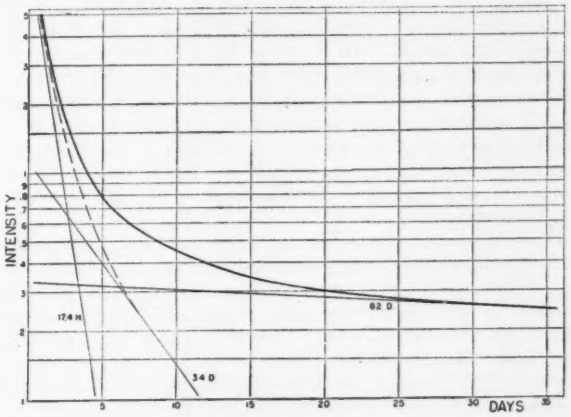

FIG. 2. The decay of activated platinum.

Since the exposure in the pile was of 2 mo. duration, the long-lived emitters were relatively strong compared with the 17.4-hr. activity. It was noted, however, by absorption in aluminum and in lead that beta-radiation whose upper energy was about 0.8 Mev and a gamma-ray of energy 2.2 Mev were present in the freshly irradiated specimen and died out rapidly. No electron conversion lines associated with this short-lived activity could be observed. The radioactive isotopes believed to exist are shown in Fig. 1.

TABLE II. Summary of gamma-energies in mercury 198.

Arbitrary designation	Energy kev	Arbitrary designation	Energy kev
1	65.0	6	131.4
2	76.6	7	133.7
3	98.3	8	138.6
4	103.0	9	157.6
5	129.2		

* This investigation was made possible by the support of the AEC and ONR.

[1] J. M. Cork and E. O. Lawrence, Phys. Rev. **49**, 788 (1936); McMillan, Karnen, and Rubin, Phys. Rev. **52**, 375 (1937); R. Krishnan and E. Nahum, Proc. Camb. Phil. Soc. **37**, 422 (1941); Sherr, Bainbridge, and Anderson, Phys. Rev. **60**, 473 (1941); and G. Wilkinson, Phys. Rev. **73**, 252 (1948).

An Improvement Effect of the Plateau in Xylene- and Argon-Filled Geiger Counters

Besim Tanyel
Norman Bridge Laboratory of Physics, California Institute of Technology, Pasadena, California
January 23, 1950

AN improvement effect of the plateau by rest has been observed in a counter tube consisting of a wire between two parallel copper-coated steel plates and filled with a xylene and argon

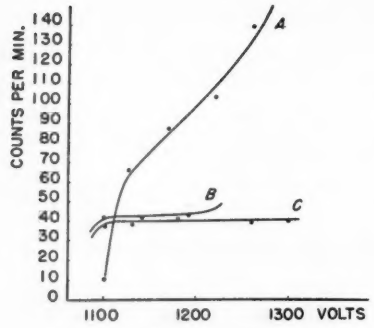

FIG. 1. Effect of rest on the plateau.

admixture near the saturation conditions of the xylene vapor. The tube, used in former experiments, was evacuated and baked at 400°C, then refilled by a xylene and argon mixture at 76 cm of mercury pressure, admitting first the xylene vapor under a pressure of 9 mm Hg. All the following tests were made on the tube sealed to a manifold. After the filling, a rest of 42 hr. was allowed and the tube was then tested. The plateau was found very unsatisfactory, as is seen in curve A of Fig. 1. After a rest period of several days the tube was tested again. The characteristic plateau curves B (after a rest of 216 hr.) and C (at the end of a total rest of 336 hr. after the filling) show an improvement of the plateau by rest.

This improvement was believed to be due to the formation of a continuous xylene film on the cathode. Indeed, for the production of good counters, beside a proper filling, the importance of formation of a suitable surface layer which prevents spontaneous discharges and electron escape from the cathode was pointed out by Trost.[1] The important role of a surface film formation in xylene-argon counters has been emphasized more recently.[2] In order to see the effect of the partial removal of this film, the tube was heated at 120°C (below the boiling point of xylene) for 10 min. and left in the oven to cool slowly, all other parts of the manifold being held at room temperature. At 40°C the plateau showed a high slope (Fig. 2, curve B). The tube was then brought to room temperature and the plateau tested 6 hr. later (Fig. 2, curve C). After 28 hr. of rest, curve D was obtained, which still shows many spurious counts toward the end of the plateau. Finally, at the end of a total rest of 76 hr. after the heating of the tube the plateau E was found to be almost the same as the initial characteristic curve (A, Fig. 2). This recovery of the plateau presents some analogy with the recovery effect observed

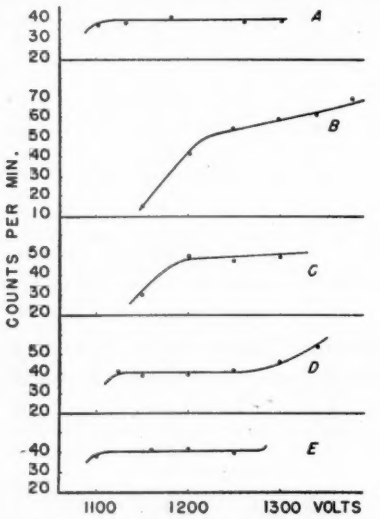

FIG. 2. Effect of film removal on the plateau.

first by Spatz in exposed alcohol- and argon-filled counters.[3] Observation of this improvement effect in a counter filled with saturated xylene vapor, and on the other hand, the absence of a recovery effect in the case of methane-argon-filled counters[3] seem to agree with the suggestions concerning the important role of a film formation on the cathode. The higher threshold voltages of characteristic curves B, C, and D in Fig. 2 show that there is a greater amount of vapor between the electrodes; in other words, according to this picture, the film formation on the plates is not complete. Furthermore, curves C and D being obtained at room temperature, the observed alteration of the plateau in curves B, C, and D would be interpreted as an alteration effect of the film rather than as a temperature effect reported by various observers.[4]

The writer is much indebted to Professor H. V. Neher who first suggested the importance of a possible film formation on the electrodes, and to whom he wishes to express here his deepest gratitude and thanks for an invaluable guidance.

[1] A. Trost, Zeits. f. Physik **105**, 399–444 (1937).
[2] J. W. Keuffel, Rev. Sci. Inst. **20**, 204 (1949).
[3] W. D. B. Spatz, Phys. Rev. **64**, 236–240 (1943).
[4] Korff, Spatz, and Hilberry, Rev. Sci. Inst. **13**, 127 (1942). J. L. Putman, Proc. Phys. Soc. London **61**, 312 (1948). Om Parkash, Phys. Rev. **76**, 568 (1949).

On Two-Component Wave Equations

F. GÜRSEY
Imperial College, London, England
January 27, 1950

IN two recent letters Jehle[1] and Kilmister[2] have drawn attention to two-component wave equations. The object of this note is to show that such equations can be regarded as degenerate cases of the general wave equation. Jehle's field free equation is equivalent to Conway's[3] form of Dirac's equation when the wave quaternion reduces to its real part, i.e., when it is self-charge conjugate. Hence Jehle's field does not represent an electromagnetic interaction, but, as Serpe[4] has shown corresponds to a pseudo-vector interaction. The equation proposed by Kilmister can be derived from a different quaternion formulation of the wave equation due to Watson[5] when the wave function is invariant under a time reflection. Thus Kilmister's equation has solutions depending only on the space coordinates and it is equivalent to two equations of Jehle's type which differ from each other by the sign of their time coordinates.

Dirac's equation can be written in the form

$$\beta^\nu\partial_\nu\Psi=\mu\Psi, \quad (\beta^\lambda\beta^\nu+\beta^\nu\beta^\lambda=-2g^{\lambda\nu}), \tag{1}$$

where $\partial_\nu=\partial/\partial x^\nu$, $(\nu=0, 1, 2, 3)$ and $x^0=ct$. If Ψ is taken as a complex quaternion, one form of Conway's equation is obtained by replacing β^ν by the linear functions

$$\beta^0\Psi=\Psi f^2, \quad \beta^n\Psi=f^n\Psi f^3, \quad (n=1, 2, 3), \tag{2}$$

where f^n is the nth quaternion unit. As such linear quaternion functions can be represented by 4×4 real matrices and the general equation can be obtained by introducing the field A_ν through the substitution $\hbar\partial_\nu\rightarrow\hbar\partial_\nu+ieA_\nu$, the complex conjugate of Ψ is also its charge conjugate. Hence the self-conjugate solutions of (1) satisfy the real quaternion equation

$$\partial_0\Phi f^2+f^n\partial_n\Phi f^3=\mu\Phi, \tag{3}$$

where $\Phi=\phi_0+f^n\phi_n$ is a real quaternion. Therefore we can rewrite (3) as a complex 2×2 matrix equation by taking

$$f^1=\begin{bmatrix} i & 0 \\ 0 & -i \end{bmatrix}, \quad f^2=\begin{bmatrix} 0 & -1 \\ 1 & 0 \end{bmatrix}, \quad f^3=\begin{bmatrix} 0 & -i \\ -i & 0 \end{bmatrix}.$$

Φ being now represented by a complex 2×2 matrix we have

$$\Phi^*=-f^2\Phi f^2, \tag{4}$$

where Φ^* denotes the complex conjugate of the matrix Φ. Hence, operating with $-f^2(\ )f^2$ on (3) we get

$$f^2\partial_0\Phi-f^3\partial_1\Phi f^1-\partial_2\Phi f^1-f^1\partial_3\Phi f^1=\mu\Phi^*. \tag{5}$$

If γ^ν denotes the matrix operating on the first column ϕ of Φ and corresponds to the linear quaternion function associated with ∂_ν in (5), we can replace (5) by the equivalent equation

$$\gamma^\nu\partial_\nu\phi=\mu\phi^*.$$

As $\gamma^\nu\phi$ corresponds to $(\beta^\nu\Phi)^*$ in the 2×2 representation it follows from (1) that the matrices γ^ν satisfy Jehle's commutation relations

$$\gamma^{*\lambda}\gamma^\nu+\gamma^{*\nu}\gamma^\lambda=-2g^{\lambda\nu}.$$

Further, under a time reflection $x_0\rightarrow-x_0$ we have $\Phi\rightarrow\Phi f^1$, hence $\phi\rightarrow\gamma^2\phi$.

Kilmister's equation reads

$$(i\partial_0+f^n\partial_n)\Phi=\mu f^2\Phi^*,$$

where Φ again is a real quaternion in its 2×2 complex matrix form. By use of Eq. (4) we can write

$$(i\partial_0+f^n\partial_n)\Phi=\mu\Phi f^2. \tag{6}$$

Operating by $-f^2(\ )f^2$ on (6) then taking the complex conjugate of both sides, we also get

$$(-i\partial_0+f^n\partial_n)\Phi=\mu\Phi f^2.$$

Hence $\partial_0\Phi$ vanishes. The two columns of (6) equated separately give rise to a pair of equations of Jehle's type differing by the sign of their first terms only. Equation (6) is related to Watson's form of Dirac's equation which can be put in the form

$$(i\partial_0+f^n\partial_n)\Psi=\mu\Psi^*f^2$$

where a 4×4 real representation is used for each f^n. This corresponds to the following "realization" of the operators β by linear quaternion functions

$$\beta^0\Psi=i\Psi^*f^2,\quad \beta^n\Psi=-f^n\Psi^*f^2.$$

In this representation Ψ changes into Ψ^* under a time reflection. Hence the solutions left invariant under $x_0\rightarrow-x_0$ are given by Kilmister's Eq. (6).

[1] H. Jehle, Phys. Rev. **75**, 1609 (1949).
[2] C. W. Kilmister, Phys. Rev. **76**, 568 (1949).
[3] A. W. Conway, Proc. Roy. Soc. (A) **162**, 147 (1937).
[4] J. Serpe, Phys. Rev. **76**, 1538 (1949).
[5] A. G. D. Watson, Proc. Camb. Phil. Soc. **43**, 491 (1947).

A Correlation between Ionospheric Phenomena and Surface Pressure*

M. W. Jones and J. G. Jones
Geophysical Institute, University of Alaska, College, Alaska

January 30, 1950

RECENTLY, we reported[1] the existence of tidal effects[2] on the ionospheric F layer. We are now able to show with some degree of reliability that the oscillations in the F layer are approximately in opposite phase to the oscillations of the air at the surface of the earth as measured by the variation in surface barometric pressure. The inverse correlation is evident in the mean curves of Fig. 1.

This is not the first time that an ionospheric characteristic has been correlated with the variations of the surface pressure.[3] However, the correlations observed in the past were usually for day to day or hour to hour variations and were seldom verified by investigators in other localities. We believe that attempts at verification were unsuccessful because the real correlation existing is one between the tidal movements at the two levels of the atmosphere. Such a relation between hourly or daily values would often be masked by large local changes due to disturbances other than tidal forces. Thus, if mean values are taken over an interval sufficient to eliminate random daily variations, tidal movements are evident in the mean curves, and the correlation existing between the curves is actually a comparison of the phases of the tidal movements at the two levels. We should expect a relation between the tidal movements at the various levels of the atmosphere to exist since all the tidal movements associated with the earth's atmosphere are attributed directly or indirectly to the tide raising forces of the sun and moon.

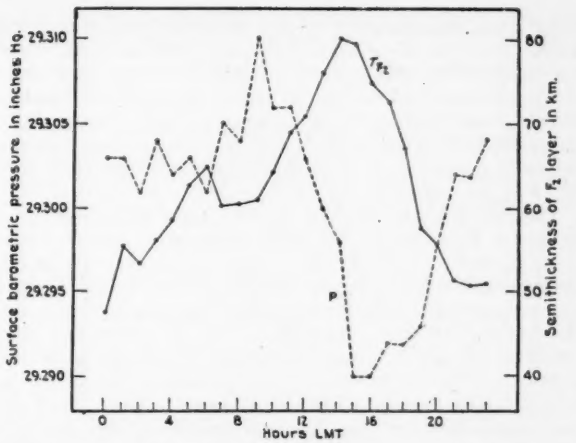

FIG. 1. Mean curves of semithickness τF_2 of the F_2 layer (College) and of surface pressure P (Fairbanks) for October, 1948 through March, 1949.

At College a mean over an interval of 6 months must be used, according to Bartels'[4] reliability test, to obtain fairly persistent pressure solar diurnal and semidiurnal waves. The same interval is sufficient for similar persistent waves in the oscillations of the semithickness of the F layer.

For further comparison of the tides at the two levels of the atmosphere, the mean variations were submitted to harmonic analyses. The harmonic components of the oscillations relative to solar time are presented in Table I.

TABLE I. Harmonic components of atmospheric oscillations.

	Diurnal component	Semidiurnal component
Surface pressure (amplitude in inches mercury)	$0.0041\sin(t+14°)$	$0.0036\sin(2t+124°)$
F layer semithickness (amplitude in kilometers)	$11.5\sin(t+256°)$	$5.6\sin(2t+323°)$

We feel that the inverse correlation demonstrated is reliable. The probabilities that the 24 and 12 hour waves in the F layer are due to chance are approximately 10^{-2} and 10^{-1}, respectively, while the probabilities for the corresponding pressure waves are 0.3 and 10^{-2}.

* This work was supported in part by Contract No. W28-099 ac-445 with the U. S. Air Force, through sponsorship of the Geophysical Research Directorate, Cambridge Research Laboratories.
[1] M. W. Jones and J. G. Jones, Phys. Rev. **76**, 581 (1949).
[2] The terms, *solar and lunar tides*, used in connection with variations of an ionospheric characteristic simply mean that the oscillations of the ionospheric phenomenon can be shown to be periodic relative to solar and lunar days.
[3] T. G. Mihran, Proc. I.R.E. **36**, 1093 (1948).
[4] J. Bartels, Terr. Mag. **40**, 1 (1935).

Coercive Force *vs.* Temperature in an Alloy with Zero Crystalline Magnetic Anisotropy

J. K. Galt
Bell Telephone Laboratories, Murray Hill, New Jersey

January 23, 1950

KITTEL,[1] Néel,[2] and Stoner and Wohlfarth[3] have shown that one expects high coercive forces in very fine powders of ferromagnetic materials. This is because each particle acts as a single domain, and work must be done against the total magnetic anisotropy when the magnetization of a particle is reversed, since the dipole moment of the whole particle must be reversed as a unit. The total magnetic anisotropy in general is the sum of contribu-

tions from demagnetizing fields, crystalline anisotropy, and magnetostriction. These high coercive forces in fine powders have been observed by several workers, especially by those in France.[4]

We have measured the coercive force of a powder of 68 percent Ni—32 percent Fe alloy at various temperatures between −200°C and +400°C. This alloy was selected because it has zero crystalline magnetic anisotropy over the range of temperatures measured.[5] The data are plotted in Fig. 1.

The material was prepared by reducing a mixed iron-nickel oxalate in H_2 at 300°C. The lattice constant as measured from x-ray powder photographs shows that the particles are in fact alloy particles of approximately the desired composition. Particle-size measurements from electron microscope pictures show that the particles are fairly uniformly distributed in the size range 500–3000A diameter. It should be mentioned that the broadening of the x-ray lines compared with lines obtained in the same set-up with 2.5μ nickel particles indicates a crystallite size of 100A. This can be explained by the presence of several crystallites in each particle and perhaps by some variation of alloy composition within the sample. In any case, x-ray line broadening is not a measure of particle size in our case.

The coercive force measurements were made using a standard ballistic technique on two separate samples. The particles in one sample were coated with divinyl benzene in order to inhibit sintering. It was only on this sample that it was possible to get measurements at 400°C.

The low temperature data in Fig. 1, however, do not fit the theoretical picture mentioned very well. This picture predicts that the coercive force will vary as the sum of two terms. One, due to demagnetizing fields, is proportional to saturation magnetization M_s. The other, due to magnetostriction, is proportional to the product of saturation magnetostriction λ, and internal stress σ. From room temperature to −200°C M_s varies by only two percent, and λ by only 10 percent.[6] Since the material was cubic it seems unlikely that the internal stress σ was appreciably changed by cooling. Moreover, while the x-ray data cannot verify the alloy composition accurately, it shows that the alloy is near enough to the zero anisotropy composition so that crystalline anisotropy cannot explain the low temperature value.

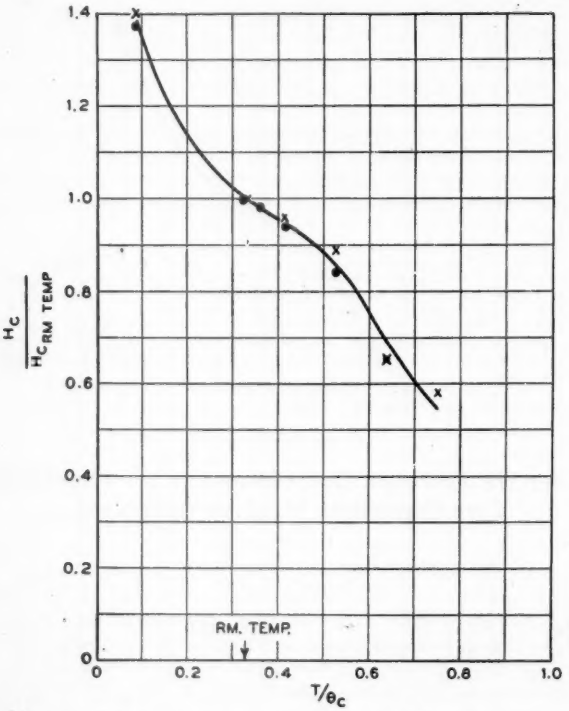

FIG. 1. H_c/H_c(rm. temp.) vs. T/θ_c, where θ_c is Curie temperature. Crosses are for coated sample, dots are for uncoated sample. H_c(rm. temp.) for uncoated sample was 200 oersteds, for coated sample it was 270 oersteds. This difference is due to the different packing densities.

According to the theoretical size conditions at present available,[7] our particles are mainly in the transition range between single domain and normal behavior. This size range has been discussed only briefly,[8] and it is possible that this is the basis for the deviations from the present theory observed here.

The author wishes to express his gratitude to A. N. Holden, E. A. Nesbitt, W. O. Baker, F. H. Winslow, and J. B. Howard for their help with various aspects of this experiment, and to C. Kittel and R. M. Bozorth for enlightening discussions.

[1] C. Kittel, Phys. Rev. **70**, 965 (1946).
[2] L. Néel, Comptes Rendus **224**, 1488–1490 (1947); **224**, 1550–1551 (1947).
[3] E. C. Stoner and E. P. Wohlfarth, Nature **160**, 650 (1947).
[4] L. Weil, Comptes Rendus **225**, 229–30 (1947); L. Weil and S. Marfoure, J. de Physique **8**, 358–61 (1947); C. Guillaud, thesis Strasbourg (1943), J. des Recherches CRNS, 267–78 (1949).
[5] H. J. Williams and R. M. Bozorth, Phys. Rev. **55**, 673A (1939).
[6] K. Honda and S. Shimizu, Phil. Mag. **10**, 548 (1905).
[7] C. Kittel, Rev. Mod. Phys. **21**, 541 (1949), see Eq. (6.1.8).
[8] C. Kittel, Phys. Rev. **73**, 810–11 (1948).

Cosmic Radiation and the Maintenance of a Potential Gradient in the Atmosphere

ROBERT E. HOLZER
Institute of Geophysics, University of California, Los Angeles, California
January 25, 1950

IN a recent Letter to the Editor, Korff[1] suggests that cosmic radiation can maintain a potential gradient in the atmosphere and implies, by citing for comparison electrical data obtained at the surface of the earth, that the proposed mechanism is partially responsible for maintaining the potential gradient near the surface.

While the mechanism described by Korff may be important at some higher level in the atmosphere, it fails to account for atmospheric electrical observations within the first few kilometers of the surface of the earth.[2] Measurements made at a large number of surface stations, including some in the polar regions, show that the potential in the atmosphere increases with height during fair weather, indicating a negative surface charge. The fair-weather air-earth current transports positive charge to the surface tending to neutralize the negative charge. Thus, a mechanism which accounts for the maintenance of the observed potential gradient must provide a means of transporting positive charge away from, or negative charge to the earth. The sign of the potential gradient and the atmospheric conduction current predicted by the proposed cosmic-ray mechanism is opposite to that observed near the surface. Further, as Korff has shown, the estimated cosmic-ray current is four orders of magnitude lower than the earth's discharging current. One must conclude that the proposed mechanism is of very minor importance in the low atmosphere. Test of the hypothesis for the upper atmosphere must await adequate data.

[1] S. A. Korff, Phys. Rev. **77**, 144 (1950).
[2] J. A. Fleming (editor), *Terrestrial Magnetism and Electricity* (McGraw-Hill Book Company, Inc., New York, 1939).

The Occurrence of Heavy Odd-Odd Isotopes in Nature

A. BRONIEWSKI*
Division of Physics, National Research Council, Ottawa, Ontario, Canada
January 24, 1950

RECENTLY two observers[1,2] have found experimentally a naturally occurring isotope of vanadium, V^{50}. As was pointed out by Leland,[2] this isotope is rather unexpected. It has both odd numbers of protons and neutrons, and also lies between two adjacent isobars, Cr^{50} and Ti^{50}. The object of this note is to point out a possible connection between the existence of such an isotope and the shell structure of nuclei.

As has been noted,[1] the existence of V^{50} is suggested by consideration of the curve of maximum stability. This is shown in Fig. 1 where the stable nuclei in the region from $Z=20$ to $Z=28$

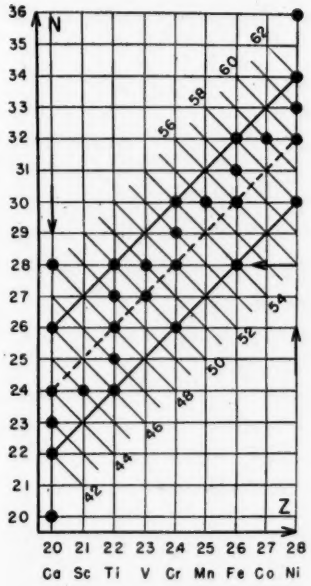

FIG. 1. The naturally occurring isotopes in the region from $Z=20$ to $Z=28$ plotted in a rectangular diagram. The arrows point to the completed shells (or sub-shells) of 20 and 28 neutrons and protons.

have been plotted in an ordinary rectangular diagram. The heavy lines passing through the heaviest and lightest isotopes of each Z indicate the limits of stability in this region. The dotted line lies exactly between these limits and one would expect the stable isotopes with odd Z to be found on the intersection of their respective ordinates with this line. Actually, no isotope thus predicted except possibly V^{50} is stable, which may be accounted for by the fact that all the odd Z isotopes in this region lying on the dotted line would have an odd number of neutrons. We must, therefore, look for a supplementary reason for the stability of V^{50} which distinguishes this particular isotope from the remaining odd-odd isotopes Sc^{46}, Mn^{54}, and Co^{58}, the radioactivity of which is well established.

It is suggested that in the case of V^{50}, there is an effect of a closed shell for neutrons somewhat different from those which have been considered hitherto. Up to now several phenomena have been interpreted by considering a closed shell itself, leading to a particularly stable nucleus or a configuration of a closed shell plus one or two nucleons, which on the contrary leads to low binding energies of the added particles. Little attention has been given to a configuration of a closed shell minus one nucleon although a spectroscopic analogy might suggest a relatively high binding energy for the last nucleon. V^{50} contains 27 neutrons, i.e., one neutron less than a shell of 28 neutrons, which is known to correspond to a completed shell or sub-shell.[3,4] There are other similar examples to be found in the table of elements. The odd-odd naturally occurring isotope, La^{138}, which also lies between two stable isobars, displays an analogous configuration, possessing 81 nucleons; i.e., one nucleon less than a closed shell of 82 nucleons. Also the existence of an incompleted closed shell or sub-shell may be connected with the occurrence of several isotopes which are radioactive but have unusually long half-lives. Thus Lu^{176}, a[u] odd-odd isotope with a half-life of 7.3×10^{10} yr., contains five neutrons in a sub-shell complete with six nucleons;[3,4] and Cl^{36}, with a half-life of 2×10^{6} yr., has one neutron less than the closed shell of 20 neutrons. These considerations may point to new stable or nearly stable isotopes such as, for instance, Tm^{168} (seven neutrons in a sub-shell of eight) about which little is known (cat. *C* in the latest table of Seaborg and Perlman[5]), Tb^{156} (nine neutrons in a sub-shell of 10 nucleons, not mentioned in this table), and Bi^{208} ((126–1) neutrons, cat. *F*).

There may be exceptions to a general rule of the type discussed due to the fact that the nucleus having one neutron less than a closed shell might lie rather far from the bottom of the mass valley as in the case of the odd Z nuclei with (50–1) neutrons, which have relatively short half-lives.

In conclusion, I wish to thank Dr. E. Pickup for his interest in this work.

* Postdoctorate fellow, National Research Council, Canada.
[1] D. C. Hess, Jr. and M. G. Inghram, Phys. Rev. **76**, 1717 (1949).
[2] W. T. Leland, Phys. Rev. **76**, 1722 (1949).
[3] M. G. Mayer, Phys. Rev. **75**, 1969 (1949); Phys. Rev. **74**, 235 (1948).
[4] Haxel, Hansen, and Suess, Phys. Rev. **75**, 1766 (1949).
[5] G. T. Seaborg and I. Perlman, Rev. Mod. Phys. **20**, 585 (1948).

The Production of Nuclear Disintegrations and Neutrons at the Geomagnetic Equator*

J. A. SIMPSON, JR. AND E. HUNGERFORD
Institute for Nuclear Studies, University of Chicago, Chicago, Illinois
January 25, 1950

MEASUREMENTS of the low energy nuclear disintegrations or stars produced by the cosmic radiations have been extended to the geomagnetic equator over a range of altitudes where the star production is in equilibrium with its producing radiations. As in the earlier measurements[1] fast, electron collection argon ionization chambers were used which measured the total ionization energy loss in the chamber due to a star event and, as shown by the measurements at higher latitudes,[1] could discriminate between star and shower events. Multichannel pulse analyzers with photographic recording as well as photographs of all ion chamber pulses using continuous motion film provided checks on all data. Concurrent measurements of the fast neutron production in air were made with boron trifluoride detectors. Since the accuracy of the measurements is dependent upon the measurement of the *true* air pressure near the B-29 aircraft, a highly corrected pressure altimeter was used. The data were obtained on August 9 and 13, 1949.

The results for three bias energies are shown in Fig. 1. The star producing radiation has an exponential dependence on atmospheric pressure and an *absorption thickness* of 210 ± 8 g/cm^2. The corresponding absorption thickness of the fast neutron producing radiation is 201 ± 5 g/cm^2 in agreement with geomagnetic equator measurements of fast neutrons made 18 months earlier.[2] The high point at 31 cm Hg on the 6.9 Mev bias curve and the low point at 22.5 cm Hg on the 8.0 Mev bias curve were due to drift of the discriminator bias during the measurement. All other biases remained within ±5 percent of their stated values.

Thus, the radiations producing stars and neutrons at $\lambda=0°$ have the same absorption in air. A similar correspondence is

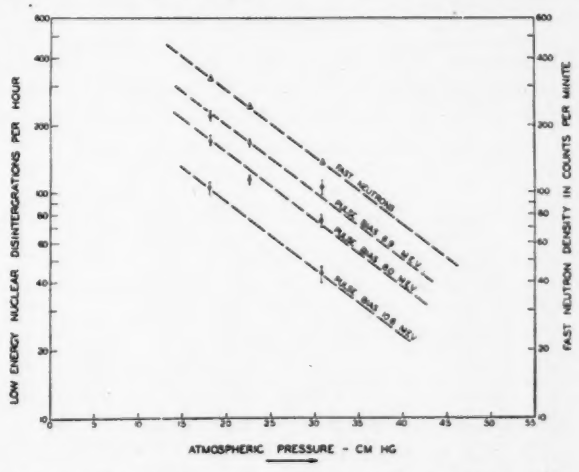
LOW ENERGY NUCLEAR DISINTEGRATIONS PER HOUR
FAST NEUTRON DENSITY IN COUNTS PER MINUTE
ATMOSPHERIC PRESSURE - CM HG
FAST NEUTRONS
STAR BIAS 6.9 MEV
STAR BIAS 8.0 MEV
STAR BIAS 2.8 MEV

FIG. 1. Star production as a function of altitude at the geomagnetic equator. The exponential absorption of the star producing radiation is 210 ± 8 g/cm^{-2}. The production of a fast neutrons measured concurrently gives an absorption of 201 ± 5 g/cm^{-2}.

obtained at $\lambda=53°$N by several observers of star production[1-4] and neutron production.[2,5]

Furthermore, the latitude dependence[1] of star production under 312 g/cm² of air (30,000-feet pressure altitude) going from $\lambda=0°$ to $\lambda=55°$N shows the same characteristic increase of a factor of approximately 3.2 as already found for the neutrons[2] in the atmosphere, the exact factor depending upon the time of the measurements.

Thus, *both* the altitude and latitude dependence of the neutrons and stars in the atmosphere provide convincing evidence that the large atmospheric neutron production of initial energies below 10 to 20 Mev arises from the low energy nuclear disintegrations in the atmosphere. The change in absorption of the star producing radiation from approximately 150–160 g/cm^{-2} at $\lambda=53°$N to 210 g/cm^{-2} at $\lambda=0°$ is consistent with star production by nucleons where longer *nuclear collision chains* are formed from the higher energy primary particles at $\lambda=0°$.

Yuan[5] has determined the intensity of slow neutrons at $\lambda=53°$N with a maximum at approximately 9 cm Hg. It is of interest to extrapolate the star and neutron production[1,2] from equilibrium air pressures to the maxima of the curves at both $\lambda=0°$ and $\lambda=53°$N. Assuming the same general shape of maximum found by Yuan it would be expected that at $\lambda=0°$ the maximum would lie at a greater depth in the atmosphere because of the 210 g/cm^{-2} absorption. The extrapolated curves predict a factor of approximately 4 for the increase of neutron and star production at the maxima between 0° and 53°N.

At present, the approximate measurements of low energy star production in photo-emulsions near the top of the atmosphere between 30° and 53° by Schein, Lord, and Salant[6] are consistent with this extrapolation.

The writers particularly wish to thank Major Wayne Gustafson, Captains G. Freyer and Shawhan and the other officers and men of the U.S.A.F. B-29 at Inyokern, California for making these flights to Lima, Peru successful.

* Assisted by the Joint Program of the ONR and the AEC.

[1] J. A. Simpson, Jr. and R. B. Uretz, Phys. Rev. **76**, 569 (1949) and references therein.
[2] J. A. Simpson, Jr., Phys. Rev. **73**, 1389 (1948).
[3] Bridge, Hazen, Rossi, and Williams, Phys. Rev. **74**, 1083 (1948).
[4] Using the sensitive emulsion method: Bernardini, Cortini, and Manfredini, Phys. Rev. **76**, 1792 (1949), and references therein.
[5] L. C. L. Yuan, Phys. Rev. **74**, 504 (1948).
[6] Echo Lake Conference on Cosmic Rays, 1949.

Additional Electron Lines from Radioactive Europium*

J. M. Cork, H. B. Keller, W. C. Rutledge, and A. E. Stoddard
Department of Physics, University of Michigan, Ann Arbor, Michigan
February 6, 1950

PREVIOUS investigations[1] have shown many internally converted gamma-rays to be emitted by activated europium. The *K–L–M* differences observed for many of the electron lines are characteristic of gadolinium ($Z=64$) as would be expected for gamma-rays following beta-emission from europium ($Z=63$). For other lines, the *K–L–M* differences are characteristic of samarium ($Z=62$). This might have indicated an impurity in the original europium, but it is now quite certain that the samarium results from the *K*-capture process in europium 152, as an alternative mode of decay with beta-emission.

Table I. Electron energies from radioactive europium.

Electron energy kev	Interpretation	Energy sum $Z=62$ kev	Energy sum $Z=64$ kev	Electron energy kev	Interpretation	Energy sum $Z=62$ kev	Energy sum $Z=64$ kev
32.0	L(Auger)(62)	39.1		341.5	M^3(64)		343.4
37.9	M(Auger)(62)	39.1		361.9	$K(-)$	408.7 or	412.2
72.9	K^1(64)		123.2	398.2	K^4(64)		448.5
75.0	K^1(62)	121.8		439.9	L^4(64)		448.3
114.6	$L_{1,2}{}^1$(62)	122.1		471.7	$K(-)$	518.5 or	522.0
115.2	$L_{1,2}{}^1$(64)		123.4	536.7	$K(-)$	583.5 or	587.0
115.8	$L_3{}^1$(64)		123.1	561.5	$K(-)$	608.3 or	611.8
120.3	M^1(62)	122.0		608.5	$K(-)$	655.3 or	658.8
121.4	M^1(64)		123.3	640.3	$K(-)$	687.1 or	690.6
122.8	N^1(64)		123.2	673.6	K^3(62)	720.4	
197.6	K^3(62)	244.4		728.5	K^3(64)		778
236.4	L^3(62)	244.2		820.6	$K(-)$	868	871
242.4	M^3(62)	244.3					
286.0	K^3(64)		366.3	917	K^4(62)	964	
293.5	K^3(64)		343.8	954	L^4(62)	963	
328.5	L^3(64)		366.6	1039	K^3(62)	1086	
335.5	L^3(64)		343.6	1066	K^3(64)		1116

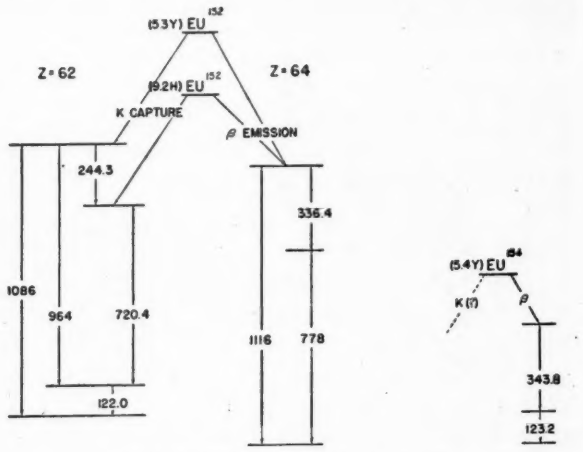

Fig. 1. Proposed europium decay schemes.

Inghram has shown by mass spectrometer studies that europium 152 and 154 have half-lives of 5.3 and 5.4 yr., respectively, and Muehlhause[2] has shown by critical absorption that *K*-capture occurred. Two of the gamma-rays observed (122 and 720 kev) are identical in energy with gamma-rays observed by Tyler in the 9.2-hr. europium activity due to *K*-capture.

In the present investigation with photographic magnetic spectrometers, the long-lived neutron activated europium yields in all about 33 electron lines as shown in column 1, Table I. Of these, about 26 lines may be uniquely identified as in samarium or gadolinium. The gamma-energies giving rise to them are summarized in Table II. For the remaining lines no *K–L* differences are observed and hence they are assumed to be *K*-lines for either samarium or gadolinium as shown in columns 3 and 4 of Table I, a choice to be made from further evidence.

By the use of a coincidence spectrometer (to be described elsewhere), Dr. C. M. Fowler has shown that electron-electron coincidences occur between the 122- and 244-kev gamma-rays and between the 123- and 344-kev gamma-rays, thus establishing certain sequences in emission, in agreement with the present interpretation.

Figure 1 indicates the complexity of the decay, and it presents that part of the existing information that seems reasonably certain and in agreement with the varied sources of information. For example, it can be seen how Tyler could observe from the 9.2-hr. activity certain, but not all, of the same gamma-energies observed here from the isomeric 5.3-yr. activity. The fit of the observed gamma-energies on the proposed level scheme is remarkably good.

Those gamma-rays due to transitions following beta-emission, and hence characteristic of gadolinium ($Z=64$), may occur in either Gd 152 or Gd 154. It is evident that a complete identifica-

Table II. Gamma-energies, identified.

Arbitrary number	$Z=62$ kev	$Z=64$ kev
1	122.0	123.2
2	244.3	336.4
3	720.4	343.8
4	964	448.4
5	1086	778
6		1116

tion of all electron lines can be made only when it is possible to obtain enriched isotopes of masses 151 and 153.

Since the sum of 336.4 and 778 kev is the observed 1115-kev line, this is arbitrarily shown as associated with Gd 152. The known sequence of 123- and 344-kev lines are shown together as arising from Gd 154. This will, of course, be much more complicated when the identification of all electron energies is complete.

* This investigation has been supported jointly by the AEC and ONR.
[1] A. W. Tyler, Phys. Rev. **66**, 125 (1939); M. G. Inghram and R. J. Hayden, Phys. Rev. **71**, 130 (1947); Cork, Schreffler, and Fowler, Phys. Rev. **72**, 1209 (1947); F. B. Shull, Phys. Rev. **74**, 917 (1948); and Hayden, Inghram, and Reynolds, Phys. Rev. **75**, 1500 (1949).
[2] C. Muehlhause, Manhattan Project Report CP-3750 (1947).

Cloud-Chamber Study of Cosmic Rays Underground*

O. L. Tiffany and W. E. Hazen
Randall Laboratory of Physics, University of Michigan, Ann Arbor, Michigan
February 6, 1950

A COUNTER-CONTROLLED Wilson cloud chamber has been operated in a salt mine at a depth of 860 mwe (8.6×10^4 g/cm²) from the top of the atmosphere. The primary aims of the experiment were two: First, to determine the character of the penetrating rays present at great depths and second, to investigate the properties of the secondaries that the penetrating rays produce in the salt roof above the cloud chamber and in lead, aluminum, and brass absorbers in the cloud chamber.

In order to determine whether or not the penetrating rays were ionizing, four one-inch lead plates were placed in the chamber with one tray of counters in the center of the chamber and the other tray below the chamber. A twofold coincidence between trays expanded the chamber and stereoscopic pictures were taken. With this arrangement, the pictures (aside from accidental coincidences) could be due to a single penetrating ionizing particle, to an electronic shower, or to a penetrating non-ionizing particle that produced two or more ionizing secondaries in the neighborhoods of the counters. Examination of the tracks in 175 pictures taken with this arrangement showed that 153 of the pictures were caused by single ionizing particles capable of traversing four inches of lead without unusual interactions. Eleven of the remaining pictures showed electronic showers, one of which was within the allowed region of the counter telescope, the remainder being side showers. Six accidentals were expected, leaving an upper limit of 5/153, or 3 percent, which might be caused by non-ionizing penetrating particles.

In order to investigate the electronic secondaries produced by the penetrating particles in the salt roof above the chamber, counter trays were placed above and in the center of the cloud chamber. The amount and nature of the absorber between the counters were then varied and the ratio of the number of soft particles with particular ranges to the number of penetrating particles was obtained. The results are summarized in Table I.

The penetrating particles were occasionally accompanied by secondary electrons upon emerging from the plates of lead, aluminum, or brass (center counter box). The ratios of accompanying secondary electrons to the producing penetrating particles are given in Table II. It is to be noted that these secondary electrons are more numerous than the knock-on electrons accompanying the penetrating component in lead at sea level. Nassar and Hazen[1] found about 6 percent for electrons of comparable energy range at sea level. The difference between the relative intensities of secondary electrons to penetrating particles in the mine and at sea level is most readily interpreted in terms of the expected difference in mean energies of the penetrating particles.

Table I. Absorption of electrons accompanying penetrating particles from salt roof.

Absorber	Penetrating particles	Electrons	Ratio electrons pen. part.
9 g/cm² Al+brass	108	75	70%
22 g/cm² Al+brass	100	16	16
66 g/cm² Pb (some Al+brass)	224	9	4

Table II. Secondary electrons produced in the chamber.

Absorber	Traversals	Electrons	Ratio-elec./p.p.
Pb	776 forward 808 backward	162 8	22 percent
Al	561	128	23
brass	420	73	17

If the penetrating particles traverse the entire layer of earth above the point of observation, we expect that a fraction $dI/I = 2.9dh/h$ would be stopped in the absorber below the counters. Of a total of 454 penetrating particles, two were stopped while the expected number was about one. Thus it is unlikely that a significant number of the penetrating ionizing particles are produced in the earth.

Occasional large electron showers from the roof of the mine were detected in the chamber. Two very large showers were initiated in the chamber by single penetrating rays.

The pictures show that the majority of the penetrating particles at 860 mwe that are capable of producing twofold coincidences in a counter telescope are ionizing. These ionizing penetrating rays interact with matter in a manner that demonstrates qualitative resemblance with the penetrating rays at sea level. Since the average number of secondary electrons is higher and showers of electrons occur more frequently than at sea level, the average energy is apparently much higher.

We wish to express our appreciation for the assistance of the administration and personnel of the Detroit mine of the International Salt Company.

* This work has been assisted by the Joint Program of the ONR and the AEC.
[1] S. Nassar and W. E. Hazen, Phys. Rev. **69**, 298 (1946).

S-Matrix in Non-Local Field Theory

Hideki Yukawa
*Columbia University, New York, New York**
January 26, 1950

RECENTLY the present author discussed certain types of quantized non-local fields, which were supposed to correspond to assemblies of elementary particles with finite radii.[1] In order to deal with the system consisting of two non-local fields, or a local field and a non-local field, which interact with each other, one must first find the substitute for the Schrödinger equation for the total system. However, it is naturally anticipated that the S-matrix in local field theory, which was obtained as the result of integration of the Schrödinger equation by successive approximations, may well find a counterpart in non-local field theory, whereas the physical interpretation of the Schrödinger wave functional itself, if it exists in non-local field theory, may be quite different from that in local field theory.

In fact, the S-matrix in non-local field theory can be obtained by a straightforward extension of the usual formalism. An arbitrary non-local operator A can be represented by a matrix $(n', x'|A|n'', x'')$, with rows and columns characterized by n', x' and n'', x'' respectively, where each of the symbols n', n'' stands for the distribution in numbers of particles in all possible quantum states while x' and x'' stand for a set of eigenvalues of four space-time operators x_μ. Further, we define $\{A\}$ for an arbitrary operator A by

$$(n'|\{A\}|n'') = \int\cdots\int (n', x'|A|n'', x'')(dx')^4(dx'')^4. \quad (1)$$

The S-matrix with matrix elements $(n'|S|n'')$ can now be written

symbolically in the form

$$S=1+(i/\hbar)\{L'\}+(i/\hbar)^2\{L'D_+L'\}+(i/\hbar)^3\{L'D_+L'D_+L'\}+\cdots \quad (2)$$

in non-local field theory as well as in local field theory, where L' is an invariant operator characterizing the interaction which can be expressed as a sum of products of non-local and local field quantities. In the particular case of the interaction between local fields, the matrix elements of L' reduce to the form

$$(n', x'|L'|n'', x'')=(n'|L'(x')|n'')\prod_{\mu=1}^{4}\delta(x_\mu'-x_\mu''), \quad (3)$$

where $(n'|L'(x')|n'')$ is the matrix element for the Lagrangian density for the interaction in the usual theory. D_+ is an invariant displacement operator with the matrix elements

$$(n', x'|D_+|n'', x'')=1, \tfrac{1}{2}, \text{ and } 0, \quad (4)$$

according as $x'-x''$ is a future-like vector, a space-like vector, and a past-like vector respectively. We can show very generally that the matrix S as defined by (2) fulfills all requirements for the S-matrix. Firstly, it is obviously relativistically invariant. Secondly, one can prove that it is unitary. Thirdly, the matrix element $(n'|S|n'')$ is different from zero only if the final and initial states, which are characterized by n' and n'' respectively, have the same total energy and momentum.[2]

As for the finiteness of the matrix S, it is not easy to draw a general conclusion. However, we can show that, for example, the self-energy of a spinor particle interacting with the non-local scalar field is finite due to the appearance of the form factor, as far as the third term of S in (2) is concerned. Further investigations are needed in order to settle the question of convergence in non-local field theory.

Detailed accounts will be published at a later date.

* On leave of absence from Kyoto University, Kyoto, Japan.
[1] H. Yukawa, Phys. Rev. **76**, 300 (1949); **76**, 1731 (1949); **77**, 219 (1950).
[2] We mean by the total energy and momentum the sums of energies and momenta respectively of the translational motion of the existing particles.

Photon Pulses from Point-to-Plane Corona

W. N. ENGLISH
Chalk River Laboratory, National Research Council of Canada, Chalk River, Ontario, Canada.
February 6, 1950

AN RCA 5819 photo-multiplier and a millimicrosecond oscilloscope have been used to study the photon pulses occurring at corona onset in air at atmospheric pressure, by use of a point-to-plane gap. Pulses of more than ten volts amplitude are obtained directly from the photo-multiplier, from single corona events which cannot be individually observed either visually or photographically. The method should be valuable for other gas discharge processes that have a similar low average, but high intrinsic, light output. It has already been used to study discharges of high average brightness such as long sparks[1] and pulsed discharges.[2]

Figure 1 shows the photon pulses obtained with 1-mm radius of curvature point and 5-cm gap. Pulses from the photo-multiplier were passed through an amplifier with pass band 100 kc to 100 Mc per second and through a coaxial line which delayed them relative to the triggering of the sweep. The photographs are a superposition of several sweeps, as can be seen in the lower picture where all the pulses do not coincide. Single sweeps were observed visually.

Studies of the induced pulses produced at the plane electrode by the corona[3] have indicated that these are due to electron motion near the point. This motion is quite slow compared to the rate of propagation of the corona, so that little of the corona process is revealed. The photon pulses do not suffer from this limitation, and give quite distinct and characteristic pulses for positive and negative point polarity.

The *positive* pre-onset streamer pulse shows a slow initial rise which may be due to the multiplication process that builds up the initial space charge necessary for the streamer to propagate. On about every tenth pulse this slow rise is replaced by a slight "bump," and the main rise of the pulse is delayed about two trace-widths. Each pulse shows a well-defined plateau, which gives the impression of two overlapping peaks. Pulse duration at 30 percent maximum amplitude is about 6×10^{-8} second. Observations with test pulses of from 3 to 8×10^{-8} second duration, inserted at the photo-multiplier anode, indicate that the plateau does not arise in the amplifier. It may be due to the nature of the decay of excitation in a single streamer channel, or again, perhaps it is possible for two successive pulses of excitation to occur in the same channel, even with a time separation as short as 3×10^{-8} second.

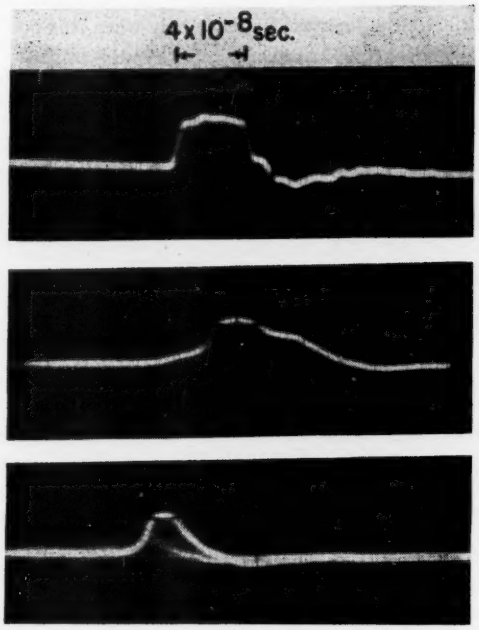

FIG. 1. Upper: Test pulse from discharge of 0.02 microsecond delay line. Middle: Photon pulse from positive point pre-onset streamer. Lower: Photon pulse from negative point "Trichel" pulse. All pulses traversed the same amplifier system.

The *negative* "Trichel" pulse shows only a slight indication of the initial multiplication process mentioned above. It rises abruptly at a rate about the same as the fast rise of the positive pulse, and decays smoothly after a duration at 30 percent maximum amplitude of about 3.5×10^{-8} second. Such a short simple pulse is surprising. The negative point corona in air has the appearance of a complete miniature glow discharge, and one might expect the process of building up the space charge formations needed to account for this structure[4] to give rise to a longer and more complex pulse.

In preliminary interpretation of the present results, it has been assumed that excitation of the gas is proportional to ionization, and that the decay of the excited states is rapid compared to the duration of the photon pulse. Further experiments with different gases, pressures, and electrode arrangements should make possible an explanation of the pulse shapes observed, and give new information of the corona processes involved.

The writer is grateful to Dr. C. Hendee of Northwestern University for suggesting the use of a photo-multiplier in the present problem. He is indebted to the Electronics Branch, Chalk River Laboratory, and especially to Mr. G. J. R. MacLusky, for loan of the oscilloscope, amplifiers and pulse generator, and for helpful advice.

[1] R. F. Saxe and J. M. Meek, Nature **162**, 263 (1948).
[2] W. S. Huxford and H. N. Olsen, Pittsburg Conference on Gaseous Electronics (November, 1949).
[3] W. N. English and A. W. Love (to be published).
[4] L. B. Loeb, J. App. Phys. **19**, 882 (1948); Phys. Rev. **71**, 712 (1947).

Gamma-Scintillations in Diphenylacetylene

C. F. RAVILIOUS, J. O. ELLIOT, AND S. H. LIEBSON
Electricity Division, Naval Research Laboratory, Washington, D. C.
January 25, 1950

KOSKI and Thomas[1] have recently reported the observation of scintillations in diphenylacetylene and have estimated the signal-to-noise ratio of diphenylacetylene to be six times better than that of stilbene. Measurements at this laboratory also show diphenylacetylene to be a more efficient phosphor and indicate its luminescence decay constant at room temperature to be 8×10^{-9} sec., assuming a pulse whose amplitude decays as $e^{-t/\tau}$. This time measurement was made by a shorted coaxial line technique in which the output pulse generated by the photo-multiplier tube is partially canceled by its own out-of-phase reflection from the variable-length shorted line. The decay constant determined by this method has not been corrected for the inherent spread in transit time of the photo-multiplier tube.

The experiment was carried out with a 931-A photo-multiplier operating at 200 v per stage which was cooled by liquid nitrogen. A radium gamma-ray source was used for excitation.

The crystals were in flake form and were made by the Bios Laboratories, Inc., of New York City.

[1] W. C. Koski and C. O. Thomas, Phys. Rev. **76**, 308 (1949).

On the Isomerism of Kr^{83}

I. BERGSTRÖM AND S. THULIN
Nobel Institute for Physics, Stockholm, Sweden

AND

G. ANDERSSON
Gustaf Werner Institute for Nuclear Chemistry, Uppsala, Sweden
January 25, 1950

IN an investigation of D-bombarded Se, Langsdorf and Segrè[1] discovered the isomerism of Kr^{83} and estimated the energy of the conversion electrons to be about 35 kev. Measurements with the β-spectrometer by Helmholtz[2] indicated two soft γ-rays of energies 29 and 46 kev (Se+D sample).

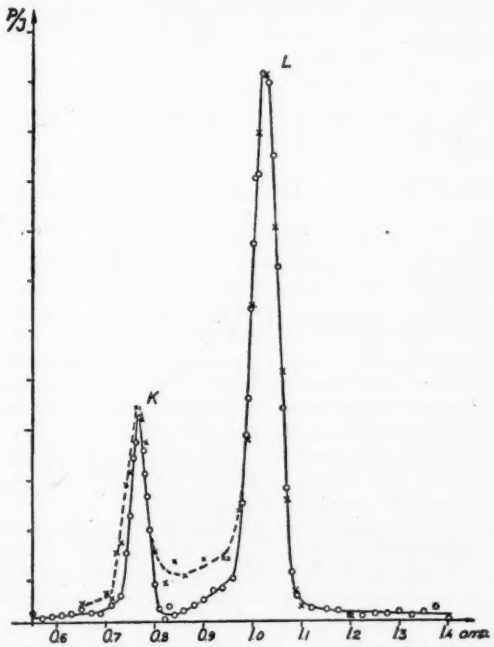

FIG. 1. Conversion lines of Kr^{83} (not corrected for absorption in the G-M tube window). Solid curve: Kr^{83} deposited on 0.15 mg Al/cm². Broken curve: Kr^{83m} deposited on 2.5 mg Al/cm².

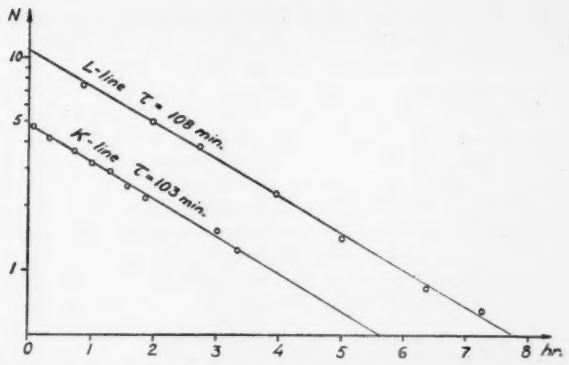

FIG. 2. Decay curves for the K- and L-lines measured in the β-spectrometer.

By separating the gaseous fission products of uranium (after cyclotron bombardment) in the electromagnetic isotope separator of the Nobel Institute,[3] it has been possible to obtain Kr^{83} with an activity sufficient for β-spectrometer investigations. This is an excellent way of preparing β-spectrometer samples. The active ions reach the collector foil with an energy of 30–60 kev and will in our case penetrate into the foil to a depth less than a hundred atomic layers[4] corresponding to an absorption thickness of the order of 1 μg/cm² in Al for the electrons from the deepest situated active atoms. It has proved possible to use 0.15 mg Al/cm² as collector foils. Thus, in most cases we obtain a mass-determined, carrier-free activity deposited on a very thin foil without any covering substance.

TABLE I. Conversion lines of Kr^{83}.

Conversion lines	$H\rho$ gauss-cm	$h\nu$ kev	Half-life (min.)	N_K/N_L line ratio	N_K/N_L surface ratio
K	446	31.5	103±10	0.44±0.06	0.39
L	598	32.5	108± 5		

The foil covered sample holder was fixed behind a circular slit (r=5 mm) in the collector arrangement of the separator and exposed to the "spot focused"[5] Kr^{83} line for about one hour. For mass number control the fission gases were mixed with stable Kr. A current of about 2 μamp. of Kr^{83} at 30 kev could be allowed during the separation without destroying the thin Al foil. The β-spectrometer data are summarized in Table I and Figs. 1 and 2.

Broken and solid lines refer to two different measurements with collector foils 2.5 and 0.15 mg Al/cm², respectively. The back-scattering effect of the thicker foil was too large to obtain an accurate value for N_K/N_L.

The absorption effect of the G-M tube window was calculated from measurements of the Co^{60} spectrum. The correction factor for N_K/N_L was 1.55 giving N_K/N_L=0.44, when comparing the ratio of the line heights and 0.39 for the line surfaces. The measurements were repeated in another lens spectrometer with a somewhat thinner G-M foil and N_K/N_L=0.40 was obtained for the ratio of the line heights. The $H\rho$-values in this case were 453 and 603 corresponding to $h\nu$=32.0 and 32.9 kev. Four measurements in two β-spectrometers gave the values 32.5, 32.5, 32.7, and 32.9 kev (mean value 32.7±0.5 kev) for the γ-energy from the L-line, which is much more accurately determined than the K-line.

Our γ-energy value of 32.7 kev probably corresponds to that of 29 kev reported by Helmholtz. It was not possible, however, to find the other converted γ-ray of 46 kev and, if it at all belongs to Kr^{83m}, the intensity of the conversion lines must be less than 1/20 of the L-line found by us. It is therefore possible that the 46-kev line belongs to Br^{83}.

The formula for the half-life given by Bethe and corrected for the theoretically calculated conversion coefficients (Hebb and Nelson) gives the half-life 2×10^{-1} sec. for $l=3$ and 3×10^{5} sec. for $l=4$ (experimental value 6.5×10^{3} sec.). According to the curves of Flügge,[6] $N_K/N_L\approx0.1$ for $l=4$ and $N_K/N_L\approx0.4$ for $l=3$ (electric radiation). The recently published curves of Tralli and Lowen[7] give $N_K/N_L\approx3$ for $l=3$ and magnetic radiation. For electric octupole radiation the agreement between the experimental value 0.44 of N_K/N_L and the theoretical one is very good. The half-life and internal conversion coefficients, however, indicate a mixture of ≈70 percent electric 2^4-pole and ≈30 percent magnetic 2^3-pole radiation. This would then still be an example of a parity forbidden isomeric transition.[8]

[1] A. Langsdorf, Jr. and E. Segrè, Phys. Rev. **57**, 105 (1940).
[2] A. C. Helmholz, Phys. Rev. **60**, 415 (1941).
[3] Bergström, Thulin, Svartholm, and Siegbahn, Arkiv f. Fys. **1**:11, 281 (1949).
[4] T. Koch, Nature **161**, 566 (1948).
[5] I. Bergström and S. Thulin, Phys. Rev. **76**, 1718 (1949).
[6] S. Flügge, Physik. Zeits. **42**, 227 (1941).
[7] N. Tralli and I. S. Lowen, Phys. Rev. **76**, 1541 (1949).
[8] P. Axel and S. M. Dancoff, Phys. Rev. **76**, 892 (1949).

The Effect of Electronic Paramagnetism on Nuclear Magnetic Resonance Frequencies in Metals

C. H. TOWNES*
Columbia University, New York, New York
CONYERS HERRING
Bell Telephone Laboratories, Murray Hill, New Jersey
AND
W. D. KNIGHT*
Trinity College, Hartford, Connecticut
January 23, 1950

THE nuclear paramagnetic resonance frequency for an atom in the metallic state usually is appreciably greater than the resonance frequency when the atom is in a non-metallic compound.[1] These frequency shifts are of the order of a few tenths of one percent, and are hence much too large to be accounted for by a simple difference in magnetic susceptibility of the materials or by differences in diamagnetic correction for the metallic and non-metallic atoms. It is proposed that such shifts are primarily due to orientation by the magnetic field of the spins of conduction electrons near the top of the Fermi distribution, and the interaction of these electrons with the nuclei. Since the conduction electrons usually have a very large probability density near the nucleus, this may be understood as an enormous concentration of the local magnetic susceptibility of the metal in the vicinity of the nuclei. It may also be compared with and calculated from the magnetic hyperfine structure interactions in an isolated atom. Diamagnetic effects of the same type appear to be very much smaller since the electronic currents responsible for the diamagnetism of the conduction electrons are appreciable only in the outer regions of the atom.

The fractional shift in nuclear resonance frequency between metal and non-metal is simply the fractional amount by which the presence of the conduction electrons increases the mean magnetic field strength H at the nucleus. Neglecting the small diamagnetic effect, we consider only the field ΔH due to the electron spins, which is $8\pi/3$ times the mean density of spin moment at the nucleus, assuming cubic symmetry. If the electron distribution is not cubically symmetric about the nucleus, then electron density at points other than at the nucleus contributes to ΔH, and ΔH will depend to some extent on orientation of the crystal with respect to H. In terms of wave functions of individual electrons in the metal the spin moment density at the nucleus can be written $\chi_p\hbar\,d\langle|\psi_F(0)|^2\rangle_{Av}$, where χ_p is the spin contribution to the macroscopic susceptibility per unit mass, M is the mass of one atom, and $\langle|\psi_F(0)|^2\rangle_{Av}$ is the average probability density at the nucleus for all electronic states on the Fermi surface. Now the hyperfine structure splitting $\Delta\nu$ for an s electron in the free atom is proportional to $|\psi_a(0)|^2$, where ψ_a is the wave function of the s electron in the free atom. Dividing the above expression for ΔH by the familiar Fermi expression for $\Delta\nu$ gives the fractional frequency shift in terms of a ratio of metallic and atomic wave functions:

$$\frac{\Delta H}{H}=\frac{hc\Delta\nu I\chi_p M}{\mu_I\mu_e(2I+1)}\,\frac{\langle|\psi_F(0)|^2\rangle_{Av}}{|\psi_a(0)|^2} \qquad (1)$$

where $hc\Delta\nu$ is the hyperfine splitting in energy units, μ_e is the Bohr magnetron, μ_I is the nuclear moment, and I the nuclear spin.

We have attempted to calculate the theoretical value of the last factor in (1) for the cases (Na, Li, Be) for which adequate calculations of metallic wave functions are at present available. This factor may be written $(|\psi_0(0)|^2/|\psi_a(0)|^2)\delta_K$, where ψ_0 is the wave function of an electron at the bottom of the conduction band and δ_K is the mean over the Fermi surface of

$$s_k=(|\psi_k(0)|^2)/(|\psi_0(0)|^2).$$

Calculations by the Wigner-Seitz method[2] give ψ_0; δ_k can be determined in either of two ways. The first, suitable only for monovalent metals, is to assume that s_k is adequately represented by the first two terms of its development in powers of the square of the electronic wave vector k:

$$s_k=1+k^2ds_k/d(k^2)+\cdots, \qquad (2)$$

and to use the expression given by Herring and Hill[3] for $ds_k/d(k^2)$ (Appendix III of this reference; a factor 6 should be inserted before α in Eq. (M).) This method was applied to the case of Na with the aid of wave functions kindly supplied by Dr. Bardeen, and gave $\delta_k=0.70$. Similar calculations were made for Li, but no results will be quoted because it was found that the available wave functions were based on an incorrect potential field for the Li ion. Comparison with the case of Be, to be discussed next, suggests that δ_k for Li may be of the order of 0.4. For Be, which is divalent, the first two terms of (2) do not give at all a good approximation, and a second procedure was therefore adopted. This consisted in dividing up the Fermi surface into six portions, estimating an average s_k for each portion from the values of s_k directly calculated for states near the Fermi surface (Table VII of reference 3), and combining with suitable weights. This gave $\delta_k=0.32$, and this value did not seem to be particularly sensitive to changes in the technique of averaging.

The quantity $|\psi_0(0)|^2/|\psi_a(0)|^2$ has approximately the values 1.16, 1.9, and 1.6, for Na, Li, and Be, respectively. For other metals its behavior can be inferred qualitatively by noting how much of the charge of the outermost s electrons of the free atom lies outside a sphere whose volume equals the atomic volume of the metal; it appears from this that $|\psi_0(0)|^2/|\psi_a(0)|^2$ should be appreciably smaller for such multivalent metals as Al, Ga, and Pb than for the mono- and divalent ones.

TABLE I. Observed shifts of nuclear resonances in metals due to free electron paramagnetism, and comparison with theory.

Nucleus	H.f.s. splitting $\Delta\nu$, in cm^{-1} for s electron	Observed shift $\Delta H/H$, (percent)	χ_p per gram $\times10^6$	$\chi_p\langle|\psi_F(0)|^2\rangle_{Av}/|\psi_a(0)|^2\times10^6$ theory	from (1)
Li^7	0.027	0.04	3.0[a]	~2.3	2.6
Na^{23}	0.060	0.10	0.98[b]	0.80	0.63
Cu^{63}	0.39	0.23	~0.11[c]		0.078
Be^9	0.040	<0.002	~0.30[d]	~0.15	<0.025[e]
Pb^{207}	2.1[f]	1.2	~0.10[c]		0.0091
Al^{27}	0.35[f]	0.16	~0.47[c]		0.21
Ca^{69}	0.58[f]	0.44	~0.20[c]		0.083

[a] Measured value with diamagnetic corrections, S. R. Rao and K. Sarithri, Proc. Ind. Acad. **6**, 207 (1942).
[b] Average of measured values with diamagnetic corrections, F. Bitter, Phys. Rev. **36**, 978 (1930).
[c] Calculated value assuming free valence electrons.
[d] Theoretical value (reference 3).
[e] The small diamagnetic contribution to the shift may increase this limit by a factor of 2 or so.
[f] Estimated from Goudsmit's formula and measured values for ionized atoms.

Table I gives some experimental values of the relative frequency shift, values of $\chi_p\langle|\psi_F(0)|^2\rangle_{Av}/|\psi_a(0)|^2$ computed from these shifts by use of (1), and, for Li, Na, and Be, the results of theoretical attempts to calculate this product by the methods outlined above. In almost all cases the most uncertain factor is probably the value of χ_p. Though no quantitative comparisons of theory and experiment can be made at present for other metals than these three, it will be noted that the figures in the table are consistent with reasonable values for χ_p, $|\psi_0(0)|^2/|\psi_a(0)|^2$, and δ_k. The case of Be is interesting in that the shift is too small to measure, indicating values of δ_k and/or χ_p still smaller than those calculated. The shift in Pb illustrates the considerable size which this paramagnetic effect may have in heavy metals.

* Work of these authors was largely performed at Brookhaven National Laboratory under contract with the AEC.

[1] W. D. Knight, Phys. Rev. **76**, 1259 (1949).
[2] E. Wigner and F. Seitz, Phys. Rev. **43**, 804 (1933).
[3] C. Herring and A. G. Hill, Phys. Rev. **58**, 132 (1940).

Relativistic Nuclear Force

T. TOYODA
St Paul's University, Tokyo, Japan
December 27, 1949

SINCE experiments on neutron-proton scattering were extended to very high voltages at Berkeley,[1] theoretical calculations[2-4] have been made to obtain the relativistic correction to nuclear forces. One of the most remarkable alterations of the nuclear force brought out by the calculations is that the $1/r^3$ singularity of the tensor force disappears in the relativistically corrected forms. This change eliminates the essential difficulty of the calculation of the deuteron ground state. However, it must be mentioned that none of these theoretical attacks has fully taken into account the retardation effect of the mesonic potential. The calculation developed in this paper starts with the explicit expression of the retarded potential and will examine additional non-negligible terms which have hitherto been overlooked. One of these terms corresponds to Breit's expression for the Møller force in the case of two electrons.

We shall take the pseudoscalar meson field with only pseudoscalar coupling, so that we have

$$(\Delta-\partial_t^2-\kappa^2)U=\varphi, \tag{1}$$

where the natural units $\hbar=c=1$ are used, and κ is the rest mass of the meson field U. The source function φ is given by the transition matrix elements of the first nucleon between two states $(E_1, u_1)\rightarrow(E_1', u_1')$, i.e.,

$$\varphi(\mathbf{r}_1, t)=fu_1'^*(\mathbf{r}_1)\rho_2^{(1)}Q^{(1)}u_1(\mathbf{r}_1)\exp(i(E_1'-E_1)t), \tag{2}$$

where f, $\rho_2^{(1)}$ and $Q^{(1)}$ are respectively the coupling constant, a Dirac matrix and an isotopic spin operator of the first particle, in the usual sense of these symbols. $u_1(\mathbf{r}_1)$ is the Dirac spinor wave function.

Now it is clear that (1) has the following special solution:

$$U(\mathbf{r}_2, t)=f\exp(i(E_1'-E_1)t)\cdot\int u_1'^*(\mathbf{r}_1)\{Q^{(1)}\rho_2^{(1)} \times\exp[-|\mathbf{r}_2-\mathbf{r}_1|(\kappa^2-(E_1'-E_1)^2)^{\frac{1}{2}}]/|\mathbf{r}_2-\mathbf{r}_1|\}u_1(\mathbf{r}_1)d\nu_1. \tag{3}$$

Since we are interested in the correction due to the retardation effect, we shall expand the exponential function in the above integrand in power series in $(E_1'-E_1)$:

$$\begin{aligned}\exp(-|\mathbf{r}_2-\mathbf{r}_1|(\kappa^2-(E_1'-E_1)^2)^{\frac{1}{2}})/|\mathbf{r}_2-\mathbf{r}_1| &=\exp(-|\mathbf{r}_2-\mathbf{r}_1|\kappa)/|\mathbf{r}_2-\mathbf{r}_1| \\ &\quad+\exp(-|\mathbf{r}_2-\mathbf{r}_1|\kappa)(E_1'-E_1)^2/2\kappa+\cdots \\ &\equiv W_0+W_1+\cdots.\end{aligned} \tag{4}$$

The first term, W_0, is the usual static Yukawa potential, and the second term, W_1, is the first correction term arising from the retardation.

The succeeding calculation can be performed in an analogous fashion to that of the Møller force between two electrons.[5] The transition matrix element $(E_1, u_1; E_2, u_2)\rightarrow(E_1', u_1'; E_2', u_2')$ is given as follows, provided the first nucleon is a proton and the second a neutron:

$$\begin{aligned}V&=\int U(\mathbf{r}_2 t)\cdot\varphi(\mathbf{r}_2, t)d\nu_2 \\ &=-f^2\exp(i(E_1'+E_2'-E_1-E_2)t)\cdot\int\int u_2'^*(\mathbf{r}_2)\cdot u_1'^*(\mathbf{r}_1)\rho_2^{(2)}\rho_2^{(1)} \\ &\quad\times\{\exp(-|\mathbf{r}_2-\mathbf{r}_1|(\kappa^2-(E_1'-E_1)^2)^{\frac{1}{2}})/ \\ &\qquad|\mathbf{r}_2-\mathbf{r}_1|\}u_2(\mathbf{r}_2)u_1(\mathbf{r}_1)d\nu_1\cdot d\nu_2 \\ &=\int\int u_2'u_1'(-f^2\rho_2^{(2)}\rho_2^{(1)}W_0-f^2\rho_2^{(2)}\rho_2^{(1)}W_1-\cdots)u_2\cdot u_1 d\nu_1\cdot d\nu_2.\end{aligned} \tag{5}$$

The operator expression in the parentheses in (5) is usually called the nuclear force between two particles, although the first and the second terms in the parentheses, as will be shown later, represent quantities of the same order. Attention has hitherto been limited to the discussion of the first term. The second term, in which we are particularly interested, can be re-written in a commutator form:

$$-f^2\rho_2^{(2)}\rho_2^{(1)}W_1=-f^2[H_2, \rho_2^{(2)}[H_1, \rho_2^{(1)}\exp(-|\mathbf{r}_2-\mathbf{r}_1|\kappa)]]/2\kappa \tag{6}$$

where H_i is the Dirac Hamiltonian of a free nucleon, i.e.,

$$H_i=-i\boldsymbol{\alpha}_i\cdot\mathrm{grad}_i+\beta_i\mu \quad (i=1, 2). \tag{7}$$

Equation (6) can be written also as

$$\begin{aligned}&-f^2\rho_2^{(2)}\rho_2^{(1)}W_1 \\ &=f^2\kappa\rho_3^{(2)}\rho_3^{(1)}\left\{(\boldsymbol{\sigma}_2, \boldsymbol{\sigma}_1)+\frac{(\boldsymbol{\sigma}_2, \mathbf{r}_{12})(\boldsymbol{\sigma}_1, \mathbf{r}_{12})}{r_{12}^2}\right\}\frac{e^{-\kappa r_{12}}}{r_{12}} \\ &\quad+f^2\kappa\rho_3^{(2)}\rho_3^{(1)}\frac{(\boldsymbol{\sigma}_2, \mathbf{r}_{12})(\boldsymbol{\sigma}_1, \mathbf{r}_{12})}{r_{12}^2}\cdot\frac{e^{-\kappa r_{12}}}{1/\kappa} \\ &\quad+4f^2\mu^2\rho_1^{(2)}\rho_1^{(1)}e^{-\kappa r_{12}} \\ &\quad-2f^2\mu\kappa i\{\rho_1^{(2)}\rho_3^{(1)}(\boldsymbol{\sigma}_1, \mathbf{r}_{12})+\rho_3^{(2)}\rho_1^{(1)}(\boldsymbol{\sigma}_2, \mathbf{r}_{21})\}\frac{e^{-\kappa r_{12}}}{r_{12}} \\ &\quad+2f^2\kappa\rho_3^{(2)}\rho_3^{(1)}\frac{e^{-\kappa r_{12}}}{r_{12}}\{(\boldsymbol{\sigma}_1, \mathbf{r}_{12})\cdot(\boldsymbol{\sigma}_2, \mathrm{grad}_2)+(\boldsymbol{\sigma}_2, \mathbf{r}_{21})(\boldsymbol{\sigma}_1, \mathrm{grad}_1)\} \\ &\quad-4f^2\rho_3^{(2)}\rho_3^{(1)}e^{-\kappa r_{12}}(\boldsymbol{\sigma}_2, \mathrm{grad}_2)(\boldsymbol{\sigma}_1, \mathrm{grad}_1) \\ &\qquad+4f^2\mu ie^{-\kappa r_{12}}\{\rho_1^{(2)}\rho_3^{(1)}(\boldsymbol{\sigma}_1, \mathrm{grad}_1)+\rho_3^{(2)}\rho_1^{(1)}(\boldsymbol{\sigma}_2, \mathrm{grad}_2)\}.\end{aligned} \tag{8}$$

The first term in this last expression (8) is the counterpart of Breit's force for the case of nuclear interaction. The second term is worth particular attention since its effect decreases with r less rapidly than the other terms. The effect of this term may, therefore, become predominant in the calculation of the quadrupole moment of the deuteron. The third and fourth terms, which contain $i\rho_1$, unfortunately cannot be reduced to simpler forms, even in Pauli's approximation. Indeed, ρ_3 is of the order of unity, while $i\rho_1$ is of the same order as ρ_2 in this approximation. Therefore, we cannot neglect these terms.

On the other hand, the last three terms in (8) are non-diagonal in the $\mathbf{r}$ representation, and express the dependence on the relative velocity of the two nucleons. When the de Broglie wave-length of an incident neutron approaches the force range $1/\kappa$, these non-diagonal parts will become of the same order as the other terms.

If we take a scalar instead of a pseudoscalar interaction, the retardation effect gives only corrections of higher order. The pseudoscalar type of interaction resembles that of the vector type in the sense that they both contain the effect of the nucleonic current. The detailed estimation of the above mentioned additional terms will be discussed in a full report.

The author should like to express his sincere gratitude to Professor Yamanouchi for his valuable suggestions.

[1] Cook, McMillan, Peterson, and Sewell, Phys. Rev. **72**, 1264 (1948).
[2] L. Van Hove, Phys. Rev. **75**, 1519 (1949).
[3] G. Araki, Phys. Rev. **75**, 1101 (1949).
[4] Y. Nambu, Soryûshiron-Kenkyû **1**, 171 (1949).
[5] H. Bethe and E. Fermi, Zeits. f. Physik **77**, 296 (1932).

Author Index to Volume 77

References with (A) are to abstracts of papers presented at meetings of the American Physical Society, and those with (T) designate title only. References with (L) are to Letters to the Editor.

Abraham, Bernard M. Properties of liquid helium 3 and of mixtures of helium 3 and helium 4—739(T)
—— (see Weinstock, B.)—400(L)
Adair, R. K. Dependence of neutron cross sections on mass number—748(A)
Adams, Edward N. II. Properties of deuteron and triton from h.f.s. measurements—755(A)
Agnew, Harold M. Beta-spectra of Cs^{137}, Y^{91}, 61^{147}, Ru^{106}, Sm^{151}, P^{32}, and Tm^{170}—655
Akeley, Edward (see Hoffman, Gerald)—761(A)
Akioka, Tetsuo (see Itoh, Junkichi)—293(L)
Alburger, D. E. (see Hughes, D. J.)—726(L)
Aldrich, L. T. and C. E. Smith. Mass spectrometric production of oxide cathodes—744(A)
Alfvén, H. On the solar origin of cosmic radiation. II—375
Allen, A. J., J. F. Nechaj, K. H. Sun, and B. Jennings. Fast neutron yield from the cyclotron—752(A)
Allen, James S. (see Klema, E. D.)—661
—— (see Smith, Philip B.)—747(A)
Allison, H. W. (see Moore, George E.)—246
Allison, S. K., J. H. Montague, and A. H. Morrish. Values of certain (p,γ) resonances below 400 kv—754(A)
Allred, J. C. Differential cross section of the reaction $He^3(d,p)He^4$ at 10.2-Mev bombarding energy and search for excited state in He^4—753(A)
Alvarez, L. W., A. Longacre, V. G. Ogren, and R. E. Thomas. Electrical detection of artificially produced mesons—752(A)
Anderson, D. L. and M. L. Pool. Radioactive xenon 125, and xenon 127—142(L)
Anderson, Roy S. (see Burkhalter, James H.)—152(L)
Anderson, Wallace E. (see Simmons, James W.)—77
Andersson, G. (see Bergström, I.)—851(L)
Anslow, Gladys A. and Hsi-teh Hsieh. Absorption bands in the ultraviolet continua of associated primary and secondary alcohols—423(A)
Arfken, G. B. (see Breit, G.)—569(L)
Arnold, W. R. Use of selenium rectifiers in a 500-kev generator—758(A)
Arnous, E. Coherent scattering of x-rays by atoms with more than one electron according to the one-electron theory and the positron theory—149(L)
Arroe, O. H. Hyperfine structure and isotope shift in barium—745(A)
Avery, R. (see Blanchard, C. H.)—756(A)

Bailey, Carl L. and William R. Stratton. Cross section of the $C^{12}(p,\gamma)N^{13}$ reaction at low energies—194
Bailey, V. A. On the relativistic electromagneto-ionic theory of wave propagation—418(L)
Baldwin, H. W. (see Simpson, J. A.)—751(A)
Ballentine, Robert (see Miller, Warren W.)—714(L)
Barbour, Ian. Magnetic deflection of cosmic-ray mesons using nuclear plates—751(A)
Bardeen, J. (see Pearson, G. L.)—303(L)
—— (see Shockley, W.)—407(L)
—— **and W. G. Pfann.** Effects of electrical forming on the rectifying barriers of *n*- and *p*-germanium transistors—401(L)
Barkas, Walter H. (see Bradner, Hugh)—462
Barschall, H. H. Use of fast neutrons for the study of nuclear energy levels—739(T)
Bartholomew, G. A. (see Kinsey, B. B.)—723(L)
Bashkin, S., B. Petree, F. P. Mooring, and R. E. Peterson. Total neutron scattering cross section of helium—748(A)
Bates, D. R. Electron recombination in helium—718(L)
Bay, Z. Calculation of decay times from coincidence experiments—419(L)
—— **and M. M. Slawsky.** General relation between genuine and chance coincidences and its application to measurement of high activity sources—414(L)
Beams, J. W. (see Snoddy, Leland B.)—572(T)
Becker, John W. Problems in newer fields in fluid mechanics—572(T)
Becker, M. and H. Y. Fan. Infra-red transmission of germanium and silicon—760(A)
Beeman, W. W. (see Dexter, D. L.)—761(A)
Beghian, L. E., M. A. Grace, G. Preston, and H. Halban. Inelastic scattering of neutrons by light nuclei—286(L)
Beiduk, F. M. (see Pruett, J. R.)—628, 755(A)
——, **J. R. Pruett, and E. J. Konopinski.** Theory of the D+D reactions. Part I. Analysis of the energy dependence—622, 755(A)
Belinfante, F. J. and J. S. Lomont. Interaction representation of general fields—757(A)
Bell, P. R. and J. M. Cassidy. Beta-spectrum of Be^{10}—301(L)
—— **and J. M. Cassidy.** Gamma-rays of K^{40}—409(L)
——, **Boyd Weaver, and J. M. Cassidy.** Beta-rays of K^{40}—399(L)
Bendt, P. J. and I. W. Ruderman. New method for determining the relative phase with which slow neutrons are scattered by nuclei—575
Bene, G. J., P. M. Denis, and C. R. Extermann. Upper limit of spin-spin interaction factor—288(L)
Benfield, A. E. D.c. magnetic generator—424(A)
—— New piezoelectric effect—762(A)
Bennett, F. D. (see Giese, J. H.)—574(A)
Bennett, W. E. (see Bradford, C. E.)—753(A)
Bergdolt, V. E. (see Giese, J. H.)—574(A)
Berger, Martin J. (see Groetzinger, Gerhart)—584
—— (see Ribe, Fred L.)—760(A)
Bergström, I. (see Grotdal, T.)—296(L)
——, **S. Thulin, and G. Andersson.** On the isomerism of Kr^{83}—851(L)
Berman, A., P. Kusch, and A. K. Mann. On the hyperfine structure of the $^2P_{\frac{1}{2}}$ state of Tl^{205} and Tl^{203}—140(L)
Berne, E. Half-life of Br^{82}—568(L)
Bernstein, Richard B. (see Ferigle, Salvador M.)—740(A)
—— (see Madigan, John R.)—740(A)
Bernstein, William (see Miller, Warren W.)—714(L)
Bershader, D. and S. I. Pai. On turbulent jet mixing in two-dimensional supersonic flow—574(A)
Bess, L. Bremsstrahlung for heavy elements at extreme relativistic energies—550
Bethe, H. A. (see Levinger, J. S.)—756(A)
——, **L. M. Brown, and J. R. Stehn.** Numerical value of the Lamb shift—370
—— **and Conrad Longmire.** Effective range of nuclear forces. II. Photo-disintegration of the deuteron—647
Bhabha, H. J. On a new theory of nuclear forces—665
Binder, Daniel. Delayed coincidence counting measurement of $Hg^{203,205}$—291(L)
Birnbaum, George. Dispersion in NH_3 in the microwave region—144(L)
Bishop, A. S. (see Bradner, Hugh)—462
Bishop, G. R., Richard Wilson, and H. Halban. Measurement of some weak γ-ray intensities—416(L)
Bjorklund, R., W. E. Crandall, B. J. Moyer, and H. F. York. High energy photons from proton-nucleon collisions—213

Blackmer, L. L. and H. E. Farnsworth. Effect of the type of support on the photoelectric work function of silver films—826
Blair, K. W. (see Burson, S. B.)—403(L)
Blanchard, C. H. and R. Avery. Low states of Li^7—756(A)
Blaser, J. P. (see Boehm, F.)—295(L)
Boehm, F., J. P. Blaser, P. Marmier, and P. Preiswerk. Nuclear gamma-radiation of Cu^{61}—295(L)
Bohr, Aage and V. F. Weisskopf. Influence of nuclear structure on the hyperfine structure of heavy elements—94
Borkowski, C. J. and E. Fairstein. Proportional counter spectrometer—759(A)
Bostick, W. H. Possible techniques in direct-electron-beam tumor therapy—564(L)
Bowen, John H. (see Harvalik, Zaboj V.)—745(A)
Bowen, W. A., Jr. (see Singer, S. F.)—398(L)
Boyer, William M. (see Ferigle, Salvador M.)—740(A)
—— (see Madigan, John R.)—740(A)
Bozorth, R. M. Recent advances in ferromagnetism—423(T)
Bradford, C. E. and W. E. Bennett. Energies of neutrons from the $Be^9(\alpha,n)$ reaction—753(A)
Bradner, Hugh (see Smith, F. M.)—562(L)
——, **Frances M. Smith, Walter H. Barkas, and A. S. Bishop.** Range-energy relation for protons in nuclear emulsions—462
Bradt, H. L. (see Goldfarb, L.)—751(A)
—— **and B. Peters.** Heavy nuclei of the primary cosmic radiation—54
Bragg, J. K., T. C. Madison, and A. H. Sharbaugh. Microwave spectrum of CH_2CFCl—148(L); Erratum—571(L)
Branyan, C. E. (see Cork, J. M.)—843(L)
Bratenahl, A., S. Fernbach, R. H. Hildebrand, C. E. Leith, and B. J. Moyer. Elastic scattering of 84-Mev neutrons—597
Bray, R. and H. J. Yearian. Dependence of the germanium high back voltage rectifier resistance on frequency—760(A)
Breit, G., G. B. Arfken, and W. W. Clendenin. Spectroscopic isotope shift and nuclear polarization—569(L)
Briggs, H. B. Infra-red absorption in silicon—727(L)
—— Optical effects in bulk silicon and germanium—287(L)
Brillouin, L. Maxwell's demon cannot do it—information and entropy—572(T)
Brittin, Wesley E. Note on the quantization of dissipative systems—396
Brockman, Frank G. Cation distribution in ferrites with spinel structure—841(L)
——, **P. H. Dowling, and Walter G. Steneck.** Dimensional effects resulting from a high dielectric constant found in a ferromagnetic ferrite—85
Broniewski, A. Occurrence of heavy odd-odd isotopes in nature—846(L)
Brown, H. (see Perez-Mendez, V.)—404(L)
Brown, L. M. (see Bethe, H. A.)—370
Brown, W. W. and A. S. McKay. Cloud-chamber study of cosmic-ray nuclear interactions at 3260 meters elevation—342
Browne, C. P., R. V. Smith, and H. T. Richards. $P-N$ reactions in light elements—754(A)
Broyles, A. A. and B. Kivel. Lower bound on the range of neutron-proton interaction—839(L)
Bruner, J., L. M. Langer, and D. Moffat. Beta-spectrum of Pr^{143}—747(A)
Bullard, E. C. Origin of terrestrial magnetism—739(T)
Burcham, W. E. and Joan M. Freeman. Erratum: short range alpha-particles from fluorine and lithium bombarded by protons—287(L)
Burgy, M. T. (see Hughes, D. J.)—291(L)
Burke, Edward (see Friedman, Raymond)—574(A)
Burkhalter, James H., Roy S. Anderson, William V. Smith, and Walter Gordy. Preliminary report on the fine structure of the microwave absorption spectrum of oxygen—152(L)
Burson, S. B., K. W. Blair, and D. Saxon. Beta-spectrum and decay scheme of $_{65}Tb^{160}$—403(L)
Cameron, A. G. W. (see Millar, C. H.)—742(A)
Campbell, W. E. (see Kittel, C.)—725 (L)
Carney, Rose A., Arnold G. Meister, and Forrest F. Cleveland. Raman and infra-red spectra for hexachloroethane and hexabromoethane, and force constants for hexachloroethane—740(A)
Carss, W. L. (see Robertson, B. E.)—747(A)
Carter, R. E. (see Koch, H. W.)—165
Cassidy, J. M. (see Bell, P. R.)—301(L), 399(L), 409(L)
Chamberlain, Owen. Neutron diffraction in liquid sulfur, lead, and bismuth—305
Chapman, Robert M. Absorption of radiation in the very near infra-red by water vapor—741(A)
Charles, George W. Study of the spectra of columbium and molybdenum in the extreme ultraviolet—120
Chew, G. F. and M. L. Goldberger. Production of fast deuterons in high energy nuclear reactions—470
Christian, Richard S. and Edward W. Hart. Neutron-proton interaction—441
Clavier, Philippe A. Active coaxial tube—302(L)
Clendenin, W. W. (see Breit, G.)—569(L)
Cleveland, Forrest F. (see Carney, Rose A.)—740(A)
—— (see El-Sabban, M. Zaki)—740(A)
—— (see Ferigle, Salvador M.)—740(A)
—— (see Lamport, J. E.)—740(A)
—— (see Madigan, John R.)—740(A)
—— (see Zietlow, James P.)—739(A)
Clotfelter, B. E. (see Fowler, R. G.)—760(A)
Coester, F. Stark-Zeeman effects on symmetric top molecules with nuclear quadrupole coupling—454
Cohen, Bernard L. $(n\text{-}2n)$ and $(n\text{-}p)$ cross sections—754(A)
Cohen, Victor W., Walter S. Koski, and T. Wentink, Jr. Nuclear spin and quadrupole coupling of S^{35}—742(A)
Coles, D. K., W. E. Good, and R. H. Hughes. Microwave spectrum of methyl alcohol—741(A)
Conn, William M. Use of "exploding wires" as a light source of very high intensity and short duration—745(A)
Conwell, E. and V. F. Weisskopf. Theory of impurity scattering in semiconductors—388
Cook, C. Sharp (see Owen, George E.)—743(A)
Coomes, E. A. Activity studies on pulsed oxide cathodes—739(T)
Cooper, E. P., and F. T. Rogers, Jr. Composite of experimental measurements of the energy-distribution among beta-particles from tritium—402(L)
Cork, J. M., H. B. Keller, W. C. Rutledge, and A. E. Stoddard. Additional electron lines from radioactive europium—848(L)
——, **A. E. Stoddard, W. C. Rutledge, C. E. Branyan, and J. M. LeBlanc.** Radioactivity in platinum by neutron capture—843(L)
Coryell, C. D. (see Glendenin, L. E.)—755(A)
——, **A. Y. Sakakura, and A. M. Ross.** Fission yields of 65-day Zr^{95} and 17-hr. Zr^{97}; search for other Zr and Nb fission chains—755(A)
Cowan, C. E. (see DeBenedetti, S.)—205
Cowley, J. M. Approximate theory of order in alloys—669
Cranberg, Lawrence. Conversion electrons of radium D—155
Crandall, W. E. (see Bjorklund, R.)—213
Crawford, D. P. (see McMurtrie, G. E.)—840(L)
Crawford, F. H. Chemical thermodynamics in Jacobian form—423(A)
Crawford, M. F. (see Kelly, F. M.)—745(A)
Curtis, C. W. (see Emrich, R. J.)—573(A)
Curtis, N. W., J. Hornbostel, D. W. Lee, and E. O. Salant. Photo-disintegration of rhodium—290(L)
Curtiss, Charles F. Entropy changes in fluid flow—572(T)
Curtiss, L. F., R. D. Evans, Warren Johnson, and Glenn T. Seaborg. Units of radioactivity—142(L)

Damask, A. C. (see Willardson, R. K.)—758(A)
Dancoff, S. M. Relativistic meson theory of the deuteron—755(A)
Danielson, G. C. (see Willardson, R. K.)—300(L), 758(A)
Daunt, J. G. Recent developments in cryogenics—739(T)
—— (see Silvidi, A. A.)—125
Davidson, Norman and A. E. Larsh, Jr. Conductivity pulses induced in insulating liquids by ionizing radiations—706
DeBenedetti, S., C. E. Cowan, W. R. Konneker, and H. Primakoff. On the angular distribution of two-photon annihilation radiation—205
de Boer, J. (see Gorter, C. J.)—569(L)
DeJuren, James and Norman Knable. Nuclear cross sections for 95-Mev neutrons—606
Dempster, A. J. and A. E. Shaw. Retardation of high velocity ions in gases—746(A)
Denis, P. M. (see Bene, G. J.)—288(L)
Deutsch, Martin and Kai Siegbahn. Internal conversion in Ni^{60}—680
—— **and W. E. Wright.** Lifetimes of excited states of Au^{197}, Fe^{57}, Cd^{111}, Hg^{198}, and Tl^{203}—139(L)
Dexter, D. L. and W. W. Beeman. Multiple diffuse small angle scattering of x-rays—761(A)
Dickson, W. C. Dependence of the F^{19} nuclear resonance position on chemical compound—736(L)
Diesendruck, Leo. Interpretation of the angular distribution of long and short range protons from the $O^{16}(d,p)O^{17}$ reaction—753(A)
Dole, Malcolm, John A. Wethington, Jr., Norman Larson, and W. P. Hettinger, Jr. Some new techniques in the calorimetry of solids—761(A)
Dow, W. G. (see Early, H. C.)—739(T)
Dowling, P. H. (see Brockman, Frank G.)—85
Dressel, Ralph, M. Goldhaber, and A. O. Hanson. Resonance scattering of x-rays by atomic nuclei—754(A)
Duckworth, Henry E. (see Johnson, Howard A.)—424(A)
—— (see Woodcock, Richard F.)—424(A)
Duffield, Robert B. and Lawrence M. Langer. Disintegration of Sn^{125}—743(A)
Duffin, R. J. On wave equation vector-matrices and their spurs—683
DuMond, Jesse W. M. "1947 values" of the atomic constants and the revision of the Faraday constant—411(L)
—— (see Lind, D. A.)—475
Dunlap, W. C., Jr. Mobility of electrons and holes in germanium—759(A)
du Pré, F. K. Non-linear I–V characteristic of Ge at very low temperatures—152(L); Erratum—571(L)
Dyson, F. J. Longitudinal photons in quantum electrodynamics—420(L)

Early, H. C. and W. G. Dow. Supersonic wind at low pressures produced by magnetically driven arc—739(T)
Eggler, C. (see Hughes, D. J.)—726(L)
Eisenstein, A. S. Leaky-condenser oxide-cathode interface—739(T)
Ekstein, H. Relation between *S*-matrix and Hamiltonian—757(A)
—— (see Schiffman, T.)—757(A)
Elliot, J. O. (see Ravilious, C. F.)—851(L)
El-Sabban, M. Zaki, and Forrest F. Cleveland. Raman and infra-red spectra of 1,1,1-trichloroethane—740(A)
Emmons, Howard W. Thermo reaction propagation in flames—572(T)
Emrich, R. J. and C. W. Curtis. Dissipation of a shock traveling in a tube—573(A)
English, W. N. Photon pulses from point-to-plane corona—850(L)
Estermann, I. (see Foner, A.)—759(A)
Evans, R. D. (see Curtiss, L. F.)—142(L)
—— (see Miller, Warren W.)—714(L)
Extermann, C. R. (see Bene, G. J.)—288(L)
Eyges, L. Straggling of electrons near the critical energy. II—81
Eyring, Henry. Relaxation theories of viscous and plastic flows—572(T)

Fairstein, E. (see Borkowski, C. J.)—759(A)
Fairweather, Alan (see Welch, A. J. E.)—403(L)
Fan, C. Y. Note on rotational universe—140(L)
Fan, H. Y. Optical behavior of semiconductors—739(T)
—— (see Becker, M.)—760(A)
Fano, U., H. Hurwitz, Jr., and L. V. Spencer. Penetration and diffusion of x-rays. V. Effect of small deflections upon the asymptotic behavior—425
Farnsworth, H. E. (see Blackmer, L. L.)—826
Faust, W. R. Multiple Compton scattering II—227
Feenberg, Eugene. Interpretation of *ft* values in the Fermi theory of beta-decay—756(A)
—— Nuclear shell models—771
Feld, B. T., I. L. Lebow, and L. S. Osborne. Showers of minimum ionizing particles from cosmic-ray induced nuclear disintegrations in nuclear emulsions—731(L)
Feldman, L. (see Macklin, P.)—137(L)
Ferigle, Salvador M., Forrest F. Cleveland, William M. Boyer, and Richard B. Bernstein. Vibrational spectra and calculated thermodynamic properties of deuterotribromomethane—740(A)
Fernbach, S. (see Bratenahl, A.)—597
Ferretti, B. and S. Gallone. On the nature of the π-meson—153(L)
Fink, Richard W., Frederick L. Reynolds, and D. H. Templeton. Neutron-deficient cesium isotopes—614
Finkelnburg, Wolfgang. Ionization potentials of higher atomic ions—304(L)
—— **and Frank Stern.** Electron screening and ionization potentials of neutral and singly ionized atoms—303(L)
Foner, A. and I. Estermann. Resistivity of germanium samples in external magnetic fields at various temperatures and orientations—759(A)
Forstat, Harold (see Jesse, William P.)—782
Forster, H. H. Evidence for a charged heavy meson—733(L)
Foss, Martin. Pole tips on the Carnegie Institute of Technology cyclotron magnet—758(A)
Fowler, J. L. and J. M. Slye, Jr. $Cu^{63}(n,2n)Cu^{62}$ cross section as a function of neutron energy near the threshold—787
Fowler, R. G., Jack S. Goldstein, R. J. Lee, and B. E. Clotfelter. Radiation transients in brief gas discharges—760(A)
Fowler, William Alfred (see Hall, Robert Noel)—197
Frankel, Sherman. β-γ angular correlation in Au^{198} and Rb^{86}—747(A)
Franzen, W., J. Halpern, and W. E. Stephens. Ionization chamber study of the disintegration of He^3 and N^{14} by thermal neutrons—641
Frauenfelder, H., M. Walter, and W. Zünti. Angular correlation of successive internal conversion electrons—557(L)
Freedman, M., B. Smaller, and J. May. Scintillation studies on potassium iodide—759(A)
Freeman, Joan M. (see Burcham, W. E.)—287(L)
Freier, G. D., E. E. Lampi, and J. H. Williams. Total cross sections of C, O, Mg, Si, and S for neutrons in the energy range 0.6 Mev and 1.8 Mev—748(A)
Freier, Phyllis (see Ney, E. P.)—752(A)
—— **and E. P. Ney.** Multiple production of mesons—337
——, **E. P. Ney, and F. Oppenheimer.** Properties of the heavy primaries—752(A)
Friedman, Lewis (see Miller, Warren W.)—714(L)
Friedman, Raymond and Edward Burke. On the one-dimensional theory of flame structure—574(A)

Fuller, Everett G. Photo-disintegration of deuterium by 4.5- to 20.3-Mev x-rays—752(A)
Fusfeld, Herbert I. and Joseph T. Gilbert. Some physical properties of titanium—302(L)

Gaerttner, E. R. and M. L. Yeater. Cross sections for the photo-disintegration of nitrogen and oxygen nuclei by 100-Mev betatron x-rays—714(L)
—— **and M. L. Yeater.** Photo-disintegration of nitrogen at energies of 20 Mev to 100 Mev—570(L)
Gallone, S. (see Ferretti, B.)—153(L)
Galt, J. K. Coercive force *vs.* temperature in an alloy with zero crystalline magnetic anisotropy—845(L)
—— (see Kittel, C.)—725(L)
Gardner, Eugene (see Smith, F. M.)—562(L)
Gasteiger, E. L. (see Koch, H. W.)—329
George, Waller (see Kauffman, John)—761(A)
Gerjuoy, E. Nuclear saturation for $V-\frac{1}{2}(1+P)J(r,\sigma_1,\sigma_2)$—568(L)
Ghiorso, A. (see Hyde, E. K.)—765
—— (see Levine, C. A.)—296(L)
—— (see Perlman, I.)—26
—— (see Thompson, S. G.)—838(L)
Gibson, R. E. Rockets and ram jets—572(T)
Giese, J. H., F. D. Bennett, and V. E. Bergdolt. Simple interferometric test for conical flow—574(A)
Gilbert, D. A. and A. Roberts. Nuclear and molecular information from the microwave spectrum of FCl—742(A)
Gilbert, Joseph T. (see Fusfeld, Herbert I.)—302(L)
Ginzberg, Arthur S. (see James, Hubert M.)—749(A)
Glendenin, L. E. and C. D. Coryell. Further interpretations of closed-shell perturbations in fission yields—755(A)
Glicksman, M. (see Millar, C. H.)—742(A)
Gold, Louis. Evaluation of the stiffness coefficients for beryllium from ultrasonic measurements in polycrystalline and single crystal specimens—390
Goldberger, M. L. (see Chew, G. F.)—470
Goldfarb, L., H. L. Bradt, and B. Peters. Primary helium flux in cosmic radiation—751(A)
Goldhaber, Gerson. Angular distribution of photo-protons from deuterium—753(A)
Goldhaber, M. (see Dressel, Ralph)—754(A)
—— (see Kubitschek, H. E.)—742(A)
Goldstein, Jack S. (see Fowler, R. G.)—760(A)
Goldstein, L., D. Sweeney, and M. Goldstein. On the theory of slow neutron scattering by liquid helium—319
Goldstein, M. (see Goldstein, L.)—319
Good, W. E. (see Coles, D. K.)—741(A)
Goodrich, M. (see Kelley, G. G.)—138(L)
Gordon, Gary D. (see Van Dyke, Karl S.)—424(A)
Gordy, Walter (see Burkhalter, James H.)—152(L)
—— (see Sheridan, John)—292(L), 719(L)
—— (see Simmons, James W.)—77
Gorter, C. J. and J. de Boer. Phase transition and vapor pressures of liquid mixtures of He^4 and He^3—569(L)
Gossick, B. R. Pd film fast neutron detector—297(L)
Grace, M. A. (see Beghian, L. E.)—286(L)
Gray, W. M. (see Kelly, F. M.)—745(A)
Green, Alex E. S. Multiple meson processes and nucleon recoil—719(L)
—— On generalized meson theories—755(A)
Gregory, B. P., B. Rossi, and J. H. Tinlot. Production of gamma-rays in nuclear interactions of cosmic rays—299(L)
Greisen, Kenneth. Nuclear cross sections of high energy pi-mesons—713(L)
Griffel, Maurice (see Stout, J. W.)—750(A)
Griffith, G. L., M. E. Remley, and P. G. Kruger. Interaction of 12–13-Mev neutrons with deuterons—748(A)
Groetzinger, Gerhart (see Ribe, Fred L.)—760(A)
——, **Martin J. Berger, and Fred L. Ribe.** Study of the multiple scattering of fast charged particles in a gas and its role in the interpretation of cloud-chamber tracks—584
—— **and Gordon W. McClure.** East-west asymmetry of positive and negative mesons—751(A)
—— **and Gordon W. McClure.** East-west asymmetry of positive and of negative mesons and the excess of the positives as a function of zenith angle and altitude—777
Grosskreutz, J. C. and K. B. Mather. Excited states of Be^7—580, 747(A)
Grotdal, T., O. M. Lönsjö, R. Tangen, and I. Bergström. On the reaction $Mg^{24}(p,\gamma)Al^{25}$—296(L)
Gupta, Suraj N. On the calculation of self-energy of particles—294(L)
Gürsey, F. On two-component wave equations—844(L)

Hackman, E. E. (see Snoddy, Leland B.)—572(T)
Hahn, E. L. Nuclear induction due to free Larmor precession—297(L)
—— Spin echoes—746(A)
Halban, H. (see Beghian, L. E.)—286(L)
—— (see Bishop, G. R.)—416(L)
Hall, Robert Noel and William Alfred Fowler. Cross section for the radiative capture of protons by C^{12} near 100 kev—197
Hall, T. A. Note on the $Li^7(p,n)Be^7$ reaction and an excited state of Be^7—411(L)
—— **and S. D. Warshaw.** Penetration of protons in several metals—754(A)
Halpern, J. (see Franzen, W.)—641
—— (see Toms, M. E.)—753(A)
Hamermesh, M. Applications of total reflection of neutrons—140(L)
Hanson, A. O. (see Dressel, Ralph)—754(A)
Harkins, William D. (see Popelka, Martin)—756(A)
—— **and M. Popelka.** Magic numbers and the principle of continuity and regularity of nuclear series—756(A)
Hart, Edward W. (see Christian, Richard S.)—441
Harvalik, Zaboj V. and John H. Bowen. Establishment of mean points of transition between spectral bands—745(A)
Haslam, R. N. H. (see Katz, L.)—289(L)
Hauptman, H. and J. Karle. Structure of atoms from diffraction studies—491
Havens, W. W. (see Tittman, J.)—748(A)
Hayden, Richard J., David C. Hess, Jr., and Mark G. Inghram. Isotopic constitution of erbium and lutecium—299(L)
Haynes, J. R. "Drift mobility" and lifetimes of injected electrons and holes in germanium—739(T)
Hazen, W. E. (see Tiffany, O. L.)—849(L)
Heidenreich, R. D. Theory of the "forbidden" (222) electron reflection in the diamond structure—271
Heller, W. R. Dielectric breakdown in simple non-polar crystals—760(A)
Henkels, Herbert W. Thermoelectric power and mobility of carriers in selenium—734(L)
Hensley, Eugene B. X-ray absorption factors for coated cylinders—744(A)
Hereford, Frank L. Concerning the knock-on secondaries of mesons—751(A)
—— Temperature effects in the spurious discharge mechanism of parallel plate counters—559(L)
Herring, Conyers (see Kittel, C.)—725(L)
—— (see Townes, C. H.)—852(L)
Herzfeld, K. F. Relation of the macroscopic to molecular viewpoint in non-equilibrium processes—572(T)
Hess, David C., Jr. (see Hayden, Richard J.)—299(L)
Hettinger, W. P., Jr. (see Dole, Malcolm)—761(A)
Heydenburg, N. P. (see Hudspeth, Emmett L.)—736(L)
Hibdon, C. T., C. O. Muehlhause, W. Selove, and W. Woolf. Resonance neutron scattering in Na^{23} at 3000 ev—730(L)

Hicks, Bruce L. Extension of the theory of diabatic flow—286(L)
—— Stability and transport characteristics of flames—572(T)
Hicks, Harry G. (see Wilkinson, Geoffrey)—314
Hildebrand, R. H. (see Bratenahl, A.)—597
Hill, R. D. (see Mihelich, J. W.)—743(A)
Hincks, E. P. and B. Pontecorvo. On the disintegration products of the 2.2-μsec. meson—102
Hirschberg, J. G., Jr. and J. E. Mack. Departure of the Lamb shift from the n^{-3} law in He^+—745(A)
Hoffman, Gerald and Edward Akeley. Electron dynamics in a standing wave accelerator—761(A)
Holden, A. N., C. Kittel, F. R. Merritt, and W. A. Yager. Determination of g-values in paramagnetic organic compounds by microwave resonance—147(L)
Hollomon, J. H. Fundamental mechanisms of diffusion in metals—739(T)
Holmes, John R. Isotope shift in the $2p^1S_1-3s^1P_1$ line of carbon—745(A)
Holt, R. B., John M. Richardson, B. Howland, and B. T. McClure. Recombination spectrum and electron density measurements in neon afterglows—239
Holzer, Robert E. Cosmic radiation and the maintenance of a potential gradient in the atmosphere—846(L)
Hopfield, J. J. Absorption spectrum of water vapor between 900 and 2000 angstroms—560(L)
Hopkins, H. H., Jr. Spallation products of arsenic with 190-Mev deuterons—717(L)
Hopkins, John I. Response of the anthracene scintillation counter to monoenergetic electrons—406(L)
Hornbostel, J. (see Curtis, N. W.)—290(L)
Hornig, Donald F. Thickness of the transition region in a shock front—572(T)
Hornyak, W. F. (see Rasmussen, V. K.)—617
—— **and T. Lauritsen.** Beta-decay of B^{12} and Li^8—160
Howard, Raydeen and William V. Smith. Temperature dependence of microwave line widths—840(L)
Howland, B. (see Holt, R. B.)—239
Howland, J. J., Jr. (see Neumann, H. M.)—720(L)
Hsieh, Hsi-teh (see Anslow, Gladys A.)—423(A)
Hu, Ning. On the treatment of quantum electrodynamics without eliminating the logitudinal field—150(L)
Hudspeth, Emmett L., Charles P. Swann, and N. P. Heydenburg. Production of C^{15}—736(L)
Hughes, D. J., M. T. Burgy, and G. R. Ringo. Coherent neutron-proton scattering by liquid mirror reflection—291(L)
——, **C. Eggler, and D. E. Alburger.** β-spectrum of Be^{10}—726(L)
Hughes, R. H. (see Coles, D. K.)—741(A)
Hulburt, H. M. Interchange of translational and vibrational energy in an asymmetric molecular potential field—572(T)
Hult, John L. (see Kundu, D. N.)—71, 743(A)
Hungerford, E. (see Simpson, J. A., Jr.)—847(L)
Hunter, L. P. Physical interpretation of type A transistor characteristics—558(L)
Hurwitz, H., Jr. (see Fano, U.)—425
Hyde, E. K., A. Ghiorso, and G. T. Seaborg. Low mass francium and emanation isotopes of high alpha-stability—765

Inghram, Mark G. (see Hayden, Richard J.)—299(L)
Inglis, D. R. On the low states of Li^7 and Be^7—724(L)
Itoh, Junkichi and Tetsuo Akioka. Ferromagnetic resonance absorption by Mo Permalloy at 2920 mc/sec.—293(L)

Jaffe, Leonard D. Distribution of phases in two-phase solids—762(A)
James, Hubert M. and Arthur S. Ginzberg. Electronic band structure in disordered alloys—749(A)
Jehle, Herbert. Charge conjugation in two component wave equations—757(A)
Jennings, B. (see Allen, A. J.)—752(A)
Jentschke, W. On the α-β and α-K branching of the heaviest natural and artificial radioactive substances—98
Jesse, William P., Harold Forstat, and John Sadauskis. Ionization in argon and in air by single alpha-particles as a function of their energy—782
Johns, H. E. (see Katz, L.)—289(L)
Johnson, E. O. and L. Malter. Double-probe method for measurements in steady and time-varying gas discharges—739(T)
Johnson, Howard A. (see Woodcock, Richard F.)—424(A)
——, **Henry E. Duckworth, Richard S. Preston, and Richard F. Woodcock.** Packing fraction of Pt^{198}—424(A)
Johnson, M. H. and B. A. Lippmann. Relativistic motion in a magnetic field—702
Johnson, V. A. Resistivity at boundaries between crystallites in semiconducting materials—760(A)
Johnson, V. R., M. J. Wilson Laubenstein, and H. T. Richards. Neutrons from $Li^7(p,n)Be^7$—413(L)
Johnson, Virgil (see Sturm, William J.)—752(A)
Johnson, Warren (see Curtiss, L. F.)—142(L)
Jones, J. G. (see Jones, M. W.)—845(L)
Jones, L. C. Pressure broadening and line shift in microwave spectra—741(A)
Jones, M. W. and J. G. Jones. Correlation between ionospheric phenomena and surface pressure—845(L)
Jurkiewicz, L. (see Miesowicz, M.)—380

Kantrowitz, Arthur R. and Robert W. Perry. Preliminary study of a converging shock wave—572(T)
Karle, J. (see Hauptman, H.)—491
Karlovitz, Bela. Investigation of turbulent flames—574(A)
Karplus, Robert and Norman M. Kroll. Fourth-order corrections in quantum electrodynamics and the magnetic moment of the electron—536
Kato, Tosio. Upper and lower bounds of eigenvalues—413(L)
Katz, L., A. S. Penfold, H. J. Moody, R. N. H. Haslam, and H. E. Johns. Determination of the maximum energy of beta-rays from Cu 62 by a new method of analyzing absorption data—289(L)
Kauffman, John and Waller George. Time delays for plastic flowing—761(A)
Kaufman, A. R. Magnetic susceptibility of metals and alloys—423(T)
Kaylor, Hoyt M. (see Talley, Robert M.)—529
Kê, T'ing-Sui. Internal friction of metals at very high temperatures—750(A)
Keepin, George R., Jr. and James H. Roberts. Measurement of fast neutron energies by observation of $Li^6(n,\alpha)H^3$ in photographic emulsions—758(A)
Keim, C. P., H. W. Savage, and Boyd Weaver. Electromagnetic concentration of Be^{10}—414(L)
Keller, H. B. (see Cork, J. M.)—848(L)
Kelley, G. G. and M. Goodrich. Temperature dependence of scintillation pulses in anthracene—138(L)
Kelly, F. M., A. L. Schawlow, W. M. Gray, and M. F. Crawford. Nuclear moments of Mg^{25}—745(A)
Kerst, D. W. (see Price, G. A.)—806
Kessler, K. G. Forbidden lines in the spectra of impure Hg^{198}—559(L)
Ketelle, B. H. and John W. Ruch. Beta-ray distribution of Tc^{99}—565(L)
Kikuchi, C. Nuclear quadrupole effects in solids—746(A)
Kinsey, B. B., G. A. Bartholomew, and W. H. Walker. Neutron capture gamma-rays from Be^9, C^{12}, and N^{14}—723(L)
Kittel, C. (see Holden, A. N.)—147(L)

——, **J. K. Galt, and W. E. Campbell.** Crucial experiment demonstrating single domain property of fine ferromagnetic powders—725(L)
—— **and Conyers Herring.** Effect of exchange interaction on ferromagnetic microwave resonance absorption—725(L)
——, **E. A. Nesbitt, and W. Shockley.** Theory of magnetic properties and nucleation in Alnico V—839(L)
Kivel, B. (see Broyles, A. A.)—839(L)
Klema, E. D. and J. S. Allen. Drift velocities of electrons in argon, nitrogen, and argon-nitrogen mixtures—661
Knable, Norman (see DeJuren, James)—606
Knight, W. D. Effect of electronic paramagnetism on nuclear magnetic resonance frequencies in metals—746(A)
—— (see Townes, C. H.)—852(L)
Koch, H. W. (see Modesitt, G. E.)—175
—— **and R. E. Carter.** Determination of the energy distribution of bremsstrahlung from 19.5-Mev electrons—165
——, **J. McElhinney, and E. L. Gasteiger.** Experimental photo-fission thresholds in $_{92}U^{235}$, $_{92}U^{238}$, $_{92}U^{233}$, $_{94}Pu^{239}$, and $_{90}Th^{232}$—329
Koch, Jørgen and Ebbe Rasmussen. Nuclear spin and isotope shift of xenon investigated with separated isotopes—722(L)
Koehler, James S. (see Neurath, Peter W.)—750(A)
—— (see Salkovitz, Edward I.)—749(A)
—— **and J. W. Marx.** Revised procedure for measuring internal friction—749(A)
Konneker, W. R. (see DeBenedetti, S.)—205
Konopinski, E. J. (see Beiduk, F. M.)—622, 755(A)
—— (see Pruett, J. R.)—628, 755(A)
Korff, S. A. Cosmic radiation and the maintenance of a potential gradient in the atmosphere—144(L)
Koski, Walter S. (see Cohen, Victor W.)—742(A)
Kraybill, H. L. Zenith angle dependence of extensive air showers—410(L)
Kroll, Norman M. (see Karplus, Robert)—536
Kruger, P. G. (see Griffith, G. L.)—748(A)
—— (see Tape, G. F.)—757(A)
Kubitschek, H. E., A. Longacre, and M. Goldhaber. Nuclear gamma-radiation from positron emitters—742(A)
Kundu, D. N., John L. Hult, and M. L. Pool. Assignment and disintegration scheme of the 6.75-hour molybdenum—71
——, **John L. Hult, and M. L. Pool.** Assignment and disintegration scheme of the 6.75-hour molybdenum activity—743(A)
Kurbatov, J. D. (see Thomas, D. G.)—151(L)
Kusch, P. (see Berman, A.)—140(L)
—— (see Mann, A. K.)—427, 435

Lampi, E. E. (see Freier, G. D.)—748(A)
Lamport, J. E. and Forrest F. Cleveland. Raman and infra-red spectra of 2,3-dibromo-2,3-dimethylbutane—740(A)
Landau, L. Concerning W. P. Allis' criticism of my paper on Coulomb interactions in a plasma—567(L)
Landé, Alfred. Interaction between elementary particles. Part II—814
Langer, Lawrence M. Beta-spectra of Cl^{38}—50, 742(A)
—— (see Bruner, J.)—747(A)
—— (see Duffield, Robert B.)—743(A)
—— (see Price, H. C., Jr.)—744(A)
——, **J. W. Motz, and H. C. Price, Jr.** Low energy beta-ray spectra: Pm^{147}, S^{35}—798
Lark-Horovitz, K. and K. W. Meissner. Reflectivity of germanium semiconductors—759(A)
Larsh, A. E., Jr. (see Davidson, Norman)—706
Larson, Norman (see Dole, Malcolm)—761(A)
Laubenstein, M. J. Wilson (see Johnson, V. R.)—413(L)
Laurila, Erkki A. Anomalous dielectric effect of vacuum-sputtered CaF_2 layers—405(L)
Lauritsen, C. C. (see Rasmussen, V. K.)—617
Lauritsen, T. (see Hornyak, W. F.)—160
—— (see Rasmussen, V. K.)—617
Lax, Melvin. Multiple scattering—756(A)
LeBlanc, J. M. (see Cork, J. M.)—843(L)
Lebow, I. L. (see Feld, B. T.)—731 (L)
Lee, D. W. (see Curtis, N. W.)—290(L)
Lee, R. J. (see Fowler, R. G.)—760(A)
Lee, T. D. Note on the coefficient of eddy viscosity in isotropic turbulence—842(L)
Leith, C. E. (see Bratenahl, A.)—597
Leland, Wallace T. Isotopic constitution of scandium, gadolinium, dysprosium, holmium, erbium, and ytterbium—634
Letner, Harold R. Measurement of small curvatures by optical interference—762(A)
Levin, F. K. and J. G. Winans. Band spectrum of GaCl—741(A)
Levine, C. A., A. Ghiorso, and G. T. Seaborg. Half-life for double beta-decay—296(L)
Levinger, J. S. and H. A. Bethe. Dipole transitions in the nuclear photo-effect—756(A)
Li, Yin-Yuan. Erratum: quasi-chemical method in the statistical theory of regular mixtures—300(L)
Lidofsky, L. (see Macklin, P.)—137(L)
Liebowitz, B. Neoclassical approach to blackbody radiation—423(A)
Liebson, S. H. (see Ravilious, C. F.)—851(L)
Lind, D. A., W. J. West, and J. W. M. DuMond. X-ray and gamma-ray reflection properties from 500 x units to nine x units of unstressed and of bent quartz plates for use in the two-meter curved-crystal focusing gamma-ray spectrometer—475
Lippmann, B. A. (see Johnson, M. H.)—702
Little, Edward M. Some circular schlieren pictures of shock wave reflections—573(A)
Lloyd, Stuart P. Elimination of the self-electromagnetic field—757(A)
Lomont, J. S. (see Belinfante, F. J.)—757(A)
Longacre, A. (see Alvarez, L. W.)—752(A)
—— (see Kubitschek, H. E.)—742(A)
Longmire, Conrad (see Bethe, H. A.)—647
Lönsjö, O. M. (see Grotdal, T.)—296(L)
Lord, J. J. and Marcel Schein. Nuclear disintegrations as detected with electron-sensitive emulsions exposed in the stratosphere—19
Lovati, A., A. Mura, G. Salvini, and G. Tagliaferri. Mean free path of the particles produced in nuclear explosions and comparison between explosions in C and Pb—284
Low, Francis. On the effects of internal nuclear motion on the hyperfine structure of deuterium—361
Lu, Hoff. Note on nuclear models—416(L)

Mack, J. E. Forbidden *s-ns* lines in alkali metal atomic absorption spectra—745(A)
—— (see Hirschberg, J. G., Jr.)—745(A)
Mackenzie, J. K. and E. H. Sondheimer. Theory of the change in the conductivity of metals produced by cold work—264
Macklin, P., L. Feldman, L. Lidofsky, and C. S. Wu. Beta-spectrum of Ca^{45}—137(L)
Madigan, John R., Forrest F. Cleveland, William M. Boyer, and Richard B. Bernstein. Vibrational spectra and calculated thermodynamic properties of deuterotrichloromethane—740(A)
Madison, T. C. (see Bragg, J. K.)—148(L), 571(L)
—— (see Sharbaugh, A. H.)—302(L)
Maienschein, Fred C. (see Mitchell, Allan C. G.)—744(A)
Mallary, E. C. and M. L. Pool. Assignment and characteristic radiations of the 14-day tin activity—75
—— **and M. L. Pool.** 14-day tin 117—743(A)
Malter, L. (see Johnson, E. O.)—739(T)
Mandeville, C. E. (see Whitehead, W. D.)—732(L)

—— **and E. Shapiro.** Investigation of the disintegration schemes of Ru^{103} and Rb^{86}—439
Mann, A. K. (see Berman, A.)—140(L)
—— **and P. Kusch.** Further data on the spin gyromagnetic ratio of the electron—435
—— **and P. Kusch.** Hyperfine structure of the stable isotopes of indium—427
Maple, E. (see Singer, S. F.)—398(L)
Marcus, Jules A. Magnetic properties of zinc alloys at low temperatures—750(A)
Marmier, P. (see Boehm, F.)—295(L)
Martin, B. (see ter Haar, D.)—721(L)
Martin, D. H. (see Smith, R. V.)—752(A)
Martinelli, E. A. and W. K. H. Panofsky. Lifetime of the positive π-meson—465
Marx, J. W. (see Koehler, J. S.)—749(A)
—— **and D. A. Patterson.** Effects of etching, annealing, and threshold deformation on the internal friction of copper—749(A)
Massalski, J. M. (see Miesowicz, M.)—380
Mather, K. B. (see Grosskreutz, J. C.)—580, 747(A)
May, Albert and Jean C. Woodhull. Virtual mass of a sphere entering water vertically—573(A)
May, J. (see Freedman, M.)—759(A)
McClure, B. T. (see Holt, R. B.)—239
McClure, Gordon W. (see Groetzinger, Gerhart)—751(A), 777
McElhinney, J. (see Koch, H. W.)—329
McGowan, F. K. 7×10^{-9} sec. isomeric state in $_{79}Au^{197}$—138(L)
McKay, A. S. (see Brown, W. W.)—342
McKay, Kenneth G. Electron bombardment conductivity in diamond—Part II—816
McKeehan, L. W. Literature of ferromagnetism—423(T)
McMurtrie, G. E. and D. P. Crawford. Thermal neutron-capture cross section of A^{36}—840(L)
McNally, J. Rand, Jr. On the classification of the spectrum of singly-ionized uranium—417(L)
Mei, J. Y. (see Mitchell, Allan C. G.)—744(A)
Meissner, K. W. (see Lark-Horovitz, K.)—759(A)
Meister, Arnold G. (see Carney, Rose A.)—740(A)
—— (see Zietlow, James P.)—739(A)
Merritt, F. R. (see Holden, A. N.)—147(L)
Miesowicz, M., L. Jurkiewicz, and J. M. Massalski. On some low ionizing radiation observed by measurements of cosmic radiation at great depths—380
Mihelich, J. W. and R. D. Hill. Radiations from long-lived tin isotopes—743(A)
Millar, C. H., A. G. W. Cameron, and M. Glicksman. γ-rays from N^{16}—742(A)
Miller, E. E. and C. B. Tanner. Direction-of-fall of sedimenting particles—761(A)
Miller, W. C., B. Waldman, J. C. Noyes, and J. E. Van Hoomissen. Voltage stabilizer for electrostatic generator—758(A)
Miller, Warren W., Robert Ballentine, William Bernstein, Lewis Friedman, A. O. Nier, and R. D. Evans. Half-life of carbon fourteen and a comparison of gas phase counter methods.—714(L)
Mingins, Charles R., Carl A. Stevens, and Robert W. Perry. Characteristics of piezoids with surfaces of cylindrical shape—762(A)
Mishra, B. Lifetimes of mercury and potassium atoms in excited states—153(L)
Mitchell, Allan C. G., J. Y. Mei, Fred C. Maienschein, and Charles L. Peacock. Disintegration of I^{124} and I^{126}—744(A)
Mizushima, Masataka. Erratum: a theory of pressure absorption—149(L)
—— On the infra-red absorption of the hydrogen molecules—150(L)
Modesitt, G. E. and H. W. Koch. Nuclear impulse in electron pair creation—175
Moffat, D. (see Bruner, J.)—747(A)
Mohr, E. I. (see Weissler, G. L.)—741(A)
Molière, G. Lateral distribution of photons in extensive air showers—715(L)
Molner, S. (see Simpson, J. A.)—751(A)
Montague, J. H. (see Allison, S. K.)—754(A)
Montroll, Elliott W. Recent advances in non-equilibrium statistical mechanics—572(T)
Moody, H. J. (see Katz, L.)—289(L)
Moore, Donald C. and Willard A. Reenstra. On the use of coaxial lines to produce and measure short time delays—761(A)
Moore, George E. and H. W. Allison. Thermionic emission of thin films of alkaline earth oxide deposited by evaporation—246
Mooring, F. P. (see Bashkin, S.)—748(A)
Morrish, A. H. (see Allison, S. K.)—754(A)
Motz, J. W. (see Langer, L. M.)—798
—— (see Price, H. C., Jr.)—744(A)
Moulton, W. G. and C. W. Sherwin. Fast neutron detector—758(A)
Moyer, B. J. (see Bjorklund, R.)—213
—— (see Bratenahl, A.)—597
Mrozowski, S. Electric resistivity of polycrystalline graphite and carbons—838(L)
Muehlhause, C. O. Resonance neutron scattering—739(T)
—— (see Hibdon, C. T.)—730(L)
Mura, A. (see Lovati, A.)—284

Naumann, R. A., F. L. Reynolds, and I. Perlman. Mass spectrographic identification of radioactive lanthanum isotopes—398(L)
Nechaj, J. F. (see Allen, A. J.)—752(A)
Nelson, M. E. and M. L. Pool. Reaction leading to Fe^{53}, Mn^{57}, and Cr^{55}—682
Nesbitt, E. A. (see Kittel, C.)—839(L)
Neumann, H. M., J. J. Howland, Jr., and I. Perlman. Possible isomeric state of RaE—720(L)
Neurath, Peter W. and J. S. Koehler. Creep of pure copper and lead single crystals—750(A)
Newell, G. F. Electric quadrupole moment of the deuteron—141(L)
Newkirk, John B. and R. Smoluchowski. Diffraction effects observed in partially ordered CoPt crystals—749(A)
Ney, E. P. (see Freier, Phyllis)—337, 752(A)
—— **and Phyllis Freier.** Multiple production of mesons—752(A)
Nicholls, R. W. Intensity distribution of the second positive ($C^3\pi\rightarrow B^3\pi$) band system of molecular nitrogen—421(L)
Nicks, P. F. (see Welch, A. J. E.)—403(L)
Nielsen, Alvin H. (see Talley, Robert M.)—529
Nielsen, Harald H. *l*-type doubling in polatomic molecules and its application to the microwave spectrum of methyl cyanide and methyl iso-cyanide—130
Nier, Alfred O. Redetermination of the relative abundances of the isotopes of carbon, nitrogen, oxygen, argon, and potassium—789
—— (see Miller, Warren W.)—714(L)
—— (see Roberts, T. R.)—746(A)
—— (see Winn, E. B.)—746(A)
Norton, James F. Response of an anthracene counter to monoenergetic electrons of energies 1.4, 2.2, and 2.6 Mev—759(A)
Novey, T. B. Ra DEF standard sources for beta-disintegration rate determinations—742(A)
Nowick, A. S. Measurement of the activation energy for motion of dislocations in single crystals of copper—750(A)
Noyes, J. C. (see Miller, W. C.)—758(A)

Ogren, V. G. (see Alvarez, L. W.)—752(A)
Oppenheimer, F. (see Freier, Phyllis)—752(A)
Osborne, D. W. (see Weinstock, B.)—400(L)
Osborne, L. S. (see Feld, B. T.)—731(L)
Owen, George E. and C. Sharp Cook. Shape of the positron spectrum of Cu^{61}—743(A)

Pai, S. I. (see Bershader, D.)—574(A)
Panofsky, W. K. H. (see Martinelli, E. A.)—465
Patterson, D. A. (see Marx, J. W.)—749(A)
Peacock, Charles L. (see Mitchell, Allan C. G.)—744(A)
Peakes, Bayard P. New theory of electricity—424(A)
Pearson, G. L. and J. Bardeen. Erratum: electrical properties of pure silicon and silicon alloys—303(L)
——, **J. D. Struthers, and H. C. Theurer.** Correlation of Geiger counter and Hall effect measurements in alloys containing germanium and radioactive antimony 124—809
Pendleton, Edward A. (see Van Dyke, Karl S.)—424(A)
Penfold, A. S. (see Katz, L.)—289(L)
Penndorf, Rudolf. Distribution of atomic and molecular oxygen in the upper atmosphere—561(L)
Perez-Mendez, V. and H. Brown. Beta-spectrum of He^6—404(L)
Perlman, I. (see Naumann, R. A.)—398(L)
—— (see Neumann, H. M.)—720(L)
——, **A. Ghiorso, and G. T. Seaborg.** Systematics of alpha-radioactivity—26
Perry, Robert W. (see Kantrowitz, Arthur R.)—572(T)
—— (see Mingins, Charles R.)—762(A)
Peters, B. (see Bradt, H. L.)—54
—— (see Goldfarb, L.)—751(A)
Peterson, R. E. Total fast neutron cross section of potassium—747(A)
—— (see Bashkin, S.)—748(A)
Petree, B. (see Bashkin, S.)—748(A)
Petrie, W. Near infra-red spectrum of the polar aurora—720(L)
Pfann, W. G. (see Bardeen, J.)—401(L)
Piccioni, O. Local production of mesons at 11,300 feet—1
—— On the secondary particles of local penetrating showers—6
Pietenpol, W. J., J. D. Rogers, and Dudley Williams. Microwave spectrum of nitrosyl chloride—741(A)
Polachek, H. (see Rawling, G.)—572(A)
Pomerance, H. Thermal-neutron capture cross sections of sixty-eight elements—747(A)
Pomerantz, M. A. Increase in the primary cosmic-ray intensity at high latitudes, and the non-existence of detectable permanent solar magnetic field—830
Pontecorvo, B. (see Hincks, E. P.)—102
Pool, M. L. (see Anderson, D. L.)—142(L)
—— (see Kundu, D. N.)—71, 743(A)
—— (see Mallary, E. C.)—75, 743(A)
—— (see Nelson, M. E.)—682
—— (see Robertson, B. E.)—747(A)
Popelka, Martin (see Harkins, William D.)—756(A)
—— **and William D. Harkins.** Principle of continuity as related to the existence of stable even N-odd P and odd N-even P nuclei—756(A)
Powell, Wilson M. (see Tracy, James)—594
Preiswerk, P. (see Boehm, F.)—295(L)
Present, R. D. Nuclear dipole vibrations and the surface symmetry energy—355
Preston, G. (see Beghian, L. E.)—286(L)
Preston, Richard S. (see Johnson, Howard A.)—424(A)
—— (see Woodcock, Richard F.)—424(A)
Price, G. A. and D. W. Kerst. Yields and angular distributions of some gamma-neutron process—806
Price, H. C., Jr. (see Langer, L. M.)—798
——, **J. Motz, and L. M. Langer.** Low energy beta-ray spectra: Pm^{147}, S^{35}—744(A)
Primakoff, H. (see DeBenedetti, S.)—205
Pringle, R. W., S. Standil, and K. I. Roulston. Recoil electron spectrum of the K^{40} gamma-ray—841(L)
Pringsheim, P. Stability of color centers in alkali-halide crystals—739(T)
Pritchard, B. S. (see Sharbaugh, A. H.)—302(L)
Proctor, W. G. and F. C. Yu. Dependence of a nuclear magnetic resonance frequency upon chemical compound—717(L)
—— **and F. C. Yu.** On the magnetic moments of Mn^{55}, Co^{59}, Cl^{37}, N^{15}, and N^{14}—716(L)
Pruett, J. R. (see Beiduk, F. M.)—622, 755(A)
——, **F. M. Beiduk, and E. J. Konopinski.** Theory of the D+D reactions. Part II. Relation to the internucleonic forces—628, 755(A)
Pryce, M. H. L. Optical detection of radiofrequency resonance—136(L)

Rainwater, J. (see Tittman, J.)—748(A)
Rall, Waldo and R. G. Wilkinson. Efficiencies of calcium tungstate and calcium fluoride as scintillators for low energy electrons—758(A)
Ramsey, Norman F. Internal diamagnetic field correction in measurements of the proton magnetic moment—567(L)
Rasmussen, Ebbe (see Koch, Jørgen)—722(L)
Rasmussen, V. K., W. F. Hornyak, C. C. Lauritsen, and T. Lauritsen. Nuclear pairs and gamma-radiation from excited states of O^{16}—617
Rathgeber, H. D. Zenith angle variation of the latitude effect of cosmic rays—566(L)
Ravilious, C. F., J. O. Elliot, and S. H. Liebson. Gamma-scintillations in diphenylacetylene—851(L)
Rawling, G. and H. Polachek. On the three-shock configuration—572(A)
Reenstra, Willard A. (see Moore, Donald C.)—761(A)
Reitz, John R. Effect of screening on beta-ray spectra and internal conversion—10
Remley, M. (see Griffith, G. L.)—748(A)
Reynolds, Frederick L. (see Fink, Richard W.)—614
—— (see Naumann, R. A.)—398(L)
Ribe, Fred L. (see Groetzinger, Gerhart)—584
——, **Martin J. Berger, and Gerhart Groetzinger.** Multiple scattering of electrons in argon—760(A)
Rice, O. K. Effect of He^3 on the λ-point of He^4—142(L)
Richards, H. T. (see Browne, C. P.)—754(A)
—— (see Johnson, V. R.)—413(L)
—— **and R. V. Smith.** P-N thresholds for calibration points on the nuclear high voltage scale—752(A)
Richardson, John M. General theory of irreversible processes—572(T)
—— (see Holt, R. B.)—239
Ridenour, L. A. High speed digital computers: an elementary survey of present developments and future trends—739(T)
Ringo, G. R. (see Hughes, D. J.)—291(L)
Roaf, D. (see Sanders, J. H.)—754(A)
Roberts, Arthur. Recent work on microwave spectroscopy at the State University of Iowa—739(T)
—— (see Gilbert, D. A.)—742(A)
Roberts, F. F. (see Welch, A. J. E.)—403(L)
Roberts, James H. (see Keepin, George R., Jr.)—758(A)
Roberts, K. V. Field dynamics. I. Classical—146(L)
—— Field dynamics. II. Quantum—146(L)
Roberts, Shepard. Theory of dielectric polarization in alkali-halide crystals—258
Roberts, T. R. and Alfred O. Nier. Atomic mass determinations with a mass spectrometer—746(A)
Robertson, B. E., W. L. Carss, and M. L. Pool. 9.0-minute La^{136}—747(A)
Robson, J. M. Radioactive decay of the neutron—747(A)
Rogers, F. T., Jr. (see Cooper, E. P.)—402(L)
Rogers, J. D. (see Pietenpol, W. J.)—741(A)

Rohrlich, F. Self-stress of the electron—357
Ross, A. M. (see Coryell, C. D.)—755(A)
Rossi, B. (see Gregory, B. P.)—299(L)
Rothstein, Jerome. Extraction of ions from solids by electrons in high fields—744(A)
Roulston, K. I. (see Pringle, R. W.)—841(L)
Ruch, John W. (see Ketelle, B. H.)—565(L)
Ruderman, I. W. (see Bendt, P. J.)—575
Rutledge, W. C. (see Cork, J. M.)—843(L), 848(L)

Sadauskis, John (see Jesse, William P.)—782
Sailor, Vance L. Nuclear energy levels in isotopes of potassium—794
Sakakura, A. Y. (see Coryell, C. D.)—755(A)
Salant, E. O. (see Curtis, N. W.)—290(L)
Salkovitz, Edward I. and James S. Koehler. Energy absorbed in twinning single crystals of zinc—749(A)
Salvini, G. (see Lovati, A.)—284
Sanders, J. H., J. Moffatt, and D. Roaf. Low energy cross section and angular distribution of the D(d,p) reaction—754(A)
Sands, Matthew. Low energy mesons in the atmosphere—180
Savage, H. W. (see Keim, C. P.)—414(L)
Saxon, D. (see Burson, S. B.)—403(L)
Schaefer, Vincent J. Confirmation of the Workman-Reynolds effect—721(L)
Schawlow, A. L. (see Kelly, F. M.)—745(A)
Schein, Marcel (see Lord, J. J.)—19
Schiffman, T. and H. Ekstein. Free vibrations of an isotropic cube—757(A)
Schulz, L. G. Growth of alkali halide crystals from the vapor phase onto substrates of mica—750(A)
Schwartz, R. N. Vibrational relaxation times in polyatomic gases—572(A)
Seaborg, Glenn T. (see Curtiss, L. F.)—142(L)
—— (see Hyde, E. K.)—765
—— (see Levine, C. A.)—296(L)
—— (see Perlman, I.)—26
—— (see Thompson, S. G.)—838(L)
Secrest, L. Functions used in Flügge's method of predicting approximate spatial neutron distributions—141(L)
Seigel, A. E. Oscillations of a cable in a stream—573(A)
Selove, W. 5-ev neutron resonance in Ag—557(L)
—— (see Hibdon, C. T.)—730(L)
Shaknov, I. (see Wu, C. S.)—136(L)
Shapiro, E. (see Mandeville, C. E.)—439
Sharbaugh, A. H. (see Bragg, J. K.)—148(L), 571(L)
——, **B. S. Pritchard, and T. C. Madison.** Microwave spectrum of CF_3Br—302(L)
Shaw, A. E. (see Dempster, A. J.)—746(A)
Sheer, C. (see Tittman, J.)—748(A)
Sheridan, John and Walter Gordy. Interatomic distances in CF_3Br, CF_3I, and CF_3CN—292(L)
—— **and Walter Gordy.** Microwave spectra and molecular constants of trifluorosilane derivatives. SiF_3H, SiF_3CH_3, SiF_3Cl, and SiF_3Br—719(L)
Sherwin, C. W. (see Moulton, W. G.)—758(A)
Shockley, W. (see Kittel, C.)—839(L)
—— **and J. Bardeen.** Energy bands and mobilities in monatomic semiconductors—407(L)
Shull, C. G. Neutron diffraction and magnetic crystallography—739(T)
Shulman, R. G. and C. H. Townes. Molecular dipole moments and Stark effects. I. Stark effects in OCS—500
—— **and C. H. Townes.** New types of microwave transitions involving l-type doubling in OCS and HCN—421(L)
Siegbahn, Kai. Disintegration of Ag^{110}—233
—— (see Deutsch, Martin)—680
Silvidi, A. A. and J. G. Daunt. Electronic specific heats in tungsten and zinc—125
Simmons, James W., Wallace E. Anderson, and Walter Gordy. Microwave spectrum and molecular constants of hydrogen cyanide—77
Šimon, I. Surface impedance of superconducting tin, mercury, and lead at 9200 Mc/sec.—384
Simpson, J. A., Jr., H. W. Baldwin, and S. Molner. Neutron production in elements at high altitudes—751(A)
—— **and E. Hungerford.** Production of nuclear disintegrations and neutrons at the geomagnetic equator—847(L)
Singer, S. F. On the nature of the cosmic radiation near the Pfotzer maximum at $\lambda = 41°N$—730(L)
—— Zenith angle dependence of the cosmic radiation above the atmosphere at $\lambda = 41°N$—729(L)
——, **E. Maple, and W. A. Bowen, Jr.** Measurement of the earth's magnetic field at high altitudes at White Sands, New Mexico—398(L)
Slawsky, M. M. (see Bay, Z.)—414(L)
Slye, J. M., Jr. (see Fowler, J. L.)—787
Smakula, Alexander. Color centers in calcium fluoride and barium fluoride crystals—408(L)
Smaller, B. (see Freedman, M.)—759(A)
Smith, C. E. (see Aldrich, L. T.)—744(A)
Smith, D. F., M. Tidwell, and V. D. P. Williams. Microwave spectrum of bromine monofluoride—420(L)
Smith, Frances M. (see Bradner, Hugh)—462
——, **Eugene Gardner, and Hugh Bradner.** Mesons produced by neutrons from the cyclotron—562(L)
Smith, Philip B. and James S. Allen. Investigation of momentum relations in the decay of Be^7—747(A)
Smith, R. V. (see Browne, C. P.)—754(A)
—— (see Richards, H. T.)—752(A)
—— **and D. H. Martin.** Deuterium (p,n) threshold and the deuteron binding energy—752(A)
Smith, William V. (see Burkhalter, James H.)—152(L)
—— (see Howard, Raydeen)—840(L)
Smoluchowski, R. (see Newkirk, John B.)—749(A)
Snoddy, Leland B., E. E. Hackman, and J. W. Beams. Combustion in long closed tubes at low pressure—572(T)
Snyder, James N. Processes involving vector mesons—143(L)
Sondheimer, E. H. (see Mackenzie, J. K.)—264
Spencer, L. V. (see Fano, U.)—425
Stabler, H. P. Utilization of a cathode-ray tube and photo-cell to synthesize integral d.c. voltages from a sequence of pulses—423(A)
Standil, S. (see Pringle, R. W.)—841(L)
Stehn, J. R. (see Bethe, H. A.)—370
Steneck, Walter G. (see Brockman, Frank G.)—85
Stephens, W. E. (see Franzen, W.)—641
—— (see Toms, M. E.)—753(A)
Stern, Frank (see Finkelnburg, Wolfgang)—303(L)
Stevens, Carl A. (see Mingins, Charles R.)—762(A)
Stever, H. Guyford. Modification of the theory of kinetics of condensation and its application to air condensation in hypersonic wind tunnels—573(A)
Stewart, Ellen S. (see Stewart, James L.)—143(L)
Stewart, James L. and Ellen S. Stewart. Ultrasonic interferometry for low acoustic impedance—143(L)
Stoddard, A. E. (see Cork, J. M.)—843(L), 848(L)
Stout, J. W. and Maurice Griffel. Paramagnetic anisotropy of manganous fluoride—750(A)
Stout, Virgil L. Luminescence of barium oxide—744(A)
Stratton, William R. (see Bailey, Carl L.)—194
Struthers, J. D. (see Pearson, G. L.)—809
Sturm, William J. and Virgil Johnson. Comparison of several nuclear absolute voltage determinations—752(A)
Sun, K. H. (see Allen, A. J.)—752(A)
Swan, P. Proton-proton scattering and the triplet range of nuclear force—288(L)
Swann, Charles P. (see Hudspeth, Emmett L.)—736(L)
Sweeney, D. (see Goldstein, L.)—319

Tagliaferri, G. (see Lovati, A.)—284
Talley, Robert M., Hoyt M. Kaylor, and Alvin H. Nielsen. Infra-red spectrum and molecular constants of HF and DF—529
Tangen, R. (see Grotdal, T.)—296(L)
Tanyel, Besim. Improvement effect of the plateau in xylene- and argon-filled Geiger counters—843(L)
Tamor, Stephen. Fast protons from the absorption of π^--mesons by nuclei—412(L)
Tanner, C. B. (see Miller, E. E.)—761(A)
Tape, G. F. and P. G. Kruger. Illinois cyclotron oscillator—757(A)
Taylor, William J. Electrostatic potential energy of crystals and molecules from x-ray and electron diffraction data—763(A)
—— Thermodynamic functions of crystals from the moments of the frequency distribution—762(A)
Teichmann, T. Some general properties of nuclear reaction and scattering cross sections—506
Templeton, D. H. (see Fink, Richard W.)—614
ter Haar, D. and B. Martin. Statistics of the three-dimensional ferromagnet—721(L)
Ter-Pogossian, Michel. On the disintegration of Sr^{85}—743(A)
Terrall, John R. On the motion of particles in a traveling wave linear accelerator—415(L)
Theurer, H. C. (see Pearson, G. L.)—809
Thirring, W. Regularization as a consequence of higher order equations—570(L)
Thomas, D. G. and J. D. Kurbatov. Search for photons emitted by long-life species of nickel—151(L)
Thomas, R. E. (see Alvarez, L. W.)—752(A)
Thompson, S. G., A. Ghiorso, and G. T. Seaborg. Element 97—838(L)
Thulin, S. (see Bergström, I.)—851(L)
Thurston, P. A. Photographic observations of air flow around moving bodies at Mach numbers up to 9.6—573(A)
Tidwell, M. (see Smith, D. F.)—420(L)
Tiffany, O. L. and W. E. Hazen. Cloud-chamber study of cosmic rays underground—849(L)
Tinlot, J. H. (see Gregory, B. P.)—299(L)
Tittman, J., C. Sheer, J. Rainwater, and W. W. Havens. Neutron scattering in the resonance region—748(A)
Toms, M. E., J. Halpern, and W. E. Stephens. Angular distribution of photo-protons from magnesium—753(A)
Townes, C. H. (see Shulman, R. G.)—421(L), 500
——, **Conyers Herring, and W. D. Knight.** Effect of electronic paramagnetism on nuclear magnetic resonance frequencies in metals—852(L)
—— **and J. Turkevich.** Hyperfine structure and exchange narrowing of paramagnetic resonance—148(L)
Toyoda, T. Relativistic nuclear force—853(L)
Tracy, James and Wilson M. Powell. Star fragments in oxygen and helium under bombardment by 90-Mev neutrons—594
Trigg, George L. Evaluation of $f_+(Z,W_2)$ in the Fermi theory of beta-decay—756(A)
Truesdell, C. A. Bernoulli's theorem for viscous compressible fluids—535
—— On the heat flux vector in moderately rarefied gases—572(T)
Turkevich, J. (see Townes, C. H.)—148(L)

Vallarta, M. S. On the energy spectrum of heavy nuclei in primary cosmic radiation—419(L)
Van Dyke, Karl S., Edward A. Pendleton, and Gary D. Gordon. Equivalent circuit of partially plated thickness-shear piezoelectric resonators—424(A)
Van Hoomissen, J. E. (see Miller, W. C.)—758(A)
Venkateswarlu, Putcha. On the emission bands of CCl—79
—— On the emission bands of CF_2—676

Waldman, B. (see Miller, W. C.)—758(A)
Walker, L. R. Electromagnetic propagation in ion streams—739(T)
Walker, W. H. (see Kinsey, B. B.)—723(L)
Walker, William D. Study of penetrating showers at 3260 meters—686
Walter, M. (see Frauenfelder, H.)—557(L)
Ward, J. C. Scattering of light by light—293(L)
Warshaw, S. D. (see Hall, T. A.)—754(A)
Watanabe, K. Thermoluminescence of calcium sulfate: Mn phosphor—748(A)
Weaver, Boyd (see Bell, P. R.)—399(L)
—— (see Keim, C. P.)—414(L)
Weber, A. H. Photoelectric emission in strong fields: a progress report—739(T)
Weinstock, B., D. W. Osborne, and B. M. Abraham. Phase relations in He^3-He^4 solutions—400(L)
Weisskopf, V. F. (see Bohr, Aage)—94
—— (see Conwell, E.)—388
Weissler, G. L. and E. I. Mohr. Absolute absorption coefficients in N_2 in the vacuum ultraviolet—741(A)
Welch, A. J. E., P. F. Nicks, Alan Fairweather, and F. F. Roberts. Natural ferromagnetic resonance—403(L)
Wentink, T., Jr. (see Cohen, Victor W.)—742(A)
West, W. J. (see Lind, D. A.)—475
Wethington, John A., Jr. (see Dole, Malcolm)—761(A)
Weyl, Hermann. Remark on the coupling of gravitation and electron—699
Whitehead, W. D. and C. E. Mandeville. Neutrons from the disintegration of beryllium by deuterons.—732(L)
Wightman, A. S. Moderation of negative mesons in hydrogen I: moderation from high energies to capture by an H_2 molecule—521
Wigner, Eugene P. Do the equations of motion determine the quantum-mechanical commutation relations?—711
Wilkinson, Geoffrey and Harry G. Hicks. Neutron deficient radioactive isotopes of rhenium—314
Wilkinson, R. G. (see Rall, Waldo)—758(A)
Willardson, R. K., A. C. Damask, and G. C. Danielson. Space-charge effects in diamond conduction counters—758(A)
—— **and G. C. Danielson.** Effect of light on a diamond conduction counter—300(L)
Williams, D. V. P. (see Smith, D. F.)—420(L)
Williams, Dudley (see Pietenpol, W. J.)—741(A)
Williams, J. H. (see Freier, G. D.)—748(A)
Wilson, H. A. Spherical shell nuclear model—516
Wilson, Richard (see Bishop, G. R.)—416(L)
Winans, J. G. Glow-to-arc transition—739(T)
—— (see Levin, F. K.)—741(A)
Winkler, Eva. Density measurements in supersonic flow by an x-ray technique—574(A)
Winn, E. B. and Alfred O. Nier. Simplified emission regulator for mass spectrometer ion sources—746(A)
Woodcock, Richard F. (see Johnson, Howard A.)—424(A)
——, **Henry E. Duckworth, Richard S. Preston, and Howard A. Johnson.** Packing fractions of W^{183} and W^{186}—424(A)
Woodhull, Jean C. (see May, Albert)—573(A)
Woolf, W. (see Hibdon, C. T.)—730(L)
Wright, S. Courtenay. Production of Li^8 from various gases—742(A)
Wright, W. E. (see Deutsch, Martin)—139(L)
Wu, C. S. (see Macklin, P.)—137(L)
—— **and I. Shaknov.** Angular correlation of scattered annihilation radiation—136(L)

Yager, W. A. (see Holden, A. N.)—147(L)
Yamamoto, Mikio. On elastic constants of nickel crystals—566(L)
Yang, C. N. Possible experimental determination of whether the neutral meson is scalar or pseudoscalar—722(L)
—— Selection rules for the dematerialization of a particles into two photons—242
Yearian, H. J. (see Bray, R.)—760(A)
Yeater, M. L. (see Gaerttner, E. R.)—570(L), 714(L)
York, H. F. (see Bjorklund, R.)—213
Yu, F. C. (see Proctor, W. G.)—716(L), 717(L)
Yuan, Luke C. L. Neutron density in the free atmosphere up to 100,000 feet—728(L)
Yukawa, Hideki. Quantum theory of non-local fields. Part I. Free fields—219
—— *S*-matrix in non-local field theory—849(L)

Zietlow, James P., Forrest F. Cleveland, and Arnold G. Meister. Raman spectrum and force constants for fluorotrichloromethane—739(A)
Zünti, W. (see Frauenfelder, H.)—557(L)

PHYSICAL REVIEW VOLUME 77, NUMBER 6 MARCH 15, 1950

Analytic Subject Index to Volume 77

References with (A) are to abstracts of papers presented at meetings of the American Physical Society. References with (L) are to Letters to the Editor.

Absorption of radiation
Infra-red in Si, H. B. Briggs—727(L)
Infra-red transmission of Ge and Si, M. Becker and H. Y. Fan—760(A)
In N_2, vacuum ultraviolet, G. L. Weisler and E. I. Mohr—741(A)
By water vapor in near infra-red, Robert M. Chapman—741(A)
Alloys (see **Crystalline states**)
Annihilation radiation (see **Radiation**)
Astrophysics
Infra-red spectrum of polar aurora, W. Petrie—720(L)
Oxygen in upper atmosphere, Rudolf Penndorf—561(L)
Atmospheric electricity (see **Meteorology**)
Atomic structure (see also **Energy states of atoms; Spectra**)
From diffraction studies, H. Hauptman and J. Karle—491
Electron screening, ionization potentials, Wolfgang Finkelnburg and Frank Stern—303(L)
Aurora
Oxygen in upper atmosphere, Rudolf Penndorf—561(L)

Biophysics
Color assignment, wave-length ranges, Zaboj V. Harvalik and John H. Bowel—745(A)
Electron-beam tumor therapy, W. H. Bostick—564(L)
Fast neutron detector, W. G. Moulton and C. W. Sherwin—758(A)
Bremsstrahlung (see **Radiation**)
Broadening of spectral lines
Microwave line widths, temperature dependence, Raydeen Howard and William V. Smith—840(L)
In microwave spectra, L. C. Jones—741(A)

Conductivity, electrical (see **Electrical conductivity; Discharge of electricity in gases**)
Constants, physical standards
Faraday constant, Jesse W. M. DuMond—411(L)
Cosmic radiation
Asymmetry of positive and negative mesons, Gerhart Groetzinger and Gordon W. McClure—777
Charged heavy meson, H. H. Forster—733(L)
Disintegrations at geomagnetic equator, J. A. Simpson, Jr. and E. Hungerford—847(L)
Disintegrations in emulsions in stratosphere, J. J. Lord and Marcel Schein—19
Distribution of photons in showers, G. Molière—715(L)
East-west asymmetry, Gerhart Groetzinger and Gordon W. McClure—751(A)
Gamma-rays, neutral meson decay, B. P. Gregory, B. Rossi, and J. H. Tinlot—299(L)
Heavy nuclei, H. L. Bradt and B. Peters—54
Heavy nuclei, energy spectrum, M. S. Vallarta—419(L)
Heavy primaries, Phyllis Freier, E. P. Ney, and F. Oppenheimer—752(A)
Interactions at 3260 meters, W. W. Brown and A. S. McKay—342
Knock-on secondaries of mesons, Frank L. Hereford—559(A)
Low ionizing radiation at great depths, M. Miesowicz, L. Jurkiewicz, and J. M. Massalski—380
Mesons at 11,300 ft., O. Piccioni—1
Mesons in atmosphere, Matthew Sands—180
Mesons, mass and charge sign in nuclear plates, Ian Barbour—751(A)
Minimum ionizing particles from disintegrations, B. T. Feld, I. L. Lebow, and L. S. Osborne—731(L)
Multiple production of mesons, Phyllis Freier and E. P. Ney—337; E. P. Ney and Phyllis Freier—752(A)
Neutron density at 100,000 ft., Luke C. L. Yuan—728(L)
Neutron production at high altitudes, J. A. Simpson, H W. Baldwin, and S. Molner—751(A)
Nuclear explosions, mean free path of particles, A. Lovati, A. Mura, G. Salvini, and G. Tagliaferri—284
Penetrating showers at 3260 meters, William D. Walker—686
Near Pfotzer maximum, S. F. Singer—730(L)
Potential gradient in atmosphere, S. A. Korff—144(L); Robert E. Holzer—846(L)
Primary α-particle flux, L. Goldfarb, H. L. Bradt, and B. Peters—751(A)
Primary intensity at high altitudes, solar magnetic field, M. A. Pomerantz—830
Protons from absorption of π-mesons, Stephen Tamor—412(L)
Secondary particles of penetrating showers, O. Piccioni—6
Solar origin, H. Alfvén—375
Underground cloud-chamber study, O. L. Tiffany and W. E. Hazen—849(L)
Zenith angle dependence, S. F. Singer—729(L)
Zenith angle of air showers, H. L. Kraybill—410(L)
Zenith angle variation of latitude effect, H. D. Rathgeber—566(L)
Cosmology
Rotational universe, C. Y. Fan—140(L)
Cross section, measurements, theory (see also **Scattering of electrons, neutrons, and ions**)
Of A^{36}, thermal neutron-capture, G. E. McMurtrie and D. P. Crawford—840(L)

Of C, O, Mg, Si, and S for neutrons, G. D. Freier, E. E. Lampi, and J. H. Williams—748(A)
Of $C^{12}(p,\gamma)N^{13}$ reaction, low energies, Carl L. Bailey and William R. Stratton—194
Of $C^{12}(p,\gamma)N^{13}$ reaction near 100 kev, Robert Noel Hall and William Alfred Fowler—197
Coherent scattering of neutrons, M. Hamermesh—140(L)
Of Cu, Ni, Mn for slow neutrons, P. J. Bendt and I. W. Ruderman—575
$Cu^{63}(n,2n)Cu^{62}$, near threshold, J. L. Fowler and J. M. Slye, Jr.—787
$D(d,p)$ reaction, low energies, angular distribution, J. H. Sanders, J. Moffatt, and D. Roaf—754(A)
Of He for neutrons, S. Bashkin, B. Petree, F. P. Mooring, and R. E. Peterson—748(A)
For $He^3(d,p)He^4$ at 10.2-Mev, excited state in He^4, J. C. Allred—753(A)
Of high energy pi-mesons, Kenneth Greisen—713(L)
Of liquid S, Pb, and Bi for neutrons, Owen Chamberlain—305
$(n\text{-}2n)$, $(n\text{-}p)$ reactions, Bernard L. Cohen—754(A)
Neutron inelastic scattering by light nuclei, L. E. Beghian, M. A. Grace, G. Preston, and H. Halban—286(L)
For neutrons, mass number, R. K. Adair—748(A)
For 95 Mev neutrons, twelve elements, James DeJuren and Norman Knable—606
Photo-disintegration of rhodium, N. W. Curtis, J. Hornbostel, D. W. Lee, and E. O. Salant—290(L)
Of K, fast neutrons, R. E. Peterson—747(A)
Production of Li^8 from various gases, S. Courtenay Wright—742(A)
For resonance radiation scattering in Pb, Ralph Dressel, M. Goldhaber, and A. O. Hanson—754(A)
Scattering cross sections, properties of nuclear reaction, T. Teichmann—506
Slow neutron scattering in resonance region, J. Tittman, C. Sheer, J. Rainwater, and W. W. Havens—748(A)
Of various elements for thermal neutrons, H. Pomerance—747(A)

Crystal structure
Cation distribution in ferrites with spinel structure, Frank G. Brockman—841(L)
CoPt crystals, partially ordered, John B. Newkirk and R. Smoluchowski—749(A)
Electron reflection in diamond, R. D. Heidenreich—271

Crystalline state
Activation energy for motion of dislocations in Cu crystals, A. S. Nowick—750(A)
Band structure in disordered alloys, Hubert M. James and Arthur S. Ginzbarg—749(A)
Color centers in CaF_2 and BaF_2, Alexander Smakula—408(L)
Conductivity, effect of cold work, J. K. Mackenzie and E. H. Sondheimer—264
Conductivity in diamond, Kenneth G. McKay—816
Creep of Cu and Pb, single crystals, Peter W. Neurath and J. S. Koehler—750(A)
Crystals grown from vapor onto mica, L. G. Schulz—750(A)
Diamond conduction counter, effect of light, R. K. Willardson and G. C. Danielson—300(L)
Dielectric breakdown in non-polar crystals, W. R. Heller—760(A)
Dielectric characteristics, CaF_2 layers, Erkki A. Laurila—405(L)
Dielectric polarization in alkali-halide crystals, Shepard Roberts—258
Elastic constants of nickel crystals, Mikio Yamamoto—566(L)
Electrostatic potential energy from diffraction data, William J. Taylor—763(A)
Energy absorbed in twinning, zinc, Edward I. Salkovitz and James S. Koehler—749(A)
Energy bands and mobilities in monatomic semiconductors, W. Shockley and J. Bardeen—407(L)
Hall effect in Ge-Sb alloys, G. L. Pearson, J. D. Struthers, and H. C. Theurer—809
Internal friction at high temperatures, T'ing-Sui Kê—750(A)
Internal friction, measurement, J. S. Koehler and J. W. Marx—749(A)
Internal friction of copper, effects of etching, annealing, threshold deformation, J. W. Marx and D. A. Patterson—749(A)
Mobility of electrons and holes in Ge, W. C. Dunlap, Jr.—759(A)
Order in alloys, theory of, J. M. Cowley—669
Paramagnetic anisotropy of MnF_2, J. W. Stout and Maurice Griffel—750(A)
Piezoid characteristics, cylindrical shape, Charles R. Mingins, Carl A. Stevens, and Robert W. Perry—762(A)
Reflectivity of Ge alloys, K. Lark-Horovitz and K. W. Meissner—759(A)
Resistivity at boundaries between crystallites, V. A. Johnson—760(A)
Scintillations in KI, effect of Th impurity, M. Freedman, B. Smaller, and J. May—759(A)
Thermoelectric power and carriers in Se, Herbert W. Henkels—734(L)
Thermoluminescence of $CaSO_4$: Mn phosphor, K. Watanabe—748(A)
X- and γ-ray reflection properties of quartz, D. A. Lind, W. J. West, and J. W. M. DuMond—475
Zn alloys, magnetic properties at low temperatures, Jules A. Marcus—750(A)

Dielectric constants (see **Dielectrics and dielectric properties**)

Dielectrics and dielectric properties
Breakdown in non-polar crystals, W. R. Heller—760(A)
Of CaF_2 layers, Erkki A. Laurila—405(L)
Of ferromagnetic ferrite, dimensional effects, Frank G. Brockman, P. H. Dowling, and Walter G. Steneck—85
Polarization in alkali-halide crystals, Shepard Roberts—258

Discharge of electricity in gases
Coulomb interactions in plasma, L. Landau—567(L)
Drift velocities in A, N, A-N mixtures, E. D. Klema and J. S. Allen—661
Extraction of ions from solids, pitting, Jerome Rothstein—744(A)
Photon pulses, point-to-plane corona, W. N. English—850(L)
Radiation transients, R. G. Fowler—760(A)
Recombination and electron density in Ne afterglows, R. B. Holt, John M. Richardson, B. Howland, and B. T. McClure—239
Retardation of ions, A. J. Dempster and A. E. Shaw—746(A)
Spurious parallel plate counters, Frank L. Hereford—559(L)

Disintegration and excitation of nucleus (see also **Radioactivity**)
Absolute voltage determinations, comparison of, William J. Sturn and Virgil Johnson—752(A)
α-particles from F and Li, W. E. Burcham and Joan M. Freeman—287(L)
Angular correlation of internal conversion electrons, H. Frauenfelder, M. Walter, and W. Zünti—557(L)
Angular distribution of $D(d,p)$, low energy cross section, J. H. Sanders, J. Moffat, and D. Roaf—754(A)
Angular distribution of protons from $O^{16}(d,p)O^{17}$, Leo Diesendruck—753(A)

Disintegration and excitation of nucleus (continued)
$C^{12}(p,\gamma)N^{13}$ reaction at low energies, Carl L. Bailey and William R. Stratton—194; Robert Noël Hall and William Alfred Fowler—197
$Cu^{63}(n,2n)Cu^{62}$, near threshold, J. L. Fowler and J. M. Slye, Jr.—787
D+D reactions, energy dependence, F. M. Beiduk, J. R. Pruett, and E. J. Konopinski—622, 755(A)
D+D reactions, internucleonic forces, J. R. Pruett, F. M. Beiduk, and E. J. Konopinski—628, 755(A)
$D(p,n)2H$ threshold, D binding energy, R. V. Smith and D. H. Martin—752(A)
Of deuterons by neutrons, G. L. Griffith, M. E. Remley, and P. G. Kruger—748(A)
Deuterons from high energy reactions, G. F. Chew and M. L. Goldberger—470
Excited state in He^4, search for, J. C. Allred—753(A)
Excited state of Be^7, T. A. Hall—411(L); J. C. Grosskreutz and K. B. Mather—580, 747(A)
Gamma-rays from neutron capture by Be, C, and N, B. B. Kinsey, G. A. Bartholomew, and W. H. Walker—723(L)
General properties, scattering cross sections, T. Teichmann—506
Of He^3 and N^{14} by thermal neutrons, reaction energies, W. Franzen, J. Halpern, and W. E. Stephens—641
High voltage scale, H. T. Richards and R. V. Smith—752(A)
Of $Mg^{24}(p,\gamma)Al^{25}$ resonances, T. Grotdal, O. M. Lönsjö, R. Tangen, and I. Bergström—296(L)
N-P reactions in light elements, C. P. Browne, R. V. Smith, and H. T. Richards—754(A)
Neutrons from Be, W. D. Whitehead and C. E. Mandeville—732(L)
Neutrons from $Li^7(p,n)Be^7$, V. R. Johnson, M. J. Wilson Laubenstein, and H. T. Richards—413(L)
Pairs and gamma-radiation of O^{16}, V. K. Rasmussen, W. F. Hornyak, C. C. Lauritsen, and T. Lauritsen—617
(p,γ) resonances below 400 kv, S. K. Allison, J. H. Montague, and A. H. Morrish—754(A)
Spallation products of arsenic with 190-Mev deuterons, H. H. Hopkins, Jr.—717(L)
Stars in O_2 and He produced by 90-Mev neutrons, James Tracy and Wilson M. Powell—594

Elasticity
Of Be crystals, Louis Gold—390
Constants of nickel crystals, Mikio Yamamoto—566(L)
Free vibrations of isotopic cube, T. Schiffman and H. Ekstein—757(A)
Of Ti rod, Herbert I. Fusfeld and Joseph T. Gilbert—302(L)
Electrical conductivity and resistance
Conductivity pulses in liquids, Norman Davidson and A. E. Larsh, Jr.—706
In diamond, electron bombardment, Kenneth G. McKay—816
Effect of cold work, J. K. Mackenzie and E. H. Sondheimer—264
Energy bands and mobilities in monatomic semiconductors, W. Shockley and J. Bardeen—407(L)
Of Ge in external magnetic fields, A. Foner and I. Estermann—759(A)
Ge rectifier, effect of frequency, R. Bray and H. J. Yearian—760(A)
Impurity scattering in semiconductors, E. Conwell and V. F. Weisskopf—388
Mobility of electrons and holes in Ge, W. C. Dunlap, Jr.—759(A)
n- and *p*-germanium transistors, electrical forming, J. Bardeen and W. G. Pfann—401(L)
Non-linear I–V characteristic of Ge at low *T*, F. K. du Pré—152(L); Erratum—571(L)
Of polycrystalline graphite, S. Mrozowski—838(L)
Resistivity at boundaries between crystallites, V. A. Johnson—760(A)
Of Si, erratum, G. L. Pearson and J. Bardeen—303(L)
Space-charge effects, diamond conduction counters, R. K. Willardson, A. C. Damask, and G. C. Danielson—758(A)
Surface impedance of Sn, Hg, and Pb, I. Šimon—384
Transistor characteristics, type *A*, L. P. Hunter—558(L)
Electrodynamics (see **Electromagnetic theory**)
Electromagnetic theory (see also **Quantum electrodynamics**)
Electron dynamics in standing wave accelerator, Gerald Hoffman and Edward Akeley—761(A)
Elimination of self-electromagnetic field, Stuart P. Lloyd—757(A)
Motion of a charge in magnetic field, M. H. Johnson and B. A. Lippmann—702
Motion of particles in linear accelerator, John R. Terrall—415(L)
New theory of electricity, Bayard P. Peakes—424(A)
Waves in ionized media, sun's atmosphere, V. A. Bailey—418(L)
Electron diffraction
"Forbidden" reflection in diamond, R. D. Heidenreich—271
Elements
Berkelium 97^{244}, S. G. Thompson, A. Ghiorso, and G. T. Seaborg—838(L)
Energy states of nucleus (see **Disintegration and excitation of nucleus; Nuclear structure**)
Errata
Electrical properties of pure silicon and silicon alloys, G. L. Pearson and J. Bardeen—303(L)
Microwave spectrum of CH_2CFCl, J. K. Bragg, T. C. Madison, and A. H. Sharbaugh—571(L)
Non-linear I–V characteristic of Ge at very low temperatures, F. K. du Pré—571(L)
Quasi-chemical method in the statistical theory of regular mixtures, Yin-Yuan Li—300(L)
Short range alpha-particles from fluorine and lithium bombarded by protons, W. E. Burcham and Joan M. Freeman—287(L)
Theory of pressure absorption, Masataka Mizushima—149(L)
Excitation of nuclei (see **Disintegration and excitation of nucleus; Nuclear structure**)

Field theory (see also **Quantum electrodynamics**)
Coupling of gravitational and electronic fields, Hermann Weyl—699
Field dynamics, *S*-matrix, K. V. Roberts—146(L)
Interaction Hamiltonian, classical, K. V. Roberts—146(L)
Non-local free fields, Hideki Yukawa—219, 849(L)
Representation of general fields, F. J. Belinfante and J. S. Lomont—757(A)
Fission of nucleus (see also **Disintegration and excitation of nucleus**)
Photo-fission thresholds in U, Pu, and Th, H. W. Koch, J. McElhinney, and E. L. Gasteiger—329
Yields, closed-shell perturbations, interpretations, L. E. Glendenin and C. D. Coryell—755(A)
Yields of $65d$ Zr^{95} and $17h$ Zr^{97}, search for other chains, C. D. Coryell, A. Y. Sakakura, and A. M. Ross—755(A)
Flame phenomena
Flame structure, Raymond Friedman and Edward Burke—574(A)
Turbulent flames, Bela Karlovitz—574(A)
Fluid dynamics (see also **Hydrodynamics; Aerodynamics**)
Bernoulli's theorem for viscous compressible fluids, C. Truesdell—535
Oscillations of a cable in a stream, A. E. Seigel—573(A)
Virtual mass of a sphere, Albert May and Jean C. Woodhull—573(A)

Friction
Activation energy for motion of dislocations in Cu crystals, A. S. Nowick—750(A)
Internal friction at high temperatures, T'ing-Sui Kê—750(A)
Internal friction in Ti rod, Herbert I. Fusfeld and Joseph T. Gilbert—302(L)
Internal friction, measurement, J. S. Koehler and J. W. Marx—749(A)
Internal friction of copper, effects of etching, annealing, threshold deformation, J. W. Marx and D. A. Patterson—749(A)

Gamma-rays (see also **Disintegration and excitation of nucleus; Radioactivity**)
Angular correlation of annihilation radiation, S. De-Benedetti, C. E. Cowan, W. R. Konneker, and H. Primakoff—205
High energy photons from proton-nucleon collisions, R. Bjorklund, W. E. Crandall, B. J. Moyer, and H. F. York—213
From N^{16}, energies measured, C. H. Millar, A. G. W. Cameron, and M. Glicksman—742(A)
From O^{16}, V. K. Rasmussen, W. F. Hornyak, C. C. Lauritsen, and T. Lauritsen—617
Selection rules for disintegration into two photons, C. N. Yang—242

Geophysics
Earth's magnetic field at high altitudes, S. F. Singer, E. Maple, and W. A. Bowen, Jr.—398(L)

Hall effect
In Ge-Sb alloys, measurements, G. L. Pearson, J. D. Struthers, and H. C. Theurer—809

Hydrodynamics
Diabatic flow, Bruce L. Hicks—286(L)
Direction-of-fall of sedimenting particles, E. E. Miller and C. B. Tanner—761(A)
Eddy viscosity in isotropic turbulence, T. D. Lee—842(L)

Hyperfine structure (see also **Nuclear moments and spin**)
Of Ba, isotope shift, O. H. Arroe—745(A)
Of deuterium, Francis Low—361
Electron spin, gyromagnetic ratio, A. K. Mann and P. Kusch—435
Exchange narrowing of paramagnetic resonance, C. H. Townes and J. Turkevich—148(L)
Of heavy elements, influence of nuclear structure, Aage Bohr and V. F. Weisskopf—94
Of In stable isotopes, interaction constants, A. K. Mann and P. Kusch—427
Quadrupole effects in solids, C. Kikuchi—746(A)
Of Tl^{205} and Tl^{203}, $^2P_{\frac{1}{2}}$ state, A. Berman, P. Kusch, and A. K. Mann—140(L)

Instruments (see Methods and instruments)

Ionization
In air and A by π-particles, William P. Jesse, Harold Forstat, and John Sadauskis—782
Waves in ionized media, V. A. Bailey—418(L)

Ionization potentials
Of higher atomic ions, Wolfgang Finkelnburg—304(L)
Of neutral and singly ionized atoms, electron screening, Wolfgang Finkelnburg and Frank Stern—303(L)

Ionosphere
Ionospheric phenomena and surface pressure, M. W. Jones and J. G. Jones—845(L)

Isomers, nuclear (see also **Nuclear structure; Radioactivity**)
Of $_{79}Au^{197}$, F. K. McGowan—138(L)
Of Kr^{83}, I. Bergström, S. Thulin, and G. Andersson—851(L)
Of RaE, H. M. Neumann, J. J. Howland, Jr., and I. Perlman—720(L)

Isotopes
Abundance ratios, C, N, O, A, and K, Alfred O. Nier—789
Of Cs, neutron-deficient activity of, Richard W. Fink, Frederick L. Reynolds, and D. H. Templeton—614
Concentration of Be^{10}, C. P. Keim, H. W. Savage, and Boyd Weaver—414(L)
Of Er and Lu, Richard J. Hayden, David C. Hess, Jr., and Mark G. Inghram—299(L)
Heavy odd-odd isotopes, A. Broniewski—846(L)
Of Sc, Gd, Dy, Ho, Er, and Yb, Wallace T. Leland—634

Liquids (see also **Hydrodynamics**)
Phase relations in He^3-He^4, B. Weinstock, D. W. Osborne, and B. M. Abraham—400(L)
Phase transition, mixtures of He^3 and He^3, C. J. Gorter and J. de Boer—569(L)
Structure from neutron diffraction, Owen Chamberlain—305

Low temperature phenomena
λ-point of He^4, effect of He^3, O. K. Rice—142(L)
Neutron scattering by liquid helium, L. Goldstein, D. Sweeney, and M. Goldstein—319
Non-linear I-V characteristic of Ge, F. K. du Pré—152(L); Erratum—571(L)
Specific heats of W and Zn, low temperatures, A. A. Silvidi and J. G. Daunt—125

Luminescence
Of barium oxide, Virgil L. Stout—744(A)

Magnetic properties (see also **Nuclear moments and spin**)
Of Alnico V, C. Kittel, E. A. Nesbitt, and W. Shockley—839(L)
Coercive force *vs.* temperature, J. K. Galt—845(L)
Exchange interaction on absorption, C. Kittel and Conyers Herring—725(L)
Of ferromagnetic ferrite, dimensional effects of dielectric constants, Frank G. Brockman, P. H. Dowling, and Walter G. Steneck—85
Paramagnetic anisotropy of MnF_2, J. W. Stout and Maurice Griffel—750(A)
Single domains in fine powders, C. Kittel, J. K. Galt, and W. E. Campbell—725(L)
Of Zn alloys at low temperatures, Jules A. Marcus—750(A)

Magnetic resonance absorption (see also **Nuclear moments and spin**)
Dependence on chemical compound, W. G. Proctor and F. C. Yu—717(L); W. C. Dickinson—736(L)
Effect of electronic paramagnetism, W. D. Knight—746(A); C. H. Townes, Conyers Herring, and W. D. Knight—852(L)
Electron spin gyromagnetic ratio, A. K. Mann and P. Kusch—435
Exchange interaction on absorption, C. Kittel and Conyers Herring—725(L)
Exchange narrowing of paramagnetic resonance, C. H. Townes and J. Turkevich—148(L)
g-values in paramagnetic organic compounds, A. N. Holden, C. Kittel, F. R. Merritt, and W. A. Yager—147(L)
Hyperfine structure of In stable isotopes, interaction constants, A. K. Mann and P. Kusch—427
Hyperfine structure of Tl^{205} and Tl^{203}, $^2P_{\frac{1}{2}}$ state, A. Berman, P. Kusch, and A. K. Mann—140(L)
Of magnesium ferrites, A. J. E. Welch, P. F. Nicks, Alan Fairweather, and F. F. Roberts—403(L)
In Mo Permalloy, Junkichi Itoh and Tetsuo Akioka—293(L)
Nuclear induction, free Larmor precession, E. L. Hahn—297(L)
Spin echoes, E. L. Hahn—746(A)
Spin-spin interaction factor, upper limit, G. J. Bene, P. M. Denis, and C. R. Extermann—288(L)

Mass spectroscopy (see also **Isotopes**)
Doublet measurements, T. R. Roberts and Alfred O. Nier—746(A)
Mean or half-life
Of Au^{197}, Fe^{57}, Cd^{111}, Hg^{198}, and Tl^{203}, excited states, Martin Deutsch and W. E. Wright—139(L)
Half-life of γ-decay of $Hg^{203,205}$, Daniel Binder—291(L)
Of positive π-meson, E. A. Martinelli and W. K. H. Panofsky—465
Of U^{238}, double beta-decay, C. A. Levine, A. Ghiorso, and G. T. Seaborg—296(L)
Mechanics, quantum—atomic structure and spectra
Lamb shift, numerical value, H. A. Bethe, L. M. Brown, and J. R. Stehn—370
Mechanics, quantum—general
Dissipative systems, Wesley E. Brittin—396
Equations of motion and commutation relations, Eugene P. Wigner—711
Higher order equations, W. Thirring—570(L)
S-matrix and Hamiltonian, H. Ekstein—757(A)
Two-component wave equations, F. Gürsey—844(L)
Upper and lower bounds of eigenvalues, Tosio Kato—413(L)
Vector-matrices and their spurs, R. J. Duffin—683
Mechanics, quantum—molecular structure and spectra
l-type doubling of methyl cyanide and methyl iso-cyanide, Harald H. Nielsen—130
Mechanics, quantum—nuclear
Bremsstrahlung for heavy elements, relativistic energies, L. Bess—550
D+D reactions, energy dependence, F. M. Beiduk, J. R. Pruett, and E. J. Konopinski—622
D+D reactions, internucleonic forces, J. R. Pruett, F. M. Beiduk, and E. J. Konopinski—628
Hyperfine structure of deuterium, internal motion effects, Francis Low—361
Multiple meson processes, Alex E. S. Green—719(L)
n-p interaction, Richard S. Christian and Edward W. Hart—441
Relativistic nuclear force, T. Toyoda—853(L)
Mechanics, statistical
Distribution of phases in two-phase solids, Leonard D. Jaffe—762(A)
Thermodynamic functions of crystals, William J. Taylor—762(A)
Of three-dimensional ferromagnet, D. ter Haar and B. Martin—721(L)
Vibrational relaxation times in polyatomic gases, R. N. Schwartz—572(A)
Mesons (see also **Cosmic radiation**)
Annihilation radiation, selection rules, C. N. Yang—242
Artificially produced, electrical detection, L. W. Alvarez, A. Longacre, V. G. Ogren, and R. E. Thomas—752(A)
Asymmetry in cosmic rays, Gerhart Groetzinger and Gordon W. McClure—777
Charged heavy meson, H. H. Forster—733(L)
Cross sections of high energy pi-mesons, Kenneth Greisen—713(L)
Disintegration products, 2.2-μsec. meson, E. P. Hincks and B. Pontecorvo—102
East-west asymmetry, Gerhart Groetzinger and Gordon W. McClure—751(A)
Gamma-rays from neutral meson, B. P. Gregory, B. Rossi, and J. H. Tinlot—299(L)
Generalized meson theories, Alex E. S. Green—755(A)
Lifetime of positive π-meson, E. A. Martinelli and W. K. H. Panofsky—465
Low energy in atmosphere, Matthew Sands—180
Mass and charge sign in nuclear plates, Ian Barbour—751(A)
Moderation in hydrogen, A. S. Wightman—521
Multiple processes, Alex E. S. Green—719(L)
Multiple production, Phyllis Freier and E. P. Ney—337; E. P. Ney and Phyllis Freier—752(A)
Neutral meson, scalar or pseudoscalar, C. N. Yang—722(L)
Produced by neutrons, F. M. Smith, Eugene Gardner, and Hugh Bradner—562(L)
Production at 11,300 ft., O. Piccioni—1
Relativistic meson theory of deuteron, S. M. Dancoff—755(A)
Spin of π-meson, B. Ferretti and S. Gallone—153(L)
Vector mesons, processes, James N. Snyder—143(L)
Metals (see **Crystalline state**)
Meteorology (see also **Ionosphere**)
Electrical potential on freezing of water, Vincent J. Schaefer—721(L)
Potential gradient in atmosphere, cosmic radiation, Robert E. Holzer—846(L)
Methods and instruments
Absorption data analysis, maximum β-ray energy from Cu^{62}, L. Katz, A. S. Penfold, H. J. Moody, R. N. H. Haslam, and H. E. Johns—289(L)
Active coaxial tube, Philippe A. Clavier—302(L)
Anthracene counter, response to monoenergetic electrons, John I. Hopkins—406(L); James F. Norton—759(A)
Calorimetry of solids, Malcolm Dole, John A. Wethington, Jr., Norman Larson, and W. P. Hettinger, Jr.—761(A)
Cathode-ray tube and photo-cell to synthesize integral d.c. voltages, H. P. Stabler—423(A)
Coaxial lines, short time delays, Donald C. Moore and Willard A. Reenstra—761(A)
Coincidences, high activity sources, Z. Bay and M. M. Slawsky—414(L)
Conductivity in diamond under electron bombardment, multiple pulses, Kenneth G. McKay—816
Conductivity pulses in liquids, ionizing radiations, Norman Davidson and A. E. Larsh, Jr.—706
Crystals grown from vapor, L. G. Schulz—750(A)
D.c. magnetic generator, A. E. Benfield—424(A)
Decay times from coincidence experiments, Z. Bay—419(L)
Diamond conduction counter, effect of light, R. K. Willardson and G. C. Danielson—300(L)
Diamond conduction counters, space-charge effects, R. K. Willardson, A. C. Damask, and G. C. Danielson—758(A)
Drift velocities of electrons in A, N, A-N mixtures, E. D. Klema and J. S. Allen—661
Electron-beam tumor therapy, W. H. Bostick—564(L)
Emission regulator for mass spectrometer, E. B. Winn and Alfred O. Nier—746(A)
Equivalent circuit of piezoelectric resonators, Karl S. Van Dyke, Edward A. Pendleton, and Gary D. Gordon—424(A)
Fast neutron detector, health physics, W. G. Moulton and C. W. Sherwin—758(A)
Fast neutron energies measured in photographic emulsions, George R. Keepin, Jr. and James H. Roberts—758(A)
Gamma-scintillations in diphenylacetylene, C. F. Ravilious, J. O. Elliot and S. H. Liebson—851(L)
Illinois cyclotron oscillator, G. F. Tape and P. G. Kruger—757(A)
Internal friction, J. S. Koehler and J. W. Marx—749(A)
Light-source high intensity exploding wires, William M. Conn—745(A)
Mass spectrograph ion retardation due to gas, A. J. Dempster and A. E. Shaw—746(A)
Mesons electrically detected, L. W. Alvarez, A. Longacre, V. G. Ogren, and R. E. Thomas—752(A)
Neutron detector, Pd film, B. R. Gossick—297(L)

Neutron diffraction in liquid structure studies, Owen Chamberlain—305
Nuclear absolute voltage determinations, comparison of, William J. Sturm and Virgil Johnson—752(A)
Nuclear high voltage scale, H. T. Richards and R. V. Smith—752(A)
Nuclear induction, free Larmor precession, E. L. Hahn—297(L)
Oxide cathodes, production of, L. T. Aldrich and C. E. Smith—744(A)
Particle size from sedimentation, E. E. Miller and C. B. Tanner—761(A)
Particle size from x-ray scattering data, D. L. Dexter and W. W. Beeman—761(A)
Particles in linear accelerator, John R. Terrall—415(L)
Phase in slow neutron scattering, P. J. Bendt and I. W. Ruderman—575
Pole tips on cyclotron, Martin Foss—758(A)
Proportional counter spectrometer, C. J. Borkowski and E. Fairstein—759(A)
Rectifier resistance dependence on frequency, R. Bray and H. J. Yearian—760(A)
Scintillation pulses in anthracene, temperature dependence, G. G. Kelley and M. Goodrich—138(L)
Scintillations in KI, effect of Th impurity, M. Freedman, B. Smaller, and J. May—759(A)
Scintillators for low energy electrons, Waldo Rall and R. G. Wilkinson—758(A)
Se rectifiers in 500-kev generator, W. R. Arnold—758(A)
Small curvatures by optical interference, Harold R. Letner—762(A)
Spurious parallel plate counters, Frank L. Hereford—559(L)
Standard sources for beta-disintegration, T. B. Novey—742(A)
Standing wave accelerator, electron dynamics in, Gerald Hoffman and Edward Akeley—761(A)
Thickness of films on coated cylinders, Eugene B. Hensley—744(A)
Transistor characteristics, type A, L. P. Hunter—558(L)
Ultrasonic interferometer for low acoustic impedance, James L. Stewart and Ellen S. Stewart—143(L)
Voltage stabilizer for electrostatic generator, W. C. Miller, B. Waldman, J. C. Noyes, and J. E. Van Hoomissen—758(A)
Xylene and argon counters, effect of rest, Besim Tanyel—843(L)

Microwaves (see also **Electromagnetic theory; Spectra, microwave**)
Hyperfine structure, exchange narrowing of paramagnetic resonance, C. H. Townes and J. Turkevich—148(L)

Mobility of electrons
Drift velocities in A, N, A-N mixtures, E. D. Klema and J. S. Allen—661

Molecular structure and constants (see also **Raman spectra; Spectra, molecular**)
Of CBr_3D, thermodynamic properties, Salvador M. Ferigle, Forrest F. Cleveland, William M. Boyer, and Richard B. Bernstein—740(A)
Of CF_3Br, CF_3I, and CF_3CN, interatomic distances, John Sheridan and Walter Gordy—292(L)
Of CF_3Br, microwave spectrum A. H. Sharbaugh, B. S. Pritchard, and T. C. Madison—302(L)
Of CCl_3F, James P. Zietlow, Forrest F. Cleveland, and Arnold G. Meister—739(A)
Of $CDCl_3$, thermodynamic properties, John R. Madigan, Forrest F. Cleveland, William M. Boyer, and Richard B. Bernstein—740(A)
Dipole moments, Stark effects in OCS, R. G. Shulman and C. H. Townes—500
Of FCl, microwave techniques, D. A. Gilbert and A. Roberts—742(A)
Of GaCl, vibrational structure, F. K. Levin and J. G. Winans—741(A)
Of HCN, microwave spectrum, James W. Simmons, Wallace E. Anderson, and Walter Gordy—77
Of HF and DF, infra-red absorption, Robert M. Talley, Hoyt M. Kaylor, and Alvin H. Nielsen—529
Of nitrosyl chloride, microwave techniques, W. J. Pietenpol, J. D. Rogers, and Dudley Williams—741(A)
Of trifluorosilane derivatives, John Sheridan and Walter Gordy—719(L)

Moments, of particles (see also **Nuclear moments and spin**)
Proton magnetic moment, diamagnetic field correction, Norman F. Ramsey—567(L)

Neutrons
From Be, W. D. Whitehead and C. E. Mandeville—732(L)
From $Be^9(\alpha,n)$ reaction, yield, energy, C. E. Bradford and W. E. Bennett—753(A)
Detector, Pd film, B. R. Gossick—297(L)
Elastic scattering at 84 Mev, A. Bratenahl, S. Fernbach, R. H. Hildebrand, C. E. Leith, and B. J. Moyer—597
At high altitudes, from C, Al, Cu, Sn, and Pb, J. A. Simpson, H. W. Baldwin, and S. Molner—751(A)
At 100,000 ft., Luke C. L. Yuan—728(L)
Phase and cross section in scattering, P. J. Bendt and I. W. Ruderman—575
Radioactive decay, J. M. Robson—747(A)
Resonance in Ag, W. Selove—557(L)
Scattering by liquid helium, L. Goldstein, D. Sweeney, and M. Goldstein—319
Spatial distributions, L. Secrest—141(L)
Total reflection, applications, M. Hamermesh—140(L)
Yield from thick targets, A. J. Allen, J. F. Nechaj, K. H. Sun, and B. Jennings—752(A)

Neutron diffraction
In liquid S, Pb, Bi, Owen Chamberlain—305

Nuclear moments and spin (see also **Hyperfine structure**)
Of Ba isotopes, O. H. Arroe—745(A)
Deuteron electrical quadrupole moment, G. F. Newell—141(L)
Of Mg^{25}, F. M. Kelly, A. L. Schawlow, W. M. Gray, and M. F. Crawford—745(A)
Magnetic resonance dependence on chemical compound, W. G. Proctor and F. C. Yu—717(L); W. C. Dickinson—736(L)
Of Mn^{55}, Co^{59}, Cl^{37}, W. G. Proctor and F. C. Yu—716(L)
Quadrupole effects in solids, C. Kikuchi—746(A)
Of S^{33}, quadrupole moment, Victor W. Cohen, Walter S. Koski, and T. Wentink, Jr.—742(A)
Of Xe isotopes, Jørgen Koch and Ebbe Rasmussen—722(L)

Nuclear spectra (see **Disintegration and excitation of nucleus; Radioactivity; Spectra, nuclear**)

Nuclear structure (see also **Disintegration and excitation of nucleus; Radioactivity; Spectra, nuclear**)
Beta-spectra of Cl^{38}, Lawrence M. Langer—50
Continuity principle applied to even N-odd P and odd N-even P nuclei, Martin Popelka and William D. Harkins—756(A)
D+D reactions, internucleonic forces, J. R. Pruett, F. M. Beiduk, and E. J. Konopinski—755(A)
Of deuteron and triton from h.f.s., Edward N. Adams, II—755(A)
Dipole vibrations and surface symmetry energy, R. D. Present—355
Excited states of Be^7, T. A. Hall—411(L); J. C. Grosskreutz and K. B. Mather—747(A)
Of Au^{198} and Rb^{86}, β-γ-angular correlation, Sherman Frankel—747(A)

Nuclear structure (continued)
Influence on h.f.s. of heavy elements, Aage Bohr and V. F. Weisskopf—94
Isotope shift and nuclear polarization, G. Breit, G. B. Arfken, and W. W. Clendenin—569(L)
Low levels in Li^7 and Be^7, D. R. Inglis—724(L)
Magic numbers, continuity and regularity of nuclear series, William D. Harkins and M. Popelka—756(A)
Neutron core model, Hoff Lu—416(L)
Nuclear forces, theory of, H. J. Bhabha—665
Nuclear saturation, E. Gerjuoy—568(L)
Nuclear shell models, Eugene Feenberg—771
Potassium energy levels, Vance L. Sailor—794
Quadrupole moment of Li^7, C. H. Blanchard and R. Avery—756(A)
Range of nuclear force, *p-p*, *n-p* interactions, P. Swan—288(L)
Spherical shell nuclear model, H. A. Wilson—516

Optical constants and properties
Of Si and Ge, H. B. Briggs—287(L)

Packing fraction (see also **Isotopes**)
Of Pt^{198}, Howard A. Johnson, Henry E. Duckworth, Richard S. Preston, and Richard F. Woodcock—424(A)
Of W^{182} and W^{186}, Richard F. Woodcock, Henry E. Duckworth, Richard S. Preston, and Howard A. Johnson—424(A)

Pair production
Nuclear impulse, G. E. Modesitt and H. W. Koch—175

Photo-disintegration
Of deuteron, 4- to 20-Mev radiation, Everett G. Fuller—752(A)
Of deuteron, use of range of forces in theory, H. A. Bethe and Conrad Longmire—647
Dipole transitions in nuclear photo-effect, J. S. Levinger and H. A. Bethe—756(A)
Of nitrogen, E. R. Gaerttner and M. L. Yeater—570(L)
Of N and O by 100-Mev x-rays, E. R. Gaerttner and M. L. Yeater—714(L)
Protons from $D^2(\gamma,n)H^1$, angular distribution, Gerson Goldhaber—753(A)
Protons from Mg, angular distribution, energy, M. E. Toms, J. Halpern, and W. E. Stephens—753(A)
Of Rh, N. W. Curtis, J. Hornbostel, D. W. Lee, and E. O. Salant—290(L)
Yields and angular distributions of neutrons, G. A. Price and D. W. Kerst—806

Photoelectric effect and properties; cells
Work function of Ag, effect of support, L. L. Blackmer and H. E. Farnsworth—826

Piezoelectric effect
Piezoid characteristics, cylindrical shape, Charles R. Mingins, Carl A. Stevens, and Robert W. Perry—762(A)
Potential gradient produced by stress gradient, A. E. Benfield—762(A)

Plasticity
Time delays, John Kauffman and Waller George—761(A)

Proceedings of the American Physical Society
New England Section, Williams College, Williamstown, Massachusetts, October 22, 1949—422
Chicago Meeting, Chicago, Illinois, November 25–26, 1949—737
Division of Fluid Dynamics, University of Virginia, Charlottesville, Virginia, December 28–30, 1949—572

Quantum electrodynamics (see also **Field theory**)
Charge conjugation in two-component wave equations, Herbert Jehle—757(A)
Elimination of self-electromagnetic field, Stuart P. Lloyd—757(A)
Interaction between elementary particles, Alfred Landé—814
Longitudinal field treatment, Ning Hu—150(L)
Longitudinal photons, F. J. Dyson—420(L)
Motion of a charge in magnetic field, M. H. Johnson and B. A. Lippmann—702
Radiative corrections, electron magnetic moment, Robert Karplus and Norman M. Kroll—536
Selection rules for annihilation radiation, C. N. Yang—242
Self-energy of particles, Suraj N. Gupta—294(L)
Self-stress of electron, F. Rohrlich—357

Quantum mechanics (see **Mechanics, quantum**)

Radiation (see also **Thermal radiation**)
Angular correlation of annihilation radiation, C. S. Wu and I. Shaknov—136(L); S. DeBenedetti, C. E. Cowan, W. R. Konneker, and H. Primakoff—205
Bremsstrahlung for heavy elements, relativistic energies, L. Bess—550

Radioactivity (see also **Disintegration and excitation of nucleus; Nuclear structure; Spectra, nuclear**)
α-β- and α-K-branching, W. Jentschke—98
Of Be^7, momentum relations, Philip B. Smith and James S. Allen—747(A)
Of Be^{10}, β-spectra, P. R. Bell and J. M. Cassidy—301(L); D. J. Hughes, C. Eggler, and D. E. Alburger—726(L)
Beta-particles from tritium, energy-distribution, E. P. Cooper and F. T. Rogers, Jr.—402(L)
Beta-ray spectra, effect of screening, John R. Reitz—10
Of B^{12} and Li^8, beta-decay, W. F. Hornyak and T. Lauritsen—160
Of Br^{82}, half-life, E. Berne—568(L)
Of Ca^{45}, β-spectra, P. Macklin, L. Feldman, L. Lidofsky, and C. S. Wu—137(L)
Of C, half-life, Warren W. Miller, Robert Ballentine, William Bernstein, Lewis Friedman, A. O. Nier, and R. D. Evans—714(L)
Of C^{15}, Emmett L. Hudspeth, Charles P. Swann, and N. P. Heydenburg—736(L)
Of Cs, Richard W. Fink, Frederick L. Reynolds, and D. H. Templeton—614
Of Cl^{38}, β-spectra, Lawrence M. Langer—50, 742(A)
Of Cu^{61}, γ-radiation, F. Boehm, J. P. Blaser, P. Marmier, and P. Preiswerk—295(L)
Of Cu^{61}, positron spectrum, George E. Owen and C. Sharp Cook—743(A)
Of Cu^{62}, maximum β-ray energy, L. Katz, A. S. Penfold, H. J. Moody, R. N. H. Haslam, and H. E. Johns—289(L)
Of Eu, conversion electrons, J. M. Cork, H. B. Keller, W. C. Rutledge, and A. E. Stoddard—848(L)
Evaluation of $f_+(Z,W_0)$, Fermi beta-decay, George L. Trigg—756(A)
Fermi beta-decay, *ft* values, Eugene Feenberg—756(A)
Of Fr and Em, E. K. Hyde, A. Ghiorso, and G. T. Seaborg—765
Gamma-radiation from positron emitters, H. E. Kubitschek, A. Longacre, and M. Goldhaber—742(A)
Of Au^{198} and Rb^{86}, β-γ angular correlation, Sherman Frankel—747(A)
Of He^6, beta-spectrum, V. Perez-Mendez and H. Brown—404(L)
Intensities of weak γ-rays, G. R. Bishop, Richard Wilson, and H. Halban—416(L)
Of I^{124} and I^{126}, Allan C. G. Mitchell, J. Y. Mei, Fred C. Maienschein, and Charles L. Peacock—744(A)
Ionization in air and A by α-particles, William P. Jesse, Harold Forstat, and John Sadauskis—782
Of Fe^{53}, Mn^{57}, and Cr^{55}, production, M. E. Nelson and M. L. Pool—682
Isomerism of Kr^{83m}, I. Bergström, S. Thulin, and G. Andersson—851(L)

Of La^{136}, B. E. Robertson, W. L. Carss, and M. L. Pool—747(A)
Of La isotopes, R. A. Naumann, F. L. Reynolds, and I. Perlman—398(L)
Of $Hg^{203,205}$, γ-ray half-life, Daniel Binder—291(L)
Of Mo^{93}, disintegration scheme, D. N. Kundu, John L. Hult, and M. L. Pool—71, 743(A)
Of neutron, J. M. Robson—747(A)
Of Ni, search for photons, D. G. Thomas and J. D. Kurbatov—151(L)
Of Ni^{60}, Martin Deutsch and Kai Siegbahn—680
Of N^{16}, gamma-rays, C. H. Millar, A. G. W. Cameron, and M. Glicksman—742(A)
Of Pt, J. M. Cork, A. E. Stoddard, W. C. Rutledge, C. E. Branyan, and J. M. LeBlanc—843(L)
Of K^{40}, M. Freedman, B. Smaller, and J. May—759(A)
Of K^{40}, beta-rays, P. R. Bell, Boyd Weaver, and J. M. Cassidy—399(L)
Of K^{40}, gamma-rays, P. R. Bell and J. M. Cassidy—409(L)
Of K^{40}, recoil electron, R. W. Pringle, S. Standil, and K. I. Roulston—841(L)
Of Pr^{143}, J. Bruner, L. M. Langer, and D. Moffat—747(A)
Production of Li^8, S. Courtenay Wright—742(A)
Of Pm^{147} and S^{35}, Fermi plots, H. C. Price, Jr., J. Motz, and L. M. Langer—744(A)
Of Pm^{147} and S^{35}, low energy β-spectra, L. M. Langer, J. W. Motz, and H. C. Price, Jr.—798
Of RaD, conversion electrons of, Lawrence Cranberg—155
Of Rh, isotopes, Geoffrey Wilkinson and Harry G. Hicks—314
Of Ru^{103} and Rb^{86}, disintegration schemes, C. E. Mandeville and E. Shapiro—439
Of Ag^{110}, disintegration scheme, Kai Siegbahn—233
Standard sources for beta-disintegration, T. B. Novey—742(A)
Of Sr^{85}, Michel Ter-Pogossian—743(A)
Systematics of alpha-radioactivity, I. Perlman, A. Ghiorso, and G. T. Seaborg—26
Of Tc^{99}, beta-ray distribution, B. H. Ketelle and John W. Ruch—565(L)
Of $_{65}Tb^{160}$, β-decay, S. B. Burson, K. W. Blair, and D. Saxon—403(L)
Of Sn, γ-transitions, J. W. Mihelich and R. D. Hill—743(A)
Of Sn^{117}, E. C. Mallary and M. L. Pool—75, 743(A)
Of Sn^{125}, Robert B. Duffield and Lawrence M. Langer—743(A)
Units, L. F. Curtiss, R. D. Evans, Warren Johnson, and Glenn T. Seaborg—142(L)
Of U^{238}, half-life, double beta-decay, C. A. Levine, A. Ghiorso, and G. T. Seaborg—296(L)
Of Xe^{125}, Xe^{127}, D. L. Anderson and M. L. Pool—142(L)

Raman spectra
Of CBr_3D, Salvador M. Ferigle, Forrest F. Cleveland, William M. Boyer, and Richard B. Bernstein—740(A)
Of CCl_3F, James P. Zietlow, Forrest F. Cleveland, and Arnold G. Meister—739(A)
Of $CDCl_3$, John R. Madigan, Forrest F. Cleveland, William M. Boyer, and Richard B. Bernstein—740(A)
Of hexachloroethane and hexobromoethane, Rose A. Carney, Arnold G. Meister, and Forrest F. Cleveland—740(A)
Of $H_3C\text{-}CCl_3$, M. Zaki El-Sabban and Forrest F. Cleveland—740(A)
Of 2,3-dibromo-2,3-dimethylbutane, J. E. Lamport and Forrest F. Cleveland—740(A)

Range of particles
Proton range-energy relation in C-2 emulsion, Hugh Bradner, Frances M. Smith, Walter H. Barkas, and A. S. Bishop—462
Of protons in several metals, T. A. Hall and S. D. Warshaw—754(A)
Straggling of electrons near critical energy, L. Eyges—81

Recombination
In He, D. R. Bates—718(L)

Relativity
Coupling of gravitational and electronic fields, Hermann Weyl—699
Motion of a charge in magnetic field, M. H. Johnson and B. A. Lippmann—702
Relativistic nuclear force, T. Toyoda—853(L)

Scattering of electrons, neutrons, protons, and ions (see also **Cross section**; **Electron diffraction**)
Cross sections for 95-Mev neutrons, twelve elements, James DeJuren and Norman Knable—606
Of 84-Mev neutrons, elastic, A. Bratenahl, S. Fernbach, R. H. Hildebrand, C. E. Leith, and B. J. Moyer—597
Lower bound, range of n-p interaction, A. A. Broyles and B. Kivel—839(L)
Multiple scattering in a gas, mass and energy, Gerhart Groetzinger, Martin J. Berger, and Fred L. Ribe—584
Multiple scattering of electrons in A, Fred L. Ribe, Martin J. Berger, and Gerhart Groetzinger—760(A)
Neutron cross section and phase, P. J. Bendt and I. W. Ruderman—575
Neutron scattering by liquid helium, L. Goldstein, D. Sweeney, and M. Goldstein—319
Of neutrons by light nuclei, L. E. Beghian, M. A. Grace, G. Preston, and H. Halban—286(L)
n-p interaction, Richard S. Christian and Edward W. Hart—441
n-p scattering by liquid mirror reflection, D. J. Hughes, M. T. Burgy, and G. R. Ringo—291(L)
Neutron resonance in Ag, W. Selove—557(L)
p-p, n-p interactions, P. Swan—288(L)
Resonance neutron scattering in Na^{23}, C. T. Hibdon, C. O. Muehlhause, W. Selove, and W. Woolf—730(L)

Scattering of radiation (see also **Raman spectra**)
Angular correlation of annihilation radiation, C. S. Wu and I. Shaknov—136(L)
Multiple Compton scattering, W. R. Faust—227
Multiple scattering, Melvin Lax—756(A)
Photon-photon scattering, J. C. Ward—293(L)

Semiconductors (see **Electrical conductivity and resistance**)

Shock waves
Dissipation in a tube, R. J. Emrich and C. W. Curtis—573(A)
Schlieren pictures on reflections, Edward M. Little—573(A)
Three-shock configuration, G. Rawling and H. Polachek—572(A)

Solid state (see **Crystalline state**)

Spallation (see **Disintegration and excitation of nucleus**)

Specific heat
Of W and Zn at low temperatures, A. A. Silvidi and J. G. Daunt—125

Spectra, absorption (see also **Absorption of radiation**)
Of GaCl, F. K. Levin and J. G. Winans—741(A)
Of H_2, vibrational lines, Masataka Mizushima—150(L)
Of HF and DF, molecular constants, Robert M. Talley, Hoyt M. Kaylor, and Alvin H. Nielsen—529
Ultraviolet continua, primary and secondary alcohols, Gladys A. Anslow and Hsi-teh Hsieh—423(A)
Of water vapor, J. J. Hopfield—560(L)
Of water vapor in near infra-red, Robert M. Chapman—741(A)

Spectra, atomic
Of Cb and Mo, George W. Charles—120
Forbidden lines in Hg^{198}, K. G. Kessler—559(L)
Forbidden s-ns lines in alkali metal, absorption, J. E. Mack—745(A)
Infra-red spectrum of polar aurora, W. Petrie—720(L)

Spectra, atomic (continued)
Isotope shift and nuclear polarization, G. Breit, G. B. Arfken, and W. W. Clendenin—569(L)
Isotope shift in C, John R. Holmes—745(A)
Isotope shift in Xe, Jørgen Koch and Ebbe Rasmussen—722(L)
Lamb shift, n^{-3} law in He^+, J. G. Hirschberg, Jr. and J. E. Mack—745(A)
Lifetimes of Hg and K, excited states, B. Mishra—153(L)
Of U II, J. Rand McNally, Jr.—417(L)
Spectra, microwave
Of BrF, D. F. Smith, M. Tidwell, and D. V. P. Williams—420(L)
Of CF_3Br, A. H. Sharbaugh, B. S. Pritchard, and T. C. Madison—302(L)
Of CF_3Br, CF_3I, and CF_3CN, interatomic distances, John Sheridan and Walter Gordy—292(L)
Of CH_2CFCl, J. K. Bragg, T. C. Madison, and A. H. Sharbaugh—148(L); Erratum—571(L)
Dispersion in NH_3, George Birnbaum—144(L)
Of FCl, D. A. Gilbert and A. Roberts—742(A)
Of HCN, molecular constants, James W. Simmons, Wallace E. Anderson, and Walter Gordy—77
l-type doubling in OCS and HCN, R. G. Shulman and C. H. Townes—421(L)
Line widths, temperature dependence, Raydeen Howard and William V. Smith—840(L)
Of methyl alcohol, D. K. Coles W. E. Good, and R. H. Hughes—741(A)
Of nitrosyl chloride, W. Pietenpol, J. D. Rogers, and Dudley Williams—741(A)
Of O_2, fine structure, James H. Burkhalter, Roy S. Anderson, William V. Smith, and Walter Gordy—152(L)
Pressure broadening, L. C. Jones—741(A)
Of S^{35}, Victor W. Cohen, Walter S. Koski, and T. Wentink, Jr.—742(A)
Of trifluorosilane derivatives, John Sheridan and Walter Gordy—719(L)
Spectra, molecular (see also **Molecular structure and constants**)
Of CCl, emission bands, Putcha Venkateswarlu—79
Of CF_2, emission, Putcha Venkateswarlu—676
Of hexachloroethane and hexabromoethane, Rose A. Carney, Arnold G. Meister, and Forrest F. Cleveland—740(A)
Of H_3C-CCl_3, M. Zaki El-Sabban and Forrest F. Cleveland—740(A)
Intensity distribution, ($C_3\pi \rightarrow B_3\pi$) system of nitrogen, R. W. Nicholls—421(L)
Stark-Zeeman effects on molecules with nuclear quadrupole coupling, F. Coester—454
Of 2,3-dibromo-2,3-dimethylbutane, J. E. Lamport and Forrest F. Cleveland—740(A)
Spectra, nuclear (see also **Disintegration and excitation of nucleus; Nuclear structure; Radioactivity**)
Beta-decay of B^{12} and Li^8, W. F. Hornyak and T. Lauritsen—160
Beta-ray spectra, effect of screening, John R. Reitz—10
Beta-spectra of Cs^{137}, Y^{91}, 61^{147}, Ru^{106}, Sm^{151}, P^{32}, and Tm^{170}, Harold M. Agnew—655
Beta-spectrum of Be^{10}, P. R. Bell and J. M. Cassidy—301(L)
Of Cu^{61}, positron, George E. Owen and C. Sharp Cook—743(A)
γ-spectra of Cu^{61}, F. Boehm, J. P. Blaser, P. Marmier, and P. Preiswerk—295(L)
Of Pr^{143}, beta-radiation, J. Bruner, L. M Langer, and D. Moffat—747(A)
Of Pm^{147} and S^{35}, beta radiation, H. C. Price, Jr., J. Motz, and L. M. Langer—744(A)
Spectroscopy, technique
Light-source, high intensity, exploding wires, William M. Conn—745(A)
Stark effect
In OCS, molecular dipole moments, R. G. Shulman and C. H. Townes—500
Stark-Zeeman effects on molecules with nuclear quadrupole coupling, F. Coester—454
Statistical mechanics (see **Mechanics, statistical**)
Supersonics (see also **Shock waves; Ultrasonics**)
Air condensation in wind tunnels, H. Guyford Stever—573(A)
Air flow around moving bodies, P. A. Thurston—573(A)
Conical flow, interferometric test, J. H. Giese, F. D. Bennett, and V. E. Bergdolt—574(A)
Density measurements, Eva Winkler—574(A)
Three-shock configuration, G. Rawling and H. Polachek—572(A)
Turbulent jet mixing, D. Bershader and S. I. Pai—574(A)

Thermal radiation (see also **Radiation**)
Neoclassical approach to blackbody radiation, B. Liebowitz—423(A)
Thermionic emission; Emitting surfaces
Of BaO and SrO, thin films, George E. Moore and H. W. Allison—246
Oxide cathodes, production of, L. T. Aldrich and C. E. Smith—744(A)
Thermodynamics
Chemical thermodynamics in Jacobian form, F. H. Crawford—423(A)
λ-point of He^4, effect of He^3, O. K. Rice—142(L)
Thermoelectric effects
Of Se, Herbert W. Henkels—734(L)
Thermoluminescence
Of $CaSO_4$: Mn phosphor, K. Watanabe—748(A)

Ultrasonics
Interferometer for low acoustic impedance, James L. Stewart and Ellen S. Stewart—143(L)

Viscosity
In isotropic turbulence, T. D. Lee—842(L)

X-rays, absorption, diffraction, scattering, reflection, refraction, and polarization
Absorption factors for coated cylinders, Eugene B. Hensley—744(A)
Coherent scattering, E. Arnous—149(L)
Penetration and diffusion, asymptotic behavior, U. Fano, H. Hurwitz, Jr., and L. V. Spencer—425
Resonance scattering in Pb, Ralph Dressel, M. Goldhaber, and A. O. Hanson—754(A)
Small angle scattering, D. L. Dexter and W. W. Beeman—761(A)
X-rays, emission
Energy distribution from 19.5-Mev electrons, H. W. Koch and R. E. Carter—165

Zeeman effect
Detection of radiofrequency resonance, M. H. L. Pryce—136(L)
Stark-Zeeman effects on molecules with nuclear quadrupole coupling, F. Coester—454

VOLUME 77 SECOND SERIES

CONTENTS

JANUARY 1, 1950

Local Production of Mesons at 11,300 Feet . . . . . O. PICCIONI 1
On the Secondary Particles of Local Penetrating Showers . . . . . O. PICCIONI 6
Effect of Screening on Beta-Ray Spectra and Internal Conversion . . . . . JOHN R. REITZ 10
Nuclear Disintegrations as Detected with Electron-Sensitive Emulsions Exposed in the Stratosphere . . . . . J. J. LORD AND MARCEL SCHEIN 19
Systematics of Alpha-Radioactivity . . . . I. PERLMAN, A. GHIORSO, AND G. T. SEABORG 26
Beta-Spectra of Cl^{38} . . . . . LAWRENCE M. LANGER 50
Heavy Nuclei of the Primary Cosmic Radiation . . . . . H. L. BRADT AND B. PETERS 54
Assignment and Disintegration Scheme of the 6.75-Hour Molybdenum . . . . . D. N. KUNDU, JOHN L. HULT, AND M. L. POOL 71
Assignment and Characteristic Radiations of the 14-Day Tin Activity . . . . . E. C. MALLARY AND M. L. POOL 75
Microwave Spectrum and Molecular Constants of Hydrogen Cyanide . . . . . JAMES W. SIMMONS, WALLACE E. ANDERSON, AND WALTER GORDY 77
On the Emission Bands of CCl . . . . . PUTCHA VENKATESWARLU 79
Straggling of Electrons near the Critical Energy. II . . . . . L. EYGES 81
Dimensional Effects Resulting from a High Dielectric Constant Found in a Ferromagnetic Ferrite . . . . . FRANK G. BROCKMAN, P. H. DOWLING, AND WALTER G. STENECK 85
Influence of Nuclear Structure on the Hyperfine Structure of Heavy Elements . . . . . AAGE BOHR AND V. F. WEISSKOPF 94
On the α-β- and α-K-Branching of the Heaviest Natural and Artificial Radioactive Substances . . . . . W. JENTSCHKE 98
On the Disintegration Products of the 2.2-μSec. Meson . E. P. HINCKS AND B. PONTECORVO 102
Study of the Spectra of Columbium and Molybdenum in the Extreme Ultraviolet . . . . . GEORGE W. CHARLES 120
Electronic Specific Heats in Tungsten and Zinc . . . . . A. A. SILVIDI AND J. G. DAUNT 125
l-Type Doubling in Polyatomic Molecules and Its Application to the Microwave Spectrum of Methyl Cyanide and Methyl Iso-Cyanide . . . . . HARALD H. NIELSEN 130

Letters to the Editor:

Angular Correlation of Scattered Annihilation Radiation . . . . . C. W. WU AND I. SHAKNOV 136
Optical Detection of Radiofrequency Reosnance . . . . . M. H. L. PRYCE 136
Beta-Spectrum of Ca^{45} . . . . . P. MACKLIN, L. FELDMAN, L. LIDOFSKY, AND C. S. WU 137
Temperature Dependence of Scintillation Pulses in Anthracene . G. G. KELLEY AND M. GOODRICH 138
7×10^{-9} Sec. Isomeric State in $_{79}Au^{197}$ . . . . . F. K. MCGOWAN 138
Lifetimes of Excited States of Au^{197}, Fe^{57}, Cd^{111}, Hg^{198}, and Tl^{203} . . . . . MARTIN DEUTSCH AND W. E. WRIGHT 139
Applications of Total Reflection of Neutrons . . . . . M. HAMERMESH 140
Note on Rotational Universe . . . . . C. Y. FAN 140
On the Hyperfine Structure of the $^2P_{\frac{1}{2}}$ State of Tl^{205} and Tl^{203} . . . . . A. BERMAN, P. KUSCH, AND A. K. MANN 140
Electric Quadrupole Moment of the Deuteron . . . . . G. F. NEWELL 141
Functions Used in Flügge's Method of Predicting Approximate Spatial Neutron Distributions . . . . . L. SECREST 141
Radioactive Xenon 125, and Xenon 127 . . . . . D. L. ANDERSON AND M. L. POOL 142
Units of Radioactivity . L. F. CURTISS, R. D. EVANS, WARREN JOHNSON, AND GLENN T. SEABORG 142
Effect of He^3 on the λ-Point of He^4 . . . . . O. K. RICE 142
Processes Involving Vector Mesons . . . . . JAMES N. SNYDER 143
Ultrasonic Interferometry for Low Acoustic Impedance . JAMES L. STEWART AND ELLEN S. STEWART 143
Cosmic Radiation and the Maintenance of a Potential Gradient in the Atmosphere . . S. A. KORFF 144
Dispersion in NH_3 in the Microwave Region . . . . . GEORGE BIRNHAM 144
Field Dynamics. I. Classical . . . . . K. V. ROBERTS 146
Field Dynamics. II. Quantum . . . . . K. V. ROBERTS 146
Determination of g-Values in Paramagnetic Organic Compounds by Microwave Resonance . . . . . A. N. HOLDEN, C. KITTEL, F. R. MERRITT, AND W. A. YAGER 147
Hyperfine Structure and Exchange Narrowing of Paramagnetic Resonance . . . . . C. H. TOWNES AND J. TURKEVICH 148
Microwave Spectrum of CH_3CFCl . . . . . J. K. BRAGG, T. C. MADISON, AND A. H. SHARBAUGH 148
Erratum: A Theory of Pressure Absorption . . . . . MASATAKA MIZUSHIMA 149
Coherent Scattering of X-Rays by Atoms with More Than One Electron According to the One Electron Theory and the Positron Theory . . . . . E. ARNOUS 149

On the Treatment of Quantum Electrodynamics without Eliminating the Longitudinal Field . . . . . NING HU 150
On the Infra-Red Absorption of the Hydrogen Molecule . . . . . MASATAKA MIZUSHIMA 150
Search for Photons Emitted by Long-Life Species of Nickel . D. G. THOMAS AND J. D. KURBATOV 151
Non-Linear I-V Characteristic of Ge at Very Low Temperatures . . . . . F. K. DU PRÉ 152
Preliminary Report on the Fine Structure of the Microwave Absorption Spectrum of Oxygen . . . . JAMES H. BURKHALTER, ROY S. ANDERSON, WILLIAM V. SMITH, AND WALTER GORDY 152
Lifetimes of Mercury and Potassium Atoms in Excited States . . . . . B. MISHRA 153
On the Nature of the π-Meson . . . . . B. FERRETTI AND S. GALLONE 153

JANUARY 15, 1950

Conversion Electrons of Radium D . . . . . LAWRENCE CRANBERG 155
Beat-Decay of B^{12} and Li^8 . . . . . W. F. HORNYAK AND T. LAURITSEN 160
Determination of the Energy Distribution of Bremsstrahlung from 19.5-Mev Electrons . . . . . H. W. KOCH AND R. E. CARTER 165
Nuclear Impulse in Electron Pair Creation . . . . . G. E. MODESITT AND H. W. KOCH 175
Low Energy Mesons in the Atmosphere . . . . . MATTHEW SANDS 180
Cross Section of the $C^{12}(p,\gamma)N^{13}$ Reaction at Low Energies . . . . . CARL L. BAILEY AND WILLIAM R. STRATTON 194
Cross Section for the Radiative Capture of Protons by C^{12} near 100 Kev . . . . . ROBERT NOEL HALL AND WILLIAM ALFRED FOWLER 197
On the Angular Distribution of Two-Photon Annihilation Radiation . . . . . S. DEBENEDETTI, C. E. COWAN, W. R. KONNEKER, AND H. PRIMAKOFF 205
High Energy Photons from Proton-Nucleon Collisions . . . . . R. BJORKLUND, W. E. CRANDALL, B. J. MOYER, AND H. F. YORK 213
Quantum Theory of Non-Local Fields. Part I. Free Fields . . . . . HIDEKI YUKAWA 219
Multiple Compton Scattering II . . . . . W. R. FAUST 227
Disintegration of Ag^{110} . . . . . KAI SIEGBAHN 233
Recombination Spectrum and Electron Density Measurements in Neon Afterglows . . . . . R. B. HOLT, JOHN M. RICHARDSON, B. HOWLAND, AND B. T. MCCLURE 239
Selection Rules for the Dematerialization of a Particle into Two Photons . . . . C. N. YANG 242
Thermionic Emission of Thin Films of Alkaline Earth Oxide Deposited by Evaporation . . . . . GEORGE E. MOORE AND H. W. ALLISON 246
Theory of Dielectric Polarization in Alkali-Halide Crystals . . . . . SHEPARD ROBERTS 258
Theory of the Change in the Conductivity of Metals Produced by Cold Work . . . . . J. K. MACKENZIE AND E. H. SONDHEIMER 264
Theory of the "Forbidden" (222) Electron Reflection in the Diamond Structure . . . . . R. D. HEIDENREICH 271
Mean Free Path of the Particles Produced in Nuclear Explosions and Comparison between Explosions in C and Pb . . A. LOVATI, A. MURA, G. SALVINI, AND G. TAGLIAFERRI 284

Letters to the Editor:

Extension of the Theory of Diabatic Flow . . . . . BRUCE L. HICKS 286
Inelastic Scattering of Neutrons by Light Nuclei . . . . . L. E. BEGHIAN, M. A. GRACE, G. PRESTON, AND H. HALBAN 286
Optical Effects in Bulk Silicon and Germanium . . . . . H. B. BRIGGS 287
Erratum: Short Range Alpha-Particles from Fluorine and Lithium Bombarded by Protons . . . . . W. E. BURCHAM AND JOAN M. FREEMAN 287
Proton-Proton Scattering and the Triplet Range of Nuclear Force . . . . . P. SWAN 288
Upper Limit of Spin-Spin Interaction Factor . . . G. J. BENE, P. M. DENIS, AND C. R. EXTERMAN 288
Determination of the Maximum Energy of Beta-Rays from Cu 62 by a New Method of Analyzing Absorption Date . L. KATZ, A. S. PENFOLD, H. J. MOODY, R. N. H. HASLAM, AND H. E. JOHNS 289
Photo-Disintegration of Rhodium . . N. W. CURTIS, J. HORNBOSTEL, D. W. LEE, AND E. O. SALANT 290
Delayed Coincidence Counting Measurement of $Hg^{203,205}$ . . . . . DANIEL BINDER 291
Coherent Neutron-Proton Scattering by Liquid Mirror Reflection . . . . . D. J. HUGHES, M. T. BURGY, AND G. R. RINGO 291
Interatomic Distances in CF_3Br, CF_3I, and CF_3CN . . . . . JOHN SHERIDAN AND WALTER GORDY 292
Scattering of Light by Light . . . . . J. C. WARD 293
Ferromagnetic Resonance Absorption by Mo Permalloy at 2920 Mc/Sec. . . . . JUNKICHI ITOH AND TETSUO AKIOKA 293
On the Calculation of Self-Energy of Particles . . . . . SURAJ N. GUPTA 294
Nuclear Gamma-Radiation of Cu^{61} . . . F. BOEHM, J. P. BLASER, P. MARMIER, AND P. PREISWERK 295
Half-Life for Double Beta-Decay . . . . . C. A. LEVINE, A. GHIORSO, AND G. T. SEABORG 296
On the Reaction $Mg^{24}(p,\gamma)Al^{25}$ . . T. GROTDAL, O. M. LÖNSJÖ, R. TANGEN, AND I. BERGSTRÖM 296
Pd Film Fast Neutron Detector . . . . . B. R. GOSSICK 297

Nuclear Induction Due to Free Larmor Precession . . . . . E. L. HAHN 297
Isotopic Constitution of Erbium and Lutecium . . . . . RICHARD J. HAYDEN, DAVID C. HESS, JR., AND MARK G. INGHRAM 299
Production of Gamma-Rays in Nuclear Interactions of Cosmic Rays . . . . . B. P. GREGORY, B. ROSSI, AND J. H. TINLOT 299
Erratum: Quasi-Chemical Method in the Statistical Theory of Regular Mixtures . . . YIN-YUAN LI 300
Effect of Light on a Diamond Conduction Counter . . . R. K. WILLARDSON AND G. C. DANIELSON 300
Beta-Spectrum of Be^{10} . . . . . P. R. BELL AND J. M. CASSIDY 301
Microwave Spectrum of CF_3Br . . . . A. H. SHARBAUGH, B. S. PRITCHARD, AND T. C. MADISON 302
Active Coaxial Tube . . . . . PHILIPPE A. CLAVIER 302
Some Physical Properties of Titanium . . . . . HERBERT I. FUSFELD AND JOSEPH T. GILBERT 302
Erratum: Electrical Properties of Pure Silicon and Silicon Alloys . G. L. PEARSON AND J. BARDEEN 303
Electron Screening and Ionization Potentials of Neutral and Singly Ionized Atoms . . . . . WOLFGANG FINKELNBURG AND FRANK STERN 303
Ionization Potentials of Higher Atomic Ions . . . . . WOLFGANG FINKELNBURG 304

FEBRUARY 1, 1950

Neutron Diffraction in Liquid Sulfur, Lead, and Bismuth . . . . . OWEN CHAMBERLAIN 305
Neutron Deficient Radioactive Isotopes of Rhenium . . . . . GEOFFREY WILKINSON AND HARRY G. HICKS 314
On the Theory of Slow Neutron Scattering by Liquid Helium . . . . . L. GOLDSTEIN, D. SWEENEY, AND M. GOLDSTEIN 319
Experimental Photo-Fission Thresholds in $_{92}U^{235}$, $_{92}U^{238}$, $_{92}U^{233}$, $_{94}Pu^{239}$, and $_{90}Th^{232}$ . . . . . H. W. KOCH, J. MCELHINNEY, AND E. L. GASTEIGER 329
Multiple Production of Mesons . . . . . PHYLLIS FREIER AND E. P. NEY 337
Cloud-Chamber Study of Cosmic-Ray Nuclear Interactions at 3260 Meters Elevation . . . . . W. W. BROWN AND A. S. MCKAY 342
Nuclear Dipole Vibrations and the Surface Symmetry Energy . . . . . R. D. PRESENT 355
Self-Stress of the Electron . . . . . F. ROHRLICH 357
On the Effects of Internal Nuclear Motion on the Hyperfine Structure of Deuterium . . . . . FRANCIS LOW 361
Numerical Value of the Lamb Shift . . . . H. A. BETHE, L. M. BROWN, AND J. R. STEHN 370
On the Solar Origin of Cosmic Radiation. II . . . . . H. ALFVÉN 375
On Some Low Ionizing Radiation Observed by Measurements of Cosmic Radiation at Great Depths . . . . . M. MIESOWICZ, L. JURKIEWICZ, AND J. M. MASSALSKI 380
Surface Impedance of Superconducting Tin, Mercury, and Lead at 9200 Mc/Sec. . . I. ŠIMON 384
Theory of Impurity Scattering in Semiconductors . . . E. CONWELL AND V. F. WEISSKOPF 388
Evaluation of the Stiffness Coefficients for Beryllium from Ultrasonic Measurements in Polycrystalline and Single Crystal Specimens . . . . . LOUIS GOLD 390
Note on the Quantization of Dissipative Systems . . . . . WESLEY E. BRITTIN 396

Letters to the Editor:

Mass Spectrographic Identification of Radioactive Lanthanum Isotopes . . . . . R. A. NAUMANN, F. L. REYNOLDS, AND I. PERLMAN 398
Measurement of the Earth's Magnetic Field at High Altitudes at White Sands, New Mexico . . . . . S. F. SINGER, E. MAPLE, AND W. A. BOWEN, JR. 398
Beta-Rays of K^{40} . . . . . P. R. BELL, BOYD WEAVER, AND J. M. CASSIDY 399
Phase Relations in He^3-He^4 Solutions . . B. WEINSTOCK, D. W. OSBORNE, AND B. M. ABRAHAM 400
Effects of Electrical Forming on the Rectifying Barriers of n- and p-Germanium Transistors . . . . . J. BARDEEN AND W. G. PFANN 401
Composite of Experimental Measurements of the Energy-Distribution among Beta-Particles from Tritium . . . . . E. F. COOPER AND F. T. ROGERS, JR. 402
Natural Ferromagnetic Resonance . . . . . A. J. E. WELCH, P. F. NICKS, ALAN FAIRWEATHER, AND F. F. ROBERTS 403
Beta-Spectrum and Decay Scheme of $_{65}Tb^{160}$ . . . . S. B. BURSON, K. W. BLAIR, AND D. SAXON 403
Beta-Spectrum of He^6 . . . . . V. PEREZ-MENDEZ AND H. BROWN 404
Anomalous Dielectric Effect of Vacuum Sputtered CaF_2 Layers . . . . . ERKKI A. LAURILA 405
Response of the Anthracene Scintillation Counter to Monoenergetic Electrons . . JOHN I. HOPKINS 406
Energy Bands and Mobilities in Monatomic Semiconductors . . . W. SHOCKLEY AND J. BARDEEN 407
Color Centers in Calcium Fluoride and Barium Fluoride Crystals . . . . . ALEXANDER SMAKULA 408
Gamma-Rays of K^{40} . . . . . P. R. BELL AND J. M. CASSIDY 409
Zenith Angle Dependence of Extensive Air Showers . . . . . H. L. KRAYBILL 410
"1947 Values" of the Atomic Constants and the Revision of the Faraday Constant . . . . . JESSE W. M. DUMOND 411
Note on the $Li^7(p,n)$ Be^7 Reaction and an Excited State of Be^7 . . . . . T. A. HALL 411
Fast Protons from the Absorption of π-Mesons by Nuclei . . . . . STEPHEN TAMOR 412
Upper and Lower Bounds of Eigenvalues . . . . . TOSIO KATO 413
Neutrons from $Li^7(p,n)$ Be^7 . . V. R. JOHNSON, M. J. WILSON LAUBENSTEIN, AND H. T. RICHARDS 413
Electromagnetic Concentration of Be^{10} . . . . . C. K. HEIM, H. W. SAVAGE, AND BOYD WEAVER 414

General Relation between Genuine and Chance Coincidences and Its Application to Measurement of High Activity Sources . . . Z. Bay and M. M. Slawsky 414
On the Motion of Particles in a Traveling Wave Linear Accelerator . . . . . John R. Terrall 415
Note on Nuclear Models . . . . . Hoff Lu 416
Measurement of Some Weak γ-Ray Intensities . G. R. Bishop, Richard Wilson, and H. Halban 416
On the Classification of the Spectrum of Singly Ionized Uranium . . . . . J. Rand McNally, Jr. 417
On the Relativistic Electromagneto-Ionic Theory of Wave Propagation . . . . . V. A. Bailey 418
Calculation of Decay Times from Coincidence Experiments . . . . . Z. Bay 419
On the Energy Spectrum of Heavy Nuclei in Primary Cosmic Radiation . . . . . M. S. Vallarta 419
Longitudinal Photons in Quantum Electrodynamics . . . . . F. J. Dyson 420
Microwave Spectrum of Bromine Monofluoride . D. F. Smith, M. Tidwell, and D. V. P. Williams 420
Intensity Distribution of the Second Positive ($C^3\pi \rightarrow B^3\pi$) Band System of Molecular Nitrogen . . . . . R. W. Nicholls 421
New Types of Microwave Transitions Involving l-Type Doubling in OCS and HCN . . . . . R. G. Shulman and C. H. Townes 421

Proceedings of the American Physicsl Society:

Minutes of the Meeting of the New England Section at Williamstown, Massachusetts, October 22, 1949 422

February 15, 1950

Penetration and Diffusion of X-Rays. V. Effect of Small Deflections upon the Asymptotic Behavior . . . . . U. Fano, H. Hurwitz, Jr., and L. V. Spencer 425
Hyperfine Structure of the Stable Isotopes of Indium . . . . . A. K. Mann and P. Kusch 427
Further Data on the Spin Gyromagnetic Ratio of the Electron . A. K. Mann and P. Kusch 435
Investigation of the Disintegration Schemes of Ru^{103} and Rb^{86} . . . . . C. E. Mandeville and E. Shapiro 439
Neutron-Proton Interaction . . . . . Richard S. Christian and Edward W. Hart 441
Stark-Zeeman Effects on Symmetric Top Molecules with Nuclear Quadrupole Coupling . . . . . F. Coester 454
Range-Energy Relation for Protons in Nuclear Emulsions . . . . . Hugh Bradner, Frances M. Smith, Walter H. Barkas, and A. S. Bishop 462
Lifetime of the Positive π-Meson . . . . . E. A. Martinelli and W. K. H. Panofsky 465
Production of Fast Deuterons in High Energy Nuclear Reactions . . . . . G. F. Chew and M. L. Goldberger 470
X-Ray and Gamma-Ray Reflection Properties from 500 X Units to Nine X Units of Unstressed and of Bent Quartz Plates for Use in the Two-Meter Curved-Crystal Focusing Gamma-Ray Spectrometer . . . . . D. A. Lind, W. J. West, and J. W. DuMond 475
Structure of Atoms from Diffraction Studies . . . . . H. Hauptman and J. Karle 491
Molecular Dipole Moments and Stark Effects. II. Stark Effects in OCS . . . . . R. G. Shulman and C. H. Townes 500
Some General Properties of Nuclear Reaction and Scattering Cross Sections . T. Teichmann 506
Spherical Shell Nuclear Model . . . . . H. A. Wilson 516
Moderation of Negative Mesons in Hydrogen I: Moderation from High Energies to Capture by an H_2 Molecule . . . . . A. S. Wightman 521
Infra-Red Spectrum and Molecular Constants of HF and DF . . . . . Robert M. Talley, Hoyt M. Kaylor, and Alvin H. Nielsen 529
Bernoulli's Theorem for Viscous Compressible Fluids . . . . . C. Truesdell 535
Fourth-Order Corrections in Quantum Electrodynamics and the Magnetic Moment of the Electron . . . . . Robert Karplus and Norman M. Kroll 536
Bremsstrahlung for Heavy Elements at Extreme Relativistic Energies . . . . . L. Bess 550

Letters to the Editor:

5-Ev Neutron Resonance in Ag . . . . . W. Selove 557
Angular Correlation of Successive Internal Conversion Electrons . . . . . H. Frauenfelder, M. Walter, and W. Zünti 557
Physical Interpretation of Type A Transitor Characteristics . . . . . L. P. Hunter 558
Forbidden Lines in the Spectra of Impure Hg^{198} . . . . . K. G. Kessler 559
Temperature Effects in the Spurious Discharge Mechanism of Parallel Plate Counters . . . . . Frank L. Hereford 559
Absorption Spectrum of Water Vapor between 900 and 2000 Angstroms . . . . . J. J. Hopfield 560
Distribution of Atomic and Molecular Oxygen in the Upper Atmosphere . . . . Rudolf Penndorf 561
Mesons Produced by Neutrons from the Cyclotron . . . . . F. M. Smith, Eugene Gardner, and Hugh Bradner 562
Possible Techniques in Direct-Electron-Beam Tumor Therapy . . . . . W. H. Bostick 564
Beta-Ray Distribution of Tc^{99} . . . . . B. H. Ketelle and John W. Ruch 565
On Elastic Constants of Nickel Crystals . . . . . Mikio Yamamoto 566

Zenith Angle Variation of the Latitude Effect of Cosmic Rays . . . . . H. D. RATHGEBER 566
Internal Diamagnetic Field Correction in Measurements of the Proton Magnetic Moment . . . . . NORMAN F. RAMSEY 567
Concerning W. P. Allis' Criticism of My Paper on Coulomb Interactions in a Plasma . . L. LANDAU 567
Nuclear Saturation for $V=\frac{1}{2}(1+P)J(r,\sigma_1,\sigma_2)$ . . . . . E. GERJUOY 568
Half-Life of Br^{82} . . . . . E. BERNE 568
Spectroscopic Isotope Shift and Nuclear Polarization . . . . . G. BREIT, G. B. ARFKEN, AND W. W. CLENDENIN 569
Phase Transition and Vapor Pressures of Liquid Mixtures of He^4 and He^3 . . . . . C. J. GORTER AND J. DE BOER 569
Regularization as a Consequence of Higher Order Equations . . . . . W. THIRRING 570
Photo-Disintegration of Nitrogen at Energies of 20 Mev to 100 Mev . . . . . E. R. GAERTTNER AND M. L. YEATER 570
Errata:
Microwave Spectrum of CH_2CFCl . . . . J. K. BRAGG, T. C. MADISON, AND A. H. SHARBAUGH 571
Non-Linear I-V Characteristic of Ge at Very Low Temperatures . . . . . F. K. DU PRÉ 571

Proceedings of the American Physical Society:

Minutes of the Meeting of the Division of Fluid Dynamics at the University of Virginia, Charlottesville, Virginia, December 28–30, 1949 572

MARCH 1, 1950

New Method for Determining the Relative Phase with Which Slow Neutrons Are Scattered by Nuclei . . . . . P. J. BENDT AND I. W. RUDERMAN 575
Excited States of Be^7 . . . . . J. C. GROSSKREUTZ AND K. B. MATHER 580
Study of the Multiple Scattering of Fast Charged Particles in a Gas and Its Role in the Interpretation of Cloud-Chamber Tracks . . . . . GERHART GROETZINGER, MARTIN J. BERGER, AND FRED L. RIBE 584
Star Fragments in Oxygen and Helium under Bombardment by 90-Mev Neutrons . . . . . JAMES TRACEY AND WILSON M. POWELL 594
Elastic Scattering of 84-Mev Neutrons . . . . . A. BRATENAHL, S. FERNBACH, R. H. HILDEBRAND, C. E. LEITH, AND B. J. MOYER 597
Nuclear Cross Sections for 95-Mev Neutrons . . . JAMES DEJUREN AND NÖRMAN KNABLE 606
Neutron-Deficient Cesium Isotopes . . . . . RICHARD W. FINK, FREDERICK L. REYNOLDS, AND D. H. TEMPLETON 614
Nuclear Pairs and Gamma-Radiation from Excited States of O^{16} . . . . . V. K. RASMUSSEN, W. F. HORNYAK, C. C. LAURITSEN, AND T. LAURITSEN 617
Theory of the D+D Reactions. Part I. Analysis of the Energy Dependence . . . . . F. M. BEIDUK, J. R. PRUETT, AND E. J. KONOPINSKI 622
Theory of the D+D Reactions. Part II. Relation to the Internucleonic Forces . . . . . J. R. PRUETT, F. M. BEIDUK, AND E. J. KONOPINSKI 628
Isotopic Constitution of Scandium, Gadolinium, Dysprosium, Holmium, Erbium, and Ytterbium . . . . . WALLACE T. LELAND 634
Ionization Chamber Study of the Disintegration of He^3 and N^{14} by Thermal Neutrons . . . . . W. FRANZEN, J. HALPERN, AND W. E. STEPHENS 641
Effective Range of Nuclear Forces. II. Photo-Disintegration of the Deuteron . . . . . H. A. BETHE AND CONRAD LONGMIRE 647
Beta-Spectra of Cs^{137}, Y^{91}, Pm^{147}, Ru^{106}, Sm^{151}, P^{32}, and Tm^{170} . . . . . HAROLD M. AGNEW 655
Drift Velocities of Electrons in Argon, Nitrogen, and Argon-Nitrogen Mixtures . . . . . E. D. KLEMA AND J. S. ALLEN 661
On a New Theory of Nuclear Forces . . . . . H. J. BHABHA 665
Approximate Theory of Order in Alloys . . . . . J. M. COWLEY 669
On the Emission Bands of CF_2 . . . . . PUTCHA VENKATESWARLU 676
Internal Conversion in Ni^{60} . . . . . MARTIN DEUTSCH AND KAI SIEGBAHN 680
Reactions Leading to Fe^{53}, Mn^{57}, and Cr^{55} . . . . . M. E. NELSON AND M. L. POOL 682
On Wave Equation Vector-Matrices and Their Spurs . . . . . R. J. DUFFIN 683
Study of Penetrating Showers at 3260 Meters . . . . . WILLIAM D. WALKER 686
Remark on the Coupling of Gravitation and Electron . . . . . HERMANN WEYL 699
Relativistic Motion in a Magnetic Field . . . . . M. H. JOHNSON AND B. A. LIPPMANN 702
Conductivity Pulses Induced in Insulating Liquids by Ionizing Radiations . . . . . NORMAN DAVIDSON AND A. E. LARSH, JR. 706
Do the Equations of Motion Determine the Quantum-Mechanical Commutation Relations? . . . . . EUGENE P. WIGNER 711

Letters to the Editor:

Nuclear Cross Sections of High Energy Pi-Mesons . . . . . KENNETH GREISEN 713
Cross Sections for the Photo-Disintegration of Nitrogen and Oxygen Nuclei by 100-Mev Betatron X-Rays . . . . . E. R. GAERTTNER AND M. L. YEATER 714
Half-Life of Carbon Fourteen and a Comparison of Gas Phase Counter Methods . WARREN W. MILLER, ROBERT BALLENTINE, WILLIAM BERNSTEIN, LEWIS FRIEDMAN, A. O. NIER, AND R. D. EVANS 714
Lateral Distribution of Photons in Extensive Air Showers . . . . . G. MOLIÈRE 715
On the Magnetic Moments of Mn^{55}, Co^{59}, Cl^{37}, N^{15}, and N^{14} . . . W. G. PROCTOR AND F. C. YU 716
Dependence of a Nuclear Magnetic Resonance Frequency upon Chemical Compound . . . . . W. G. PROCTOR AND F. C. YU 717
Spallation Products of Arsenic with 190-Mev Deuterons . . . . . H. H. HOPKINS, JR. 717
Electron Recombination in Helium . . . . . D. R. BATES 718
Microwave Spectra and Molecular Constants of Trifluorosilane Derivatives SiF_3H, SiF_3CH_3, SiF_3Cl, and SiF_3Br . . . . . JOHN SHERIDAN AND WALTER GORDY 719
Multiple Meson Processes and Nucleon Recoil . . . . . ALEX E. S. GREEN 719
Near Infra-Red Spectrum of the Polar Aurora . . . . . W. PETRIE 720
Possible Isomeric State of RaE . . . . H. M. NEUMANN, J. J. HOWLAND, JR., AND I. PERLMAN 720
Confirmation of the Workman-Reynolds Effect . . . . . VINCENT J. SCHAEFER 721
Statistics of the Three-Dimensional Ferromagnet . . . . . D. TER HAAR AND B. MARTIN 721
Nuclear Spin and Isotope Shift of Xenon Investigated with Separated Isotopes . . . . . JØRGEN KOCH AND EBBE RASMUSSEN 722
Possible Experimental Determination of Whether the Neutral Meson is Scalar or Pseudoscalar . . . . . C. N. YANG 722
Neutron Capture Gamma-Rays from Be^9, C^{13}, and N^{14} . . . . . B. B. KINSEY, G. A. BARTHOLOMEW, AND W. H. WALKER 723
On the Low States of Li^7 and Be^7 . . . . . D. R. INGLIS 724
Crucial Experiment Demonstrating Single Domain Property of Fine Ferromagnetic Powders . . . . . C. KITTEL, J. K. GALT, AND W. E. CAMPBELL 725
Effect of Exchange Interaction on Ferromagnetic Microwave Resonance Absorption . . . . . C. KITTEL AND CONYERS HERRING 725
Beta-Spectrum of Be^{10} . . . . . D. J. HUGHES, C. EGGLER, AND D. E. ALBURGER 726
Infra-Red Absorption in Silicon . . . . . H. B. BRIGGS 727
Neutron Density in the Free Atmosphere up to 100,000 Feet . . . . . LUKE C. L. YUAN 728
Zenith Angle Dependence of the Cosmic Radiation above the Atmosphere at $\lambda = 41°$N . S. F. SINGER 729
On the Nature of the Cosmic Radiation near the Pfotzer Maximum at $\lambda = 41°$N . . . S. F. SINGER 730
Resonance Neutron Scattering in Na^{23} at 3000 Ev . . . . . C. T. HIBDON, C. O. MUEHLHAUSE, W. SELOVE, AND W. WOOLF 730
Showers of Minimum Ionizing Particles from Cosmic-Ray Induced Nuclear Disintegrations in Nuclear Emulsions . . . . . B. T. FELD, I. L. LEBOW, AND L. S. OSBORNE 731
Neutrons from the Disintegration of Beryllium by Deuterons . . . . . W. D. WHITEHEAD AND C. E. MANDEVILLE 732
Evidence for a Charged Heavy Meson . . . . . H. H. FORSTER 733
Thermoelectric Power and Mobility of Carriers in Selenium . . . . . HERBERT W. HENKELS 734
Production of C^{15} . . . . EMMETT L. HUDSPETH, CHARLES P. SWANN, AND N. P. HEYDENBURG 736
Dependence of the F^{19} Nuclear Resonance Position on Chemical Compound . . . W. C. DICKINSON 736

Proceedings of the American Physical Society:

Minutes of the Meeting at Chicago, November 25 and 26, 1949 737

MARCH 15, 1950

Low Mass Francium and Emanation Isotopes of High Alpha-Stability . . . . . E. K. HYDE, A. GHIORSO, AND G. T. SEABORG 765
Nuclear Shell Models . . . . . EUGENE FEENBERG 771
East-West Asymmetry of Positive and of Negative Mesons and the Excess of the Positives as a Function of Zenith Angle and Altitude . . . . . GERHART GROETZINGER AND GORDON W. MCCLURE 777
Ionization in Argon and in Air Single Alpha-Particles as a Function of Their Energy . . . . . WILLIAM P. JESSE, HAROLD FORSTAT, AND JOHN SADAUSKIS 782
$Cu^{63}(n,2n)Cu^{62}$ Cross Section as Function of Neutron Energy near the Threshold . . . . . J. L. FOWLER AND J. M. SLYE, JR. 787
Redetermination of the Relative Abundances of the Isotopes of Carbon, Nitrogen, Oxygen, Argon, and Potassium . . . . . ALFRED O. NIER 789
Nuclear Energy Levels in Isotopes of Potassium . . . . . VANCE L. SAILOR 794
Low Energy Beta-Ray Spectra: Pm^{147} S^{35} . L. M. LANGER, J. W. MOTZ, AND H. C. PRICE, JR. 798
Yields and Angular Distributions of Some Gamma-Neutron Process . . . . . G. A. PRICE AND D. W. KERST 805
Correlation of Geiger Counter and Hall Effect Measurements in Alloys Containing Germanium and Radioactive Antimony 124 . G. L. PEARSON, J. D. STRUTHERS, AND H. C. THEUERER 809
Interaction between Elementary Particles. Part II . . . . . ALFRED LANDÉ 814
Electron Bombardment Conductivity in Diamond. Part II . . . . . KENNETH G. MCKAY 816

Effect of the Type of Support on the Photoelectric Work Function of Silver Films . . . . . L. L. BLACKMER AND H. E. FARNSWORTH 826

Increase in the Primary Cosmic-Ray Intensity at High Latitudes, and the Non-Existence of a Detectable Permanent Solar Magnetic Field . . . . . MARTIN A. POMERANTZ 830

Letters to the Editor:

Electric Resistivity of Polycrystalline Graphite and Carbons . . . . . S. MROZOWSKI 838
Element 97 . . . . . S. G. THOMPSON, A. GHIORSO, AND G. T. SEABORG 838
Lower Bound on the Range of Neutron-Proton Interaction . . . . A. A. BROYLES AND B. KIVEL 839
Theory of Magnetic Properties and Nucleation in Alnico V . . . . . C. KITTEL, E. A. NESBITT, AND W. SHOCKLEY 839
Thermal Neutron-Capture Cross Section of A^{36} . . . . G. E. MCMURTRIE AND D. P. CRAWFORD 840
Temperature Dependence of Microwave Line Widths . RAYDEEN HOWARD AND WILLIAM V. SMITH 840
Recoil Electron Spectrum of the K^{40} Gamma-Ray . R. W. PRINGLE, S. STANDIL, AND K. I. ROULSTON 841
Cation Distribution in Ferrites with Spinel Structure . . . . . FRANK G. BROCKMAN 841
Note on the Coefficient of Eddy Viscosity in Isotropic Turbulence . . . . . T. D. LEE 842
Radioactivity in Platinum by Neutron Capture . . . . . J. M. CORK, A. E. STODDARD, W. C. RUTLEDGE, C. E. BRANYAN, AND J. M. LEBLANC 843
Improvement Effect of the Plateau in Xylene- and Argon-Filled Geiger Counters . . BESIM TANYEL 843
On Two-Component Wave Equations . . . . . F. GÜRSEY 844
Correlation between Ionospheric Phenomena and Surface Pressure . M. W. JONES AND J. G. JONES 845
Coercive Force *vs.* Temperature in an Alloy with Zero Crystalline Magnetic Anisotropy . J. K. GALT 845
Cosmic Radiation and the Maintenance of a Potential Gradient in the Atmosphere . . . . . ROBERT E. HOLZER 846
Occurrence of Heavy Odd-Odd Isotopes in Nature . . . . . A. BRONIEWSKI 846
Production of Nuclear Disintegrations and Neutrons at the Geomagnetic Equator . . . . . J. A. SIMPSON, JR. AND E. HUNGERFORD 847
Additional Electron Lines from Radioactive Europium . . . . . J. M. CORK, H. B. KELLER, W. C. RUTLEDGE, AND A. E. STODDARD 848
Cloud-Chamber Study of Cosmic Rays Underground . . . . . O. L. TIFFANY AND W. E. HAZEN 849
***S*-Matrix in Non-Local Field Theory** . . . . . HIDEKI YUKAWA 849
Photon Pulses from Point-to-Plane Corona . . . . . W. N. ENGLISH 850
Gamma-Scintillations in Diphenylacetylene . C. F. RAVILIOUS, J. O. ELLIOT, AND S. H. LIEBSON 851
On the Isomerism of Kr^{83} . . . . . I. BERGSTRÖM, S. THULIN, AND G. ANDERSSON 851
Effect of Electronic Paramagnetism on Nuclear Magnetic Resonance Frequencies in Metals . . . . . C. H. TOWNES, CONYERS HERRING, AND W. D. KNIGHT 852
Relativistic Nuclear Force . . . . . T. TOYODA 853

Author Index to Volume 77 854
Analytic Subject Index to Volume 77 864
Volume Table of Contents iii

THE AMERICAN INSTITUTE OF PHYSICS

INCORPORATED

57 East 55th Street New York 22, N.Y.

MEMBER SOCIETIES:

American Physical Society
KARL K. DARROW, *Secretary*, Columbia University, New York 27, New York

Optical Society of America
ARTHUR C. HARDY, *Secretary*, Massachusetts Institute of Technology, Cambridge 39, Massachusetts

Acoustical Society of America
WALLACE WATERFALL, *Secretary*, 57 East 55th Street, New York 22, New York

Society of Rheology
C. J. DUTHIE, *Secretary*, North American Aviation, Inc., P. O. Box 30, Downey, California

American Association of Physics Teachers
R. F. PAUL, *Secretary*, University of Illinois, Urbana, Illinois

AFFILIATED SOCIETIES:

Electron Microscopy Society of America
Physical Society of Pittsburgh
Physics Club of Chicago
Physics Club of Philadelphia
Cleveland Physics Society
Physics Club of the Lehigh Valley

ASSOCIATES:

Over seventy-five leading industrial corporations and other institutions which contribute to the support of the Institute.

JOURNALS:

The Physics Teacher
JOHN T. TATE, *Editor*, University of Minnesota, Minneapolis, Minnesota

Reviews of Modern Physics
L. W. NORDHEIM, *Editor*, University of Minnesota, Minneapolis, Minnesota

Journal of the Optical Society of America
WALLACE R. BROCK, *Editor*, National Bureau of Standards, Washington 25

The Journal of the Acoustical Society of America
FLOYD A. FIRESTONE, *Editor*, 3318 Forest Grove Street, N.W., Washington, D.C.

American Journal of Physics
THOMAS H. OSGOOD, *Editor*, Michigan State College, East Lansing, Michigan

The Review of Scientific Instruments
GAYLORD P. HARNWELL, *Editor*, Room 301, Morgan Laboratory of Physics, University of Pennsylvania, Philadelphia, Pennsylvania

The Journal of Chemical Physics
JOSEPH E. MAYER, *Editor*, Kent Chemical Laboratory, University of Chicago, Chicago 37, Illinois

Journal of Applied Physics
ELMER HOUSTON, *Editor*, Case Institute of Technology, Cleveland 6, Ohio

Physics Today
DAVID ADLER, *Editor*, Associate Editor of Physics, 57 East 55 Street, New York 22, New York

OFFICERS

GEORGE R. HARRISON, *Chairman*
Massachusetts Institute of Technology

GEORGE B. PEGRAM, *Treasurer*
Columbia University

JOHN T. TATE,
Adviser on Publications
University of Minnesota

GOVERNING BOARD

LUIS W. ALVAREZ
I. W. BEAMS
WALLACE R. BROCK
E. U. CONDON
W. F. FAIR, JR.
HARVEY FLETCHER
GEORGE R. HARRISON
W. V. HOUSTON
PAUL KIRKPATRICK
PAUL E. KLOPSTEG
F. W. LOOMIS
PHILIP M. MORSE
J. R. OPPENHEIMER
GEORGE B. PEGRAM
HAROLD K. SCHILLING
JOHN T. TATE
WALLACE WATERFALL
M. W. WHITE

Consultant on Printing
MELVIN LOOS

ADMINISTRATIVE STAFF

GEORGE A. BARTON, *Director*
WALLACE WATERFALL,
Executive Secretary
THEODORE VORBURGER,
Assistant Treasurer and Comptroller
RUTH F. BRYANS,
Publication Manager
BETTY HOFSTADTER,
Assistant Secretary
HELEN B. NEUBERGER,
Circulation Manager

THE American Institute of Physics was founded in 1931 as a federation of leading societies in the field of Physics. It combines also one operating agency whose functions on behalf of physics which can best be done by the Societies jointly. Its purpose is the advancement and diffusion of physics and its applications to human welfare. To this end it publishes the journals of the Societies the nine journals listed on this page; promotes unity and effectiveness of effort among all who are interested in physics; renders numerous direct services to physicists and to the public; and cooperates with government agencies, national associations, educational institutions, scientific industries, and others in such manner as to realize the opportunities and fulfill the responsibilities of physics as an important and constructive human activity.

CONTENTS

THE PHYSICAL REVIEW, SECOND SERIES, VOLUME 77, NO. 6 MARCH

Low Mass Francium and [illegible] of High Alpha-Stability . . . . . E. K. HYDE, A. GHIORSO, AND G. T. SEABORG

Nuclear Shell Models . . . . . EUGENE FEENBERG

East-West Asymmetry of [illegible] and of Negative Mesons and the Excess of the Latter as a Function of [illegible] and Altitude . . . . . GEORGE GROETZINGER AND GORDON W. MACDIARMID

Ionization in Argon and in [illegible] Alpha-Particles as a Function of Their Energy . . . . . CHRISTIAN P. JUNGE, HAROLD FORSTAT, AND JOHN SAMUEL

$Cu^{63}(n,2n)Cu^{62}$ Cross Section [illegible] of Neutron Energy near the Threshold . . . . . J. L. FOWLER AND J. M. [illegible]

Redetermination of the [illegible] Abundances of the Isotopes of Carbon, Nitrogen, Argon, and Potassium . . . . . ALFRED O. NIER

Nuclear Energy Levels in [illegible] Formation . . . . . VANCE L. SAILOR

Low Energy Beta-Ray Spectra of Sr^{90} . . . . . L. M. LANGER, J. W. MOTZ, AND H. C. PRICE, JR.

Yields and Angular Distributions of Some Gamma-Electron Processes . . . . . G. A. PRICE AND D. [illegible]

Correlation of Geiger Counter [illegible] Effect Measurements in Alloys Containing Gold and Radioactive [illegible] . . . . . G. L. PEARSON, J. D. STRUTHERS, AND H. C. THOMAS

Interaction between [illegible] Particles. Part II . . . . . ALFRED LANDÉ

Electron Bombardment [illegible] in Diamond. Part II . . . . . KENNETH G. MCKAY

Effect of the Type of [illegible] on Photoelectric Work Function of Silver Films . . . . . L. L. BLACKMER AND H. E. FARNSWORTH

Increase in the Primary Cosmic Radiation Intensity at High Latitudes, and the Non-Existence of Detectable Permanent Magnetic Fields . . . . . MARTIN A. POMERANTZ

Letters to the Editor:

Electric Resistivity of [illegible] and Cadmium . . . . . S. MIDDLEMAN

Element 97 . . . . . S. G. THOMPSON, A. GHIORSO, AND G. T. SEABORG

Lower Bound on the [illegible] Scattering . . . . . A. A. BROYLES AND R. KARPLUS

Theory of Magnetic [illegible] . . . . . C. ZENER, R. A. NEBIUT, AND W. SHOCKLEY

Thermal Neutron [illegible] of Ag^{107} . . . . . G. K. MCMURTRIE AND D. P. CRAWFORD

Temperature Dependence of [illegible] . . . . . RAYMOND HOWARD AND WILLIAM V. HOUSTON

Recoil Electron [illegible] . . . . . W. PRIMAKOFF, S. STANDIL, AND K. I. ROULSTON

Cation Distribution [illegible] . . . . . FRANK G. BROCKMAN

Note on the Coefficient [illegible] . . . . . S. S. [illegible]

Radioactivity in [illegible] . . . . . J. J. [illegible]

Improvement [illegible] . . . . . W. C. ROENTGEN, C. E. BRANTAN, AND J. M. [illegible]

On Two-Component [illegible] . . . . . F. [illegible]

Correlation between [illegible] . . . . . M. W. JONES AND J. G. [illegible]

Coercive Force of [illegible] . . . . . J. K. [illegible]

Cosmic Radiation [illegible] . . . . . ROBERT S. RICHARDSON

Occurrence of [illegible] . . . . . A. [illegible]

Production of [illegible] . . . . . J. A. SIMPSON, JR. AND R. [illegible]

Additional Electron [illegible] . . . . . W. C. ROENTGEN, AND A. J. [illegible]

Cloud-Chamber [illegible] . . . . . O. L. TIFFANY AND W. E. [illegible]

S-Matrix in Non-[illegible] . . . . . HERBERT [illegible]

Photon Pulses from [illegible] . . . . . W. R. [illegible]

Gamma-Scintillation [illegible] . . . . . C. F. RAPHAEL, J. O. ELLIOTT, AND S. H. [illegible]

On the Isomerism [illegible] . . . . . I. BERGSTRÖM, S. THULIN, AND G. [illegible]

Effect of Electron [illegible] . . . . . Nuclear Resonance Frequencies in Metals . . . . . C. [illegible], CONYERS HERRING, AND W. J. [illegible]

Relativistic Nuclear [illegible] . . . . . T. [illegible]

Author Index to Volume [illegible] . . . . .

Analytic Subject Index [illegible] . . . . .

Volume Table of Contents [illegible] . . . . .

LANCASTER PRESS, INC., [illegible]